CARDIOVASCULAR DISEASES RELATED TO DIABETES AND OBESITY VOLUME II

EDITED BY: Lu Cai, Ying Xin, Jamie Lynn Young and Rajesh Mohanraj
PUBLISHED IN: Frontiers in Endocrinology

frontiers Research Topics

ISSN 1664-8714
ISBN 978-2-83250-541-0
DOI 10.3389/978-2-83250-541-0

About Frontiers

Frontiers is more than just an open-access publisher of scholarly articles: it is a pioneering approach to the world of academia, radically improving the way scholarly research is managed. The grand vision of Frontiers is a world where all people have an equal opportunity to seek, share and generate knowledge. Frontiers provides immediate and permanent online open access to all its publications, but this alone is not enough to realize our grand goals.

Frontiers Journal Series

The Frontiers Journal Series is a multi-tier and interdisciplinary set of open-access, online journals, promising a paradigm shift from the current review, selection and dissemination processes in academic publishing. All Frontiers journals are driven by researchers for researchers; therefore, they constitute a service to the scholarly community. At the same time, the Frontiers Journal Series operates on a revolutionary invention, the tiered publishing system, initially addressing specific communities of scholars, and gradually climbing up to broader public understanding, thus serving the interests of the lay society, too.

Dedication to Quality

Each Frontiers article is a landmark of the highest quality, thanks to genuinely collaborative interactions between authors and review editors, who include some of the world's best academicians. Research must be certified by peers before entering a stream of knowledge that may eventually reach the public - and shape society; therefore, Frontiers only applies the most rigorous and unbiased reviews.
Frontiers revolutionizes research publishing by freely delivering the most outstanding research, evaluated with no bias from both the academic and social point of view. By applying the most advanced information technologies, Frontiers is catapulting scholarly publishing into a new generation.

What are Frontiers Research Topics?

Frontiers Research Topics are very popular trademarks of the Frontiers Journals Series: they are collections of at least ten articles, all centered on a particular subject. With their unique mix of varied contributions from Original Research to Review Articles, Frontiers Research Topics unify the most influential researchers, the latest key findings and historical advances in a hot research area! Find out more on how to host your own Frontiers Research Topic or contribute to one as an author by contacting the Frontiers Editorial Office: frontiersin.org/about/contact

CARDIOVASCULAR DISEASES RELATED TO DIABETES AND OBESITY VOLUME II

Topic Editors:
Lu Cai, University of Louisville, United States
Ying Xin, Jilin University, China
Jamie Lynn Young, University of Louisville, United States
Rajesh Mohanraj, United Arab Emirates University, United Arab Emirates

Citation: Cai, L., Xin, Y., Young, J. L., Mohanraj, R., eds. (2022). Cardiovascular Diseases Related to Diabetes and Obesity Volume II. Lausanne: Frontiers Media SA. doi: 10.3389/978-2-83250-541-0

Table of Contents

frontiers | Frontiers in Endocrinology

TYPE Editorial
PUBLISHED 05 October 2022
DOI 10.3389/fendo.2022.1044326

OPEN ACCESS

EDITED AND REVIEWED BY
Gaetano Santulli,
Albert Einstein College of Medicine,
United States

*CORRESPONDENCE
Jamie L. Young
jamie.young.1@louisville.edu
Lu Cai
lu.cai@louisville.edu

SPECIALTY SECTION
This article was submitted to Cardiovascular Endocrinology, a section of the journal Frontiers in Endocrinology

RECEIVED 14 September 2022
ACCEPTED 26 September 2022
PUBLISHED 05 October 2022

CITATION
Young JL, Xin Y, Rajesh M and Cai L (2022) Editorial: Cardiovascular diseases related to diabetes and obesity – volume II.
Front. Endocrinol. 13:1044326.
doi: 10.3389/fendo.2022.1044326

Editorial: Cardiovascular diseases related to diabetes and obesity – volume II

Jamie L. Young[1]*, Ying Xin[2], Mohanraj Rajesh[3] and Lu Cai[1,4]*

[1]Department of Pharmacology and Toxicology, University of Louisville School of Medicine, Louisville, KY, United States, [2]Key Laboratory of Pathobiology, Ministry of Education, Jilin University, Changchun, China, [3]Department of Pharmacology and Therapeutics, College of Medicine and Health Sciences, United Arab Emirates University, Al Ain, United Arab Emirates, [4]Pediatric Research Institute, Department of Pediatrics, the University of Louisville School of Medicine, Louisville, KY, United States

KEYWORDS

metabolic syndrome, obesity, cardiovascular disease, multifactorial, biomarkers

Editorial on the Research Topic
Cardiovascular diseases related to diabetes and obesity volume II

Metabolic diseases are multifactorial, multifaceted, and even intertwined making understanding the etiopathogenesis of such diseases more complex than originally thought. This concept of intimately intertwined health conditions is exemplified in the relationship between obesity, diabetes, and cardiovascular diseases (CVDs), of which the prevalence of all three diseases are growing in parallel with one another. Nearly tripling in prevalence since 1975, obesity is considered a leading global health concern and continues be the number one risk factor for diabetes and CVDs (1). Despite our advances at the bench and in the clinic, approximately 17.9 million people die each year from CVDs, accounting for 32% of all deaths globally (2). Therefore, it is imperative to rigorously investigate the underlying mechanisms involved in the pathogenesis of obesity- and diabetes-related cardiovascular events to develop more effective, targeted therapies aimed at prevention and attenuation of disease progression. Reflective of the significance of this topic, a second volume of this special issue has been created, further compiling recent clinical, pre-clinical and basic research studies as well as review articles aimed at filling the knowledge gaps and expanding our understanding of the complicated and intertwined relationship between obesity, diabetes, and CVDs.

The multifactorial, intertwined nature of metabolic diseases has become increasingly apparent. In fact, the term "metabolic syndrome" is used to describe a group of conditions that work together to increase the risk of diabetes and CVDs. It is pertinent to note obesity is the main risk factor for metabolic syndrome. A major contributor to CVDs is premature myocardial infarction (PMI), referring to myocardial infarction that occurs in men less than 55 years old and women less than 65 years old. In an observational study by Gao et al. (2022) 772 patients less than 45 years old diagnosed with acute myocardial infarction were divided into groups based on whether they had

metabolic syndrome or not and followed up for approximately 42 months for major adverse cardiovascular events (MACE). Metabolic syndrome was an independent risk factor for MACE with hyperglycemia being an independent predictor for both coronary artery lesions and MACE. These results highlight the complex association between metabolic diseases as well as the need for early intervention in both metabolic syndrome and PMI.

Further highlighting the multifactorial traits of cardiovascular diseases, Wen et al. (2022) demonstrated the increased risk of cardiovascular complications, specifically coronary heart disease (CHD), associated with obstructive sleep apnea hypopnea syndrome (OSAHS) are related to inflammatory factors, glycol-lipid metabolism, obesity status, and HOMA-IR. In patients with OSAHS and CHD there was a significant increase in triglycerides, serum inflammatory factors C-reactive protein (CRP), tumor necrosis factor-α (TNF-α), interleukin-6 (IL-6), and interferon-γ (IFN-γ) when compared to patients with OSAHS alone. Results from this study emphasize the inseparable relationship of OSAHS with inflammatory factors, obesity status and heart disease, demonstrating the importance of considering the influence of these factors in prevention and treatment of OSAHS.

The multifactorial pathogenesis of diabetic cardiomyopathy is eloquently reviewed in the article by Chen et al. (2022) highlighting the involvement of key cellular networks involved in inflammation and oxidative stress that result in abnormal lipid and glucose metabolism (a key characteristic of obesity) and ultimately diabetic cardiomyopathy. The potential pathways by which glycol- and lipid-metabolism disorders damage the diabetic heart are substantial. Detrimental alterations in cellular events that contribute to dysregulated lipid and glucose metabolism, such as the up regulation of CD36, the AGEs/RAGE system, hexamine biosynthesis and NLRP inflammasome activation, have all attracted considerable research attention making them potential targets for therapeutic interventions for not only diabetic cardiomyopathy, but also chronic inflammatory diseases and cancer. With such advances, there is a need for researchers to reevaluate the exact effects of the established, first-line drugs (i.e., metformin and thiazolidinediones) on diabetic cardiomyopathy.

An alternative approach to developing new drugs is the repurposing of established, already approved therapies, a strategy that is gaining traction because it builds on already available information including structure, formulations and potential toxicity while decreasing cost and improving the rates of clinical success. This approach was applied in an integrated bioinformatics study by Guo et al. (2022) who identified 5 potential immune biomarkers in diabetic cardiomyopathy patients using existing microarray data from the Gene Expression Omnibus (GEO) database. Expression levels of the 5 immune biomarkers were confirmed in an animal model of diabetic cardiomyopathy, with endothelin-1 (EDN1) showing significant expression differences in both the dataset and animal model. The authors then screened for potential, known therapeutic drugs that could regulate EDN1 upstream transcription factors and identified 9 candidate compounds for potential drug repurposing followed by molecular docking simulations. This data is compelling, suggesting EDN1 is a potential biomarker of diabetic cardiomyopathy while highlighting the potential of drug repurposing, which needs urgent validation using robust *in vivo* models. In support of this notion, Wang et al. (2022) targeted endothelial dysfunction, an early pathological event in diabetic angiopathy, with curcumin, a natural polyphenol shown to attenuate diabetes-associated endothelial dysfunction, and baicalein, a phytochemical shown to inhibit vascular inflammation. Both *in vivo* and *in vitro* results revealed curcumin and baicalein synergistically restored endothelial cell survival and blood vessel structure repair as well as decreases blood sugar and lipid levels in rats. Although this study did not focus on diabetic cardiomyopathy, this novel combination of therapies on the endothelial system creates a platform for investigating this combination therapy for all diabetic CVDs.

The discovery of novel biomarkers of CVDs is key to the advancement of preventative measures and disease treatment. Yang et al. (2022) investigated the role of postprandial hyperglycemia in the pathogenesis of coronary artery disease in 2970 Chinese patients who underwent coronary angiography. Patients were categorized by whether they had diabetes or not and 1,5-Anhydroglucitol (1,5-AG) was measured in their serum. In contrast to hemoglobin A1c (HbA1c) (reflective of average blood sugar levels over the past 2-3 months), 1,5-AG reflects short-term, circulating glucose fluctuations, thus predictive of postprandial hyperglycemia. The prevalence and severity of coronary artery disease in Chinese patients undergoing coronary angiography was significantly associated with low serum 1,5-AG and this effect was stronger in patients with diabetes. These results add to previous evidence highlighting the use of 1,5-AG as an effective glycometabolic marker. In another study using a transcriptomics approach to identify novel biomarker, Yu et al. (2022) used 10 human carotid atherosclerotic plaque samples from diabetic and non-diabetic patients to sequence coding RNA, non-coding RNA and identify potential biomarkers and RNA regulatory pathways associated with plaque formation and diabetes. Many of the genes and all RNA regulatory pathways associated with carotid atherosclerotic plaques in diabetic patients had not been reported, thus providing a platform for further studies validating these novel potential biomarkers.

Using established, already existing datasets to test hypothesis and build analytical models has proven to be a useful predictive tool in understanding disease development. Yang et al. (2022) used 2 high-quality critically ill databases to screen intensive care unit patients with both heart failure and diabetes with the goal of developing a composite indicator of predicting hospital mortality for patients. These patients have worse prognosis and higher mortality than patients with either heart failure or

diabetes alone. A machine learning model was used to find indicators associated with hospital mortality for patients with both diabetes and heart failure, resulting in the creation of a novel composite indicator that combines three major attributes related to mortality risk [Acute Physiology Score (APS) III, Sepsis-related Organ Failure Assessment (SOFA), and Max lactate]. Studies such as these that use existing data to create novel disease outcome predictors with better clinical value are extremely valuable and have potential to help reduce mortality risk.

As our knowledge base increases, both technically and conceptually, there is a need to reevaluate existing practices and guidelines. Although CVDs are the result of a combination of risk factors, current guidelines do not account for the multitude of risk factors involved, nor do they take into account the heterogeneity among patients. As indicated by Li et al. (2022), the paradigm is shifting to ensure the intensity of treatments adequately match the risk level. A new risk stratification was applied to a Chinese cohort of 9,944 patients with atherosclerotic CVD (ASCVD). Among patients in various subgroups of ASCVD, worse outcomes were significantly associated with diabetes thus implicating a need to adjust ASCVD treatment in diabetic patients.

Finally, in a comprehensive review, Al Kury et al. (2022) emphasized the need for more studies focused on diabetes-induced sinoatrial node remodeling. Sinoatrial node dysfunction results in slow heart rate, eventually resulting in high blood pressure and coronary heart disease. Of note is the fact that chronic treatments for diabetes (including metformin, insulin, and rosiglitazone) adversely affect the sinoatrial node, and thus negatively impact cardiac function. Therefore, more adequate therapies are need for diabetic patients who also have impaired cardiac function.

Overall, the above-mentioned articles published in the second volume of this Research Topic highlight the broad scope of research being conducted to advance our technical and conceptual understanding of the interconnectedness of obesity, diabetes, and CVDs. We continue to expand our understanding of the cellular, molecular, and pathological processes involved in these chronic diseases, applying what we know to advance the discovery of novel biomarkers and therapies. However, it is clear there is much work to be done, data gaps to be filled and discoveries to be made.

Author contributions

JY and LC made the first draft. MR, JY, YX, and LC revised and approved the final submitted version.

Conflict of interest

The authors declare that the research was conducted in the absence of any commercial or financial relationships that could be construed as a potential conflict of interest.

Publisher's note

References

1. ADA (American Diabetes Assocition). *Diabetes complications: Cardiovascular disease* (2022). Available at: https://diabetes.org/diabetes/cardiovascular-disease (Accessed September 3, 2022).

2. WHO (World Health Organization). *Cardiovascular disease: Fact sheet* (2022). Available at: https://www.who.int/news-room/fact-sheets/detail/cardiovascular-diseases-(cvds) (Accessed September 3, 2022).

frontiers | Frontiers in Endocrinology

ORIGINAL RESEARCH
published: 28 April 2022
doi: 10.3389/fendo.2022.860698

Current Guideline Risk Stratification and Cardiovascular Outcomes in Chinese Patients Suffered From Atherosclerotic Cardiovascular Disease

*Sha Li, Hui-Hui Liu, Yuan-Lin Guo, Cheng-Gang Zhu, Na-Qiong Wu, Rui-Xia Xu, Qian Dong, Jie Qian, Ke-Fei Dou and Jian-Jun Li**

Cardiometabolic Center, State Key Laboratory of Cardiovascular Disease, FuWai Hospital, National Center for Cardiovascular Diseases, Chinese Academy of Medical Sciences, Peking Union Medical College, Beijing, China

OPEN ACCESS

Edited by:
Jamie Lynn Young, University of Louisville, United States

Reviewed by:
Nicolas Renna, Universidad Nacional de Cuyo, Argentina
Lamija Ferhatbegovic (Pojskic), Cantonal Hospital Zenica, Bosnia and Herzegovina

***Correspondence:**
Jian-Jun Li
Lilijianjun938@126.com

Specialty section:
This article was submitted to Cardiovascular Endocrinology, a section of the journal Frontiers in Endocrinology

Received: *23 January 2022*
Accepted: *29 March 2022*
Published: *28 April 2022*

Citation:
Li S, Liu H-H, Guo Y-L, Zhu C-G, Wu N-Q, Xu R-X, Dong Q, Qian J, Dou K-F and Li J-J (2022) Current Guideline Risk Stratification and Cardiovascular Outcomes in Chinese Patients Suffered From Atherosclerotic Cardiovascular Disease. Front. Endocrinol. 13:860698. doi: 10.3389/fendo.2022.860698

Background and Aims: Heterogeneity exists among patients with atherosclerotic cardiovascular disease (ASCVD) with regard to the risk of recurrent events. Current guidelines have definitely refined the disease and we aimed to examine the practicability in Chinese population.

Methods: A cohort of 9944 patients with ASCVD was recruited. Recurrent events occurred during an average of 38.5 months' follow-up were collected. The respective and combinative roles of major ASCVD (mASCVD) events and high-risk conditions, being defined by 2018 AHA/ACC guideline, in coronary severity and outcome were studied.

Results: The number of high-risk conditions was increased with increasing number of mASCVD events (1.95 ± 1.08 vs. 2.16 ± 1.10 vs. 2.42 ± 1.22). Trends toward the higher to the highest frequency of multi-vessel coronary lesions were found in patients with 1- (71.1%) or ≥2 mASCVD events (82.8%) when compared to those without (67.9%) and in patients with 2- (70.5%) or ≥3 high-risk conditions (77.4%) when compared to those with 0-1 high-risk condition (61.9%). The survival rate was decreased by 6.2% between none- and ≥2 mASCVD events or by 3.5% between 0-1 and ≥3 high-risk conditions. Interestingly, diabetes was independently associated with outcome in patients with 1- [1.54(1.06-2.24)] and ≥2 mASCVD events [1.71(1.03-2.84)]. The positive predictive values were increased among groups with number of mASCVD event increasing (1.10 vs. 1.54 vs. 1.71).

Conclusion: Propitious refinement of ASCVD might be reasonable to improve the survival. Concomitant diabetes was differently associated with the incremental risk among different ASCVD categories, suggesting the need of an appropriate estimate rather than a 'blanket' approach in risk stratification.

Keywords: ASCVD, risk stratification, Chinese, high-risk conditions, outcome

INTRODUCTION

Atherosclerotic cardiovascular disease (ASCVD) is the leading cause of death worldwide, especially in China (1–3). Traditionally, ASCVD is considered to be a result from the combination of multiple cardiovascular risk factors (RFs). However, the overall risk of ASCVD remains high despite optimal medical management for RFs (4, 5). It is increasingly recognized that heterogeneity exists among patients with ASCVD, which has been defined into the same risk category with a 'blanket' approach in the past (6–8). Currently, the paradigm of guidelines has proposed the risk refinement, targeting that the intensity of treatments matches the risk level (9–12). Emerging data strongly indicate that the patients at very-high-risk (VHR) deserves a more veritable approach for clinical management.

Given the disease burden and heterogeneity of ASCVD, we sought to examine the practicability of the newest stratification in a Chinese cohort. Specially, in the present study, we determined 1) the patterns of high-risk conditions, coronary severity, and outcomes among patients with different number of major ASCVD (mASCVD) events at enrolment (0 vs. 1 vs. ≥2 mASCVD events); 2) the associations of coronary severity or outcome with high-risk conditions (0-1 vs. 2 vs. ≥3 high-risk conditions); and 3) the respective and combinative roles of mASCVD events and high-risk conditions, especially diabetes in outcomes.

MATERIALS AND METHODS

Study Design and Populations

Our study complied with the Declaration of Helsinki and was approved by the hospital's ethical review board (Fu Wai Hospital & National Center for Cardiovascular Diseases, Beijing, China). Informed written consents were obtained from all patients enrolled in this study.

In this observational study with a prospective cohort design, a total of 9944 adults with established ASCVD who were hospitalized in our division of Fu Wai Hospital were consecutively collected from April 2011 through July 2018. Patients with ASCVD were those with coronary artery disease (CAD) including chronic CAD and acute coronary syndrome (ACS), ischemic stroke, and/or peripheral artery disease (PAD) (10). Of the 9944 participants with baseline medical history records, 9806 had CAD, 403 had stroke, and 189 had PAD. Diabetes in this study were all type 2 diabetes. Patients with severe levels of triglycerides (TG, >5.6mmol/L), significant hematologic disorders (white blood cell <3.0 or $>10\times10^9$), infectious or systematic inflammatory disease, thyroid dysfunction, severe liver/renal insufficiency and/or malignant disease were excluded from the study (**Supplemental Figure 1**).

Baseline Data Collection and Measurement

Clinical variables of each participant were obtained as described by our previous study (13, 14). The study patients were subjected to elective coronary angiography (CAG). Obstructive CAD defined as the detection of 50-99% diameter stenosis in any of the four major epicardial coronary arteries including left main (LM), left anterior descending (LAD), left circumflex (LCX), and right coronary artery (RCA). Occlusive CAD defined as 100% occlusion of ≥1 coronary artery. The severity and extent of coronary stenosis were assessed using the number of diseased vessels and the Gensini scoring system (15). High-risk conditions and mASCVD events were defined according to 2018 AHA/ACC cholesterol guideline (10).

Follow-Up and Endpoints Assignment

Follow-up data were obtained at outpatient visits or by telephone contact with every 6-months. We followed-up the cohort mapping for clinical outcomes until the study end date (February 26, 2019, with a window period of 30 days). The primary end points included cardiovascular death, nonfatal myocardial infarction (MI), heart failure (HF), and stroke (13). After all, the data were obtained from 9783 patients and a total of 407 primary events were documented during an average of 38.5 months' follow-up.

Statistical Analysis

Statistical analysis was performed with SPSS version 26.0 software (SPSS Inc., Chicago, IL, USA). P values <0.05 were considered statistically significant. Categorical variables were presented as numbers with relative frequencies (percentages) and continuous variables as mean with standard deviation (SDs) or median with inter-quartile range (IQR) as appropriate. Categorical variables were presented as number (percentage) and analyzed by chi-squared statistic test. Differences between groups were determined using the ANOVA or nonparametric test where appropriate. Kaplan-Meier survival curves and Log-rank tests were used to analyze the survival outcomes among the different groups. Cox regression analyses were performed to calculate hazard ratios (HRs) and 95% confidence intervals (CIs) to analyze survival outcome with the high-risk conditions. The covariates including a given high-risk condition and adjusted factors named age, gender, body mass index (BMI), prior percutaneous coronary intervention/coronary artery bypass grafting (PCI/CABG), and current smoking were entered into the multivariable Cox regression model 1, respectively. All covariates above were added simultaneously to the Cox model 2.

RESULTS

Baseline Characteristics

Baseline characteristics of patients according to the number of mASCVD events were showed in **Table 1**. Most patients (67.1%) presented with stable event or without mASCVD event followed by patients with 1- (25.0%) or ≥2 mASCVD events (7.8%). Both the number of high-risk conditions (**Supplemental Figure 2**) and the coronary severity (**Figure 1**) were increased with increasing number of mASCVD events. Similarity, we also

TABLE 1 | Baseline characteristics by ASCVD categories.

	Without mASCVD event	With 1 mASCVD event	With ≥2 mASCVD events	P for trend
Demographic characteristics				
N	6676	2489	779	
Male,%(n)	67.5(4503)	83.8(2085)	87.3 (680)	<0.001
Age (y)	59.1 ± 8.9	54.7 ± 12.3	56.2 ± 11.7	<0.001
BMI (kg/m2)	25.9 ± 3.2	26.1 ± 3.2	26.0 ± 3.2	0.018
Clinical characteristics				
Hypertension,%(n)	66.6 (4445)	59.9 (1490)	63.4 (494)	<0.001
Hypercholesterolemia*,%(n)	5.5 (367)	6.5 (161)	7.6 (59)	0.026
Diabetes,%(n)	33.2 (2215)	32.2 (801)	36.7 (286)	0.034
CKD3/4,%(n)	3.4 (225)	4.0 (100)	4.9 (38)	0.056
History of congestive HF,%(n)	1.0 (69)	7.2 (179)	18.0 (140)	<0.001
Current smoker,%(n)	33.3 (2220)	46.3 (1152)	46.0 (358)	<0.001
History of PCI/CABG,%(n)	24.1 (1612)	38.2 (951)	41.1 (320)	<0.001
Physical/Laboratory values				
SBP (mmHg)	127.81 ± 16.97	123.91 ± 16.81	123.40 ± 17.53	<0.001
DBP (mmHg)	77.96 ± 10.54	77.20 ± 11.10	76.53 ± 10.84	<0.001
TG (mmol/L)	1.49 (1.09-2.09)	1.52 (1.12-2.13)	1.50 (1.14-2.13)	<0.001
LDL-C (mmol/L)	2.53 ± 0.95	2.44 ± 1.02	2.49 ± 1.01	<0.001
HDL-C (mmol/L)	1.09 ± 0.29	1.01 ± 0.28	0.98 ± 0.26	<0.001
Lipoprotein(a) (mg/L)	142.94 (63.58-351.32)	152.81 (70.07-385.57)	201.82 (80.82-453.40)	<0.001
Glucose (mmol/L)	5.93 ± 1.75	6.00 ± 1.93	6.08 ± 1.98	0.028
HbA1C (%)	6.33 ± 1.10	6.41 ± 1.23	6.52 ± 1.26	<0.001
Cr (umol/L)	77.55 ± 22.35	80.98 ± 18.62	83.31 ± 17.53	<0.001
NT-proBNP (pg/ml)	123.90 (41.70-470.92)	352.75 (81.97-649.67)	494.05 (155.47-883.37)	<0.001
Medications at enrolment				
Anti-platelet,%(n)	61.5 (4109)	69.1 (1720)	69.6 (542)	<0.001
ACEI/ARB,%(n)	16.7 (1117)	23.3 (581)	22.2 (173)	<0.001
β-bloker,%(n)	33.1 (2209)	42.1 (1048)	43.4 338)	<0.001
Statins,%(n)	69.8 (4660)	76.9 (1915)	77.4 (603)	<0.001

Data shown are %(n), mean ± SD, or median (IQR). P values are shown for trend. mASCVD, major atherosclerotic cardiovascular disease; BMI, body mass index; CKD, chronic kidney disease; HF, heart failure; PCI, percutaneous coronary intervention; CABG, coronary artery bypass grafting; SBP, systolic blood pressure; DBP, diastolic blood pressure; TG, triglycerides; LDL-C, low-density lipoprotein cholesterol; HDL-C, high-density lipoprotein cholesterol; HbA1C, hemoglobin A1C; Cr, creatinine; NT-proBNP, N-terminal pro-B-type natriuretic peptide; ACEI, angiotensin converting enzyme inhibitors; ARB, angiotensin receptor blocker.

found that the more high-risk conditions, the severer intensity of coronary lesions (**Figure 2**). The specific descriptions were showed in the **Supplementary Material** section.

Clinical Outcomes

Patients with multi-mASCVD events were associated with a higher rate of recurrent events (**Figure 3A**). Those with multi-high-risk conditions showed the similar results (**Figure 3B**). As shown in **Figure 3C**, the estimated survival rate was the lowest in patients with ≥2mASCVD events combined ≥3 or 2 high-risk conditions. The highest survival rate was found in patients with none mASCVD events combined 0-1 or 2 high-risk conditions and those with 1 mASCVD events combined 0-1 high-risk conditions. The survival rates in the other combinations ranged from low to high were patients who had 1 mASCVD events and ≥3 high-risk conditions, ≥2 mASCVD events and 0-1 high-risk conditions, 1 mASCVD events and 2 high-risk conditions, and 0 mASCVD events and ≥3 high-risk conditions.

The different association of a given high-risk condition with outcome at different ASCVD group was found (**Figure 4**). The rates of recurrent events were stepwise among the exposures to the number of mASCVD events and diabetes (3.2% vs. 3.8% vs. 4.3% vs. 6.3% vs. 7.2% vs. 10.4%). Of note, patients with mASCVD alone (mASCVD+/diabetes-) presented a higher event rate compared to those with diabetes alone (mASCVD-/diabetes+). In the multivariable Cox regression analysis, only diabetes presented a significantly independent risk for outcome in either groups of patients with 1- or ≥2 mASCVD events. The predictive values (HRs) were increased with increasing number of mASCVD events (Model 1, 1.15 vs. 1.61 vs. 1.72, Model 2, 1.10 vs. 1.54 vs. 1.71).

DISCUSSION

In this study of 9944 patients with documented ASCVD from a Chinese cohort, our findings were substantially important in two respects. First, in baseline analysis, we found that levels of high-risk conditions were far from ideal although the treatment coverage of secondary preventions gradually increased with increasing number of mASCVD events. Moreover, patients with more mASCVD events or high-risk conditions had severer coronary lesions. Clearly, the biology of ASCVD is complex but a majority of the risk can be explained by known modifiable RFs. While the cut-offs of the optimal values are lowering (16–21). Studies have reported a better benefit from successfully recanalized occlusion in patients with multi-vessel CAD compared to those with single-vessel CAD (22, 23). These findings might emphasize the need to focus patients at VHR on RFs achievement and revascularization.

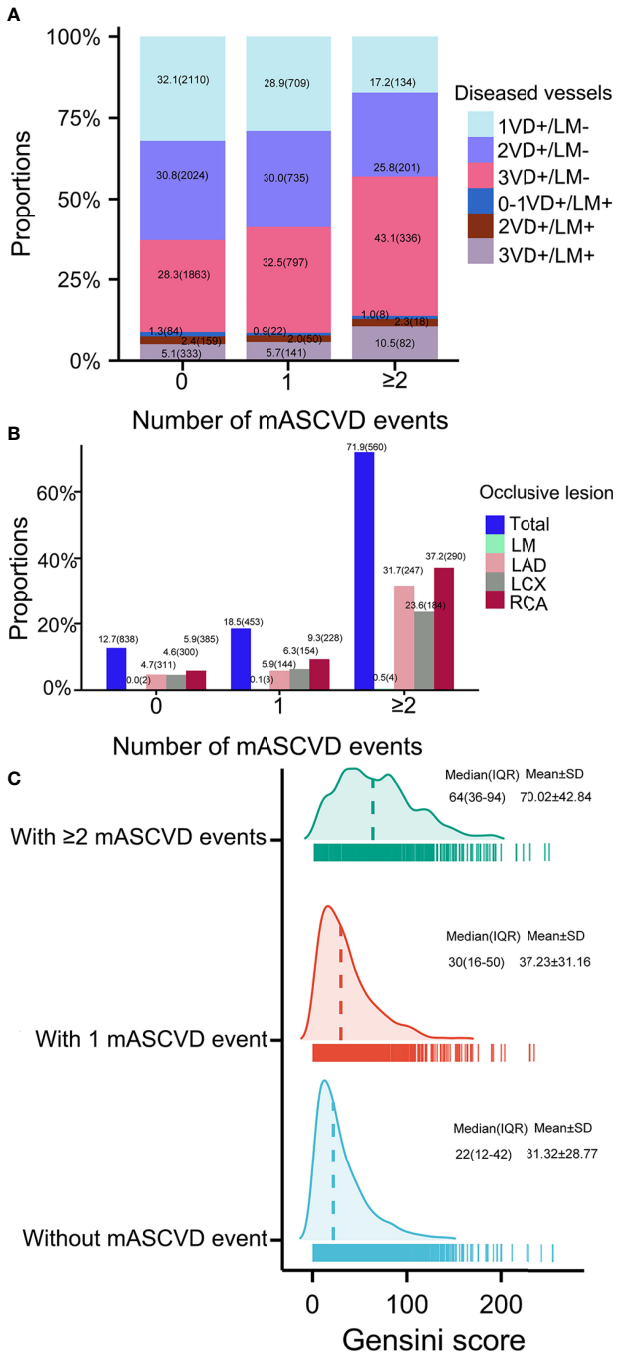

FIGURE 1 | Coronary severity according to number of mASCVD events. Coronary severity was assessed by **(A)** number of diseased arteries, **(B)** occlusive lesion, and **(C)** Gensini score. MASCVD, major atherosclerotic cardiovascular disease; VD, vessel disease; LM, left main; LAD, left anterior descending; LCX, left circumflex; RCA, right coronary artery.

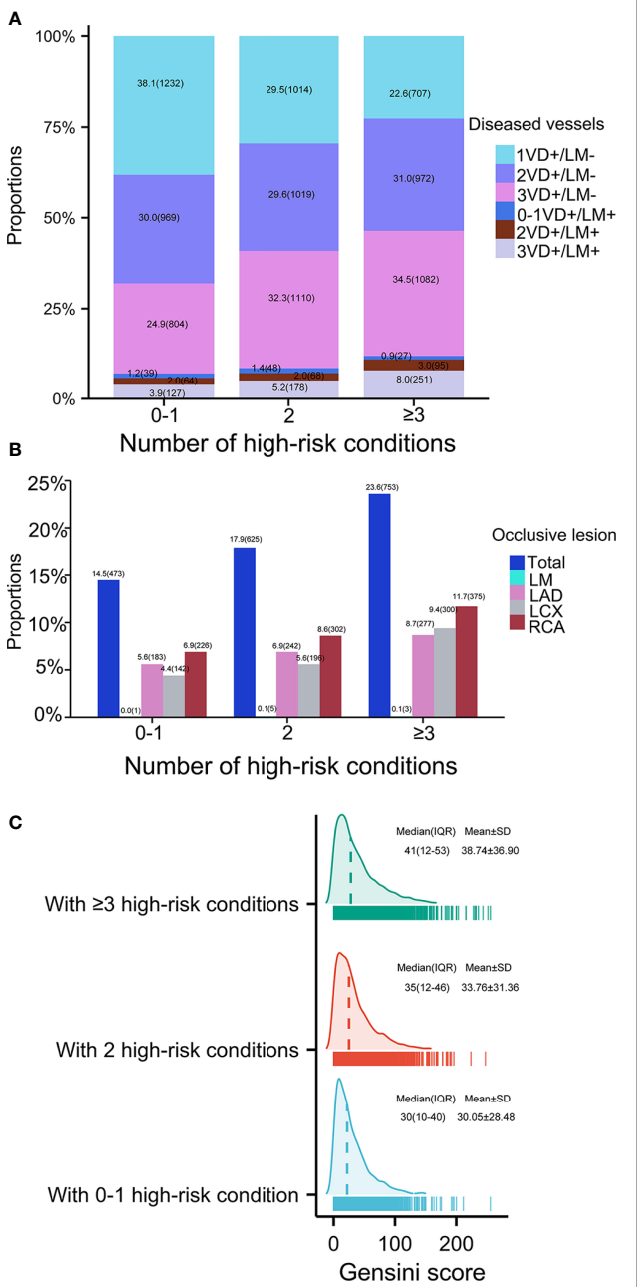

FIGURE 2 | Coronary severity according to number of high-risk conditions. Coronary severity was assessed by **(A)** number of diseased arteries, **(B)** occlusive lesion, and **(C)** Gensini score. VD, vessel disease; LM, left main; LAD, left anterior descending; LCX, left circumflex; RCA, right coronary artery.

Second, during the follow-up period, we found that the more numbers of mASCVD events or high-risk conditions, the lower the survival rates. The current risk stratification might be appropriate for Chinese and further refinement of ASCVD might be necessary to improve the cardiovascular outcome. Furthermore, we found that diabetes was increasingly associated with risk of recurrent events according to the subgroups of ASCVD. Therefore, individuals with diabetes for risk stratification should be recognized as a patient rather than a 'blanket' factor (1).

Current practice guidelines have stratified the subgroup of VHR, a more ominous ASCVD category associated with greater

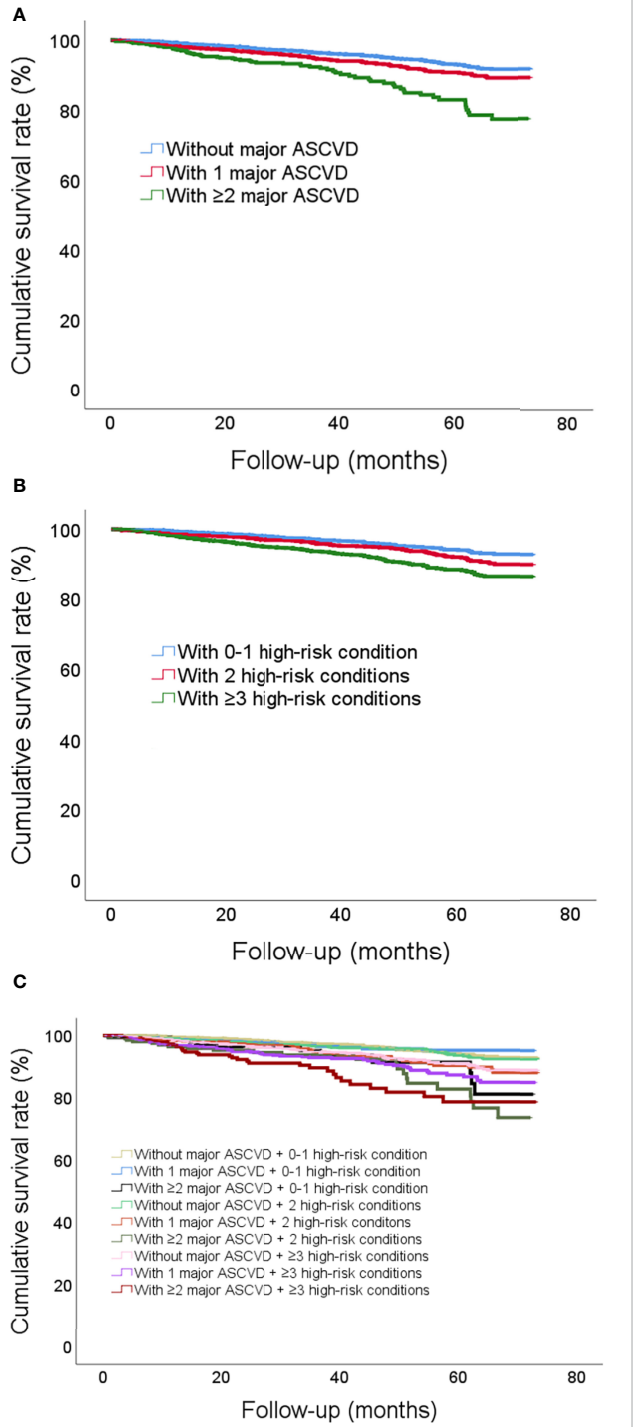

FIGURE 3 | Cumulative incidence curves illustrating the risk of future recurrent events according to **(A)** number of mASCVD events, **(B)** number of high-risk conditions, and **(C)** combinations with number of mASCVD events and high-risk conditions. MASCVD, major atherosclerotic cardiovascular disease.

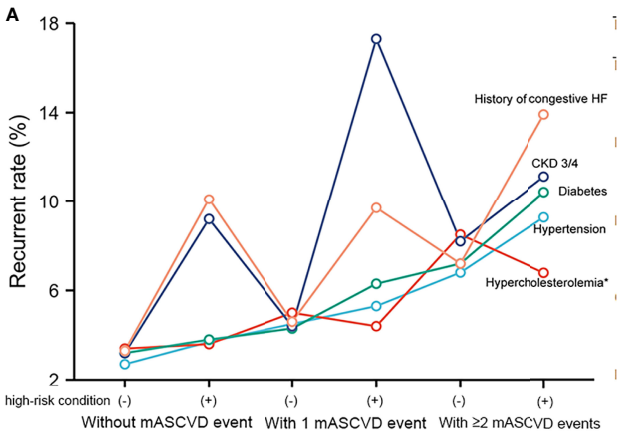

B

Predictors	Events,%(n)		Adjusted HR(95%CI)	
	Without condition	With condition	Model 1	Model 2
Hypertension				
Without mASCVD event	2.7(60)	3.7(161)	1.27(0.94-1.73)	1.23(0.90-1.67)
With 1 mASCVD event	4.5(44)	5.3(78)	1.06(0.72-1.56)	1.00(0.68-1.48)
With ≥2 mASCVD events	6.8(19)	9.3(45)	1.05(0.60-1.85)	1.01(0.57-1.80)
Hypercholesterolemia*				
Without mASCVD event	3.4(208)	3.6(13)	1.14(0.65-2.01)	1.07(0.61-1.88)
With 1 mASCVD event	5.0(115)	4.4(7)	1.19(0.55-2.56)	1.01(0.47-2.21)
With ≥2 mASCVD events	8.5(60)	6.8(4)	1.00(0.35-2.88)	1.10(0.38-3.13)
Diabetes				
Without mASCVD event	3.2(139)	3.8(82)	1.15(0.87-1.52)	1.10(0.83-1.45)
With 1 mASCVD event	4.3(72)	6.3(50)	1.61(1.11-2.33)	1.54(1.06-2.24)
With ≥2 mASCVD events	7.2(35)	10.4(29)	1.72(1.04-2.85)	1.71(1.03-2.84)
CKD3/4				
Without mASCVD event	3.2(201)	9.2(20)	2.84(1.75-4.59)	2.73(1.69-4.43)
With 1 mASCVD event	4.4(105)	17.3(17)	3.26(1.89-5.64)	2.99(1.72-5.23)
With ≥2 mASCVD events	8.2(60)	11.1(4)	1.27(0.44-3.71)	1.17(0.40-3.44)
History of congestive HF				
Without mASCVD event	3.3(214)	10.1(7)	2.84(1.33-6.03)	2.82(1.32-6.01)
With 1 mASCVD event	4.6(105)	9.7(17)	2.27(1.36-3.80)	2.28(1.36-3.81)
With ≥2 mASCVD events	7.2(45)	13.9(19)	1.97(1.14-3.39)	1.97(1.14-3.41)

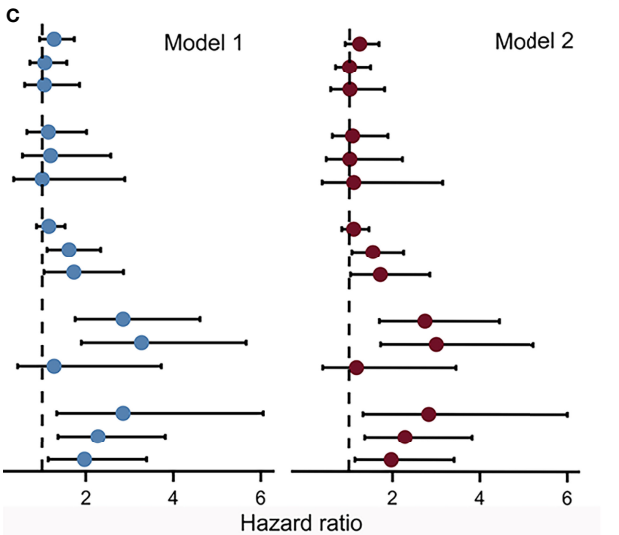

FIGURE 4 | Recurrent event rates **(A, B)** and hazard ratios **(B, C)** for a given high-risk condition among different stages of ASCVD. Model 1 was a given high-risk condition with adjustment for age, gender, BMI, prior PCI/CABG, and current smoking. All covariates including the above covariables and high-risk conditions were added simultaneously to Model 2. MASCVD, major atherosclerotic cardiovascular disease; CKD, chronic kidney disease; HF, heart failure.

morbidity and mortality (9–12). In fact, identifying those patients at VHR is challenging, as the risk assessment by mASCVD events and high-risk conditions is not adequate. The heterogeneity of mASCVD events for recurrent events might exemplify the necessity of reappraisal (24, 25). Moreover, each high-risk condition possessed different weight for ASCVD risk among different populations (26, 27), underscoring the need for native-data to evaluate the suitable risk stratifications.

The current study had several potential limitations. Firstly, the majority of our patients were CAD, the number of individuals suffered from other ASCVD events was relatively small. Moreover, the definition of high-risk conditions might be not completely accurate. For example, the condition of familial hypercholesterolemia was considered according to clinical diagnosis rather than genetic testing in the present study. Finally, the analysis was a single-center nature and the sampling framework of this study might be not nationally representative.

CONCLUSIONS

The current study might replenish the knowledge of current ASCVD refinement and provide data on Chinese patients. Our results demonstrated that within patients with ASCVD, the number of mASCVD events and/or high-risk conditions was significantly associated with worse patterns of coronary severity and outcome. The weight of a given high-risk condition discriminated across numeracy levels of mASCVD events. Importantly, diabetes was significantly and differently associated with increased risk of the worse outcome among patients at various subgroups of ASCVD.

DATA AVAILABILITY STATEMENT

The raw data supporting the conclusions of this article will be made available by the authors, without undue reservation.

ETHICS STATEMENT

The studies involving human participants were reviewed and approved by The hospital's ethical review board (Fu Wai Hospital & National Center for Cardiovascular Diseases, Beijing, China). The patients/participants provided their written informed consent to participate in this study.

AUTHOR CONTRIBUTIONS

J-JL have full access to all of the data in the study. SL and J-JL take responsibility for the integrity of the data and the data analysis. Concept and design: J-JL, SL. Acquisition, analysis, or interpretation of data: SL, H-HL. Statistical analysis: SL, R-XX. Patient recruitment: Y-LG, C-GZ, N-QW, QD, JQ, K-FD, J-JL. Drafting the manuscript: SL, J-JL. All authors contributed to the article and approved the submitted version.

FUNDING

This work was supported by the Capital Health Development Fund [grant number 201614035] and CAMS Major Collaborative Innovation Project [grant number 2016-I2M-1-011] awarded to Dr. Jian-Jun Li, MD, PhD. The study sponsors did not participate in the study design; the collection, analysis, or interpretation of data; the writing of the report; or the decision to submit the paper for publication.

ACKNOWLEDGMENTS

The authors thank all the staff and participants of this study for their important contributions.

SUPPLEMENTARY MATERIAL

The Supplementary Material for this article can be found online at: https://www.frontiersin.org/articles/10.3389/fendo.2022.860698/full#supplementary-material

REFERENCES

1. Figtree GA, Broadfoot K, Casadei B, Califf R, Crea F, Drummond GR, et al. A Call to Action for New Global Approaches to Cardiovascular Disease Drug Solutions. *Eur Heart J* (2021) 42:1464–75. doi: 10.1093/eurheartj/ehab068
2. Zhao D, Liu J, Wang M, Zhang X, Zhou M. Epidemiology of Cardiovascular Disease in China: Current Features and Implications. *Nat Rev Cardiol* (2019) 16:203–12. doi: 10.1038/s41569-018-0119-4
3. Khera R, Valero-Elizondo J, Nasir K. Financial Toxicity in Atherosclerotic Cardiovascular Sisease in the United States: Current State and Future Directions. *J Am Heart Assoc* (2020) 9:e017793. doi: 10.1161/JAHA.120.017793
4. Vernon ST, Coffey S, Bhindi R, Soo Hoo SY, Nelson GI, Ward MR, et al. Increasing Proportion of ST Elevation Myocardial Infarction Patients With Coronary Atherosclerosis Poorly Explained by Standard Modifiable Risk Factors. *Eur J Prev Cardiol* (2017) 24:1824–30. doi: 10.1177/2047487317720287
5. Vernon ST, Coffey S, D'Souza M, Chow CK, Kilian J, Hyun K, et al. ST-Segment-Elevation Myocardial Infarction (STEMI) Patients Without Standard Modifiable Cardiovascular Risk Factors-How Common Are They, and What Are Their Outcomes? *J Am Heart Assoc* (2019) 8:e013296. doi: 10.1161/JAHA.119.013296
6. Goff DC Jr, Lloyd-Jones DM, Bennett G, Coady S, D'Agostino RB Sr, Gibbons R, et al. 2013 ACC/AHA Guideline on the Assessment of Cardiovascular Risk. A Report of the American College of Cardiology/American Heart Association Task Force on Practice Guidelines. *J Am Coll Cardiol* (2014) 63:2935–59. doi: 10.1161/01.cir.0000437741.48606.98
7. Catapano AL, Graham I, De Backer G, Wiklund O, Chapman MJ, Drexel H, et al. ESC/EAS Guidelines for the Management of Dyslipidaemias. *Eur Heart J* (2016) 37:2999–3058. doi: 10.1093/eurheartj/ehw272
8. Rosenblit PD. Extreme Atherosclerotic Cardiovascular Disease (ASCVD) Risk Recognition. *Curr Diabetes Rep* (2019) 19:61. doi: 10.1007/s11892-019-1178-6
9. Jellinger PS, Handelsman Y, Rosenblit PD, Bloomgarden ZT, Fonseca VA, Garber AJ, et al. AACE/ACE Guidelines American Association of Clinical Endocrinologists and American College of Endocrinology Guidelines for Management of Dyslipidemia and Prevention of Cardiovascular Disease. *Endocr Pract* (2017) 23:1–87. doi: 10.4158/EP171764.APPGL

10. Grundy SM, Stone NJ, Bailey AL, Beam C, Birtcher KK, Blumenthal RS, et al. 2018 AHA/ACC/AACVPR/AAPA/ABC/ACPM/ADA/AGS/APhA/ASPC/NLA/PCNA Guideline on the Management of Blood Cholesterol: A Report of the American College of Cardiology/American Heart Association Task Force on Clinical Practice Guidelines. *Circ* (2019) 139:e1082–143. doi: 10.1161/CIR.0000000000000698
11. Mach F, Baigent C, Catapano AL, Koskinas KC, Casula M, Badimon L, et al. 2019 ESC/EAS Guidelines for the Management of Dyslipidaemias: Lipid Modification to Reduce Cardiovascular Risk. *Eur Heart J* (2020) 41:111–88. doi: 10.1093/eurheartj
12. Visseren FLJ, Mach F, Smulders YM, Carballo D, Koskinas KC, Bäck M, et al. ESC Guidelines on Cardiovascular Disease Prevention in Clinical Practice. *Eur Heart J* (2021) 42:3227–337. doi: 10.1093/eurheartj
13. Li S, Liu HH, Guo YL, Zhu CG, Wu NQ, Xu RX, et al. Improvement of Evaluation in Chinese Patients With Atherosclerotic Cardiovascular Disease Using the Very-High-Risk Refinement: A Population-Based Study. *Lancet Reg Health West Pac* (2021) 17:100286. doi: 10.1016/j.lanwpc.2021.100286
14. Jin JL, Cao YX, Liu HH, Zhang HW, Guo YL, Wu NQ, et al. Impact of Free Fatty Acids on Prognosis in Coronary Artery Disease Patients Under Different Glucose Metabolism Status. *Cardiovasc Diabetol* (2019) 18:134. doi: 10.1186/s12933-019-0936-8
15. Rampidis GP, Benetos G, Benz DC, Giannopoulos AA, Buechel RR. A Guide for Gensini Score Calculation. *Atherosclerosis* (2019) 287:181–3. doi: 10.1016/j.atherosclerosis.2019.05.012
16. Yusuf S, Hawken S, Ounpuu S, Dans T, Avezum A, Lanas F, et al. Effect of Potentially Modifiable Risk Factors Associated With Myocardial Infarction in 52 Countries (the INTERHEART Study): Case-Control Study. *Lancet* (2004) 364:937–52. doi: 10.1016/S0140-6736(04)17018-9
17. Vasan RS, Sullivan LM, Wilson PW, Sempos CT, Sundström J, Kannel WB, et al. Relative Importance of Borderline and Elevated Levels of Coronary Heart Disease Risk Factors. *Ann Intern Med* (2005) 142:393–402. doi: 10.7326/0003-4819-142-6-200503150-00005
18. Yusuf S, Joseph P, Rangarajan S, Islam S, Mente A, Hystad P, et al. Modifiable Risk Factors, Cardiovascular Disease, and Mortality in 155 722 Individuals From 21 High-Income, Middle-Income, and Low-Income Countries (PURE): A Prospective Cohort Study. *Lancet* (2020) 395:795–808. doi: 10.1016/S0140-6736(19)32008-2
19. Penson PE, Pirro M, Banach M. LDL-C: Lower Is Better for Longer—Even at Low Risk. *BMC Med* (2020) 18:320. doi: 10.1186/s12916-020-01792-7
20. Chatterjee S, Khunti K, Davies MJ. Type 2 Diabetes. *Lancet* (2017) 389:2239–51. doi: 10.1016/S0140-6736(17)30058-2
21. Whelton PK, Carey RM, Aronow WS, Casey DE Jr, Collins KJ, Dennison Himmelfarb C, et al. ACC/AHA/AAPA/ABC//ACPM/AGS/APhA/ASH/ASPC/NMA/PCNA Guideline for the Prevention, Detection, Evaluation, and Management of High Blood Pressure in Adults: A Report of the American College of Cardiology/American Heart Association Task Force on Clinical Practice Guidelines. *J Am Coll Cardiol* (2018) 71:e127–248. doi: 10.1161/HYP.0000000000000076
22. Jones DA, Weerackody R, Rathod K, Behar J, Gallagher S, Knight CJ, et al. Successful Recanalization of Chronic Total Occlusions Is Associated With Improved Long-Term Survival. *JACC Cardiovasc Interv* (2012) 5:380–8. doi: 10.1016/j.jcin.2012.01.012
23. Toma A, Stähli BE, Gick M, Gebhard C, Nührenberg T, Mashayekhi K, et al. Impact of Multi-Vessel Versus Single-Vessel Disease on Outcomes After Percutaneous Coronary Interventions for Chronic Total Occlusions. *Clin Res Cardiol* (2017) 106:428–35. doi: 10.1007/s00392-016-1072-z
24. Crea F, Libby P. Acute Coronary Syndromes: The Way Forward From Mechanisms to Precision Treatment. *Circ* (2017) 136:1155–66. doi: 10.1161/CIRCULATIONAHA.117.029870
25. Kaski JC, Crea F, Gersh BJ, Camici PG. Reappraisal of Ischemic Heart Disease. *Circ* (2018) 138:1463–80. doi: 10.1161/CIRCULATIONAHA.118.031373
26. Morris AA, Ko YA, Hutcheson SH, Quyyumi A. Race/Ethnic and Sex Differences in the Association of Atherosclerotic Cardiovascular Disease Risk and Healthy Lifestyle Behaviors. *J Am Heart Assoc* (2018) 7:e008250. doi: 10.1161/JAHA.117.008250
27. Katsiki N, Banach M, Mikhailidis DP. Is Type 2 Diabetes Mellitus a Coronary Heart Disease Equivalent or Not? Do Not Just Enjoy the Debate and Forget the Patient! *Arch Med Sci* (2019) 15:1357–64. doi: 10.5114/aoms.2019.89449

Conflict of Interest: The authors declare that the research was conducted in the absence of any commercial or financial relationships that could be construed as a potential conflict of interest.

Publisher's Note: All claims expressed in this article are solely those of the authors and do not necessarily represent those of their affiliated organizations, or those of the publisher, the editors and the reviewers. Any product that may be evaluated in this article, or claim that may be made by its manufacturer, is not guaranteed or endorsed by the publisher.

frontiers | Frontiers in Endocrinology

ORIGINAL RESEARCH
published: 29 June 2022
doi: 10.3389/fendo.2022.917838

A Novel Composite Indicator of Predicting Mortality Risk for Heart Failure Patients With Diabetes Admitted to Intensive Care Unit Based on Machine Learning

Boshen Yang[1†], Yuankang Zhu[2†], Xia Lu[1] and Chengxing Shen[1*]*

[1] Department of Cardiology, Shanghai Jiao Tong University Affiliated Sixth People's Hospital, Shanghai, China, [2] Department of Gerontology, Xinhua Hospital affiliated to Shanghai Jiaotong University School of Medicine, Shanghai, China

OPEN ACCESS

Edited by:
Ying Xin,
Jilin University, China

Reviewed by:
Matsumoto Kotaro,
Kurume University, Japan
Nickolas Savarimuthu,
National Institute of Technology, Tiruchirappalli, India

****Correspondence:***
Chengxing Shen
shencx@sjtu.edu.cn
Xia Lu
18851730292@163.com

†These authors have contributed equally to this work and share first authorship

Specialty section:
This article was submitted to Cardiovascular Endocrinology, a section of the journal Frontiers in Endocrinology

Received: *11 April 2022*
Accepted: *11 May 2022*
Published: *29 June 2022*

Citation:
Yang B, Zhu Y, Lu X and Shen C (2022) A Novel Composite Indicator of Predicting Mortality Risk for Heart Failure Patients With Diabetes Admitted to Intensive Care Unit Based on Machine Learning. Front. Endocrinol. 13:917838. doi: 10.3389/fendo.2022.917838

Background: Patients with heart failure (HF) with diabetes may face a poorer prognosis and higher mortality than patients with either disease alone, especially for those in intensive care unit. So far, there is no precise mortality risk prediction indicator for this kind of patient.

Method: Two high-quality critically ill databases, the Medical Information Mart for Intensive Care IV (MIMIC-IV) database and the Telehealth Intensive Care Unit (eICU) Collaborative Research Database (eICU-CRD) Collaborative Research Database, were used for study participants' screening as well as internal and external validation. Nine machine learning models were compared, and the best one was selected to define indicators associated with hospital mortality for patients with HF with diabetes. Existing attributes most related to hospital mortality were identified using a visualization method developed for machine learning, namely, Shapley Additive Explanations (SHAP) method. A new composite indicator ASL was established using logistics regression for patients with HF with diabetes based on major existing indicators. Then, the new index was compared with existing indicators to confirm its discrimination ability and clinical value using the receiver operating characteristic (ROC) curve, decision curve, and calibration curve.

Results: The random forest model outperformed among nine models with the area under the ROC curve (AUC) = 0.92 after hyper-parameter optimization. By using this model, the top 20 attributes associated with hospital mortality in these patients were identified among all the attributes based on SHAP method. Acute Physiology Score (APS) III, Sepsis-related Organ Failure Assessment (SOFA), and Max lactate were selected as major attributes related to mortality risk, and a new composite indicator was developed by combining these three indicators, which was named as ASL. Both in the initial and external cohort, the new indicator, ASL, had greater risk discrimination ability with AUC higher than 0.80 in both low- and high-risk groups compared with existing attributes. The decision curve and

calibration curve indicated that this indicator also had a respectable clinical value compared with APS III and SOFA. In addition, this indicator had a good risk stratification ability when the patients were divided into three risk levels.

Conclusion: A new composite indicator for predicting mortality risk in patients with HF with diabetes admitted to intensive care unit was developed on the basis of attributes identified by the random forest model. Compared with existing attributes such as APS III and SOFA, the new indicator had better discrimination ability and clinical value, which had potential value in reducing the mortality risk of these patients.

Keywords: heart failure, diabetes, machine learning, hospital mortality, indicator

INTRODUCTION

Heart failure (HF) is the end-stage manifestation of cardiovascular disease and the leading cause of death, which affects more than 40 million people worldwide (1–3). With the development of the global population growth and the acceleration of population aging, the absolute number of patients with heart failure has been increasing (4, 5). Meanwhile, the proportion of patients with HF with hypertension, atrial fibrillation, and diabetes increased significantly (6–8). Existing studies have found that diabetes could increase the risk of HF and lead to a poor prognosis for patients with HF, especially for those in intensive care unit (ICU) (4, 6, 9). Mechanistic hypotheses related to hyperglycemia, oxidative stress, or inflammation have been explored (10). Some researchers further found that the increased risk of events associated with diabetes was partially explained by structural and functional abnormalities of heart (11). However, the exact pathophysiological mechanisms have not been fully elucidated, and the specific treatment measures for patients with HF with diabetes still need to be further developed. Some clinically widely used severity score indicators, such as Simplified Acute Physiology Score II (SAPS-II) and Acute Physiology and Chronic Health Evaluation II (APACHE-II), were not specifically evolved for patients with HF (12, 13). Therefore, these indicators did not show any outstanding performance to predict mortality risk for these patients, especially for those high-risk patients with HF with diabetes.

In recent years, artificial intelligence (AI) has increasingly penetrated into the medical field (14). Through appropriate "learning", computers can replace the human brain to deal with a large number of complex tasks. AI is capable of helping process image information, support diagnosis, recognize patterns of disease, and so on, so that clinicians could provide patients with better healthcare (14). Notably, unsupervised learning enables the discovery of latent structures or patient subgroups in specific cohorts, especially in ICU-related tasks (15). Some clinical decision support studies have demonstrated the ability of sophisticated machine learning models in solving certain ICU-related tasks and gained satisfying performance (16–19).

This is the first study that focused on predicting mortality risk for a specific group of high-risk populations, namely, patients with HF with diabetes in ICU. In Medical Information Mart for Intensive Care IV (MIMIC-IV) population, we used clustering algorithm to classify candidates into high-risk or low-risk groups, and then, nine machine learning models were employed to identify the major indicators for all-cause in-hospital mortality in these populations and two subgroups. Taking this as the cornerstone, a new composite indicator, ASL, was established and externally validated in the eICU cohort. Our study showed that ASL had a better performance in forecasting mortality risk in patients with HF with diabetes.

METHOD

Data Sources

This study used two high-quality large public databases. First is the MIMIC-IV database, which consisted of more than 53,000 patients in ICU between 2008 and 2019 at Beth Israel Deaconess Medical Center (20). The database contained the basic demographic information, vital signs, and biochemical indexes of each patient during ICU. Nurses recorded these data every other hour to ensure authenticity and reliability. Users were required to apply for and pass the test to obtain database permissions. Informed consent was not required for this database for all patient information was processed anonymously. Second is the eICU Collaborative Research Database, a multi-center emergency database, which included ICU records of more than 200,000 patients from 208 hospitals across the United States (21).

Study Population and Study Design

This study focused on critically ill patients with HF complicated with diabetes. The inclusion criteria of the study population were as followed: (1) 18 years old or older, (2) had experience in ICU, and (3) diagnosis of HF and diabetes. Those who had no ICU experience or stayed in ICU for less than 24 h were excluded. For patients with multiple admissions or ICU history, only the first ICU experience at the first admission was included. This study was a large multi-center cohort study, and the study flowchart is shown in **Figure 1**.

Data Extraction and Preprocessing

SQL language and International Classification of Diseases and Ninth Revision (ICD-9) codes were used to extract data from the two databases. We enrolled patients admitted to ICU with a

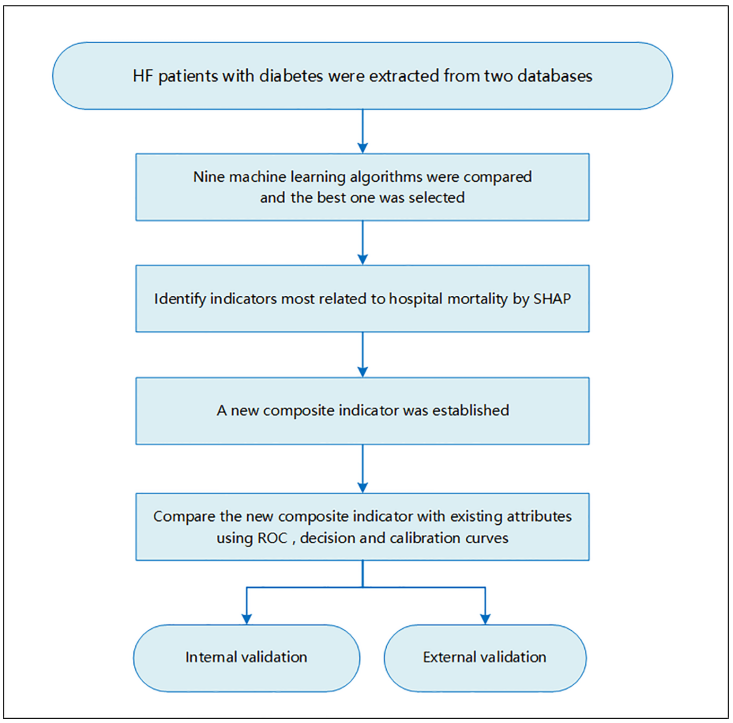

FIGURE 1 | Flowchart of this study.

diagnosis of HF and diabetes on hospital admission. The patient's basic demographic information, such as sex, age, and laboratory indicators like blood glucose, creatinine, and urea, were extracted one by one. Scores related to the severity of the disease, such as Sepsis-related Organ Failure Assessment (SOFA) Score, Systemic Inflammatory Response Syndrome (SIRS) criteria, Acute Physiology Score (APS) III, and some common comorbidities or drugs were also included in the final cohort. Data with missing values of more than 30% were deleted, and other vacant values were filled by multiple interpolation. This process was implemented in Stata (version 14.0). To find out all possible hidden connections, each continuous index was divided into three groups of Min, Max, and Mean. The Max or Min value referred to the maximum or minimum value of all the measured values of the attribute during this ICU stay. Mean represented the average of the maximum and minimum value. The primary outcome was all-cause in-hospital mortality.

Machine Learning Model Comparisons and Identify Risk Indicators

Nine machine learning models were established and validated, including Logistic Regression, Support Vector Classifier (SVC), Decision Tree, Bagging, Gradient Boosting Machine (GBM), K-nearest neighbors (KNN), Random Forest, XGBoost, and LightGBM. A total of 80% of the study population was randomly selected as the training set, and the remaining 20% was used for internal validation. Each model was validated by five times cross-folding, and the average accuracy was obtained. We used areas under the receiver operating characteristic (ROC) curves (AUCs) to evaluate the performance of models as well as the precision and recall rate. The model with the best efficiency was further adjusted by hyper-parameters to optimize its performance. Then, a "perfect" model was established to define risk indicators most related to hospital mortality using SHAP in the three groups: patients with HF with diabetes, high-risk cohort, and low-risk cohort. All the steps were performed using Python.

Shapley Additive Explanations (SHAP) is a visual method to interpret the results of machine learning algorithm. We used SHAP to identify the top 20 indicators associated with in-hospital mortality based on machine learning models. This method assessed the importance of each feature using a game-theoretic approach (22). To obtain the importance of each feature at the overall level, the SHAP values of all features for all samples were drawn, and then, they were sorted in descending order according to the sum of the SHAP values. The color represents the importance of the feature (red represents high, and blue represents low), and each point represents a sample.

In addition, to further obtain the subgroups in the patient population, we used the R package called "ConsensusClusterPlus". On the basis of this, we can further identify risk factors and test predictive effectiveness in more subdivided patient subgroups. This is an unsupervised clustering method based on the quantity of each index. To prevent the redundancy of work, we divided patients into high-risk groups and low-risk groups.

Comparison Between the New Composite Indicator and Existing Attributes

After the new composite indicator was established by linear fitting using logistics regression, we introduced three analyses to compare the performance between the new indicator and existing attributes, including ROC curve, decision curve analysis (DCA), and calibration curve. The AUC curve only measures the diagnostic accuracy of the predictive model and fails to take into account the clinical utility of a specific model, whereas the advantage of DCA is that it integrates the preferences of patients or decision-makers into the analysis. In the calibration curve analysis, by drawing the fitting of the actual probability under different conditions and the probability predicted by the model, the evaluation of the prediction effect of the model on the actual results is judged.

Statistical Analysis

Data were presented in the tables according to different distributions and types of variables. Categorical variables were presented as numbers (percentages) and tested by Chi-square (or Fisher's exact) tests. Continuous variables were presented as mean ± standard deviation or median (25–75 percentiles) and were tested by student's t-test or Wilcoxon rank sum tests. The composite indicator was generated using logistics regression, which was implemented in SPSS (version 23.0). To address the possibility of confounding differences and selection bias, propensity score matching (PSM) was performed using a 1:1 greedy nearest-neighbor algorithm within specified calliper widths. Locally weighted scatter plot smoothing (Lowess) could better deal with this problem by fitting a line in line with the overall trend, so as to better expose the hidden trend.

All statistical analyses in this study were performed using SPSS (version 23.0) or Stata (version 14.0). SHAP and machine learning algorithms were implemented using Python (version 3.9.7). Cluster analysis is implemented using R language (version 4.1.3) (**Supplementary Figure 1**). Lowess and PSM were analyzed with Stata (version 14.0). A P-value lower than 0.05 was set for statistical significance in this study.

RESULTS

Baseline Characteristics and Cluster Analysis

After screening for inclusion and exclusion criteria, a total of 3,210 MIMIC-IV patients were included in the study cohort. As shown in **Supplementary Table 1**, 395 patients died during hospitalization, whereas 2,815 patients survived. After cluster analysis of study participants using R language, all patients were divided into two subgroups, namely, cluster 1 and cluster 2 (**Figure 2A**). Since entering ICU, the survival curves of the two clusters of patients were drawn and the log-rank test was less than 0.001 (**Figure 2B**). The risk of death in the cluster 2 patients was significantly higher than that in the cluster1 group with hazard ratio (HR) = 1.93 (1.59–2.35). Therefore, we defined cluster 1 as the low-risk group and the other one as the high-risk group. As the **Table 1** shown, the patients in high-risk group were older and consisted of more male patients. There was no significant difference in heart rate (HR) and Mean respiratory rate (RR) between these two groups. The difference of value between body temperature and SpO_2 was mild, although there was a statistical difference between the two groups. Notably, overall, the systolic blood pressure, diastolic blood pressure, and mean blood pressure of the high-risk group were significantly lower than that of the low-risk group. In terms of biochemical indicators, the high-risk group had lower glucose, HbA1c, platelet, and bicarbonate, whereas blood urea nitrogen and creatinine were significantly higher than the other group, and urine output was lower, indicating that the high-risk group had a worse renal function. For some indexes, reflecting the degree of heart damage, the CK-MB, Troponin-T, and NT-Pro-BNP of the high-risk group

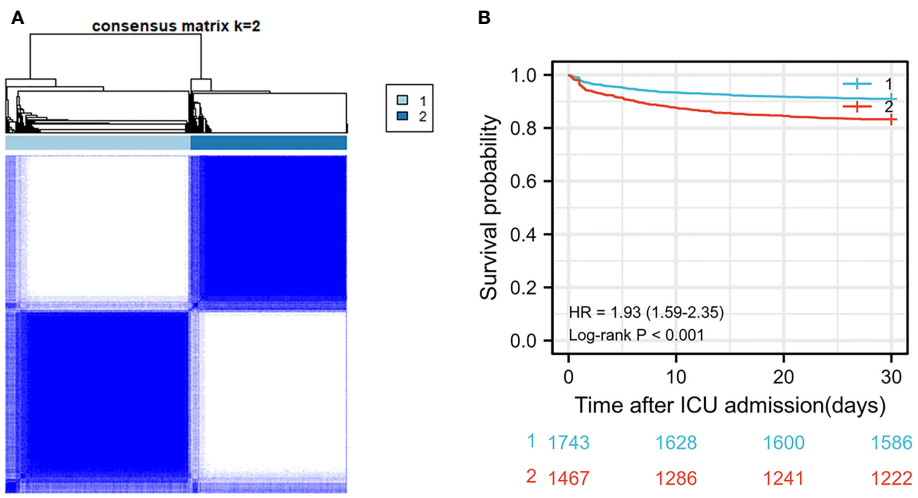

FIGURE 2 | **(A)** Cluster diagram in MIMIC-IV population. **(B)** Survival curve between two clusters of patients in MIMIC-IV population.

TABLE 1 | Baseline characteristics of the low-risk group and high-risk group after cluster analysis in MIMIC-IV cohort.

	Cluster 1 (Low-Risk Group, N = 1,743)	Cluster 2 (High-Risk Group, N = 1,467)	P-Value
Age (years)	72 (63–81)	75 (67–83)	<0.001
Males (n (%))	886 (50.8)	849 (57.9)	<0.001
Min HR (/min)	69 (60–79)	68 (60–78)	0.034
Max HR (/min)	98 (86–112)	96 (84–111)	0.189
Mean HR (/min)	82 (72–92)	81 (71–91)	0.075
Min RR (/min)	13 (11–15)	12 (10–15)	0.002
Max RR (/min)	28 (24–32)	27 (24–31)	0.028
Mean RR (/min)	19 (17–22)	19 (17–21)	0.002
Min Temperature (°C)	36.4 (36.1–36.7)	36.3 (35.9–36.5)	<0.001
Max Temperature (°C)	37.2 (36.9–37.6)	37.1 (36.8–37.4)	<0.001
Mean Temperature (°C)	36.8 (36.6–37.0)	36.7 (36.4–36.9)	<0.001
Min SpO_2 (%)	92 (89–94)	92 (89–95)	0.758
Max SpO_2 (%)	100 (99–100)	100 (100–100)	0.009
Mean SpO_2 (%)	97 (95–98)	97 (96–99)	0.001
Min SBP (mmHg)	91 (82–102)	89 (80–100)	<0.001
Max SBP (mmHg)	148 (132–165)	143 (130–160)	<0.001
Mean SBP (mmHg)	118 (107–131)	114 (104–127)	<0.001
Min DBP (mmHg)	43 (37–50)	41 (35–48)	<0.001
Max DBP (mmHg)	86 (74–100)	81 (70–95)	<0.001
Mean DBP (mmHg)	60 (53–68)	57 (51–64)	<0.001
Min MBP (mmHg)	57 (51–64)	55 (49–62)	<0.001
Max MBP (mmHg)	100 (89–115)	97 (86–110)	<0.001
Mean MBP (mmHg)	75 (69–82)	73 (67–80)	<0.001
Lab events			
Min Glucose (mmol/L)	120 (93–152)	107 (82–140)	<0.001
Max Glucose (mmol/L)	216 (170–285)	200 (158–257)	<0.001
Mean Glucose (mmol/L)	164 (133–210)	148 (124–191)	<0.001
Min WBC (K/μl)	4.3 (3.0–5.9)	4.9 (3.1–6.5)	<0.001
Max WBC (K/μl)	18.5 (13.3–24.9)	17.7 (12.9–23.7)	0.068
Mean WBC (K/μl)	8.3 (6.6–10.7)	8.5 (6.7–11.0)	0.092
Min RBC (m/μl)	2.8 (2.4–3.1)	2.7 (2.4–3.0)	<0.001
Max RBC (m/μl)	4.6 (4.2–5.1)	4.3 (3.9–4.8)	<0.001
Mean RBC (m/μl)	3.5 (3.1–4.0)	3.4 (3.0–3.7)	<0.001
Min Platelet (K/μl)	133 (106–161)	126 (92–157)	0.001
Max Platelet (K/μl)	386 (294–493)	334 (251–440)	<0.001
Mean Platelet (K/μl)	231 (177–295)	203 (151–266)	<0.001
Min Hemoglobin (g/dl)	7.9 (6.8–8.9)	7.8 (6.9–8.7)	0.117
Max Hemoglobin (g/dl)	13.4 (12.6–14.4)	12.8 (11.7–13.7)	<0.001
Mean Hemoglobin (g/dl)	10.3 (9.1–11.3)	9.8 (9.0–10.8)	<0.001
Min anion gap (mEq/L)	9 (7–10)	10 (8–11)	<0.001
Max anion gap (mEq/L)	21 (19–25)	22 (19–26)	0.028
Mean anion gap (mEq/L)	15 (14–17)	16 (14–18)	<0.001
Min bicarbonate (mEq/L)	19 (16–22)	18 (15–21)	<0.001
Max bicarbonate (mEq/L)	34 (31–37)	32 (29–35)	<0.001
Mean bicarbonate (mEq/L)	26 (24–29)	25 (23–28)	<0.001
Min Sodium (mmol/L)	131 (127–134)	131 (127–135)	0.027
Max Sodium (mmol/L)	146 (143–148)	145 (142–148)	<0.001
Mean Sodium (mmol/L)	139 (137–141)	139 (136–141)	0.006
Min Potassium (mmol/L)	3.2 (3.0–3.5)	3.3 (3.0–3.6)	<0.001
Max Potassium (mmol/L)	5.9 (5.2–6.9)	5.7 (5.1–6.6)	<0.001
Mean Potassium (mmol/L)	4.3 (4.0–4.7)	4.4 (4.0–4.8)	<0.001
Min Chloride (mmol/L)	92 (87–96)	93 (88–97)	<0.001
Max Chloride (mmol/L)	110 (107–113)	110 (106–113)	0.258
Mean Chloride (mmol/L)	101 (99–104)	101 (98–104)	0.427
Min Calcium (mmol/L)	7.7 (7.2–8.2)	7.7 (7.2–8.1)	0.219
Max Calcium (mmol/L)	9.9 (9.5–10.3)	9.6 (9.2–10.2)	0.001
Mean Calcium (mmol/L)	9.0 (8.8–9.2)	8.9 (8.7–9.2)	<0.001
Min BUN (mg/dl)	12 (8–16)	16 (11–24)	<0.001
Max BUN (mg/dl)	59 (38–91)	73 (47–104)	<0.001
Mean BUN (mg/dl)	22 (17–32)	32 (22–46)	<0.001
Min Creatinine (mg/dl)	0.8 (0.6–1.0)	1.0 (0.8–1.4)	<0.001
Max Creatinine (mg/dl)	2.2 (1.5–3.6)	2.9 (1.8–5.2)	<0.001
Mean Creatinine (mg/dl)	1.1 (0.9–1.5)	1.5 (1.1–2.2)	<0.001
Min Lactate (mg/dl)	1.0 (0.8–1.2)	1.0 (0.8–1.4)	<0.001
Max Lactate (mg/dl)	3.2 (2.2–4.6)	2.9 (1.8–5.2)	0.153
Mean Lactate (mg/dl)	1.6 (1.2–2.1)	1.5 (1.1–2.1)	0.289
Min ALT (IU/L)	12 (8–17)	13 (9–21)	0.001
Max ALT (IU/L)	48 (28–123)	50 (25–191)	0.033
Mean ALT (IU/L)	22 (16–33)	23 (15–44)	<0.001
Min Bilirubin (mg/dl)	0.3 (0.2–0.4)	0.3 (0.2–0.5)	<0.001
Max Bilirubin (mg/dl)	0.8 (0.5–1.6)	1.0 (0.5–1.8)	0.002
Mean Bilirubin (mg/dl)	0.5 (0.3–0.7)	0.5 (0.3–0.9)	<0.001
Min Albumin (g/dl)	3.0 (2.6–3.5)	3.0 (2.5–3.4)	<0.001
Max Albumin (g/dl)	4.2 (3.8–4.5)	3.9 (3.5–4.3)	<0.001
Min Urine output (ml)	30 (12–62)	20 (5–40)	<0.001
Max Urine output (ml)	460 (300–680)	375 (240–500)	<0.001
Mean Urine output (ml)	200 (100–350)	120 (50–230)	<0.001
Min CK-MB (ng/ml)	2.0 (2.0–4.0)	3.0 (2.5–3.4)	<0.001
Max CK-MB (ng/ml)	7.0 (4.0–19.0)	9.0 (4.0–26.0)	0.010
Min Troponin-T (ng/ml)	0.02 (0.01–0.11)	0.06 (0.02–0.24)	<0.001
Max Troponin-T (ng/ml)	0.28 (0.07–1.19)	0.41 (0.11–1.66)	0.001
Min NT-Pro-BNP (pg/ml)	1,052 (381–2367)	6,817 (4,563–11,696)	<0.001
Max NT-Pro-BNP (pg/ml)	3,972 (1,797–8,848)	13,316 (8,786–23,503)	<0.001
Mean NT-Pro-BNP (pg/ml)	1,625 (607–3123)	9,068 (6,419–14,854)	<0.001
Min HbA1c (%)	6.3 (5.9–6.9)	6.3 (5.9–6.9)	0.187
Max HbA1c (%)	7.6 (6.8–9.3)	7.1 (6.5–8.1)	<0.001
Mean HbA1c (%)	6.9 (6.3–8.0)	6.7 (6.2–7.5)	<0.001
Disease score			
APS III	46 (37–60)	53 (43–68)	<0.001
SOFA	4 (2–7)	6 (4–8)	<0.001
SIRS	2 (2–3)	2 (2–3)	0.162
Comorbidity			
Hypertension (n (%))	1,044 (59.9)	864 (58.9)	0.588
Arrhythmia (n (%))	672 (38.6)	565 (38.5)	1.000
Cardiomyopathy (n (%))	405 (23.2)	350 (23.9)	0.707
Coronary disease (n (%))	1061 (60.9)	877 (59.8)	0.538
MI (n (%))	528 (30.3)	413 (28.2)	0.186
Peripheral vascular disease (n (%))	342 (19.6)	273 (18.6)	0.472
Cerebral disease (n (%))	280 (16.1)	236 (16.1)	1.000
Valvular disease (n (%))	404 (23.2)	301 (20.5)	0.072
COPD (n (%))	252 (14.5)	235 (16.0)	0.236
Respiratory failure (n (%))	430 (24.7)	369 (25.2)	0.774
Pulmonary heart diseases (n (%))	454 (26.0)	338 (23.0)	0.053
AKI (n (%))	1005 (57.7)	819 (55.8)	0.300
CKD (n (%))	922 (52.9)	752 (51.3)	0.357
Hyperlipidemia (n (%))	1163 (66.7)	948 (64.6)	0.218
Hypothyroidism (n (%))	330 (18.9)	280 (19.1)	0.928
Hemopathy (n (%))	467 (26.8)	385 (26.2)	0.748
Drug use			
Insulin (n (%))	549 (31.5)	432 (29.4)	0.218
Loop diuretic (n (%))	1,354 (77.7)	1,154 (78.7)	0.520
β-blocker (n (%))	1,205 (69.1)	1,006 (68.6)	0.760
Digoxin (n (%))	138 (7.9)	132 (9.0)	0.278
Albumin (n (%))	263 (15.1)	211 (14.4)	0.583
Dobutamine (n (%))	66 (3.8)	49 (3.3)	0.507
ACEI/ARB (n (%))	664 (38.1)	516 (35.2)	0.091

(Continued)

TABLE 1 | Continued

	Cluster 1 (Low-Risk Group, N = 1,743)	Cluster 2 (High-Risk Group, N = 1,467)	P-Value
Epinephrine (n (%))	128 (7.3)	86 (5.9)	0.102
Norepinephrine (n (%))	409 (23.5)	323 (22.0)	0.332
CCB (n (%))	291 (16.7)	241 (16.4)	0.849

HR, heart rate; RR, respiratory rate; SBP, systolic blood pressure; DBP, diastolic blood pressure; MBP, mean blood pressure; WBC, white blood cell; RBC, red blood cell; BUN, blood urea nitrogen; ALT, alanine aminotransferase; CK-MB, creatine kinase-MB; NT-Pro-BNP, N-terminal pro-B-type natriuretic peptide; APS, Acute Physiology Score; SOFA, Sepsis-related Organ Failure Assessment; SIRS, Systemic Inflammatory Response Syndrome; MI, myocardial infarction; COPD, chronic obstructive pulmonary disease; AKI, acute kidney injury; CKD, chronic kidney disease; ACEI, angiotensin-converting enzyme inhibitors; ARB, angiotensin receptor blockers; CCB, Calcium channel blocker.

were significantly higher than those in the low-risk group. For sodium, potassium, and other indicators, the two groups were very approximate in value.

Development and Comparison of Machine Learning Models

Nine machine learning models were employed in this study, including Logistic Regression, SVC, Decision Tree, Bagging, GBM, KNN, Random Forest, XGBoost, and LightGBM. These were all commonly used models for solving binary classification problems. Each model was verified by five cross-fold validation, and their AUC and Precision-Recall (P-R) curves were drawn in **Figure 3**. Among them, the random forest algorithm had the finest discrimination ability with precision = 0.511 and AUC = 0.850 (**Table 2**), so we chose it to establish the final model. After hyper-parameter optimization using grid and random hyper-parameter search, the final random forest model reached AUC = 0.92, and the confusion matrix was displayed (**Figure 4**). All demographic information, vital signs, laboratory indicators, complications, and drug medications were included in the final analysis. Whereafter, we respectively analyzed the related factors of the overall population, high-risk group, and low-risk group using the final RM algorithm.

TABLE 2 | Comparisons of nine different machine learning models.

Model	Precision	AUC
Logistics regression	0.473	0.815
SVC	0.462	0.752
Decision tree	0.165	0.576
Bagging	0.498	0.823
GBM	0.451	0.799
KNN	0.164	0.584
Random Forest	0.511	0.850
XGBoost	0.487	0.836
LightGBM	0.457	0.795

Major Indicators Defined by SHAP

To make the output of the model more visual, we introduced SHAP to identify the factors that have the greatest correlation with hospital mortality. As shown in **Figure 5**, for the entire population, a total of 20 factors were identified. Among them, the top five indicators were APS III, SOFA, Min urine output, Max lactate, and age. After that, we analyzed the low-risk group and high-risk

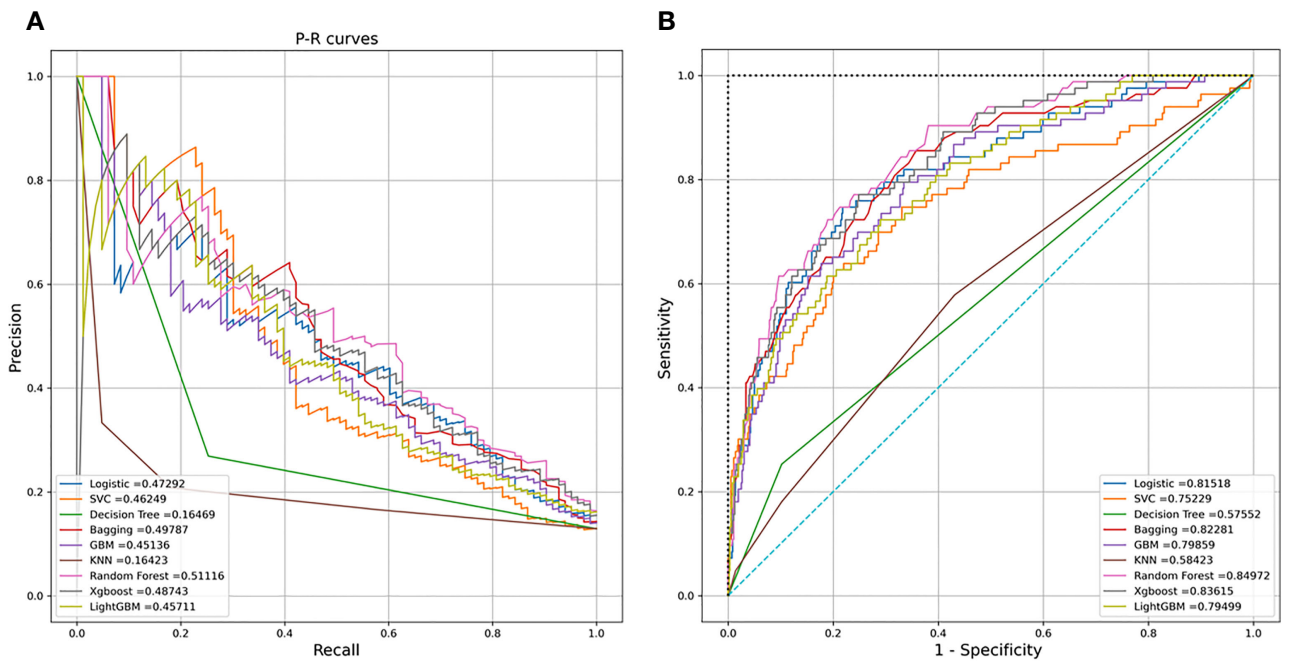

FIGURE 3 | **(A)** Receiver operating characteristic (ROC) curves of the nine models. **(B)** Precision-Recall (P-R) curves of the nine models.

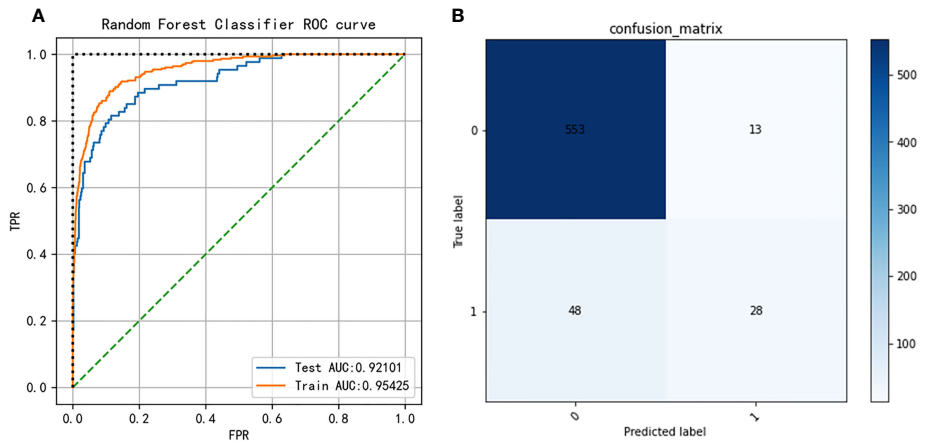

FIGURE 4 | **(A)** Receiver operating characteristic (ROC) curves of the Random Forest model after hyper-parameter optimization. **(B)** Confusion matrix of the Random Forest model after hyper-parameter optimization.

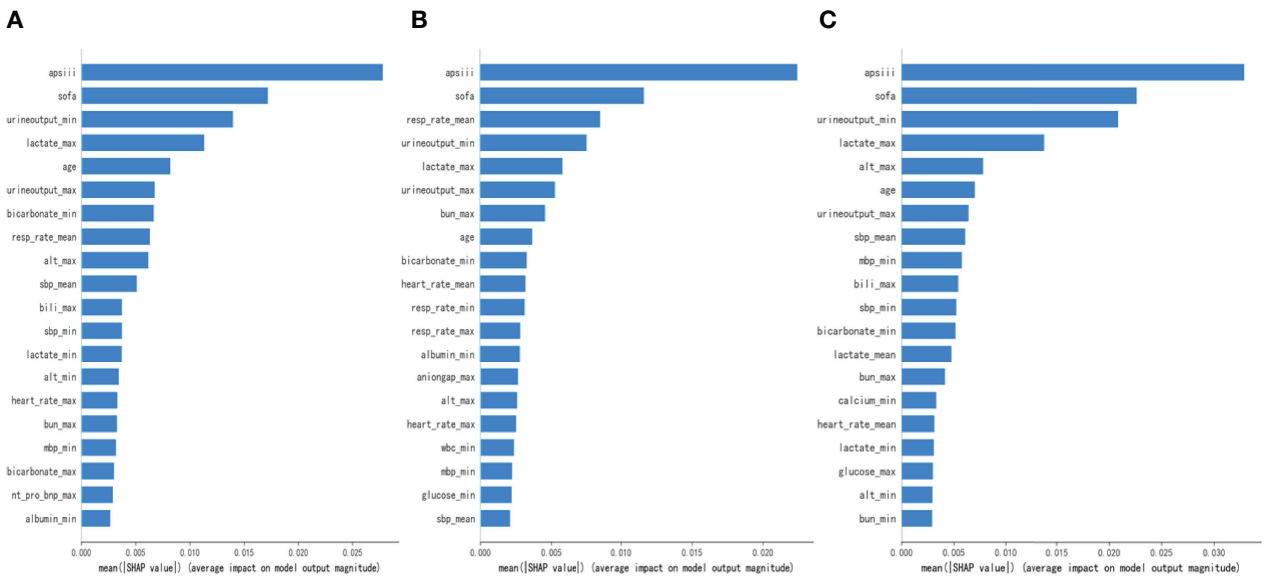

FIGURE 5 | Bar charts that rank the importance of 20 indicators identified by Shapley Additive Explanations (SHAP) values. **(A)** The overall MIMIC-IV population. **(B)** Low-risk group. **(C)** High-risk group.

group, respectively. Among the top five factors in the low-risk group, the only factor that was different from the overall population was Mean RR. Interestingly, in the high-risk group, Mean RR was not significantly associated with hospital mortality but was replaced by Max ALT. From the SHAP plot (**Figure 6**), a rough but imprecise trend could be observed. Among the three groups, patients with higher APS III, SOFA, Max lactate, and lower Min urine output had a greater risk of death. In the low-risk group, the higher Mean RR corresponded to the higher risk of death, whereas in the high-risk group, it was replaced by Max ALT.

Establishment of a New Composite Indicator and Internal Validation

As shown in **Figures 5**, **6**, APS III, SOFA, and Max lactate were common indicators associated with in-hospital mortality in patients with HF with diabetes and two subclusters. On the basis of the three indicators mentioned above, logistics regression was employed to establish a novel composite indicator, which was named ASL. We validated this new indicator in MIMIC-IV cohort and found that, compared with APS III and SOFA, ASL had a more significant enhancement in predicting mortality risk in

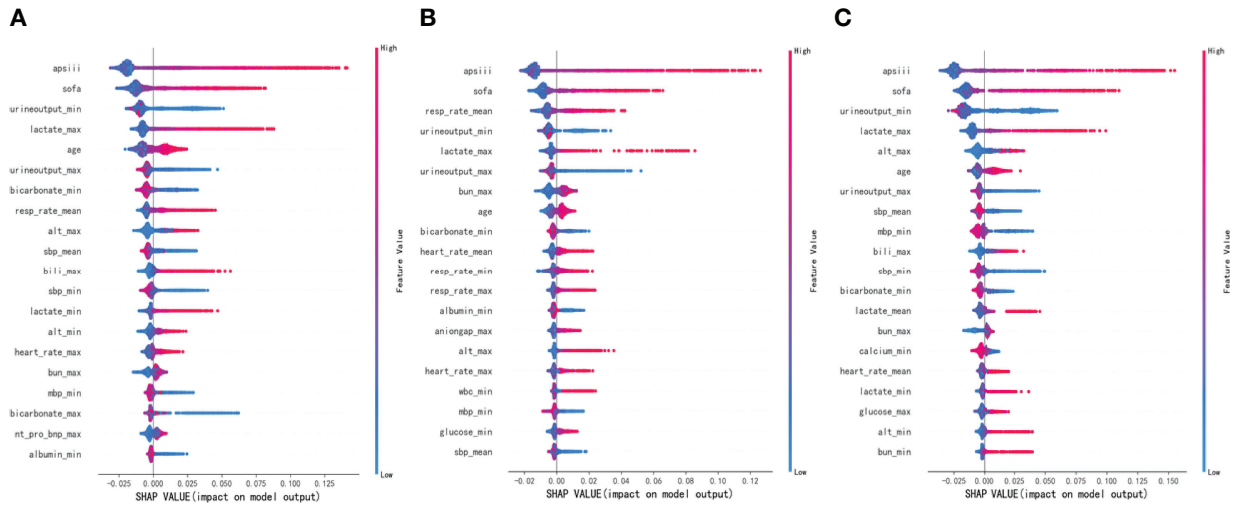

FIGURE 6 | Distribution of the impact each feature had on the full model output using Shapley Additive Explanations (SHAP) values. **(A)** The overall MIMIC-IV population. **(B)** Low-risk group. **(C)** High-risk group.

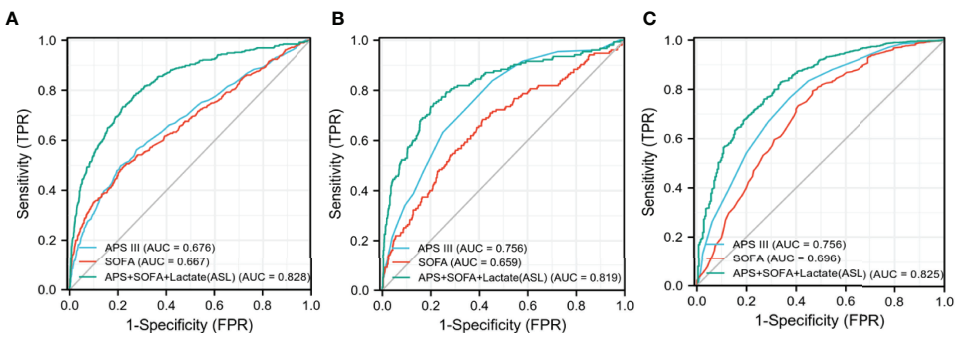

FIGURE 7 | Receiver operating characteristic (ROC) curves of three different indicators in MIMIC-IV cohort. **(A)** The overall MIMIC-IV population. **(B)** Low-risk group. **(C)** High-risk group.

patients with HF with diabetes with AUC = 0.828 (**Figure 7**), independent of high-risk or low-risk group.

External Validation in the eICU Cohort

To further confirm the predictive ability of ASL, we extracted patients with HF with diabetes from a multi-center database for external validation, namely, the eICU database.

A total of 3,862 patients were included in the eICU cohort. As shown in **Table 3**, non-survivors were older and had higher lactate, SOFA, and APS III. Compared with APS III and SOFA, ROC curve showed that ASL had a favorable performance in this external validation cohort, and the DCA curve, along with calibration curve, indicated that this indicator also had respectable clinical value (**Figures 8A–C**). Taken together, this novel predictive indicator had acceptable sensitivity and specificity either in the derivation and validating cohort with a promising clinical value.

Association Between ASL and Hospital Mortality Using Lowess

To further discover the exact relationship between major indicators and hospital mortality, we used the Lowess curve to analyze the overall population. For the general population, the relationship between APS III, SOFA, Max Lactate, and hospital mortality was approximately linear as a whole (**Supplementary Figure 2**). After using logistics regression to generate ASL, it is not surprising that there was also a linear positive correlation between ASL and mortality in MIMIC-IV cohort and eICU cohort (**Figures 8D, E**). Then, we divided the patients into low-risk, middle-risk, and high-risk groups according to ASL and found that there were significant differences of mortality among the three groups both in MIMIC-IV cohort and eICU cohort, which showed that this indicator had great risk stratification ability (**Table 4**). To further confirm the relationship between drug medication and prognosis, patients were divided into

TABLE 3 | Baseline characteristics of the survivors and non-survivors in eICU cohort.

	All patients(N = 3,862)	Survivors(N = 3,315)	Non-survivors(N = 501)	P-value
Age (years)	70 (61–77)	70 (60–77)	71 (65–79)	<0.001
Males (n (%))	2090 (54.12)	1,790 (85.65)	300 (14.35)	0.712
Min Lactate (mmol/L)	1.62 (1.00–2.29)	1.60 (1.00–2.20)	1.70 (1.10–2.54)	<0.001
Max Lactate (mmol/L)	2.84 (1.50–4.16)	2.80 (1.50–4.00)	3.20 (1.80–5.30)	<0.001
Mean Lactate (mmol/L)	2.12 (1.30–3.00)	2.10 (1.25–2.90)	2.37 (1.50–3.65)	<0.001
SOFA	4 (2–6)	3 (2–6)	6 (3–9)	<0.001
APS III	46 (34–61)	44 (33–58)	60 (44–82)	<0.001

APS, Acute Physiology Score; SOFA, Sepsis-related Organ Failure Assessment.

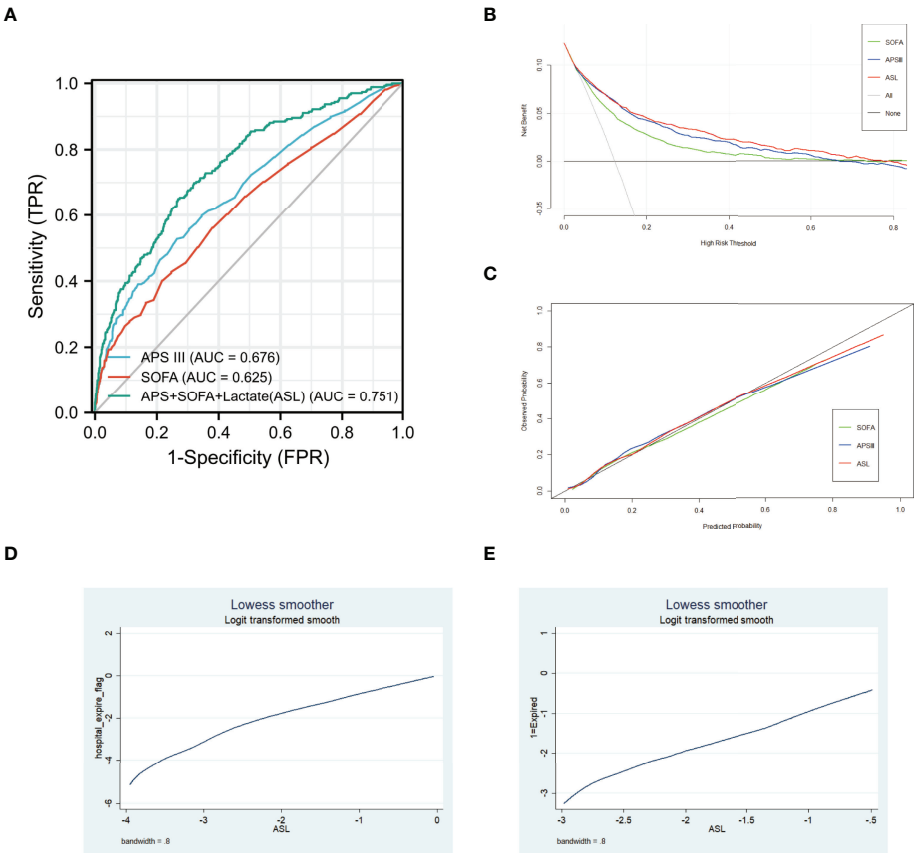

FIGURE 8 | **(A)** Receiver operating characteristic (ROC) curves of three different indicators in eICU cohort. **(B)** DCA curves of three different indicators in eICU cohort. **(C)** Calibration curves of three different indicators in eICU cohort. **(D)** Association between ASL and hospital mortality in MIMIC-IV cohort using Lowess. **(E)** Association between ASL and hospital mortality in eICU cohort using Lowess.

medication group and non-medication group according to 1:1 matching. All 20 related factors were corrected by PSM. As displayed in **Supplementary Tables 2**, **3**, the use of diuretics and insulin had no significant effect on hospital mortality.

DISCUSSION

In this study, we developed a novel composite indicator for predicting hospital mortality for patients with HF with diabetes. The AUCs of ROC curves demonstrated that, compared with SOFA and APS III, ASL had greater risk discrimination ability in these patients, independent of high-risk or low-risk groups. DCA and calibration curve further ensured the effectiveness and security of this indicator. Compared with existing attributes, this study proved that this novel composite indicator had a distinctive mortality risk prediction ability for this specific population and provided potential guiding values for clinical healthcare in ICU.

With the development of AI, machine learning has been more and more applied in the field of cardiovascular medicine, especially for patients with HF. Current HF diagnosis and

TABLE 4 | Risk stratification using ASL in MIMIC-IV and eICU cohort.

Risk Stratification	Total Patients	Non-Survivors	Hospital Mortality
MIMIC-IV cohort			
Low risk	1,748	61	3.5%
Middle risk	920	142	15.4%
High risk	218	83	38.1%
eICU cohort			
Low risk	1,644	123	7.5%
Middle risk	1,349	181	13.4%
High risk	486	130	26.7%

management rely on physical examination, both laboratory and imaging data of patients (23). The advantage of machine learning is that it can learn from vast amounts of existing data and output the most valuable results. For example, machine learning has been applied to the diagnosis of HF, the prediction of mortality, and readmission rate and achieved good performance (24–30). Previous studies have also confirmed that the random forest model had outstanding ability to identify risk factors in patients with HF, and the left ventricular ejection fraction was successfully identified as the most relevant feature in predicting the mortality risk of patients (31). In our study, the random forest model stood out among the nine algorithms, which proved that it had the best prediction ability for this specific population. Our study is the first to apply machine learning algorithms to patients with HF with diabetes in the environment of ICU. Even with the development of medical treatment, the mortality rate in ICU remained at a high level with 11.3% in 1996 and 12.0% in 2010 (32). Therefore, predicting the mortality risk of critically ill patients could provide useful guidance for clinical healthcare.

Cardiovascular disease caused 18 million deaths worldwide each year, and the coexistence of diabetes made cardiovascular mortality risk higher (33, 34). Meanwhile, diabetes, especially type 2 diabetes, affected more than 400 million people worldwide (35). Its pathophysiological mechanism has been widely studied, and it has been proved that it is closely related to microvascular and macrovascular complications, especially for the development of HF (36, 37). Therefore, the number of patients with these two common diseases had been already quite widespread and the risk of death might be greatly increased in patients with HF with diabetes. However, there is no risk assessment tool for this type of patient, especially for critical ill patients. Currently, there are many ICU scoring systems, whereas the predictive effect of these scoring systems on the mortality risk varies among different populations, including Acute Physiology and Chronic Health Evaluation (APACHE) (II, III, and IV), SIRS criteria, and SOFA score (38, 39). In terms of their purposes of creation and previous related studies, although they can estimate patients' conditions quickly within 10 min so that doctors can acquire clinical dynamics of disease changes and give feedback strategies, due to the heterogeneity of the patient population, the performance of the existing scoring system in common use had inevitably volatility (40–43), for example, the SIRS may lack sufficient sensitivity and specificity to identify and risk-stratify patients in some cases. To ensure the monitoring ability of common use scoring systems for HF with diabetes patients, our study selected the APS III, SOFA, and SIRS, which were commonly used in ICU in America. We found that APS III and SOFA performed best in both high-risk and low-risk groups, whereas SIRS performed poorly. APS III was designed to predict the in-hospital mortality of ICU patients; focused on the lowest score of several vital signs, laboratory examinations, and nervous system in the first 24 h; and has been widely used to predict the clinical outcome of mixed critically ill patients now (44, 45). SOFA could describe the dysfunction or failure of one or more organs and evaluate the degree from mild dysfunction to severe failure, from repeated measures of the occurrence and progression of dysfunction in one or all organs. The items in SOFA are continuous variables that are objective, accessible, and reliable to avoid confusion and bias from the source of patients, entities, and demographics (46). Therefore, these two scoring systems complement each other in ASL and fully demonstrate their ability for real-time assessment and long-term dynamic monitoring in the time dimension. Moreover, it not only includes intuitive results such as vital signs and laboratory tests but also objectively collects the changes of various tissues and organs, so as to pay more attention to the overall changes in the spatial dimension (47). Although both urine output and lactate were identified to be highly correlated with hospital mortality based on random forest model, only lactate was selected in the composite indicator for urine output was already included in the APS III score, whereas lactate was not. Lactate, an end-stage product of anaerobic cell metabolism, always occurs during hypoxic conditions and has been reported to be associated with multiple organ dysfunction, poor prognosis, and higher in-hospital mortality. The metabolism of glucose in sensitive tissues is severely altered in diabetes patients or patients with HF who are in a state of oxygen imbalance and depletion, including defective glycogen synthesis and impaired glucose oxidative metabolism, following multiple tissues and organs that act negatively in processing the elevated lactate concentration so that the production of lactic acid increased with the increase of non-oxidized glycolysis in blood (48, 49). Because of the exquisite recognition ability of the machine learning model, the final composite indicator performed better than the existing scoring system in predicting mortality risk in patients with HF with diabetes.

At present, there is no in-depth study on the specific treatment measures for this kind of patient. As displayed in **Supplementary Tables 2**, **3**, we found that diuretics and insulin did not significantly improve the prognosis of these patients after PSM, which indicated that these patients might have unelucidated pathophysiological mechanisms and required more specific treatment. Sodium-glucose co-transporter 2 inhibitors (SGLT2is), which are initially introduced as oral anti-diabetic drugs to reduce blood glucose by inhibition of sodium-glucose cotransporters in kidney, are now known to reduce the combined risk of cardiovascular death in patients with HF with or without diabetes (50, 51). By combining with ASL indicator, we could identify high-risk patients and improve their clinical treatment strategies, such as replacing or adding SGLT2 drugs. The effect of those promising drugs on critical ill patients remained to be further studied in the future.

There were several limitations to this study. First, this was a retrospective study, although we used two databases of multiple centers for internal and external validation respectively, more extensive research studies were still required in the future. Second, there were multiple subtypes of HF and diabetes,

which were not subdivided in this study. Nevertheless, this study was the first to focus on patients with HF with diabetes in a critical care environment and was expected to help improve the prognosis of these patients in the future.

CONCLUSION

In this study, we developed a novel composite indicator for predicting hospital mortality for patients with HF with diabetes admitted to ICU, which was validated in internal and external cohorts. Compared with existing attributes such as APS III and SOFA, the new indicator had better discrimination ability and clinical value, which had potential value in reducing the mortality risk of these patients.

DATA AVAILABILITY STATEMENT

Subject to the databases' license, the raw data supporting the conclusions of this article will be made available by the authors, without undue reservation.

ETHICS STATEMENT

Ethical review and approval was not required for the study on human participants in accordance with the local legislation and institutional requirements. Written informed consent for participation was not required for this study in accordance with the national legislation and the institutional requirements.

AUTHOR CONTRIBUTIONS

BY and YZ conceived the theme and wrote the manuscript. CS and XL improved the manuscript. All authors contributed to the article and approved the submitted version.

FUNDING

CS was supported by the National Natural Science Foundation of China (81871105) and the Shanghai Shenkang Hospital Development Center (SHDC2020CR1042B).

SUPPLEMENTARY MATERIAL

The Supplementary Material for this article can be found online at: https://www.frontiersin.org/articles/10.3389/fendo.2022.917838/full#supplementary-material

Supplementary Figure 1 | Consensus index and Delta area of cluster analysis.

Supplementary Figure 2 | Association between SOFA, APS III, Max Lactate and hospital mortality in MIMIC-IV cohort using Lowess.

REFERENCES

1. Groenewegen A, Rutten FH, Mosterd A, Hoes AW. Epidemiology of Heart Failure. *Eur J Heart Fail* (2020) 22:1342–56. doi: 10.1002/ejhf.1858
2. Jones NR, Roalfe AK, Adoki I, Hobbs FDR, Taylor CJ. Survival of Patients With Chronic Heart Failure in the Community: A Systematic Review and Meta-Analysis. *Eur J Heart Fail* (2019) 21:1306–25. doi: 10.1002/ejhf.1594
3. Baman JR, Ahmad FS. Heart Failure. *JAMA* (2020) 324:1015. doi: 10.1001/jama.2020.13310
4. Gerber Y, Weston SA, Redfield MM, Chamberlain AM, Manemann SM, Jiang R, et al. A Contemporary Appraisal of the Heart Failure Epidemic in Olmsted County, Minnesota, 2000 to 2010. *JAMA Internal Med* (2015) 175(6):996–1004. doi: 10.1001/jamainternmed.2015.0924
5. Pfeffer MA, Shah AM, Borlaug BA. Heart Failure With Preserved Ejection Fraction In Perspective. *Circ Res* (2019) 124:1598–617. doi: 10.1161/CIRCRESAHA.119.313572
6. Lam CSP. Heart Failure in Southeast Asia: Facts and Numbers. *ESC Heart Fail* (2015) 2:46–9. doi: 10.1002/ehf2.12036
7. Tromp J, Ferreira JP, Janwanishstaporn S, Shah M, Greenberg B, Zannad F, et al. Heart Failure Around the World. *Eur J Heart Fail* (2019) 21:1187–96. doi: 10.1002/ejhf.1585
8. Tromp J, Teng T-H, Tay WT, Hung CL, Narasimhan C, Shimizu W, et al. Heart Failure With Preserved Ejection Fraction in Asia. *Eur J Heart Fail* (2019) 21:23–36. doi: 10.1002/ejhf.1227
9. van den Berge JC, Constantinescu AA, Boiten HJ, van Domburg RT, Deckers JW, Akkerhuis KM, et al. Short- and Long-Term Prognosis of Patients With Acute Heart Failure With and Without Diabetes: Changes Over the Last Three Decades. *Diabetes Care* (2018) 41:143–9. doi: 10.2337/dc17-0544
10. Marwick TH, Ritchie R, Shaw JE, Kaye D. Implications of Underlying Mechanisms for the Recognition and Management of Diabetic Cardiomyopathy. *J Am Coll Cardiol* (2018) 71:339–51. doi: 10.1016/j.jacc.2017.11.019
11. Inciardi RM, Claggett B, Gupta DK, Cheng S, Liu J, Echouffo Tcheugui JB, et al. Cardiac Structure and Function and Diabetes-Related Risk of Death or Heart Failure in Older Adults. *J Am Heart Assoc* (2022) 11:e022308. doi: 10.1161/JAHA.121.022308
12. Godinjak A, Iglica A, Rama A, Tančica I, Jusufović S, Ajanović A, et al. Predictive Value of SAPS II and APACHE II Scoring Systems for Patient Outcome in a Medical Intensive Care Unit. *Acta Med Acad* (2016) 45(2):97–103. doi: 10.5644/ama2006-124.165
13. Kądziołka I, Świstek R, Borowska K, Tyszecki P, Serednicki W.. Validation of APACHE II and SAPS II Scales at the Intensive Care Unit Along With Assessment of SOFA Scale at the Admission as an Isolated Risk of Death Predictor. *Anaesthesiol Intensive Ther* (2019) 51:107–11. doi: 10.5114/ait.2019.86275
14. Hamet P, Tremblay J. Artificial Intelligence in Medicine. *Metabol: Clin Exp* (2017) 69S:S36–40. doi: 10.1016/j.metabol.2017.01.011
15. Su L, Zhang Z, Zheng F, Pan P, Hong N, et al. Five Novel Clinical Phenotypes for Critically Ill Patients With Mechanical Ventilation in Intensive Care Units: A Retrospective and Multi Database Study. *Respir Res* (2020) 21:325. doi: 10.1186/s12931-020-01588-6
16. Hanson CW, Marshall BE. Artificial Intelligence Applications in the Intensive Care Unit. *Crit Care Med* (2001) 29:427–35. doi: 10.1097/00003246-200102000-00038
17. Greco M, Caruso PF, Cecconi M. Artificial Intelligence in the Intensive Care Unit. *Semin Respir Crit Care Med* (2021) 42:2–9. doi: 10.1055/s-0040-1719037
18. Komorowski M, Celi LA, Badawi O, Gordon AC, Faisal AA. The Artificial Intelligence Clinician Learns Optimal Treatment Strategies for Sepsis in Intensive Care. *Nat Med* (2018) 24:1716–20. doi: 10.1038/s41591-018-0213-5
19. Rueckel J, Kunz WG, Hoppe BF, Patzig M, Notohamiprodjo M, Meinel FG, et al. Artificial Intelligence Algorithm Detecting Lung Infection in Supine Chest Radiographs of Critically Ill Patients With a Diagnostic Accuracy Similar to Board-Certified Radiologists. *Crit Care Med* (2020) 48:e574–e83. doi: 10.1097/CCM.0000000000004397
20. Johnson A, Bulgarelli L, Pollard T, Horng S, Celi LA, Mark R. MIMIC-IV (Version 1.0). *PhysioNet* (2021). doi: 10.13026/s6n6-xd98
21. Pollard TJ, Johnson AEW, Raffa JD, Celi LA, Mark RG, Badawi O, et al. The eICU Collaborative Research Database, a Freely Available Multi-Center

Database for Critical Care Research. *Sci Data* (2018) 5:180178. doi: 10.1038/sdata.2018.178
22. Lundberg SM, Erion G, Chen H, De Grave A, Prutkin JM, Nair B, et al. From Local Explanations to Global Understanding With Explainable AI for Trees. *Nat Mach Intell* (2020) 2:56–67. doi: 10.1038/s42256-019-0138-9
23. Ponikowski P, Voors AA, Anker SD, Bueno H, Cleland JG, Coats AJ, et al. [2016 ESC Guidelines for the Diagnosis and Treatment of Acute and Chronic Heart Failure]. *Kardiol Polska* (2016) 74:1037–147. doi: 10.5603/KP.2016.0141
24. Tabassian M, Sunderji I, Erdei T, Sanchez-Martinez S, Degiovanni A, Marino P, et al. Diagnosis of Heart Failure With Preserved Ejection Fraction: Machine Learning of Spatiotemporal Variations in Left Ventricular Deformation. *J Am Soc Echocardiogr: Off Publ Am Soc Echocardiogr* (2018) 31(12):1272–84.e9. doi: 10.1016/j.echo.2018.07.013
25. Sanchez-Martinez S, Duchateau N, Erdei T, Kunszt G, Aakhus S, Degiovanni A, et al. Machine Learning Analysis of Left Ventricular Function to Characterize Heart Failure With Preserved Ejection Fraction. *Circ Cardiovasc Imaging* (2018) 11:e007138. doi: 10.1161/CIRCIMAGING.117.007138
26. Mortazavi BJ, Downing NS, Bucholz EM, Dharmarajan K, Manhapra A, Li SX, et al. Analysis of Machine Learning Techniques for Heart Failure Readmissions. *Circ Cardiovasc Qual Outcomes* (2016) 9:629–40. doi: 10.1161/CIRCOUTCOMES.116.003039
27. Frizzell JD, Liang L, Schulte PJ, Yancy CW, Heidenreich PA, Hernandez AF, et al. Prediction of 30-Day All-Cause Readmissions in Patients Hospitalized for Heart Failure: Comparison of Machine Learning and Other Statistical Approaches. *JAMA Cardiol* (2017) 2:204–9. doi: 10.1001/jamacardio.2016.3956
28. Jing L, Ulloa Cerna AE, Good CW, Sauers NM, Schneider G, Hartzel DN, et al. A Machine Learning Approach to Management of Heart Failure Populations. *JACC Heart Fail* (2020) 8:578–87. doi: 10.1016/j.jchf.2020.01.012
29. Adler ED, Voors AA, Klein L, Macheret F, Braun OO, Urey MA, et al. Improving Risk Prediction in Heart Failure Using Machine Learning. *Eur J Heart Fail* (2020) 22:139–47. doi: 10.1002/ejhf.1628
30. Angraal S, Mortazavi BJ, Gupta A, Khera R, Ahmad T, Desai NR, et al. Machine Learning Prediction of Mortality and Hospitalization in Heart Failure With Preserved Ejection Fraction. *JACC Heart Fail* (2020) 8:12–21. doi: 10.1016/j.jchf.2019.06.013
31. Chicco D, Jurman G. Machine Learning can Predict Survival of Patients With Heart Failure From Serum Creatinine and Ejection Fraction Alone. *BMC Med Informatics Decis Mak* (2020) 20:16. doi: 10.1186/s12911-020-1023-5
32. Sjoding MW, Prescott HC, Wunsch H, Iwashyna TJ, Cooke CR.. Longitudinal Changes in ICU Admissions Among Elderly Patients in the United States. *Crit Care Med* (2016) 44:1353–60. doi: 10.1097/CCM.0000000000001664
33. World Health Organization Cardiovascular Disease Risk Charts: Revised Models to Estimate Risk in 21 Global Regions. *Lancet Global Health* (2019) 7:e1332–e45. doi: 10.1016/S2214-109X(19)30318-3
34. Viswanathan V, Jamthikar AD, Gupta D, Shanu N, Puvvula A, Khanna NN, et al. Low-Cost Preventive Screening Using Carotid Ultrasound in Patients With Diabetes. *Front Biosci (Landmark Edition)* (2020) 25:1132–71. doi: 10.2741/4850
35. Ogurtsova K, da Rocha Fernandes JD, Huang Y, Linnenkamp U, Guariguata L, Cho NH, et al. IDF Diabetes Atlas: Global Estimates for the Prevalence of Diabetes for 2015 and 2040. *Diabetes Res Clin Pract* (2017) 128:40–50. doi: 10.1016/j.diabres.2017.03.024
36. Defronzo RA. Banting Lecture. From the Triumvirate to the Ominous Octet: A New Paradigm for the Treatment of Type 2 Diabetes Mellitus. *Diabetes* (2009) 58:773–95. doi: 10.2337/db09-9028
37. Rosano GM, Vitale C, Seferovic P. Heart Failure in Patients With Diabetes Mellitus. *Cardiac Fail Rev* (2017) 3:52–5. doi: 10.15420/cfr.2016:20:2
38. Salluh JIF, Soares M. ICU Severity of Illness Scores: APACHE, SAPS and MPM. *Curr Opin Crit Care* (2014) 20:557–65. doi: 10.1097/MCC.0000000000000135
39. Le Gall JR, Lemeshow S, Saulnier F. A New Simplified Acute Physiology Score (SAPS II) Based on a European/North American Multicenter Study. *JAMA* (1993) 270:2957–63. doi: 10.1001/jama.270.24.2957
40. Arabi Y, Haddad S, Goraj R, Al-Shimemeri A, Al-Malik S. Assessment of Performance of Four Mortality Prediction Systems in a Saudi Arabian Intensive Care Unit. *Crit Care (London England)* (2002) 6:166–74. doi: 10.1186/cc1477
41. Khwannimit B, Geater A. A Comparison of APACHE II and SAPS II Scoring Systems in Predicting Hospital Mortality in Thai Adult Intensive Care Units. *J Med Assoc Thailand = Chotmaihet Thangphaet* (2007) 90:643–52.
42. Gupta R, Arora VK. Performance Evaluation of APACHE II Score for an Indian Patient With Respiratory Problems. *Indian J Med Res* (2004) 119:273–82.
43. Tempe A, Wadhwa L, Gupta S, Bansal S, Satyanarayana L. Prediction of Mortality and Morbidity by Simplified Acute Physiology Score II in Obstetric Intensive Care Unit Admissions. *Indian J Med Sci* (2007) 61:179–85. doi: 10.4103/0019-5359.31151
44. Zhang Z, Chen K, Chen L. APACHE III Outcome Prediction in Patients Admitted to the Intensive Care Unit With Sepsis Associated Acute Lung Injury. *PLos One* (2015) 10:e0139374. doi: 10.1371/journal.pone.0139374
45. Keegan MT, Gajic O, Afessa B. Comparison of APACHE IV, SAPS 3, and MPM0III and Influence of Resuscitation Status on Model Performance. *Chest* (2012) 142:851–8. doi: 10.1378/chest.11-2164
46. Lambden S, Laterre PF, Levy MM, Francois B. The SOFA Score-Development, Utility and Challenges of Accurate Assessment in Clinical Trials. *Crit Care (London England)* (2019) 23:374. doi: 10.1186/s13054-019-2663-7
47. Raith EP, Udy AA, Bailey M, McGloughlin S, MacIsaac C, Bellomo R, et al. Prognostic Accuracy of the SOFA Score, SIRS Criteria, and qSOFA Score for In-Hospital Mortality Among Adults With Suspected Infection Admitted to the Intensive Care Unit. *JAMA* (2017) 317:290–300. doi: 10.1001/jama.2016.20328
48. Adeva-Andany M, López-Ojén M, Funcasta-Calderón R, Ameneiros-Rodríguez E, Donapetry-García C, Vila-Altesor M, et al. Comprehensive Review on Lactate Metabolism in Human Health. *Mitochondrion* (2014) 17:76–100. doi: 10.1016/j.mito.2014.05.007
49. Del Prato S, Bonadonna RC, Bonora E, Gulli G, Solini A, Shank M, et al. Characterization of Cellular Defects of Insulin Action in Type 2 (non-Insulin-Dependent) Diabetes Mellitus. *J Clin Invest* (1993) 91:484–94. doi: 10.1172/JCI116226
50. Zannad F, Ferreira JP, Pocock SJ, Anker SD, Butler J, Filippatos G, et al. SGLT2 Inhibitors in Patients With Heart Failure With Reduced Ejection Fraction: A Meta-Analysis of the EMPEROR-Reduced and DAPA-HF Trials. *Lancet (London England)* (2020) 396:819–29. doi: 10.1016/S0140-6736(20)31824-9
51. Zelniker TA, Wiviott SD, Raz I, Im K, Goodrich EL, Bonaca MP, et al. SGLT2 Inhibitors for Primary and Secondary Prevention of Cardiovascular and Renal Outcomes in Type 2 Diabetes: A Systematic Review and Meta-Analysis of Cardiovascular Outcome Trials. *Lancet (London England)* (2019) 393:31–9. doi: 10.1016/S0140-6736(18)32590-X

Conflict of Interest: The authors declare that the research was conducted in the absence of any commercial or financial relationships that could be construed as a potential conflict of interest.

frontiers | Frontiers in Endocrinology

ORIGINAL RESEARCH
published: 30 June 2022
doi: 10.3389/fendo.2022.920470

Impact of Metabolic Syndrome and Its Components on Clinical Severity and Long-Term Prognosis in Patients With Premature Myocardial Infarction

Jing Gao[1,2,3†], Yuan Wang[2†], Ya-Nan Yang[4], Xiao-Yuan Wu[2], Yan Cui[2], Zhong-He Zou[2], Zhuang Cui[5] and Yin Liu[2,6*]*

[1] Chest Hospital, Tianjin University, Tianjin, China, [2] Thoracic Clinical College, Tianjin Medical University, Tianjin, China, [3] Cardiovascular Institute, Tianjin Chest Hospital, Tianjin, China, [4] Cancer Department, Daping Hospital, Army Medical University, Chongqing, China, [5] Epidemiology and Biostatistics Institute, School of Public Health, Tianjin Medical University, Tianjin, China, [6] Department of Cardiology, Tianjin Chest Hospital, Tianjin, China

OPEN ACCESS

Edited by:
Ying Xin,
Jilin University, China

Reviewed by:
Muammer Karakayalı,
Kafkas University, Turkey
Chenxi Song,
Chinese Academy of Medical Sciences and Peking Union Medical College, China

***Correspondence:**
Zhuang Cui
cuizhuang@tmu.edu.cn
Yin Liu
liuyin2088@163.com

†These authors share first authorship

Specialty section:
This article was submitted to Cardiovascular Endocrinology, a section of the journal Frontiers in Endocrinology

Received: *14 April 2022*
Accepted: *01 June 2022*
Published: *30 June 2022*

Citation:
Gao J, Wang Y, Yang Y-N, Wu X-Y, Cui Y, Zou Z-H, Cui Z and Liu Y (2022) Impact of Metabolic Syndrome and its Components on Clinical Severity and Long-Term Prognosis in Patients With Premature Myocardial Infarction. Front. Endocrinol. 13:920470. doi: 10.3389/fendo.2022.920470

Background: The effects of metabolic syndrome (MS) on premature myocardial infarction (PMI) are not clear to date. This study aimed to investigate the impact of MS and its components on clinical severity and long-term prognosis in patients with PMI.

Methods: We enrolled 772 patients aged ≤45 years old who were diagnosed with acute myocardial infarction (AMI) at our hospital consecutively between 2015 and 2020. The patients were divided into an MS group and non-MS group. The parameters of clinical severity were compared using regression analysis. Patients were followed for median of 42 months for major adverse cardiovascular events (MACE).

Results: Hyperglycemia was associated with multi-vessel disease [odds ratio*(OR)* =1.700, *95%* confidence interval (*CI*)=1.172-2.464, *P*=0.005] and Syntax score ≥33 (*OR*=2.736, *95% CI*=1.241-6.032, *P*=0.013). Increased MACE were observed in the MS group(17.9% vs 10.3%, *P*=0.004).The Kaplan-Meier curve also showed significant differences (*P*< 0.001). MS was an independent risk factor for MACE. Of each component of MS, BMI ≥28 kg/m^2 (hazard ratio [*HR*]=2.022, *95% CI* =1.213-3.369, *P*=0.007] and hyperglycemia (*HR=2.904, 95% CI=1.847-4.567, P<0.001*) were independent risk factors for MACE.

Conclusions: In patients with PMI, 1) hyperglycemia usually indicates more severe lesions; 2) MS as a whole was an independent risk factor for MACE; 3) BMI ≥28.0 kg/m^2 and hyperglycemia were associated with MACE.

Keywords: metabolic syndrome, premature myocardial infarction, clinical severity, long-term prognosis, MACE

INTRODUCTION

Metabolic syndrome (MS) is classified as a collection of risk factors, including hyperglycemia, atherogenic dyslipidemia, central obesity, hypertension, prothrombotic and proinflammatory states, that increase the risk of coronary artery disease (CAD), cardiovascular disease (CVD) and diabetes mellitus type 2 (1). It is estimated that MS affects about 1/4 of the global population and has become a major threat to public health in contemporary society (2).

With the rapid development of the social economy, the lifestyle of young people has also undergone great changes, including that lack of exercise, irregular eating habits. And also, often staying up late has become a common phenomenon among today's young people. As a result, the population of obesity and hyperglycemia in China is increasing year by year, while both of them are important components of MS. Therefore, the individuals with MS are more likely to be younger (3). MS is highly prevalent in younger adults (<45 years) with acute myocardial infarction(AMI) (4–6). At the same time, the prevalence and mortality of myocardial infarction also follows a younger trend (7–10).This indicates that MS may play an important role in the development of AMI in this population. At present, no unified standard has been established on the age limit of premature myocardial infarction(PMI) at home and abroad, but most of the existing studies on AMI in younger adults have set the age at 45 years (11–13), so this study includes the adult population below the cut-off point of 45 years.

PMI leads to premature incapacity to work, increases public health care costs, and creates a huge social and economic burden. Studies at home and abroad have shown that MS increases the risk of coronary heart disease and death, and is associated with a poor prognosis and occurrence of MACE in patients aged >45 years with AMI (3, 14–17). Moreover, few studies have focused on the impact of MS on the severity of AMI lesions in patients >45 years of age, and the results are also different (14, 18). However, there is a lack of research on the effect of MS on PMI (≤45 years). Therefore, the purpose of this study was to investigate the impact of MS and its components on the severity of coronary artery lesions and long-term prognosis in patients with PMI.

METHODS

Study Design and Participants

Consecutive patients ≤45 years of age who were diagnosed with AMI in Tianjin Chest Hospital from 2015 to 2020 were included. We diagnosed AMI according to the fourth edition of the global definition of myocardial infarction (19): Clinical evidence of acute myocardial injury accompanied by acute myocardial ischemia, that is, cTn is detected to be worthy of increase and or decrease (at least once exceeding the upper limit of 99 percentile),and at least one of the following: 1) symptoms of myocardial ischemia; 2) new ischemic ECG changes; 3) pathological Q waves; 4) imaging evidence that new patterns of myocardial inactivation or new focal wall motion abnormalities are consistent with ischemic pathological changes; and 5) coronary thrombosis found by radiography or autopsy. After excluding patients with severe liver or kidney diseases, malignant tumors and lack of diagnostic data related to MS, 772 patients were finally included.

Ethical Considerations

The study protocol was approved by the Internal Review Board of Tianjin Chest Hospital (No. 2017KY-007-01) and all included patients provided signed informed consent prior to study participation. All procedures performed were in accordance with the ethical standards of the Helsinki Declaration and its later amendments, or comparable ethical standards.

Diagnostic Criteria of MS

MS was defined according to the criteria of the 2005 National Cholesterol Education Program (20). In detail, the definition of MS requires the existence of any 3 of the following 5 criteria: 1) Hypertension: blood pressure ≥130/85 mmHg or consistent hypertensive patients undergoing treatment; 2) Hypertriglyceridemia: fasting plasma triglyceride ≥1.7 mmol/L; 3) Fasting HDL -cholesterol <1.0 mmol/L in men and <1.3 mmol/L in women. 4) Hyperglycemia: fasting blood glucose level ≥6.1 mmol/L or known diabetic patients undergoing treatment; 5) Central obesity: waist circumference >90 cm for men and >80 cm for women. Since the waist circumference of the patient was not measured in this study, we used BMI ≥28.0 kg/m^2 as the diagnostic criterion of obesity as proposed by the working group on obesity in China (WGOC) (21).

Clinical and Biochemical Measurements

The basic data of sex, age, BMI and medical history of all patients were recorded on admission, and the admission conditions of the patients were evaluated, including sitting blood pressure (measured by senior doctors on the non-dominant arm supported by the heart level), Killip class and the type of AMI. The emergency laboratory indexes of admission (hypersensitive troponin T, CK, CK-MB, etc.) were recorded. After fasting overnight for 12 hours, fasting blood glucose (FBG), triglyceride (TG), high density lipoprotein cholesterol (HDL-C), low density lipoprotein cholesterol (LDL-C) and total cholesterol were measured. Coronary angiography and PCI were performed by an independent physician with qualification for coronary artery diagnosis and treatment in Tianjin Chest Hospital and multi-position projection head position was used in coronary angiography. Postoperative antiplatelet therapy with aspirin 100 mg/d and clopidogrel 75 mg/d or ticagrelor 90 mg twice per day was recommended for at least one year. The Syntax score, which is widely used to evaluate the severity of coronary artery disease, as well as to guide risk stratification and revascularization strategies in patients with coronary heart disease (22), was calculated for the present study by two or more physicians with experience performing percutaneous coronary intervention (PCI) who were blinded to the study and the patient's condition. For risk stratification of the severity of the disease based on Syntax scores, patients with scores ≤ 22 were at low risk, scores 23-32 were at moderate risk, and those ≥ 33 were at high risk. According to clinical standards and current echocardiographic guidelines, all patients had at least one echocardiographic examination in the first week after AMI (23).

Follow-Up and Outcomes

The patients were followed after discharge by telephone and/or by interview after the initial appointment by trained nurses or cardiologists blinded to laboratory test results, The average follow-up time was 42 months. The end points were defined as MACE, which was a composite outcome consisting target vessel

revascularization (TVR), re-hospitalization for heart failure (HF), cardiac death, recurrent myocardial infarction and stroke. TVR is defined as ischemic symptoms or event-driven revascularization of any lesion, including PCI and CABG, which is unplanned. Heart failure was diagnosed according to the guidelines from the European Society of Cardiology (24). Cardiac death is mainly caused by sudden cardiac death, congestive heart failure, AMI, severe arrhythmia, stroke or other structural/functional heart diseases. Myocardial infarction was diagnosed comprehensively by symptoms such as chest pain, changes in myocardial enzymes and electrocardiogram results. Stroke was defined as acute cerebral infarction according to imaging results or typical symptoms. All outcomes were adjudicated centrally by two independent cardiologists, and any disagreement was resolved by consensus.

Statistical Analysis

Continuous variables were tested for normality using the Kolmogorov-Smirnov test. The continuous data of normal distribution were expressed as mean ± standard deviation, the comparison between the two groups was performed by independent student t test, the continuous data of skewness distribution was expressed by M (Q1 ~ Q3), and the comparison between the two groups was performed by Mann Whitney U test. The categorical data were expressed as frequency and percentage, and the comparison between the two groups was made by Chi-square test or Fisher exact probability method (when the theoretical frequency< 1 or the number of cases <40). Multivariate logistic regression model was used to analyze the effects of MS and its components on lesion severity. The survival curves of MS patients and non-MS patients were drawn using the Kaplan-Meier method and were compared with the logarithmic rank test. Cox proportional hazards models were adjusted for age, sex, smoking history, family history of coronary heart disease, Killip ≥II, left ventricular ejection fraction (LVEF)< 40%, Syntax score ≥33, multi-vessel disease, PCI, the use of ACEI/ARB and Beta-blocker. The hazard ratios (HR) of MS and its five components were calculated to evaluate their effects on MACE. To evaluate the incremental prognostic value of MS and two of its components (BMI ≥28.0 kg/m^2, hyperglycemia) on MACE, we established model 1 (basic model) to include the above 11 variables. Model 2a includes basic model + BMI ≥28.0 kg/m^2. Model 2b includes variables in the basic model plus hyperglycemia. Model 3 includes the basic model + MS, we compared the AUC difference, calculate NRI,(Net Reclassification) and IDI(Integrated Discrimination Improvement) between ① model 3 and model 2a and ② model 3 and model 2b. Bilateral P <0.05 was established as statistical significance. All statistical analyses were determined using SPSS software version 26.0 (IBM SPSS Statistics, Chicago, IL, USA) and R software (version 4.2.0).

RESULTS

Comparison of Baseline Characteristics

After excluding patients with severe liver or kidney diseases, malignant tumors and lack of diagnostic data related to MS, 772 patients were finally included. As shown in **Table 1**, among the 772 patients included in this study, 417 (54%) met the diagnostic criteria of MS and 355 (46%) were in the non-MS group. Males accounted for the majority of the two groups. Compared with the non-MS group, the MS group had more history of diabetes, hypertension, smoking and chronic kidney disease. In terms of MS and its components, the BMI value of the MS group was higher than that of the non-MS group, and the proportion of BMI ≥ 28.0 kg/m^2, hypertension, hyperglycemia, hypertriglyceridemia and low HDL-C was significantly higher than that of the non-MS group (P< 0.001) (**Supplementary Figure**). In the MS group, the most common MS component was hypertension (90.2%), followed by low HDL-C (89%), hypertriglyceridemia (88.2%), hyperglycemia (65.2%) and BMI ≥28.0 kg/m^2 (24.5%) (**Supplementary Figure**). On admission, systolic and diastolic blood pressure values were higher in the MS group than in the non-MS group. For type of MI, NSTEMI was the most common type in the MS group (32.1% vs 22.5%, P=0.003), while STEMI was more frequent in the non-MS group (77.5% vs 67.9%, P=0.003). Among laboratory indexes, the levels of fasting glucose, hypersensitive C-reactive protein, total cholesterol and triglyceride were higher in the MS group than those in the non-MS group, while the level of HDL-C in the MS group was significantly lower than that in non-MS group.

Coronary Angiography and Treatment

Among the 772 patients, 726 (94%) underwent CAG. In terms of treatment, 112 (14.5%) patients received conservative drug therapy, 11 (1.4%) patients received thrombolytic therapy, and 12 (1.6%) patients underwent CABG; a total of 637 (82.5%) patients received percutaneous coronary intervention (PCI). There was no significant difference in the above treatments between MS group and non-MS group(P>0.05). Among the patients undergoing CAG, single-vessel disease was dominant in the non-MS group (45.5% vs 37.3%, P=0.026), and the proportion of three-vessel disease and multi-vessel disease in the MS group was significantly higher than that in the non-MS group (32.0% vs 24.4%, P=0.024; 62.7% vs 54.5%, P=0.026). No differences were noted in Syntax scores between the two groups (**Table 1**).

Comparison of Logistic Regression Analysis of Clinical Severity Between the Two Groups

Multi-vessel disease and Syntax scores ≥33 were taken as dependent variables, MS and its five components were divided into independent variables for univariate and multivariate Logistic regression analysis (**Figure 1**). The results suggest that hyperglycemia is an independent risk factor for multi-vessel disease in the multivariate regression model (*OR*=1.700, *95% CI*=1.172-2.464, P=0.005) (**Figure 1A**). In the multivariate regression model with Syntax scores ≥33 as dependent variables, hyperglycemia was also an independent risk factor (*OR*=2.736, *95% CI*=1.241-6.032, P=0.013) (**Figure 1B**).

Comparison of Clinical Prognosis Between the Two Groups

Patients were followed for median of 42 months for major adverse cardiovascular events (MACE), a total of 63(8.2%)

TABLE 1 | Demographic and clinical characteristics of patients with premature myocardial infarction.

Variables	non-MS group (n = 355)	MS group (n = 417)	*P*
Age (year)	41 (36-43.3)	41 (38-43)	0.616
Male,n (%)	335 (94.4)	405 (97.1)	0.056
BMI (kg/m^2)	24.8 (23.1-26.2)	25.9 (23.9-27.9)	P<0.001
Medical history			
History of Diabetes, n, (%)	24 (6.8)	138 (33.1)	*P*<0.001
History of Hypertension, n, (%)	112 (31.5)	254 (60.9)	*P*<0.001
Previous angina pectoris, n, (%)	75 (21.1)	97 (23.3)	0.477
History of MI, n, (%)	14 (3.9)	22 (5.3)	0.382
Family history of CVD,n, (%)	57 (16.1)	60 (14.4)	0.52
History of smoking,n, (%)	265 (74.4)	339 (81.3)	0.026
History of drinking,n, (%)	155 (43.7)	167 (40)	0.31
Renal insufficiency,n, (%)	1 (0.3)	9 (2.2)	0.022
Previous PCI,n, (%)	11 (3.1)	12 (2.9)	0.857
Previous CABG,n, (%)	1 (0.1)	2 (0.3)	1
Cerebrovascular disease,n, (%)	11 (3.1)	13 (3.1)	0.988
Admission			
Systolic blood pressure (mmHg)	120 (110-145)	133 (125-151.5)	*P*<0.001
Diastolic blood pressure (mmHg)	75 (69.8-87.8)	85.5 (70-94.3)	*P*<0.001
Killip class			0.627
I	343 (96.6)	407 (97.6)	
II	9 (2.5)	6 (1.4)	
III	2 (0.6)	3 (0.7)	
IV	1 (0.3)	1 (0.2)	
Killip ≥II, n, (%)	12 (3.4)	10 (2.4)	0.414
Type of MI			
STEMI, n, (%)	275 (77.5)	283 (67.9)	0.003
NSTEMI, n, (%)	80 (22.5)	134 (32.1)	0.003
Laboratory			
LVEF<40%, n, (%)	22 (6.2)	22 (5.3)	0.594
LVEF (%)	53 (48-58)	53 (47-58)	0.47
Fasting blood glucose (mmol/L)	5.1 (4.6-5.6)	6.7 (5.3-8.4)	*P*<0.001
CK (U/L)	1728 (725.3-3064.8)	1599.5 (630.3-3020)	0.126
CK MB (U/L)	159.5 (47.3-258.3)	122 (52.8-229.3)	0.111
Hypersensitive C-reactive protein (mmol/L)	5.3 (2.4-15)	6.3 (3.2-14.6)	0.045
Total cholesterol (mmol/L)	4.8 ± 1.2	5.0 ± 1.2	0.002
Triglyceride (mmol/L)	1.5 (1.2-2.1)	2.5 (2-3.5)	*P*<0.001
HDL-C (mmol/L)	1 (0.9-1.2)	0.9 (0.7-0.9)	*P*<0.001
Hypersensitive troponin T (ug/L)	2.9 (1-5.7)	3.2 (1.1-6.8)	0.206
LDL-C (mmol/L)	3.1 (2.5-3.8)	3.2 (2.6-3.9)	0.215
CAG and treatment			
CAG, n, (%)	332 (93.5)	394 (94.5)	0.573
Conservative treatment, n (%)	51 (14.4)	61 (14.6)	0.918
Thrombolysis, n (%)	6 (1.7)	5 (1.2)	0.566
CABG, n (%)	6 (1.7)	6 (1.4)	0.778
PCI, n (%)	292 (82.3)	345 (82.7)	0.861
Severity of coronary artery lesion, n (%)			
Single vessel disease	151 (45.5)	147 (37.3)	0.026
Two-vessel disease	90 (27.1)	115 (29.2)	0.535

(Continued)

TABLE 1 | Continued

Variables	non-MS group (n = 355)	MS group (n = 417)	*P*
Three-vessel disease	81 (24.4)	126 (32.0)	0.024
Left main	10 (3.0)	6 (1.5)	0.173
multi-vessel disease	181 (54.5)	247 (62.7)	0.026
Syntax score	16 (9-22)	15.5 (10-22.5)	0.526
Syntax ≤ 22	252 (75.9)	289 (73.4)	0.432
Syntax (23-32)	50 (15.1)	60 (15.2)	0.950
Syntax≥33	19 (5.7)	25 (6.3)	0.726
Baseline medication, n, (%)			
DAPT	353 (99.4)	410 (98.3)	0.150
Beta-blocker	281 (79.2)	332 (79.6)	0.874
ACEI/ARB	242 (68.2)	273 (65.5)	0.427
Statin	353 (99.4)	410 (98.3)	0.150
Anticoagulants	341 (96.1)	389 (93.3)	0.091

MS, metabolic syndrome; MI, myocardial infarction; CVD, cardiovascular disease; PCI, percutaneous coronary intervention; CABG, coronary artery bypass graft; STEMI, ST-segment elevation myocardial infarction; NSTEMI, non-ST segment elevation myocardial infarction; CK, creatine kinase; CK-MB, creatine kinase isoenzyme; HDL-C, high density lipoprotein cholesterol; LDL-C, low density lipoprotein cholesterol; CAG, coronary angiography; DAPT, dual antiplatelet; ACEI/ARB, angiotensin-converting enzyme inhibitor/angiotensin receptor blocker.

people were lost to follow-up. We compared the baseline characteristics between patients lost to follow-up (n=63) and all (n=772) patients. The results exhibited that patients' baseline characteristics were not significantly different between the two groups (all P >0.05, **Supplementary Table**). This shows that the people who lost follow-up have no effect on the conclusion of this study. After follow-up, 102 (14.4%) patients had MACE, including 68 (9.6%) cases of TVR, 20 (2.8%) cases of heart failure, 10 (1.4%) cases of cardiac death, 33 (4.7%) cases of recurrent MI, and 7 (1.0%) cases of stroke. A significant difference was found in the occurrence of MACE between the MS and non-MS groups (17.9% vs 10.3%, P=0.004), mainly due to significantly higher TVR and HF in the MS group than in the non-MS group (12.1% vs 6.7%, P=0.014; 4.7% vs 0.6%, P=0.001) (**Table 2**). In addition, AMI patients with prior PCI, prior CABG, LVEF <40%, high fasting blood glucose, high CK, high CK-MB, high hs-CRP, high hs-TNT, multi-vessel disease, or Syntax score ≥33 were positively associated with the occurrence of MACE (all P<0.05, **Supplementary Table**).

A significant difference was found in the KM curve between the two groups (P < 0.001) (**Figure 2A**). Cox regression analysis showed that MS was an independent risk factor for MACE (*HR*=2.082, 95% *CI*=1.324-3.273, P=0.001), mainly due to the increased risk of TVR (*HR*=1.964, 95% *CI*=1.155-3.340, P=0.013)

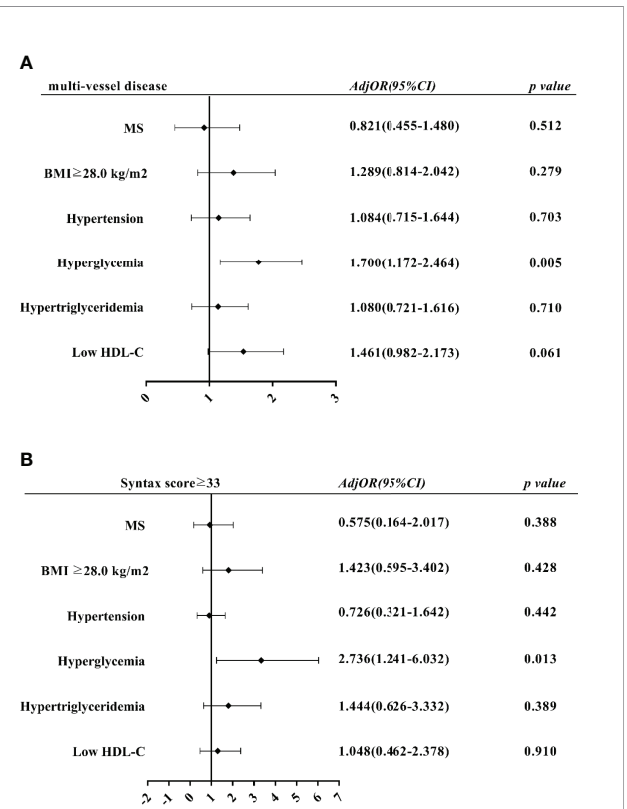

FIGURE 1 | Multivariate logistic regression analysis of impact of MS components on PMI severity. **(A)** Effects of MS and its components on multi-vessel disease. **(B)** Effects of MS and its components on Syntax score ≥33 Adj OR, adjusted odds ratio; CI, confidence interval.

TABLE 2 | Comparison of clinical outcomes between MS group and non-MS group.

Variables	non-MS group (n = 330)	MS group (n = 379)	*P*
MACE, n, (%)	34 (10.3)	68 (17.9)	0.004
TVR, n, (%)	22 (6.7)	46 (12.1)	0.014
HF, n, (%)	2 (0.6)	18 (4.7)	0.001
Cardiac death, n, (%)	4 (1.2)	6 (1.6)	0.676
Recurrent MI, n, (%)	14 (4.2)	19 (5.0)	0.627
Stroke, n, (%)	3 (0.9)	4 (1.1)	1.000

MS, metabolic syndrome; MACE, major adverse cardiovascular events; TVR, target vessel revascularization; HF, re-hospitalization for heart failure; MI, myocardial infarction.

and HF (*HR*=8.301, *95% CI*=1.798 -38.332, *P*=0.007) (**Table 3**). Subsequent COX regression analysis of each component of MS showed that BMI ≥28.0 kg/m^2 (*HR*=2.022, *95% CI*=1.213-3.369, *P* =0.007) and hyperglycemia (*HR*=2.904, *95% CI*=1.847-4.567, *P*<0.001) were independent risk factors for the occurrence of MACE (**Figure 2B**). In addition, LVEF <40% (*HR*=3.920, 95% *CI*=2.113-7.273, *P*<0.001) and Syntax scores ≥33(*HR*=2.315, 95% *CI*=1.237-4.334, *P*=0.009) were also independent risk factor for the occurrence of MACE.

The analysis of the incremental prognostic value of MS and its components on MACE showed the AUC values of model 1, model 2a and 2b were 0.6381, 0.6751 and 0.6847, respectively, and the AUC of model 3 was 0.6665, which indicated that MS, BMI ≥28.0 kg/m^2 and hyperglycemia all increased the predictive value of MACE. Furthermore, the NRI and IDI of AUC between model 3 and model 2a and between model 3 and model 2b were calculated. The NRI of model 3 vs model 2a and model 3 vs model 2b were 0.0411 and 0.0029 respectively, and the IDI of model 3 vs model 2a and model 3 vs model 2b was 0.008, 0.003, respectively. The results show that model 3 has better ability to predict MACE than model 2, that is, MS as a whole can better predict the poor prognosis of people with premature myocardial infarction (**Figure 3**).

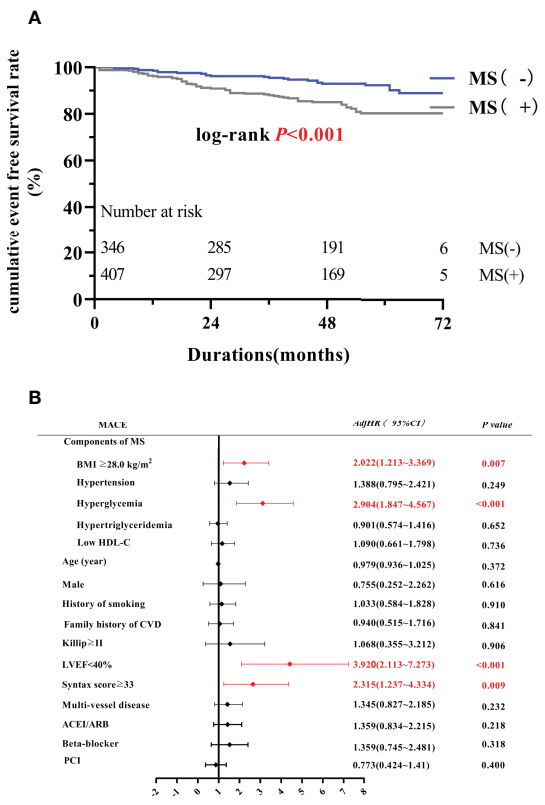

FIGURE 2 | MS and PMI prognosis. **(A)** The Kaplan-Meier curve between MS group and non-MS group. **(B)** Multivariate Cox regression analysis of MACE. MACE, major adverse cardiovascular events; LVEF, left ventricular ejection fraction; ACEI/ARB, angiotensin converting enzyme inhibitor/angiotensin II receptor blocker; AdjHR, adjusted hazard ratio; CI, confidence interval; PCI, percutaneous coronary intervention.

DISCUSSION

Results of the present study highlights that: 1) In the PMI population of the present study, the prevalence rate of MS was 54%, and males accounted for the majority. NSTEMI was dominant in the MS group, while STEMI was higher in the non-MS group; 2) No correlations were found between MS as a whole and the severity of coronary artery lesions, but hyperglycemia in the MS components often predicted more severe coronary heart disease; 3) After median 42 months of follow-up, the incidence of MACE in the MS group was significantly higher than that found in the non-MS group, and MS was an independent risk factor for MACE, especially for the occurrence of TVR and HF. MS components, including BMI ≥28.0 kg/m^2 and hyperglycemia, were independently associated with the occurrence of MACE in these patients.

MS is common in patients with coronary heart disease, especially in patients with AMI (15, 17, 25). Myocardial infarction is now showing a younger trend, affecting adults in middle age and younger (7–10). Studies have been conducted previously on the prevalence and distribution of MS components in people with PMI (4, 26, 27). A case-control study conducted by Kazemi et al. (26)in the AMI population ≤50 years old found that the prevalence of MS in the case group was significantly higher than that in the control group (34.7% vs 16.3%, respectively), and high triglycerides were the most common component. Gadepalli et al (4)estimated that the prevalence rate of MS in AMI patients ≤45 years old was about 62.74%, and the decrease in HDL level was the most common indicator. A meta-analysis of 34 large studies(age range 18–30 years old) suggested that MS was found in 4.8%-7% of younger adults (27). In that study, atherosclerotic dyslipidemia defined by low levels of HDL-C was the most common MS component (26.9%-

TABLE 3 | COX multivariate regression analysis of each adverse event in patients with PMI and MS.

Variables	*HR*	*95%CI*	*P*
MACE	2.082	1.324-3.273	0.001
TVR	1.964	1.155-3.340	0.013
HF	8.301	1.798-38.332	0.007
Cardiac death	2.355	0.351-15.801	0.378
Recurrent MI	1.360	0.645-2.867	0.419
Stroke	1.216	0.162-9.119	0.849

MS, metabolic syndrome; MACE, major adverse cardiovascular events; TVR, target vessel revascularization; HF, re-hospitalization for heart failure; MI, myocardial infarction HR, hazard ratio; CI, confidence interval.

41.2%), followed by elevated blood pressure (16.6%-26.6%), abdominal obesity (6.8%-23.6%), elevated triglycerides (8.6%-15.6%) and elevated fasting blood glucose (2.8%-15.4%). In the present study, MS accounted for 54% of people with PMI, and the most common component was hypertension (90.2%), followed by low HDL-C (89%), hypertriglyceridemia (88.2%), hyperglycemia (65.2%) and BMI ≥28.0 kg/m^2 (24.5%). This results basically consistent with the results of previous studies, that is, MS accounts for about half of the patients with PMI, and dyslipidemia accounts for a large proportion.

MS has been reported to increase the risk of cardiovascular disease. Mottillo et al. (28) conducted a meta-analysis of 87 prospective studies, and the final results showed that MS was associated with an increased risk of cardiovascular disease with an *RR* of 2.35 (*95% CI*=2.02-2.73). Although the exact pathogenesis of MS is not completely clear, current studies suggest that MS increases the risk of cardiovascular disease in the following ways (29–32) (1): Insulin resistance: insulin resistance increases the entry of free fatty acids into the liver and increases the synthesis of triglyceride and very low-density lipoprotein. Compensatory hyperinsulinemia damages vascular endothelium and is conducive to lipid deposition, thus leading to the occurrence and development of atherosclerosis (2); Obesity and chronic inflammation: fat metabolites are released into the blood of obese patients, resulting in the accumulation of lipid metabolites, the penetration and activation of macrophages, and the chronic inflammatory state of the body, decreased adiponectin levels and increased interleukin-6 and plasminogen activator inhibitors, resulting in a state of high inflammation and high thrombosis.

MS not only increases the risk of CVD, especially AMI, but also affects the disease severity and prognosis of AMI patients (>45 years). These studies connect MS with more severe CAD. According to Mornar et al (33), more multi-vessel lesions are found in patients with MS. This observation was also noted in the present PMI population. In addition, Lovic et al. (14) used Syntax scores to assess the severity of coronary heart disease between patients with and without MS, and the results showed that patients with MS had higher Syntax scores. According to several studies, the higher the Syntax score, the worse the prognosis (34–36) (37). The present study expanded these findings and further demonstrated this observation in PMI patients, because in the long run (median 42 months of follow-up), Syntax scores ≥33 was independently associated with the occurrence of MACE. Although no differences were found in Syntax scores between groups, in order to evaluate the severity of lesions between the MS group and non-MS group, we classified the disease into low risk (≤22), moderate risk 23-32 and high risk (≥ 33) according to Syntax scores. As far as we know, this is the first study to apply this classification to delineate risk.

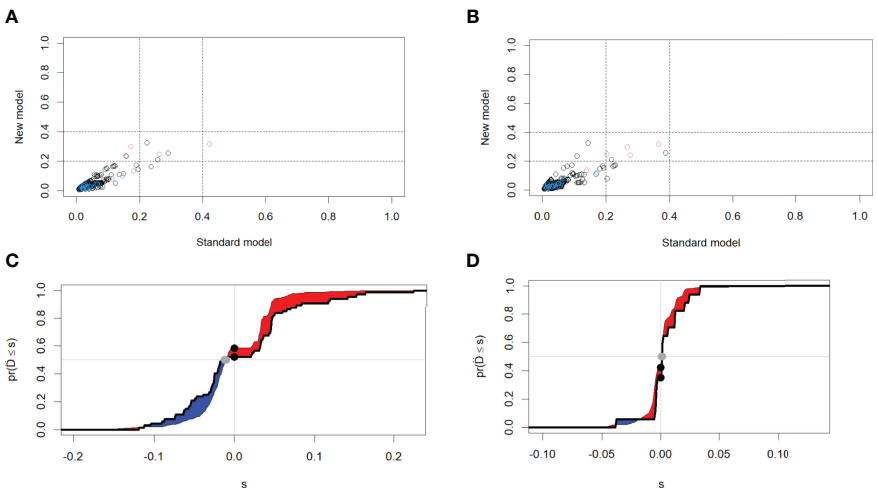

FIGURE 3 | NRI and IDI between ① model 3 and model 2a ② model 3 and model 2b. **(A)**NRI for ① **(B)** NRI for ② **(C)** IDI for① **(D)** IDI for ② NRI, Net Reclassification; IDI, Integrated Discrimination Improvement.

In the setting of ACS, the prognostic value of assessing the presence of MS as a comprehensive diagnosis remains uncertain (38–41). In fact, the various components of MS have different relationships with the outcome, which may affect the observed incremental risk stratification (38, 41, 42). In the present study, we found that MS as a whole can better predict the poor prognosis of people with premature myocardial infarction.

In present study, hyperglycemia in the MS components is an independent risk factor for multi-vessel disease and Syntax ≥33 in PMI patients Nevertheless, inconsistent with some previous studies, multivariate regression analysis adjusted by MS and five components did not find that dyslipidemia was associated with the severity of coronary artery disease. The possible reasons are as follows. Firstly, earlier studies have shown that diabetes is a challenging factor for the effects of MS on the severity of AMI, because it can independently increase the severity of coronary heart disease (43). The definition of hyperglycemia in MS diagnostic criteria also includes people with diabetes. So when MS and its components are included in multivariate adjustment analysis, hyperglycemia has become the main and robust factor affecting coronary artery disease. Secondly, it may be because we include people in the same area, and there is no significant difference in eating habits. However, it is worth noting that hyperglycemia in MS includes not only people with diabetes, but also patients with fasting blood glucose ≥6.1 mmol/L, some of whom may be in a prediabetic state or in a stage of insulin resistance. Levantesi et al. (44) pointed out that MS is a powerful predictor of delayed diabetes after myocardial infarction. Therefore, when clinicians diagnose MS as a whole, we pay particular attention to hyperglycemia, which in the present study usually indicated a more serious degree of coronary artery lesions; this is therefore helpful for identifying high-risk PMI patients with poor prognosis as early as possible, allowing implementation of more timely intervention measures to improve the prognosis of these younger adult patients. Therefore, we suggest that MS can serve as an early indicator of increased risk for PMI.

After median 42 months of follow-up, we found that MS was independently associated with MACE in PMI patients, which was consistent with the results of previous studies (>45 years) (3, 14, 45). We also found that this was due to the increased risk of TVR and HF, which is also consistent with previous studies of patients >45 years (25). In the present study, we found that among the MS components, hyperglycemia and BMI ≥28.0 kg/m^2 were independent risk factors for MACE. Hyperglycemia induces the expression of cytokines and inflammatory factors, induces the production of growth factors that promote restenosis, smooth muscle cell proliferation and extracellular matrix production, and eventually leads to intimal hyperplasia and restenosis (46). Therefore, the revascularization rate in the MS group was significantly higher than that in the non-MS group. Also, previous studies have shown that MS is a major related factor in the risk of developing severe heart failure (47, 48), which is also observed in our population. In addition, obese patients are in a state of chronic inflammation and prethrombotic state, which plays an important role in the process of atherosclerosis and will lead to adverse cardiovascular events during follow-up (47). Early research has confirmed that abdominal obesity is independently associated with cardiovascular disease (49, 50). Consistent with our study results, Azarfarin et al. (51)pointed out that the left ventricular function was decreased in patients with abnormal BMI (P<0.05), suggesting that anthropometric indicators (e.g., BMI, waist circumference) have an impact on cardiac function after MI. Also, as mentioned above, the present study has shown that hyperglycemia in MS is independently associated with multi-vessel disease and Syntax score ≥33, while previous studies have shown that they all predict a poor prognosis (34, 52), which has been confirmed in long-term follow-up of the included PMI patients.

CONCLUSIONS

Previous studies have confirmed that MS affects the occurrence, development and prognosis of acute myocardial infarction. As far as we know, this is the first observational study to explore the impact of MS on the clinical severity and prognosis of PMI in adults aged 45 years and younger, suggesting that MS component hyperglycemia is as an independent predictor for coronary artery lesions and MACE. This may be useful for improving the awareness of adults aged 45 years and younger about risk factors for PMI, MS and MACE, and to encourage starting intervention measures as early as possible to help prevent PMI and MS.

LIMITATIONS

The present study has several limitations, including: 1) This was a single-center observational study and the sample size does not represent the overall prevalence of MS in patients with PMI; 2) The blood glucose and blood lipids measured during the onset of MI may be different from the daily levels, which may affect the diagnosis of MS; 3) The use of BMI instead of abdominal circumference to diagnose MS will likely have an impact on the results; 4) MS is independently related to the occurrence of MACE, but the results of exploratory analysis of each event of MACE, especially the occurrence of cardiac death, need to be further confirmed by larger sample size and longer follow-up time.

DATA AVAILABILITY STATEMENT

The original contributions presented in the study are included in the article/**Supplementary Material**. Further inquiries can be directed to the authors.

AUTHOR CONTRIBUTIONS

(I) Conception and design: JG YW and YL; (II) Administrative support: None; (III) Provision of study materials or patients: JG

and YL; (IV) Collection and assembly of data: YW, X-YW, YC, Z-HZ and Y-NY; (V) Data analysis and interpretation: ZC, JG and YW; (VI) Manuscript writing: All authors; (VII) Final approval of manuscript: All authors.

FUNDING

This research was supported by the Key Project of Scientific and Technological Support Plan of Tianjin in 2020 (No.20YFZCSY00820).

ACKNOWLEDGEMENTS

The author especially thanks all the selected patients for their participation.

SUPPLEMENTARY MATERIAL

The Supplementary Material for this article can be found online at: https://www.frontiersin.org/articles/10.3389/fendo.2022.920470/full#supplementary-material

REFERENCES

1. Expert Panel On Detection EATO, Expert Panel On Detection EATO. Executive Summary of the Third Report of the National Cholesterol Education Program (NCEP) Expert Panel on Detection, Evaluation, and Treatment of High Blood Cholesterol in Adults (Adult Treatment Panel III). *JAMA* (2001) 285(19):2486–97. doi: 10.1001/jama.285.19.2486
2. Saklayen MG. The Global Epidemic of the Metabolic Syndrome. *Curr Hypertens Rep* (2018) 20(2):12. doi: 10.1007/s11906-018-0812-z
3. Cavallari I, Cannon CP, Braunwald E, Goodrich EL, Im K, Lukas MA, et al. Metabolic Syndrome and the Risk of Adverse Cardiovascular Events After an Acute Coronary Syndrome. *Eur J Prev Cardiol* (2018) 25(8):830–8. doi: 10.1177/2047487318763897
4. Ramesh G, Sai NVB, Gururaj P, Bhupal R, Patel N. Association of Metabolic Syndrome and Level of Hs-CRP, Lp(a), and Serum Ferritin in Young Asian Patients (≤45 Years) With Acute Myocardial Infarction. *Interventional Med Appl Science.* (2018) 10(2):65–9. doi: 10.1556/1646.10.2018.14
5. Chung EH, Curran PJ, Sivasankaran S, Chauhan MS, Gossman DE, Pyne CT, et al. Prevalence of Metabolic Syndrome in Patients ≤45 Years of Age With Acute Myocardial Infarction Having Percutaneous Coronary Intervention. *Am J Cardiol* (2007) 100(7):1052–5. doi: 10.1016/j.amjcard.2007.05.028
6. Milionis HJ, Kalantzi KJ, Papathanasiou AJ, Kosovitsas AA, Doumas MT, Goudevenos JA. Metabolic Syndrome and Risk of Acute Coronary Syndromes in Patients Younger Than 45 Years of Age. *Coronary Artery Dis* (2007) 18 (4):247–52. doi: 10.1097/MCA.0b013e328035f8c4
7. Tweet MS. Sex Differences Among Young Individuals With Myocardial Infarction. *Eur Heart J* (2020) 41(42):4138–40. doi: 10.1093/eurheartj/ehaa682
8. Gulati R, Behfar A, Narula J, Kanwar A, Lerman A, Cooper L, et al. Acute Myocardial Infarction in Young Individuals. *Mayo Clin Proc* (2020) 95 (1):136–56. doi: 10.1016/j.mayocp.2019.05.001
9. Arora S, Stouffer GA, Kucharska-Newton AM, Qamar A, Vaduganathan M, Pandey A, et al. Twenty Year Trends and Sex Differences in Young Adults Hospitalized With Acute Myocardial Infarction. *Circulation.* (2019) 139 (8):1047–56. doi: 10.1161/CIRCULATIONAHA.118.037137
10. Gupta A, Wang Y, Spertus JA, Geda M, Lorenze N, Nkonde-Price C, et al. Trends in Acute Myocardial Infarction in Young Patients and Differences by Sex and Race, 2001 to 2010. *J Am Coll Cardiol* (2014) 64(4):337–45. doi: 10.1016/j.jacc.2014.04.054
11. Ricci B, Cenko E, Vasiljevic Z, Stankovic G, Kedev S, Kalpak O, et al. Acute Coronary Syndrome: The Risk to Young Women. *J Am Heart Assoc* (2017) 6 (12).e007519 doi: 10.1161/JAHA.117.007519
12. Li Y, Dong R, Hua K, Liu TS, Zhou SY, Zhou N, et al. Outcomes of Coronary Artery Bypass Graft Surgery Versus Percutaneous Coronary Intervention in Patients Aged 18-45 Years With Diabetes Mellitus. *Chin Med J (Engl).* (2017) 130(24):2906–15. doi: 10.4103/0366-6999.220305
13. Hoit BD, Gilpin EA, Henning H, Maisel AA, Dittrich H, Carlisle J, et al. Myocardial Infarction in Young Patients: An Analysis by Age Subsets. *Circ (New York N.Y.).* (1986) 74(4):712–21. doi: 10.1161/01.CIR.74.4.712
14. Lovic MB, Djordjevic DB, Tasic IS, Nedeljkovic IP. Impact of Metabolic Syndrome on Clinical Severity and Long-Term Prognosis in Patients With Myocardial Infarction With ST-Segment Elevation. *Hell J Cardiol* (2018) 59 (4):226–31. doi: 10.1016/j.hjc.2018.02.002
15. Lee SH, Jeong MH, Kim JH, Kim MC, Sim DS, Hong YJ, et al. Influence of Obesity and Metabolic Syndrome on Clinical Outcomes of ST-Segment Elevation Myocardial Infarction in Men Undergoing Primary Percutaneous Coronary Intervention. *J Cardiol* (2018) 72(4):328–34. doi: 10.1016/j.jjcc.2018.03.010
16. Ji MS, Jeong MH, Ahn YK, Kim SH, Kim YJ, Chae SC, et al. Comparison of Resolute Zotarolimus-Eluting Stents Versus Everolimus-Eluting Stents In Patients With Metabolic Syndrome and Acute Myocardial Infarction: Propensity Score-Matched Analysis. *Int J Cardiol* (2015) 199:53–62. doi: 10.1016/j.ijcard.2015.07.010.
17. Arnold SV, Lipska KJ, Li Y, Goyal A, Maddox TM, McGuire DK, et al. The Reliability and Prognosis of In-Hospital Diagnosis of Metabolic Syndrome in the Setting of Acute Myocardial Infarction. *J Am Coll Cardiol* (2013) 62 (8):704–8. doi: 10.1016/j.jacc.2013.02.062
18. Synetos A, Papanikolaou A, Toutouzas K, Georgiopoulos G, Karanasos A, Drakopoulou M, et al. Metabolic Syndrome Predicts Plaque Rupture in Patients With Acute Myocardial Infarction. An Optical Coherence Study. *Int J Cardiol* (2016) 209:139–41. doi: 10.1016/j.ijcard.2016.02.006
19. Thygesen K, Alpert JS, Jaffe AS, Chaitman BR, Bax JJ, Morrow DA, et al. Fourth Universal Definition of Myocardial Infarction (2018). *J Am Coll Cardiol* (2018) 72(18):2231–64. doi: 10.1016/j.jacc.2018.08.1038
20. Grundy SM, Cleeman JI, Daniels SR, Donato KA, Eckel RH, Franklin BA, et al. Diagnosis and Management of the Metabolic Syndrome - An American Heart Association/National Heart, Lung, and Blood Institute Scientific Statement. *Circulation.* (2005) 112(17):2735–52. doi: 10.1161/CIRCULATIONAHA.105.169404
21. Zhou BF. Effect of Body Mass Index on All-Cause Mortality and Incidence of Cardiovascular Diseases–Report for Meta-Analysis of Prospective Studies Open Optimal Cut-Off Points of Body Mass Index in Chinese Adults. *BioMed Environ Sci* (2002) 15(3):245–52.
22. Sianos G, Morel M, Kappetein AP, Morice M, Colombo A, Dawkins K, et al. The SYNTAX Score: An Angiographic Tool Grading the Complexity of Coronary Artery Disease. *EuroIntervention.* (2005) 1(2):219–27
23. Cheitlin MD, Armstrong WF, Aurigemma GP, Beller GA, Bierman FZ, Davis JL, et al. ACC/AHA/ASE 2003 Guideline Update for the Clinical Application of Echocardiography: Summary Article. *J Am Soc Echocardiog.* (2003) 16 (10):1091–110. doi: 10.1016/S0894-7317(03)00685-0
24. McMurray JJ, Adamopoulos S, Anker SD, Auricchio A, Böhm M, Dickstein K, Falk V, Filippatos G, Fonseca C, Gomez-Sanchez MA, Jaarsma T, Køber L, Lip GY, Maggioni AP, Parkhomenko A, Pieske BM, Parkhomenko A , Pieske BM,, Popescu BA, Rønnevik PK, Rutten FH, Schwitter J, Seferovic P, Stepinska J, Trindade PT, Voors AA, Zannad F,Zeiher A; ESC Guidelines for the Diagnosis and Treatment of Acute and Chronic Heart Failure 2012: The Task Force for the Diagnosis and Treatment of Acute and Chronic Heart Failure 2012 of the European Society of Cardiology. Developed in Collaboration With the Heart Failure Association (HFA) of the ESC. *Eur Heart J* (2012) 33(14):1787–847.doi: 10.1093/eurheartj/ehs104.
25. Ji MS, Jeong MH, Ahn Y, Kim YJ, Chae SC, Hong TJ, et al. One-Year Clinical Outcomes Among Patients With Metabolic Syndrome and Acute Myocardial Infarction. *Korean Circ J* (2013) 43(8):519. doi: 10.4070/kcj.2013.43.8.519
26. Kazemi T, Sharifzadeh G, Zarban A, Fesharakinia A. Comparison of Components of Metabolic Syndrome in Premature Myocardial Infarction in an Iranian Population: A Casewfi 2-Control Study. *Int J Prev Med* (2013) 4 (1):110–4.

27. Nolan PB, Carrick-Ranson G, Stinear JW, Reading SA, Dalleck LC. Prevalence of Metabolic Syndrome and Metabolic Syndrome Components in Young Adults: A Pooled Analysis. *Prev Med Rep* (2017) 7:211–5. doi: 10.1016/j.pmedr.2017.07.004
28. Mottillo S, Filion KB, Genest J, Joseph L, Pilote L, Poirier P, et al. The Metabolic Syndrome and Cardiovascular Risk. *J Am Coll Cardiol* (2010) 56 (14):1113–32. doi: 10.1016/j.jacc.2010.05.034
29. Rochlani Y, Pothineni NV, Kovelamudi S, Mehta JL. Metabolic Syndrome: Pathophysiology, Management, and Modulation by Natural Compounds. *Ther Adv Cardiovasc Disease*. (2017) 11(8):215–25. doi: 10.1177/1753944717711379
30. Nilsson PM, Tuomilehto J, Rydén L. The Metabolic Syndrome – What Is It and How Should It Be Managed? *Eur J Prev Cardiol* (2019) 26(2_suppl):33–46. doi: 10.1177/2047487319886404
31. Zafar U, Khaliq S, Ahmad HU, Manzoor S, Lone KP. Metabolic Syndrome: An Update on Diagnostic Criteria, Pathogenesis, and Genetic Links. *Hormones*. (2018) 17(3):299–313. doi: 10.1007/s42000-018-0051-3
32. McCracken E, Monaghan M, Sreenivasan S. Pathophysiology of the Metabolic Syndrome. *Clin Dermatol*. (2017) 36(1):14–20. doi: 10.1016/j.clindermatol.2017.09.004.
33. Mornar JM. Metabolic Syndrome: Influence on Clinical Severity and Prognosis in Patients With Acute ST-Elevation Myocardial Infarction Treated With Primary Percutaneous Coronary Intervention. *Acta Cardiol*. (2015)Apr.70(2)149–56. doi: 10.1080/ac.70.2.3073505.
34. Girasis C, Garg S, Raber L, Sarno G, Morel M, Garcia-Garcia HM, et al. SYNTAX Score and Clinical SYNTAX Score as Predictors of Very Long-Term Clinical Outcomes in Patients Undergoing Percutaneous Coronary Interventions: A Substudy of SIRolimus-Eluting Stent Compared With Paclitaxel-Eluting Stent for Coronary Revascularization (SIRTAX) Trial. *Eur Heart J* (2011) 32(24):3115–27. doi: 10.1093/eurheartj/ehr369
35. Magro M, Nauta S, Simsek C, Onuma Y, Garg S, van der Heide E, et al. Value of the SYNTAX Score in Patients Treated by Primary Percutaneous Coronary Intervention for Acute ST-Elevation Myocardial Infarction: The MI SYNTAXscore Study. *Am Heart J* (2011) 161(4):771–81. doi: 10.1016/j.ahj.2011.01.004
36. Capodanno D, Di Salvo ME, Cincotta G, Miano M, Tamburino C, Tamburino C. Usefulness of the SYNTAX Score for Predicting Clinical Outcome After Percutaneous Coronary Intervention of Unprotected Left Main Coronary Artery Disease. *Circ-Cardiovasc Inte*. (2009) 2(4):302–8. doi: 10.1161/CIRCINTERVENTIONS.108.847137
37. Karabağ Y, Çağdaş M, Rencuzogullari I, Karakoyun S, Artaç İ, İliş D, et al. Comparison of SYNTAX Score II Efficacy With SYNTAX Score and TIMI Risk Score for Predicting in-Hospital and Long-Term Mortality in Patients With ST Segment Elevation Myocardial Infarction. *Int J Cardiovasc Imaging*. (2018) 34(8):1165–75. doi: 10.1007/s10554-018-1333-1
38. Won K, Kim B, Chang H, Shin D, Kim J, Ko Y, et al. Metabolic Syndrome Does Not Impact Long-Term Survival in Patients With Acute Myocardial Infarction After Successful Percutaneous Coronary Intervention With Drug-Eluting Stents. *Catheter Cardio Inte*. (2014) 83(5):713–20. doi: 10.1002/ccd.25150
39. Boulon C, Lafitte M, Richeboeuf V, Paviot B, Pradeau V, Coste P, et al. Prevalence of Metabolic Syndrome After Acute Coronary Syndrome and its Prognostic Significance. *Am J Cardiol* (2006) 98(11):1429–34. doi: 10.1016/j.amjcard.2006.07.025
40. Dohi T, Miyauchi K, Kasai T, Kajimoto K, Kubota N, Tamura H, et al. Impact of Metabolic Syndrome on 10-Year Clinical Outcomes Among Patients With Acute Coronary Syndrome. *Circ J* (2009) 73(8):1454–8. doi: 10.1253/circj.CJ-08-1122
41. Mehta RH, Westerhout CM, Zheng Y, Giugliano RP, Huber K, Prabhakaran D, et al. Association of Metabolic Syndrome and its Individual Components With Outcomes Among Patients With High-Risk non-ST-Segment Elevation Acute Coronary Syndromes. *Am Heart J* (2014) 168(2):182–8. doi: 10.1016/j.ahj.2014.04.009
42. Lee Y, Lim Y, Shin J, Park J, Shin J, Kim K. The Impact of Metabolic Syndrome on Clinical Outcomes After Everolimus-Eluting Stent Implantation. *Am J Cardiol* (2015) 116(5):717–24. doi: 10.1016/j.amjcard.2015.05.041
43. Hajsadeghi S, Chitsazan M, Chitsazan M, Haghjoo M, Babaali N, Norouzzadeh Z, et al. Metabolic Syndrome is Associated With Higher Wall Motion Score and Larger Infarct Size After Acute Myocardial Infarction. *Res Cardiovasc Med* (2015) 4(1):3. doi: 10.5812/cardiovascmed.25018
44. Levantesi G, Macchia A, Marfisi R, Franzosi MG, Maggioni AP, Nicolosi GL, et al. Metabolic Syndrome and Risk of Cardiovascular Events After Myocardial Infarction. *J Am Coll Cardiol* (2005) 46(2):277–83. doi: 10.1016/j.jacc.2005.03.062
45. Bin H, Yujie Z, Yuyang L, Dongmei S, Yingxin Z, Dean J, et al. Impact of Metabolic Syndrome on Clinical Outcomes After Drug-Eluting Stent Implantation in Patients With Coronary Artery Disease. *Angiology* (2011) 62(6):440–6. doi: 10.1177/0003319711398473
46. Wang L, Gao P, Zhang M, Huang Z, Zhang D, Deng Q, et al. Prevalence and Ethnic Pattern of Diabetes and Prediabetes in China in 2013. *JAMA* (2017) 317(24):2515–23. doi: 10.1001/jama.2017.7596
47. Perrone-Filardi P, Paolillo S, Costanzo P, Savarese G, Trimarco B, Bonow RO. The Role of Metabolic Syndrome in Heart Failure. *Eur Heart J* (2015) 36 (39):2630–4. doi: 10.1093/eurheartj/ehv350
48. Haffner S, Taegtmeyer H. Epidemic Obesity and the Metabolic Syndrome. *Circulation*. (2003) 108(13):1541–5. doi: 10.1161/01.CIR.0000088845.17586.EC
49. Lakka HM, Lakka TA, Tuomilehto J, Salonen JT. Abdominal Obesity is Associated With Increased Risk of Acute Coronary Events in Men. *Eur Heart J* (2002) 23(9):706–13. doi: 10.1053/euhj.2001.2889
50. Coutinho T, Goel K, Corrêa DSD, Kragelund C, Kanaya AM, Zeller M, et al. Central Obesity and Survival in Subjects With Coronary Artery Disease: A Systematic Review of the Literature and Collaborative Analysis With Individual Subject Data. *J Am Coll Cardiol* (2011) 57(19):1877–86. doi: 10.1016/j.jacc.2010.11.058
51. Azarfarin R, Samadikhah J, Shahvalizadeh R, Golzari SE. Evaluation of Anthropometric Indices of Patients With Left Ventricle Dysfunction Fallowing First Acute Anterior Myocardial Infarction. *J Cardiovasc Thorac Res* (2012) 4(1):11–5. doi: 10.5681/jcvtr.2012.003
52. Widimsky P, Holmes DR. How to Treat Patients With ST-Elevation Acute Myocardial Infarction and Multi-Vessel Disease? *Eur Heart J* (2011) 32 (4):396–403. doi: 10.1093/eurheartj/ehq410

Conflict of Interest: The authors declare that the research was conducted in the absence of any commercial or financial relationships that could be construed as a potential conflict of interest.

Publisher's Note: All claims expressed in this article are solely those of the authors and do not necessarily represent those of their affiliated organizations, or those of the publisher, the editors and the reviewers. Any product that may be evaluated in this article, or claim that may be made by its manufacturer, is not guaranteed or endorsed by the publisher.

frontiers | Frontiers in Endocrinology

ORIGINAL RESEARCH
published: 01 July 2022
doi: 10.3389/fendo.2022.854142

Research on the Association Between Obstructive Sleep Apnea Hypopnea Syndrome Complicated With Coronary Heart Disease and Inflammatory Factors, Glycolipid Metabolism, Obesity, and Insulin Resistance

Yumei Wen, Haibin Zhang, Yu Tang and Rui Yan*

Department of Cardiology, Beijing Luhe Hospital, Capital of Medical University, Beijing, China

The aim of this study is to explore the association between obstructive sleep apnea hypopnea syndrome (OSAHS) complicated with coronary heart disease (CHD) and inflammatory factors, glycolipid metabolism, obesity, and insulin resistance. A total of 400 patients diagnosed with OSAHS who underwent polysomnography (PSG) monitoring in the Sleep Diagnosis and Treatment Center of Beijing Luhe Hospital from March 2015 to September 2018 were selected and divided into the OSAHS group (n = 200) and the OSAHS + CHD group (n = 200) according to disease condition. The questionnaire survey was conducted, the somatology indexes were measured, and the PSG, insulin, glycolipid metabolism parameters, and serum inflammatory factors were detected. Body weight, body mass index, waist circumference, and Epworth sleepiness scale (ESS) score were all significantly increased in the OSAHS + CHD group compared with those in the OSAHS group ($p < 0.05$). The microarousal index (MAI), apnea hypopnea index (AHI), cumulative percentage of time spent at oxygen saturation below 90% (CT90%), oxygen desaturation index (ODI), lowest oxygen saturation ($LSaO_2$), total apnea time (TAT), and mean oxygen saturation ($MSaO_2$) had statistically significant differences between the OSAHS + CHD group and the OSAHS group ($p < 0.05$). According to the Spearman correlation analysis of AHI, $LSaO_2$, $MSaO_2$, CT90%, ODI, and MAI with HOMA-IR in both groups, MAI, AHI, CT90%, and ODI were positively correlated with HOMA-IR ($r > 0$), while $LSaO_2$ and $MSaO_2$ were negatively correlated with HOMA-IR ($r < 0$). Compared with the OSAHS group, the OSAHS + CHD group had an obviously increased level of triglyceride (TG) ($p < 0.05$), and obviously increased levels of serum inflammatory factors C-reactive protein

OPEN ACCESS

Edited by:
Lu Cai,
University of Louisville, United States

Reviewed by:
Leila Warszawski,
Instituto Estadual de Diabetes e Endocrinologia Luiz Capriglione, Brazil
Guliz Kozdag Gold,
Albert Einstein College of Medicine, United States

***Correspondence:**
Haibin Zhang
zhangtunwo13069@163.com

Specialty section:
This article was submitted to Cardiovascular Endocrinology, a section of the journal Frontiers in Endocrinology

Received: *13 January 2022*
Accepted: *29 April 2022*
Published: *01 July 2022*

Citation:
Wen Y, Zhang H, Tang Y and Yan R (2022) Research on the Association Between Obstructive Sleep Apnea Hypopnea Syndrome Complicated With Coronary Heart Disease and Inflammatory Factors, Glycolipid Metabolism, Obesity, and Insulin Resistance. Front. Endocrinol. 13:854142. doi: 10.3389/fendo.2022.854142

(CRP), tumor necrosis factor-α (TNF-α), interleukin-6 (IL-6), and interferon-γ (IFN-γ) ($p < 0.05$). The occurrence of OSAHS complicated with CHD is related to inflammatory factors, glycolipid metabolism, obesity rate, and HOMA-IR.

Keywords: obstructive sleep apnea hypopnea syndrome, coronary heart disease, obesity, inflammation, glycolipid metabolism

INTRODUCTION

Obstructive sleep apnea hypopnea syndrome (OSAHS), whose morbidity rate is annually increasing, is mainly manifested as sleep structure disorder, drowsiness, breath blockage, apnea, snoring, etc. (1), which increases the risks of cardiovascular complications and multiple organ damage in patients. OSAHS not only harms the respiratory system but also affects the cardio-cerebrovascular system of patients, and causes such complications as heart failure and coronary heart disease (CHD), seriously affecting the quality of life and lifespan of patients (2, 3). OSAHS has a high morbidity rate in middle-aged and elderly people, and it is also affected by genetics, unhealthy living habits, and social pressure (4). CHD is caused by the myocardial tissue lesions due to stenosis or obstruction of the arterial lumen (5). CHD has become a common cardio-cerebrovascular disease in recent years, and it frequently occurs in the elderly, but patients have become increasingly younger nowadays, with an increasing annual morbidity rate (6). The etiology of CHD is complex, and the effective prevention and control of its risk factors has an important significance to reduce its morbidity rate (7). CHD seriously threatens human health; thus, it has gradually attracted widespread attention in society (8). According to a large number of studies in China and other countries, OSAHS is closely related to CHD (9). Studies have also shown that the morbidity rate of OSAHS in CHD patients is higher than that in the general population, and OSAHS complicated with CHD will raise the mortality rate (10). Therefore, this paper conducted a questionnaire survey of patients with CHD, measured somatic indexes, and detected polysomnography (PSG), insulin, glucose and lipid metabolism parameters, and serum inflammatory factors, so as to analyze the expression differences in inflammatory factors, and glucose and lipid metabolism in patients with OSAHS complicated with CHD. Insulin resistance (HOMA-IR) was evaluated by obesity rate and a homeostasis model to explore the relationship between OSAHS combined with CHD and inflammatory factors, glucose and lipid metabolism, obesity, and IR of cardiovascular disease.

OBJECTS AND METHODS

Objects of the Study

A total of 400 patients diagnosed with OSAHS who underwent PSG monitoring in the Sleep Diagnosis and Treatment Center of Beijing Luhe Hospital from March 2015 to September 2018 were selected and divided into the OSAHS group ($n = 114$) and the OSAHS + CHD group ($n = 286$) according to disease condition.

Inclusion and Exclusion Criteria

Inclusion criteria were as follows: patients with such clinical symptoms as loud snoring with apnea during nighttime sleep, mouth breathing, frequent urination at night, mouth dryness in the morning, memory deterioration, and daytime sleepiness [Epworth sleepiness scale (ESS) score ≥9 points]; those with an apnea hypopnea index (AHI) ≥ 5 times/h according to PSG; those with upper airway stenosis and obstruction shown in the examination; those diagnosed with OSAHS; and those with an ESS score <9 points but AHI ≥5 times/h. According to the international common visual diameter method, the degree of vascular stenosis = (normal vessel diameter near the heart of the stenosis site − diameter of the stenosis site)/vessel diameter near the heart of the stenosis segment × 100%, and coronary angiography showed that the stenosis degree of the inner diameter of the main branches was more than 50%, which could also be diagnosed as OSAHS complicated with CHD. Exclusion criteria were as follows: patients with upper airway resistance syndrome, simple snoring, or narcolepsy; those with a clear history of diabetes earlier than OSAHS; those with IR caused by other factors, such as pancreatic exocrine disease or endocrine diseases; and those with severe malformations of the mouth, nose, or neck.

Questionnaire Survey and Measurement of Somatology Indexes

The main contents of questionnaire survey are as follows:

1. Basic information: gender and age.
2. Past medical history: with or without a history of upper respiratory diseases (such as acute and chronic rhinitis, sinusitis, pharyngitis, angina, severe sinusitis, and deviation of nasal septum), cardiovascular/cerebrovascular diseases, hypertension, and diabetes.
3. Personal history: with or without a history of smoking and alcoholism.
4. Family history: with or without a family history of OSAHS, heart disease, and diabetes.
5. ESS score: The daytime sleepiness was scored in all subjects according to the ESS (**Table 1**).

Somatology indexes are as follows:

1. Body weight: After fasting, patients wore thin clothes, took off their shoes, and urinated before their body weight (kg) was measured using a weighing scale and recorded.

TABLE 1 | ESS.

Are you sleepy in the following conditions?	Never	Rarely	Sometimes	Often
Sit reading books				
Watch TV				
Sit still somewhere				
Long-time riding (>1 h)				
Lie down for rest at noon				
Sit chatting with people				
Sit quietly at noon without drinking				
Stop at the traffic light in traffic jam				

Never, 0 point; rarely, 1 point; sometimes, 2 points; often, 3 points. "Never": not occur at all, "Rarely": once-twice a week, "Sometimes": 3-4 times a week, "Often": more than 5 times a week.

2. Waist circumference: the circumference (cm) of the plane at the midpoint between the inferior margin of rib and the crista iliaca.
3. Height: The patients kept their body upright and their heels were placed together, and then the height (cm) was measured and recorded.
4. Body mass index (BMI) = weight/height^2 (kg/m^2).
5. Waist-to-height ratio (WHtR) = waist circumference (cm)/height (cm).

PSG Monitoring

In the daytime, the patients did not sleep without eating food containing stimulants and sedatives that affected sleep. The sleep process (more than 7 h overnight) was monitored *via* PSG from 9:00 p.m. to 8:00 a.m. the next day. The following indexes were recorded and analyzed: cumulative percentage of time spent at oxygen saturation below 90% (CT90%), oxygen desaturation index (ODI), microarousal index (MAI), AHI, lowest oxygen saturation ($LSaO_2$), mean oxygen saturation ($MSaO_2$), longest apnea time (LAT), and total apnea time (TAT).

Detection of Fasting Plasma Glucose and Fasting Insulin

After fasting for more than 8 h overnight, the peripheral venous blood (elbow venous blood samples) was drawn in the morning to detect FPG and FINS through hexokinase assay and chemiluminescence assay. The IR level was evaluated using homeostasis model assessment of IR (HOMA-IR): HOMA-IR = FINS (mIU/ml) × FPG (mmol/L)/22.5.

Detection of Glycolipid Metabolism Parameters

After fasting for more than 8 h overnight, the peripheral venous blood (elbow venous blood samples) was drawn in the morning to routinely detect FPG, total cholesterol (TC), triglyceride (TG), high-density lipoprotein (HDL), and low-density lipoprotein (LDL).

Detection of Serum Inflammatory Factors

After fasting overnight, 3–4 ml of venous blood was drawn from patients and centrifuged at 3,000 rpm for 15 min. Then, the supernatant was taken using a micropipettor and stored at −80°C. The levels of C-reactive protein (CRP), tumor necrosis factor-α (TNF-α), interleukin-6 (IL-6), and interferon-γ (IFN-γ) in both groups were determined repeatedly 3 times *via* enzyme-linked immunosorbent assay (ELISA) according to the instructions, and the results were averaged.

Statistical Methods

SPSS 20.0 software was used for statistical analysis. The differences in inflammatory factors, glycolipid metabolism, obesity rate, and HOMA-IR were compared between the two groups using *t*-test. $p < 0.05$ suggested that the difference was statistically significant.

RESULTS

Clinical Data

Body weight, BMI, waist circumference, and ESS score were all found to be significantly increased in the OSAHS + CHD group compared with those in the OSAHS group, and the differences were statistically significant ($p < 0.05$), while other indexes had no statistically significant differences between the two groups ($p > 0.05$) (**Table 2**).

PSG Monitoring Results in Both Groups

MAI, AHI, CT90%, ODI, $LSaO_2$, TAT, and $MSaO_2$ had statistically significant differences between the OSAHS + CHD group and the OSAHS group ($p < 0.05$) (**Table 3**).

TABLE 2 | Clinical data in OSAHS + CHD group and OSAHS group.

Item	OSAHS group	OSAHS + CHD group	χ2	*p*
Age (years old)	45.68±7.56	47.25±8.71	0.03	0.830
Weight (kg)	74.12±11.95	82.78±10.69	6.47	0.006
BMI (kg/m2)	25.48±1.98	29.34±2.14	4.02	0.005
Waist circumference (cm)	98.15±12.35	102.49±13.78	3.08	0.003
WHtR	0.55±0.01	0.56±0.02	0.06	0.745
ESS score	8.56±3.24	11.23±4.19	5.47	0.029
Gender (male/female)	112/88	146/54	4.48	0.092
Smoking history	95	103	3.32	0.126
Drinking history	82	98	1.42	0.623

TABLE 3 | PSG monitoring results in both groups.

Item	OSAHS group	OSAHS + CHD group	χ2	*p*
AHI (times/h)	16.48±3.46	51.86±9.48	24.69	0.003
LSaO2 (%)	88.46±10.65	61.87±13.49	13.45	0.004
CT90% (%)	5.14±7.26	38.16±4.23	14.26	0.005
ODI (times/h)	19.16±4.03	35.09±9.61	10.03	0.005
MSaO2 (%)	96.05±2.04	88.74±1.95	7.12	0.004
TAT (min)	40.38±190.23	164.29±20.46	19.45	0.002
MAI (times/h)	20.31±9.01	34.16±12.73	6.09	0.004

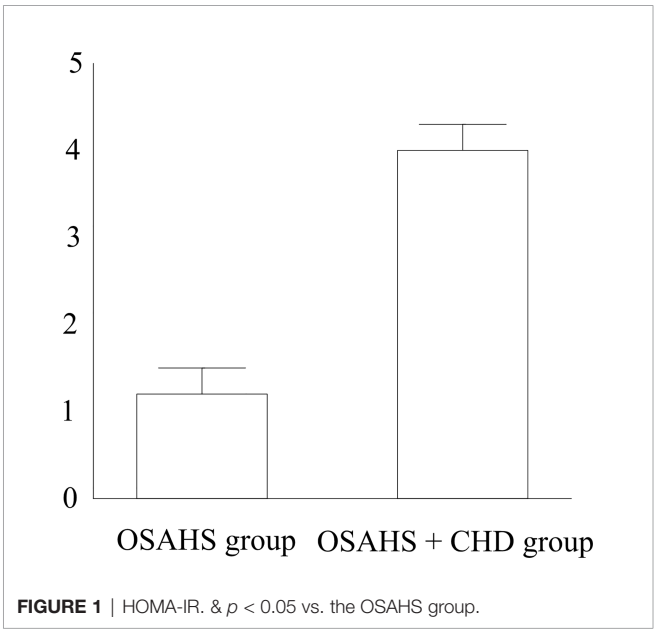

FIGURE 1 | HOMA-IR. & $p < 0.05$ vs. the OSAHS group.

HOMA-IR

HOMA-IR was the highest (4.65 ± 0.71) in the OSAHS + CHD group and the lowest (1.24 ± 0.25) in the OSAHS group ($p < 0.05$) (**Figure 1**). According to the Spearman correlation analysis of AHI, $LSaO_2$, $MSaO_2$, CT90%, ODI, MAI, and TAT with HOMA-IR in both groups, AHI, CT90%, ODI, MAI, and TAT were positively correlated with HOMA-IR ($r > 0$), while $LSaO_2$ and $MSaO_2$ were negatively correlated with HOMA-IR ($r < 0$) (**Table 4**).

Glycolipid Metabolism Parameters

There were no obvious differences in the FPG, TC, HDL, and LDL between the OSAHS + CHD group and the OSAHS group ($p > 0.05$). Compared with the OSAHS group, the OSAHS + CHD group had an obviously increased level of TG, showing a statistically significant difference ($p < 0.05$) (**Table 5**).

Serum Inflammatory Factors

Compared with the OSAHS group, the OSAHS + CHD group had obviously increased levels of serum inflammatory factors CRP, TNF-α, IL-6, and IFN-γ, and there were also statistically significant differences ($p < 0.05$) (**Table 6**).

DISCUSSION

There are at least over 50 million patients with OSAHS in China, and most of them receive no active and effective treatment. On the one hand, patients regard "snoring" as a normal phenomenon rather than a disease. On the other hand, there is still a lack of effective biological indexes for early detection of OSAHS-related complications currently (11–14). Therefore, raising the patient's awareness of the disease and its complications, and strengthening the early detection of OSAHS-related complications contribute to the treatment of

TABLE 4 | Correlation analysis of variables with HOMA-IR.

Item	Weight	BMI	Waist circumference	ESS score	AHI	LSaO2	MSaO2	CT90%	ODI	MAI	TAT
r	0.16	0.15	0.18	0.21	0.83	-0.25	-0.22	0.82	0.12	0.18	0.35
p	0.002	0.002	0.001	0.002	0.001	0.001	0.002	0.004	0.013	0.001	0.13

TABLE 5 | Glycolipid metabolism parameters.

Item	OSAHS group	OSAHS + CHD group	*p*
FPG (mmol/L)	4.92±0.08	5.95±0.12	0.061
TC (mmol/L)	4.19±0.35	5.81±0.25	0.076
TG (mmol/L)	1.43±0.07	6.61±0.43	0.016
HDL (mmol/L)	1.59±0.15	1.06±0.36	0.091
LDL (mmol/L)	3.42±0.04	2.98±0.13	0.106

TABLE 6 | Content of serum inflammatory factors in both groups.

Item	OSAHS group	OSAHS + CHD group	*p*
CRP	2.38±1.08	15.30±2.14	0.009
TNF-α	21.91±4.25	39.16±3.94	0.010
IL-6	8.19±3.49	13.07±1.80	0.005
IFN-γ	76.09±15.55	104.06±20.72	0.003

disease and improvement of the prognosis of patients (15). The pathogenesis of OSAHS is upper airway obstruction (16), and OSAHS patients have neurohumoral abnormality (17). OSAHS can cause lesions in the cardiovascular system, and different types of CHD and OSAHS can also promote each other; thus, there is a complicated pathophysiological relation between OSAHS and CHD (18).

In the present study, body weight, BMI, waist circumference, and ESS score were all significantly increased in the OSAHS + CHD group compared with those in the OSAHS group, and the differences were statistically significant ($p < 0.05$). MAI, TAT, AHI, CT90%, ODI, $LSaO_2$, and $MSaO_2$ had obvious differences between the OSAHS + CHD group and the OSAHS group ($p < 0.05$). There were no obvious differences in the FPG, TC, HDL, and LDL between the OSAHS + CHD group and the OSAHS group ($p > 0.05$). Compared with the OSAHS group, the OSAHS + CHD group had an obviously increased level of TG, and there was a statistically significant difference ($p < 0.05$). To sum up, OSAHS has a significant correlation with obesity. OSAHS patients have such symptoms as daytime sleepiness, greasy food preference, and fat accumulation, which will aggravate the obesity of patients. The number of obesity patients with OSAHS + CHD is remarkably larger than those with OSAHS. Therefore, increasing the amount of exercise and reducing the intake of excessive high-calorie food can effectively improve the symptoms of OSAHS. In this study, among the glycolipid metabolism parameters, only TG had obvious changes in OSAHS + CHD compared with OSAHS, but no remarkable changes were observed in other parameters. Such a result is consistent with the conclusion made by Qing who used the SAS score and 4 different kinds of questionnaires as the screening tools for OSAHS such that the excessive fat accumulation in the thorax due to obesity leads to a decline in chest wall compliance and an increase in respiratory muscle resistance, which are most apparent in a supine position, and hypoxemia occurs in severe cases, forming a vicious cycle (19).

In this study, HOMA-IR was the highest in the OSAHS + CHD group and the lowest in the OSAHS group ($p < 0.05$). According to the Spearman correlation analysis of AHI, $LSaO_2$, $MSaO_2$, CT90%, ODI, and MAI with HOMA-IR in both groups, AHI, CT90%, ODI, and MAI were positively correlated with HOMA-IR ($r > 0$), while $LSaO_2$ and $MSaO_2$ were negatively correlated with HOMA-IR ($r < 0$). Moreover, compared with the OSAHS group, the OSAHS + CHD group had obviously increased levels of serum inflammatory factors CRP, TNF-α, IL-6, and IFN-γ, displaying statistically significant differences ($p < 0.05$). Hotamisligil et al. studied and found that IR is closely related to plasma pro-inflammatory factors, and the enhanced IR corresponds to the increased secretion of pro-inflammatory cytokines. Due to the increase in respiratory resistance, the patient experiences hypoxia, and a large number of inflammatory cytokines are expressed, thereby increasing the concentration of inflammatory factors in plasma. Such a result is consistent with the conclusion made by Cai et al. in their study on respiratory resistance in OSAHS patients that there is an inseparable relationship between OSAHS and IR, heart disease, and inflammatory factors, which demonstrates that detection of IR, heart disease, and inflammatory factors in patients may have an important significance for the prevention and treatment of OSAHS (20).

In conclusion, glycolipid metabolism, obesity rate, HOMA-IR, and inflammatory factors are all significantly increased in OSAHS + CHD compared with OSAHS.

DATA AVAILABILITY STATEMENT

The original contributions presented in the study are included in the article/supplementary material. Further inquiries can be directed to the corresponding author.

ETHICS STATEMENT

The study was approved by the ethics committee of Beijing Luhe Hospital, and written informed consents were signed by the patients and/or guardians. The patients/participants provided their written informed consent to participate in this study.

AUTHOR CONTRIBUTIONS

YW wrote the manuscript. YW and HZ were responsible for questionnaire survey and measurement of somatology indexes. YT and RY performed ELISA. All authors contributed to the article and approved the submitted version.

REFERENCES

1. Patel SV, Gill H, Shahi D, Rajabalan A, Patel P, Sonani R, et al. High Risk for Obstructive Sleep Apnea Hypopnea Syndrome Predicts New Onset Atrial Fibrillation After Cardiac Surgery: A Retrospective Analysis. *Sleep Breath* (2018) 22:1117–24. doi: 10.1007/s11325-018-1645-3
2. Zhou L, Ouyang R, Chen P, Luo H, Liu H, Liu G. A Case of Severe Obstructive Sleep Apnea Hypopnea Syndrome With Urinary and Anal

Incontinence. *J Cent S Univ (Med Sci)* (2018) 43:333–6. doi: 10.11817/j.issn.1672-7347.2018.03.016
3. Vena D, Bradley TD, Millar PJ, Floras JS, Rubianto J, Gavrilovic B, et al. Heart Rate Variability Responses of Individuals With and Without Saline-Induced Obstructive Sleep Apnea. *J Clin Sleep Med* (2018) 14:503–10. doi: 10.5664/jcsm.7032
4. Zhan X, Fang F, Wu C, Pinto JM, Wei Y. A Retrospective Study to Compare the Use of the Mean Apnea-Hypopnea Duration and the Apnea-Hypopnea Index With Blood Oxygenation and Sleep Patterns in Patients With Obstructive Sleep Apnea Diagnosed by Polysomnography. *Med Sci Monit* (2018) 24:1887–93. doi: 10.12659/MSM.909219
5. Lundetrae RS, Saxvig IW, Pallesen S, Aurlien H, Lehmann S, Bjorvatn B. Prevalence of Parasomnias in Patients With Obstructive Sleep Apnea. A Registry-Based Cross-Sectional Study. *Front Psychol* (2018) 9:1140. doi: 10.3389/fpsyg.2018.01140
6. Archontogeorgis K, Voulgaris A, Nena E, Strempela M, Karailidou P, Tzouvelekis A, et al. Cardiovascular Risk Assessment in a Cohort of Newly Diagnosed Patients With Obstructive Sleep Apnea Syndrome. *Cardiol Res Pract* (2018) 6572785:2018. doi: 10.1155/2018/6572785
7. Fang SY, Wan Abdul Halim WH, Mat Baki M, Din NM. Effect of Prolonged Supine Position on the Intraocular Pressure in Patients With Obstructive Sleep Apnea Syndrome. *Graefes Arch Clin Exp Ophthalmol* (2018) 256:783–90. doi: 10.1007/s00417-018-3919-7
8. Liu YT, Zhang HX, Li HJ, Chen T, Huang YQ, Zhang L, et al. Aberrant Interhemispheric Connectivity in Obstructive Sleep Apnea-Hypopnea Syndrome. *Front Neurol* (2018) 9:314. doi: 10.3389/fneur.2018.00314
9. Stavrou V, Bardaka F, Karetsi E, Daniil Z, Gourgoulianis KI. Brief Review: Ergospirometry in Patients With Obstructive Sleep Apnea Syndrome. *J Clin Med* (2018) 7:191(1-6). doi: 10.3390/jcm7080191
10. Su J, Tian JH, Gao XX, Wu YF, Zu JM, Dong KF, et al. Multimodal Analgesic Analgesia in Patients With Obstructive Sleep Apnea Hypopnea Syndrome With Multiple Planar Surgery. *J Clin Otorhinolaryngol Head Neck Surg* (2018) 32:850–3. doi: 10.13201/j.issn.1001-1781.2018.11.012
11. Cadeddu JA. Re: Airway Resistance in Patients With Obstructive Sleep Apnea Syndrome Following Robotic Prostatectomy. *J Urol* (2018) 199:14. doi: 10.1016/j.juro.2017.09.097
12. Aydin S, Ozdemir C, Kucukali CI, Sokucu SN, Giris M, Akcan U, et al. Reduced Peripheral Blood Mononuclear Cell ROCK1 and ROCK2 Levels in Obstructive Sleep Apnea Syndrome. *In Vivo* (2018) 32:319–25. doi: 10.21873/invivo.11240
13. Wang X, Fan JY, Zhang Y, Nie SP, Wei YX. Association of Obstructive Sleep Apnea With Cardiovascular Outcomes After Percutaneous Coronary Intervention: A Systematic Review and Meta-Analysis. *Med (Baltimore)* (2018) 97:e0621. doi: 10.1097/MD.0000000000010621
14. De Backer W. Obstructive Sleep Apnea/Hypopnea Syndrome. *Panminerva Med* (2013) 55:191–5.
15. Vaquerizo-Villar F, Alvarez D, Kheirandish-Gozal L, Gutierrez-Tobal GC, Barroso-Garcia V, Crespo A, et al. Utility of Bispectrum in the Screening of Pediatric Sleep Apnea-Hypopnea Syndrome Using Oximetry Recordings. *Comput Methods Programs BioMed* (2018) 156:141–9. doi: 10.1016/j.cmpb.2017.12.020
16. Zhao EF, Chen SM, Du YJ, Zhang YS. Association Between Sleep Apnea Hypopnea Syndrome and the Risk of Atrial Fibrillation: A Meta-Analysis of Cohort Study. *BioMed Res Int* (2018) 1(1-9):5215868. doi: 10.1155/2018/5215868
17. Zhang J, Song Y, Ji Y. Correlation Between Coronary Artery Disease and Obstructive Sleep Apnea Syndrome and Analysis of Risk Factors. *Exp Ther Med* (2018) 15(6):4771–6. doi: 10.3892/etm.2018.6070
18. Jia S, Zhou YJ, Yu Y. Obstructive Sleep Apnea is Associated With Severity and Long-Term Prognosis of Acute Coronary Syndrome. *J Geriatric Cardiol* (2018) 15(2):146–52. doi: 10.11909/j.issn.1671-5411.2018.02.005
19. Qing S. Comparison of the No SAS Score With Four Different Questionnaires as Screening Tools for Obstructive Sleep Apnea-Hypopnea Syndrome. *China Med Abstracts* (2018) 41(2):213–9.
20. Cai Z, Taoping LI, Xiaoxia LU. Alterations of Respiratory Resistance in Patients With Obstructive Sleep Apnea Hypopnea Syndrome. *J South Med Univ* (2018) 38(6):765–8. https://www.j-smu.com/CN/Y2018/V38/I06/765

Conflict of Interest: The authors declare that the research was conducted in the absence of any commercial or financial relationships that could be construed as a potential conflict of interest.

Publisher's Note: All claims expressed in this article are solely those of the authors and do not necessarily represent those of their affiliated organizations, or those of the publisher, the editors and the reviewers. Any product that may be evaluated in this article, or claim that may be made by its manufacturer, is not guaranteed or endorsed by the publisher.

frontiers | Frontiers in Endocrinology

REVIEW
published: 07 July 2022
doi: 10.3389/fendo.2022.946313

Structural and Electrical Remodeling of the Sinoatrial Node in Diabetes: New Dimensions and Perspectives

Lina T. Al Kury[1†], Stephanie Chacar[2†], Eman Alefishat[3,4,5], Ali A. Khraibi[2,5] and Moni Nader[2,5*]*

[1] Department of Health Sciences, College of Natural and Health Sciences, Zayed University, Abu Dhabi, United Arab Emirates, [2] Department of Physiology and Immunology, College of Medicine and Health Sciences, Khalifa University of Science and Technology, Abu Dhabi, United Arab Emirates, [3] Department of Pharmacology, College of Medicine and Health Sciences, Khalifa University of Science and Technology, Abu Dhabi, United Arab Emirates, [4] Department of Biopharmaceutics and Clinical Pharmacy, School of Pharmacy, The University of Jordan, Amman, Jordan, [5] Center for Biotechnology, Khalifa University of Science and Technology, Abu Dhabi, United Arab Emirates

OPEN ACCESS

Edited by:
Lu Cai,
University of Louisville, United States

Reviewed by:
Di Lang,
University of Wisconsin-Madison, United States
Henggui Zhang,
The University of Manchester, United Kingdom

***Correspondence:**
Lina T. Al Kury
Lina.AlKury@zu.ac.ae
Moni Nader
moni.nader@ku.ac.ae

[†]These authors have contributed equally to this work

Specialty section:
This article was submitted to Cardiovascular Endocrinology, a section of the journal Frontiers in Endocrinology

Received: *17 May 2022*
Accepted: *14 June 2022*
Published: *07 July 2022*

Citation:
Al Kury LT, Chacar S, Alefishat E, Khraibi AA and Nader M (2022) Structural and Electrical Remodeling of the Sinoatrial Node in Diabetes: New Dimensions and Perspectives. Front. Endocrinol. 13:946313. doi: 10.3389/fendo.2022.946313

The sinoatrial node (SAN) is composed of highly specialized cells that mandate the spontaneous beating of the heart through self-generation of an action potential (AP). Despite this automaticity, the SAN is under the modulation of the autonomic nervous system (ANS). In diabetes mellitus (DM), heart rate variability (HRV) manifests as a hallmark of diabetic cardiomyopathy. This is paralleled by an impaired regulation of the ANS, and by a pathological remodeling of the pacemaker structure and function. The direct effect of diabetes on the molecular signatures underscoring this pathology remains ill-defined. The recent focus on the electrical currents of the SAN in diabetes revealed a repressed firing rate of the AP and an elongation of its tracing, along with conduction abnormalities and contractile failure. These changes are blamed on the decreased expression of ion transporters and cell-cell communication ports at the SAN (i.e., HCN4, calcium and potassium channels, connexins 40, 45, and 46) which further promotes arrhythmias. Molecular analysis crystallized the RGS4 (regulator of potassium currents), mitochondrial thioredoxin-2 (reactive oxygen species; ROS scavenger), and the calcium-dependent calmodulin kinase II (CaMKII) as metabolic culprits of relaying the pathological remodeling of the SAN cells (SANCs) structure and function. A special attention is given to the oxidation of CaMKII and the generation of ROS that induce cell damage and apoptosis of diabetic SANCs. Consequently, the diabetic SAN contains a reduced number of cells with significant infiltration of fibrotic tissues that further delay the conduction of the AP between the SANCs. Failure of a genuine generation of AP and conduction of their derivative waves to the neighboring atrial myocardium may also occur as a result of the anti-diabetic regiment (both acute and/or chronic treatments). All together, these changes pose a challenge in the field of cardiology and call for further investigations to understand the etiology of the structural/functional remodeling of the SANCs in diabetes. Such an understanding may lead to more adequate therapies that can optimize glycemic control and improve health-related outcomes in patients with diabetes.

Keywords: sinoatrial node, diabetes, action potential, ion channels, gap junctions, structural remodeling, metabolic changes

1 THE SINOATRIAL NODE AS A PACEMAKER OF THE HEART

Cardiac rhythm is controlled by the activity of a heterogeneous collection of highly specialized cells forming the SAN, located at the wall (epicardium) of the right atrium, laterally to the entrance of the superior vena cava, and in the vicinity to the cristae terminalis (1, 2). Since its discovery about a century ago (1907) by Arthur Keith and Martin Flack, the SAN has attracted the attention of scientists to decipher its characteristics (3).

The length of the SAN ranges from 8-21.5 mm, comprising the head, the central area and the tail (4, 5). Optical mapping techniques identified several spots, within the SAN, that discharge action potentials (APs), ultimately leading to the depolarization of the atrial muscle (6). The unique electrophysiological properties of the SAN cells (SANCs) are conducive to self-excitation yielding spontaneous depolarization, thus pacemaker activity, in the absence of external stimuli (7). This is mandated by the ingress of sodium (funny current) and calcium ions through the sarcolemma (8) which constantly lifts up the unstable resting membrane potential (~ 60 mV) of SANCs towards the threshold (~ -40 mV), before the upstroke of the AP arises (9, 10). Despite this, the self-excitation process *per se* is insufficient; it still requires a special cellular organization/structure that promotes the exit of the AP throughout well-defined pathways to spread through, and efficiently depolarize the adjacent myocardium (left atrium) (11). These include a remarkable cell-cell communication profile implicating low conductance gap junctions with a particular transmission pattern of the electrical signals, along with an electrical insulator (connective tissue) surrounding the grouped SANCs (12). The connective tissue is needed to avoid the random dissipation of the depolarization wave and to focus its trajectory through specific exit pathways for an effective propagation of the AP through the atrial myocardium (13). The blood supply to the SAN is mainly through the right coronary artery in most cases, to a lesser extent by the circumflex of the left coronary artery, and by both coronary arteries in a very minor portion of the population (14–16). Therefore, the safety of cardiac rhythm highly hinges on a properly functioning SAN that must be constantly supplied by the appropriate amount of oxygen/nutrients.

2 SAN CELLS LINEAGE AND DEVELOPMENTAL CHANGES

SANCs are structurally and functionally different from the surrounding cardiomyocytes (17, 18). The SAN comprises a collection of weakly connected cells (pacemaker cells, adipocytes, myocytes, and fibroblasts) out of which those defining the pacemaker activity of the node are divided into three main types of cells; the elongated spindle shaped cells (~80 μm in length), the spindle cells (~ 40μm), and the spider-shaped cells [reviewed in (19)]. A careful inspection of human SAN revealed the presence of mainly three different types of cells: the pale (P) cells organized in clusters with elongated cytoplasmic extensions, the transitional (T) cells that resemble cardiomyocytes but with fewer sarcomeres, and the fibroblast-like cells with long bi-tripolar contacting cells (20). All together, these cells are insulated by fibrous tissues from the rest of the atrial myocardium. This insulation shields the SANCs from atrial hyperpolarization and provides a unidirectional route for the depolarization wave initiated at the SAN center to spread in mainly three directions (outside the superior vena cava, outside the inferior vena cava, and between both venae cava) and therefore to invade the atrial muscle (21). Despite the heterogeneity of these cells, along with the difference in their distribution across the SAN (cristae terminals vs atrial septum), there are unifying active electrical properties at the plasma membrane that support the pacing activity under normal circumstances. At the initial stages of cardiac development, all cardiac cells possess pacemaker activity, however, the majority develop into working myocardium and few cells form the conduction system of the heart (SAN, Atrioventricular node, and His-Purkinje fibers). This is achieved by localized and targeted repression of differentiation of specific genes that drive these cells into cardiac muscle *via* an interplay between different modulators of the transcription (example: Tbx5, Nkx-5, Tbx-2, Tb-3, and Id2) (22). A primordium SAN is shown as early as Embryonic (E) day 10.5 in mouse hearts (23). At this stage, SANCs are relatively poor in organelles and myofibrils compared to the other cardiomyocytes at E16 and E18 in mice, and they are characterized by a strikingly poor proliferative capacity at embryonic levels (compared with cardiomyocytes) (24). At birth, the pacing of the SAN overrides all other parts of the conduction system (Atrioventricular node and His-Purkinje fibers) and guarantees a heart rate of about 70-90 beats per min in healthy subjects. Heart rate variability (HRV) is tightly linked to changes in the activity of the SAN (intrinsic or extrinsic factors). With age, the decrease in the volume of nodal cells and SAN tissues, along with the development of fibrosis can result in dysfunction of the SAN (25, 26).

3 REGULATION OF SAN BY THE AUTONOMIC NERVOUS SYSTEM AND THE COUPLED-CLOCK SYSTEM

Under physiological conditions, HRV is regulated by two main signaling cascades: the autonomic nervous system (ANS) and the coupled-clock system within the SANCs (27). The involvement of the ANS implicates the brain as a modulator of the SANCs automaticity through a balanced control of G-protein-coupled receptors (GPCRs) from both ANS branches: the sympathetic and the parasympathetic nervous system (SNS and PNS). Stimulation of the sympathetic nervous system (SNS) increases HR while stimulation of the parasympathetic nervous system (PNS) decreases the HR (28, 29). Acetylcholine that is released upon PNS stimulation acts on muscarinic receptors (M2R) in the SAN of the human heart and reduces its rate of firing (29).

The sympathetic activation of the heart (adrenergic), *via* the release of its neurotransmitter norepinephrine (NE), leads to the activation of the β-adrenergic receptors (β-AR) expressed at the sarcolemma of SANCs, thus causing the activation of the β-AR cyclase. The β-AR pathway involves the activation of adenylyl cyclase (AC), *via* the stimulatory guanosine triphosphate (GTP) regulatory protein (Gs), which converts adenosine triphosphate (ATP) into adenosine 3′, 5′-monophosphate (cAMP), which in turn stimulates cAMP-dependent protein kinase A (PKA) (30). PKA is a central mediator of β-AR regulation of cardiac function. Subsequently, a multitude of target proteins including the ryanodine receptors (RyR) and the sarco-/endoplasmic reticulum Ca^{2+} ATPase (SERCA) Ca^{2+} pumps in the SAN are phosphorylated by PKA to evoke intracellular Ca^{2+} $[(Ca^{2+})_i]$ oscillations affecting currents through the Na^{+}/Ca^{2+} exchanger (NCX) (31). This surge of $[Ca^{2+}]_i$ ultimately increases the slope of the spontaneous diastolic depolarization (SDD) and consequently the heart rate (HR) (positive chronotropic effect) (32). There is increasing evidence that SAN pacemaker activity is subject to an intrinsic regulation by CaMKII *via* modulation of L-type Ca^{2+} currents ($I_{Ca,L}$)inactivation and reactivation (31, 33). Additionally, the hyperpolarization-activated cyclic nucleotide-gated (HCN) channel gene family is a key determinant of mechanisms underlying chronotropic effects of β-AR stimulation (34). HCN4 channels are the most prevalent in SAN. These channels are regulated by PKA and therefore they are involved in the auto-pacing activity of SAN, as well as in the autonomic modulation of the HR (35).

In contrast, the parasympathetic input represses the rhythm of SANCs through the release of acetylcholine (ACh) which reduces the production of cAMP in SANCs. More importantly, ACh activates the potassium channels driving the SANCs into the hyperpolarized state. This leads to a reduced slope of SDD and a decrease in HR (negative chronotropic effect) (36). Nonetheless, exposure of SAN cells to adrenaline or acetylcholine revealed a shift in the pacemaker locus across the SAN tissues, thus implying a different expression pattern of the effectors/signaling cascades (to these neurotransmitters) by SANCs and reinstating their heterogeneity (18).

Although debatable, the "coupled-clock" system is believed to regulate the automaticity of the SANCs (7). It comprises an ensemble of highly dynamic membranes: the surface membrane (Sarcolemma-SL) and the sarcoplasmic reticulum (SR) membrane. The SL and SR membranes express ion channels and transporters defining the membrane clock or "M clock" and "Ca^{2+} clock". Both clocks work interdependently but synergistically contribute to SDD, triggering the AP upstroke (37). The degree of the coupling between the "M" and the "Ca^{2+}" clocks delineates the normal pacemaker function (7).

Electrophysiological studies identified electrical currents that form the pacemaker AP in SANCs. The ionic currents defining the "M clock" include the funny current (I_f) carried by HCN channel (38), T-type (Cav3.1) calcium current ($I_{Ca,T}$) (39), L-type (Cav1.3 and Cav1.2) calcium currents ($I_{Ca,L}$) (40), sodium-calcium exchange current (I_{NCX}) (41), and rapid and slow delayed rectifier potassium currents ($I_{K,r}$ and $I_{K,s}$) (42, 43). Proteins defining the "Ca^{2+} clock" include RyR_2 (44) and SERCA (45).

In general, local diastolic Ca^{2+} releases (LCRs) from the SR occur rhythmically. This promotes the Na^{+}/Ca^{2+} exchange (NCX) current (I_{NCX}) to generate a local AP which subsequently spreads as a depolarization wave over the SANCs and the neighboring myocardium (46). It is believed that the Ca^{2+}-cAMP-PKA pathway is also involved in regulating the clock coupling (45). In fact, Ca^{2+} release stimulates both the CaMKII and PKA *via* Ca^{2+}-calmodulin activated ACs. These kinases phosphorylate the SL "M clock" proteins and the SR Ca^{2+} cycling proteins, which promotes SR Ca^{2+} release, thus further promoting the Ca^{2+} -calmodulin-activated ACs and CaMKII (32). It has been shown that withdrawal of β-AR stimulation uncouples the clocks, thus failing to generate a spontaneous AP in SANCs (45). Recently, Sirenko and colleagues reported that the inhibition of the phosphoprotein phosphatases (PP) increases the firing rate of APs *via* the coupled-clock mechanism, including respective increases in the SR Ca^{2+} pumping rate, $I_{Ca,L}$, and I_{NCX} (46).

4 SAN REMODELING AND DYSFUNCTION IN DIABETES

Diabetes mellitus (DM) is a global health problem that affects hundreds of millions of people worldwide (47). The chronic hyperglycemia seen in diabetes is precipitated due to abnormalities in insulin secretion, insulin action, or a combination of both in the form of insulin resistance. The prevalence worldwide ranges from around 5% to more than 15%. In the Middle East, the prevalence is reported to be among the highest in the world, with an average of 11.4% (48). The prevalence of cardiovascular risk factors is high among patients with diabetes and in those with earlier onset of the disease, where higher cardiovascular risks and poorer cardiovascular outcomes and mortality are seen (49). In fact, the leading cause of mortality among patients with diabetes is cardiovascular disease (50). Besides mechanical changes, alteration in the electrical function is another main characteristic of a diabetic heart.

Overall, metabolic abnormalities have been linked to a reduction in sympathetic activity and atypical SAN function (51, 52). This is mainly blamed on nerve growth factor production by adipocytes (53). Such release of growth factors can also account for the higher level of innervation seen in the nodal tissue (53). For example, the adipocyte-derived metabolic hormone leptin has also been suggested to be linked to the SAN function. Leptin receptor-deficient mice are at higher risk of developing arrhythmias due to a reduction in SAN recovery time and relative autonomic denervation (54). The SAN function has also been linked to metabolic changes through the role of free fatty acids (FFA) whereby the I_f current is upregulated by FFA and sympathetic innervation, which results in increasing intracellular Ca^{2+} level and I_{st} current (55, 56). Collectively,

these studies demonstrate that diabetes induces metabolism-mediated dysfunction of the SAN.

4.1 Effects of the Impaired Autonomic Nervous System on SAN Function in Diabetic Conditions

One of the most important determinants of cardiac function and performance is the HR, which is modulated by the intrinsic rhythmical firing of the SAN. DM is associated with significant cardiovascular complications and neuropathies (57, 58). The regulation of HR by the ANS has been shown to be impaired in diabetic patients (59, 60). This condition is referred to as cardiovascular autonomic neuropathy (CAN), one of the earliest manifestations of DM (59). Up to 90% of diabetic patients exhibit CAN, which is often accompanied by impairment of the nerves of the heart and possible damage to the PNS mechanisms regulating HR (59, 60). These findings are of crucial clinical significance since DM patients with CAN have increased mortality as compared to patients with DM who do not exhibit CAN (61).

In type 2 DM (T2DM), PNS activity is impaired (59, 62). In addition, in type 1 DM (T1DM), there is an impairment in the mechanisms regulating HR by PNS, and that this impairment is accompanied by a change in the response of the SAN to PNS agonists such as carbachol (CCh) (63, 64). The impaired PNS activity and CAN are demonstrated earlier in T2DM as compared to T1DM (59); however, the mechanisms that are involved in the impaired regulation of HR by PNS in T2DM are not completely understood. It appears that the cardiac autonomic dysfunction that is associated with T2DM is mainly caused by direct damage to the autonomic nerves themselves (59, 65, 66); however, a direct impairment of the SAN function with T2DM cannot be ruled out at this time.

It is important to note that screening diabetic patients for cardiac autonomic neuropathy is highly recommended, especially in those patients with a history of macrovascular or microvascular complications, increased cardiovascular risk, and poor glycemic control (67). While cardiovascular reflex tests are still standard of care, the measurement of HRV is one of the most convenient, pain-free ways to reliably assess the cardiac autonomic neuropathy (68, 69). HRV is defined as the variation between two consecutive heartbeats. A decrease in ANS function has been reported to precede the progression into hypertension (70). Higher HRV indicates higher parasympathetic activity and reflects better adaptations to microenvironmental changes (71), and low HRV is reported as a marker of increased cardiovascular risk (69, 72). Among the general population, increased systolic blood pressure, abdominal diameter, waist–hip ratio, and body mass index (BMI) have been associated with decreased HRV (73, 74). HRV was reported to be improved following weight loss (75). No substantial data is available on the relationship of these parameters in the diabetic state, and the present data on HRV among patients with diabetes is contradictory (76, 77). Nevertheless, it has been reported that HRV is reduced in T1DM youth patients (78).

4.2 Cellular and Molecular Changes Within the Diabetic SAN Tissue

Irrespective of the modality of diabetes (T1DM vs. T2DM), manifestations of the sympathetic and parasympathetic axes certainly precipitate variabilities in cardiac rhythm. Despite this direct modulation of the SAN by the ANS, the cellular, molecular, and structural changes within the SAN tissue in hyperglycemic conditions remain ill-defined.

Spontaneous and rhythmical APs are generated by the SANCs, the primary pacemaker of the heart. Under normal circumstances, these spontaneous APs, and the slow diastolic depolarization between successive APs, contribute to the determination of the intrinsic HR (29). The length of time between successive APs in the myocytes of the SAN is determined by the contributions of ionic currents that can affect the transition from the maximum diastolic potential (MDP) to the threshold and the initiation of the next AP. The ionic currents include the hyperpolarization-activated current or funny current (I_f), and a rapidly activating delayed rectifier K^+ currents (I_{Kr}) generated by ether-a-go-go (ERG) channels (7, 28, 79). The PNS reduces HR by activation of inhibitory G proteins associated with M2R and attenuating spontaneous firing of AP in SAN myocytes (58). While the primary pacemaker activity of the SAN is spontaneously generated, the rate of this activity and, therefore the HR, can be modified by factors such as ANS, hormones and neurotransmitters, medications, ions, hypoxia, as well as disease states.

In a recent study, Liu et al. (58) examined the effects of carbachol (CCh) on HR and SAN function in isolated SAN cardiomyocytes of male and female db/db mice, an animal model exhibiting features of T2DM. CCh showed an attenuated effect on slowing the spontaneous AP firing which was associated with a smaller decrease in the slope of diastolic depolarization and a reduced hyperpolarization of the MDP. CCh did not produce significant hyperpolarization in SAN cardiomyocytes isolated from male and female db/db mice (58). The results of this study provided some evidence for cellular and molecular mechanisms that might lead to the attenuated regulation of PNS on HR in T2DM (58). The acetylcholine-activated K^+ current (I_{KACh}) becomes desensitized and its amplitude diminishes in the presence of an M2R agonist such as CCh (80–82). This channel, I_{KACh}, which mediates the activation of PNS in the SAN, was found to exhibit increased desensitization and faster deactivation kinetics in the SAN of db/db mice, resulting in an attenuated effect of CCh on HR in these mice. Furthermore, the impaired I_{KACh} in SAN myocytes was attributed to altered G protein signaling 4 (RGS4) and phosphatidylinositol (3,4,5) P3 (PIP3) signaling. The authors concluded that their findings may identify new interventions that might benefit diabetic patients with CAN, and with attenuated ANS signaling to the SAN (58). In support of this contention, earlier studies have also shown that the kinetics of I_{KACh} are regulated by RGS4 and PIP3 signaling in the SAN (83). RGS4 is inhibited by PIP3 which is activated by insulin-mediated phosphoinositide-3 kinase (PI3K) signaling. Therefore, impaired insulin and PI3K signaling in T2DM

could result in enhanced RGS4 activity due to a loss of PIP3-mediated inhibition of RGS4 (84–86).

At the molecular level, the CaMKII pathway, known to maintain the pacemaker activity of SAN (33) is altered in diabetes and could lead to SAN anomalies. This is mainly achieved through the oxidation of CaMKII into ox-CaMKII which slows down the pacemaker activity of the SAN and promotes apoptosis of SANCs leading to high mortality in human and in experimentally diabetic animal models (33, 87, 88). In fact, inhibition of CaMKII oxidation (mice lacking active NADPH oxidase), or pharmacological inhibition of CaMKII concedes resistance to apoptosis and fibrosis for injured SAN (87). Furthermore, using antioxidants in streptozotocin (STZ)-treated rats successfully reversed this process (87–89).

In addition to CaMKII sustained activity, hyperglycemia furthers the production of detrimental ROS that damage the cells and induce apoptosis leading to reduced SAN function. High blood glucose levels in diabetes increases diacylglycerol (DAG) content that activates protein kinase C (PKC). This in turn phosphorylates NADPH-oxidase, leading to further production of ROS. Such inflammatory reactions may also be associated with the action of advanced glycation end products (AGEs), which interact with their respective receptors (RAGE) on the cell surfaces, to produce the proinflammatory cytokines. Collectively, these promote inflammation, oxidative stress, and cellular death (90).

In SAN, basal PKC activity is crucial for normal spontaneous SANC activity. In freshly isolated rabbit SANCs, inhibition of PKC suppressed SR Ca^{2+} cycling and the spontaneous beating of the cells. Normally, SANCs firing is regulated by local subsarcolemmal Ca^{2+} release from the SR. Such release takes place during the SDD and stimulates NCX leading to an increased rate of SDD and acceleration of spontaneous SANC activity (91).

The pathological remodeling of the SAN in diabetic conditions resembles the one noticed in the elderly, whereby nodal cells are atrophied and are surrounded by infiltrated fibrous tissues (25, 26) (**Figure 1**). This profoundly alters the electrical conduction between the SANCs. In fact, the diabetes-induced fibrosis in STZ-treated rats detrimentally reduces the conduction properties of SAN tissues, often depicted by a wider P wave on the ECG tracings (92, 93). In contrast, the remodeling of the SAN in obese rats is manifested by hypertrophied SANCs and enlarged SAN tissues (94). Moreover, in diabetic conditions, the adenosine receptor AR1 is upregulated in the heart (95). Functional analysis showed that the upregulation of AR1 promotes SAN dysfunction and nodal conduction abnormalities (96). Thus, the direct effect of diabetes on SAN safety cannot be simply ignored. In addition, the indirect effect of diabetes on SAN tissues exemplified by the hypoperfusion of the SAN by the coronary arteries, due to their pathological remodeling in hyperglycemic conditions, profoundly alters SAN function.

4.3 Insights on Ion Channels Dysfunction and Cytoskeletal Remodeling in Diabetic SAN

Disruption of cardiac electrical activity has been widely observed in the hearts of both T1DM and T2DM patients (97). For example, prolongation of QRS and QT segments (98), disturbance in automaticity of SAN, atrioventricular block, and left bundle branch block have been commonly reported (99–101). T2DM patients have a high risk of atrial fibrillation (102, 103), ventricular arrhythmia (104), and fibrillation (105).

Similarly, prolonged QRS and QT intervals have also been reported in animal studies on diabetes. In isolated perfused hearts of non-obese Goto-Kakizaki (GK) T2DM rats, spontaneous HR was lower compared to control rats. This

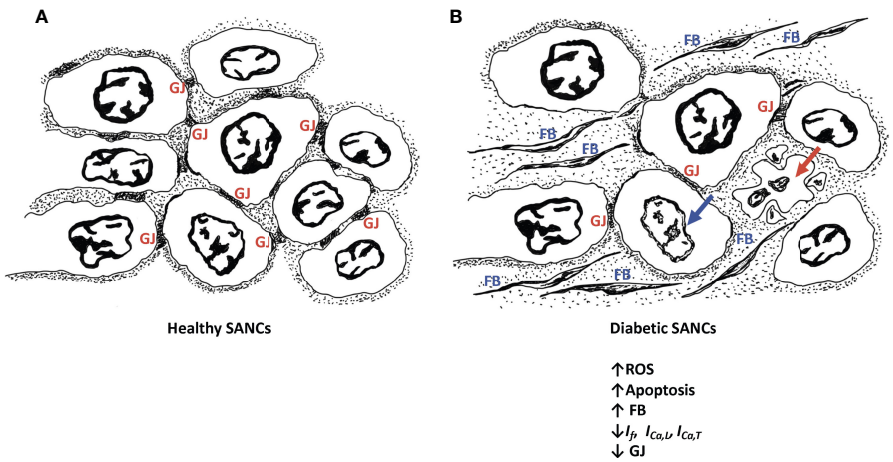

FIGURE 1 | Schematic diagram of healthy SANCs showing intact gap junctions (GJ) **(A)** and remodeling of the diabetic SANCs showing decreased GAP junctions, infiltration of fibrous tissues, and apoptosis of SANCs **(B)**. Red arrow represents cell apoptosis; blue arrow represents nuclear blebbing; GJs are characterized by altered expression of connexins. Fibroblasts (FB) are populating in the extracellular matrix.

observation implies that the changes are, at least in part, due to an intrinsic abnormality in the cardiac electrical conduction system (106). Although earlier studies in animal models have reported a profound decrease in HR and increased mortality in diabetic animals (106), reports on SAN remodeling in diabetes are limited. In STZ-treated diabetic rats, HR was found to be slower compared to controls. Furthermore, SAN conduction and pacemaker cycle length and time were prolonged (107). Recently, in a recent, in leptin-receptor deficient T2DM diabetic mice, disturbance of systolic and diastolic activity of the heart, prolongation of SAN recovery time and relative autonomic denervation were reported (54).

Structural and/or functional channelopathies are thought to play a role in the electrical abnormalities reported in the diabetic heart. At the cellular level, diabetes reduces the velocity of SAN conduction and the slope of SDD and prolongs the duration of cardiac AP which is attributed to the altered expression and electrophysiological properties of various ion channels (97, 108–110) (**Figure 2**).

4.3.1 SAN Ion Channels

As mentioned earlier, the pacemaker activity of the SAN is regulated by several ion channels that are thought to contribute to the SDD. Specifically, the pacemaker activity is determined by a net inward current caused by the deactivation of outward current ($I_{K,s}$) and the activation of inward currents, carried mainly by voltage-gated sodium channels (Nav1.5), hyperpolarization-activated cyclic nucleotide-gated channels (HCN), Cav3.1 channels and Cav1.3 channels (1, 12, 111). Therefore, disruption of one or more of these ion channels would alter the electrophysiological properties of the SAN. **Figure 3** shows the main ionic currents involved in the AP of SANCs.

4.3.1.1 Voltage Gated Sodium Channel (Nav1.5)

The voltage-gated sodium channel (Nav1.5) is predominantly expressed in the heart and governs the upstroke of the AP in the atrial and ventricular cells (112). However, its expression and distribution in the SAN tissues remain debatable. While studies showed the presence of the Nav1.5 in SAN tissues, others

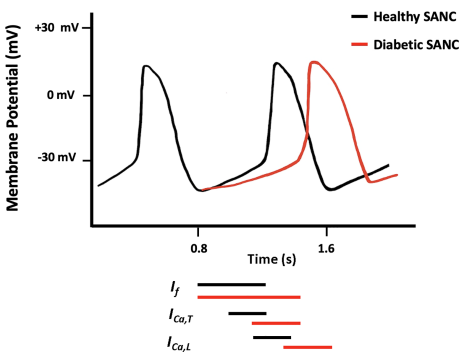

FIGURE 2 | Schematic diagram showing action potential (AP) pattern of SANCs in control (black) and diabetic (red) SAN.

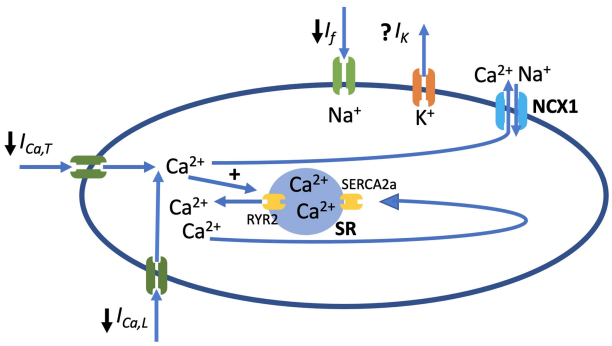

FIGURE 3 | Schematic diagram of SANC showing main ion channels that play a role in AP generation and along with ryanodine receptor 2 (RyR2), the sarcoplasmic reticulum (SR) calcium pump (SERCA2a) and the Na^+/Ca^{2+} exchanger (NCX1). ↓ represents the currents that play a main role in generation of AP and are inhibited in diabetes. I_f, funny current; $I_{Ca,T}$, current conducted by T-type voltage-gated Ca^{2+} channel; $I_{Ca,L}$, current conducted by L-type voltage-gated Ca^{2+} channel.

indicated that they are mainly expressed at the periphery but absent from the center of the SAN (113). Moreover, developmental studies showed that this particular isoform of the sodium channel is highly expressed at an early stage during development, and its expression is reduced later on when the heart adopts a slower rate of contraction (114). From the functional point of view, while studies showed an implication of Nav1.5 in the conduction of SANCs (115), others indicated that Nav1.5 rescues the pacing activity of SANs in hyperpolarization conditions (114).

In heterozygous knockout mice Nav1.5$^{+/-}$, delayed conduction and arrhythmia were reported (116). In alloxan-induced diabetic rabbits, the protein level of Nav1.5 and the density of I_{Na} in the ventricle were significantly reduced (117). In agreement with this finding, Zhang et al. found that Nav1.5 was significantly decreased in the left atrium and right ventricle by 33% and 37%, respectively (118). However, Ferdous, et al. (2016) showed an upregulation of the gene encoding Nav1.5 in the SAN of STZ diabetic heart compared to normal (107). Such change in the expression of Nav1.5 could be an important determinant for arrhythmogenesis observed in diabetes. Furthermore, increased production of ROS in diabetic hearts, which is known to modify the properties of Na^+ channels, could also contribute to the impaired SAN function in diabetes (119, 120).

4.3.1.2 Hyperpolarization-Activated Cyclic Nucleotide-Gated Channel

HCN channel conducts the hyperpolarization current (funny current; I_f). The channel activity is responsible for the spontaneous diastolic membrane depolarization of the SANCs and therefore the generation of spontaneous SAN AP. The channel is a tetramer that is composed of four HCN subunits that are made of six transmembrane segments. Although four HCN gene family members (HCN1, HCN2, HCN3 and HCN4) have been found in the heart, HCN4 is the prominent HCN in human SAN (121).

The HCN channel is modulated by cAMP (122). Specifically, the activity of the channel rises with the increase in intracellular concentrations of cAMP, which binds to the C-terminus of the channel (123). While cAMP activates the channel, muscarinic agonists inhibit the inward current at diastolic potentials by shifting the activation curve to more negative values (124). It is believed that regulation of HCN4 by cAMP in the heart is essential for HR modulation by the ANS. While cAMP-dependent increase in HCN4 activity is needed for the acceleration of the HR under ANS stimulation, a drop in the levels of cAMP following vagal stimulation lessens HCN4 activity and decreases HR (28, 123).

Studies in animal models have reported that SANCs from knockout mice lacking HCN4 have a parallel decrease of 75% in I_f (125). In STZ T1DM, altered mRNA expression of HCN4 channels was reported (107). In support of this finding, a recent study conducted by Zhang et al. (2019) has shown a significant disturbance in the ECG characteristics of STZ-treated diabetic rats. This change was marked by prolongation of the PR interval, RR interval, QT interval and QRS complex. In addition, the beating rate of SAN was slower compared to control. Electrophysiological experiments showed that blocking of HCN4 channels with CsCl resulted in reduction of the beating rate of rat SAN preparations, indicating that HCN4 channels play a vital role in sustaining the spontaneous pacemaker activity. Along with the downregulation of HCN4 in the SAN, I_f was significantly reduced which could explain the observed reduction in SAN function (118).

Similarly, altered expression of HCN4 was reported in T2DM animals. *In vivo* experiments conducted in GK diabetic rats have shown that a decrease in the HR of young animals was coupled to downregulation of the expression of HCN4 gene (126). It is important to note that downregulation of HCN4 and I_f might be partly responsible for bradyarrhythmia observed in diabetic patients (127).

Although elevated ROS is a consistent finding in cardiovascular complications of diabetes, data on defined molecular targets and pathways that connect increased oxidation with SAN function are very limited. In sick sinus syndrome, mitochondrial oxidative stress was found to induce HCN4 downregulation (128). A recent study found that this effect involves the inhibition of mitochondrial thioredoxin-2, an important ROS scavenger that regulates the mitochondrial apoptosis signaling pathway. Indeed, the deletion of thioredoxin-2 in the whole mouse heart caused dilated cardiomyopathy, atrioventricular block and sinus bradycardia. The mice also displayed reduced expression of HCN4 in SANCs and typical electrophysiological signs of sick sinus syndrome (129).

4.3.1.3 T-Type Voltage-Gated Ca^{2+} Channel (Cav3.1)

The T-type voltage-gated Ca^{2+} channel plays a key role in cell excitation and Ca^{2+} handling in the heart. Three types of T-type Ca^{2+} channels were cloned; Cav3.1 (α1G), $Ca_v3.2$ (α1H) and $Ca_v3.3$ (α1I) (130). The Cav3.1 is highly expressed in the SAN and atrioventricular node, while it is poorly expressed in the myocardium. Cav3.1 contributes to the total Ca^{2+} current in the SAN. It was found to play a vital role in pace-making and impulse conduction in both mice and humans (131). The current generated by Cav3.1($I_{Ca,T}$) is marked by delayed activation at voltages expanding over the diastolic depolarization phase, and rapid inactivation (132). It was reported that mice deficient in Cav3.1 had slower SAN recovery time, decelerated pacemaker activity of SAN and HR, and delayed atrioventricular conduction. These findings show that Cav3.1 is a major contributor to the generation of cardiac rhythmicity (132). An earlier study demonstrated that $I_{Ca,T}$ of mouse SAN is activated by isoproterenol in a PKA-dependent manner; however, the physiological role of adrenergic control of $I_{Ca,T}$is not well-understood (130).

Studies on the expression of Cav3.1 in diabetic animals reported conflicting results. Ferdous et al. (2016) have shown that in the SAN of STZ diabetic rats, mRNA expression of Cav3.1 is upregulated (107). In agreement with this finding, earlier studies have reported upregulation of Cav3.1 in the ventricle from the GK and the Zucker diabetic fatty rat (133, 134). It is expected that the upregulation of Cav3.1 upsurges T-type Ca^{2+} current and, consequently the slope of the pacemaker potential and HR in STZ rats. In contrast and in a more recent study, it has been shown that the expression of Cav3.1 gene is downregulated by three folds in GK rats. As a result, reductions in pacemaker activity and the slope of diastolic depolarization are expected (126, 132).

4.3.1.4 L-Type Voltage-Gated Ca^{2+} Channel (Cav1.3)

Two types of L-type voltage-gated Ca^{2+} channels, namely Cav1.2 and Cav1.3 are expressed in the heart; however, Cav1.3 is predominantly expressed in the SAN and atrioventricular node. In SAN, Cav1.3 not only contributes to the pacemaker activity but also to the initiation of diastolic depolarization and regulation of Ca^{2+} release from SR during SAN pacemaker activity (135, 136). Evidence shows that downregulation of the Cav1.3 gene in mice causes a reduction in pacemaker activity and causes spontaneous arrhythmia in SANCs (135).

Experiments in isolated perfused hearts of STZ diabetic animals have shown that decreased HR and prolonged SAN AP were associated with a significant decrease (32%) in the expression of Cav1.3 gene in diabetic SAN compared to control SAN (118). Previous studies have shown that deletion of the channel ($Cav1.3^{-/-}$) caused the prolongation of the PR interval and the complete block of the atrioventricular conduction (137). As a result, downregulation of Cav1.3 could be a source of bradyarrhythmia and heart block in patients with T1DM. In GK diabetic rats, SAN Cav1.3 was also downregulated (126). This reduction in $I_{Ca,T}$ observed in diabetes may be attributed to the change in the activation/inactivation kinetics of the channels, the expression of the channel proteins, or the change in the single-channel conductance. Although several studies have investigated the effect of diabetes on such electrophysiological properties in ventricular myocytes, the data on SAN Cav1.3 is scarce (138).

An earlier study examined the effect of CaMKII on SAN spontaneous excitation and modulation of $I_{Ca,L}$ in freshly isolated rabbit single SANCs. It was found that inhibition of CaMKII can completely arrest SANCs largely as a result of

depressed $I_{Ca,\ L}$ amplitude, reduced window current, and slowed recovery of L-type Ca^{2+} channels from inactivation. This finding shows a key role of CaMKII in regulating cardiac pacemaker activity (33).

4.3.2 SAN Cytoskeletal Proteins

Cytoskeleton proteins support cell shape, elasticity, and contractility. For example, collagen I is an extracellular protein that provides a structural framework to the cardiac myocytes, stiffness to the myocardial wall, and assists in force transmission (139). Therefore, changes in the level of expression of this protein affects the conduction properties in the heart, thus promoting arrhythmogenesis. In fact, several studies have shown that collagen I is overexpressed in diabetic rat hearts, which would contribute to the decreased ventricular compliance (140). A recent study in STZ diabetic rats has shown an increase in the level of collagen I expression throughout the conduction system in the heart including the SAN (118).

Caveolin-3 is a structural and regulatory protein that modulates the function of ion channels, including those involved in pace-making (141). Mutations in the gene encoding caveolin-3 have been linked to several cardiac diseases such as long QT syndrome, myocardial hypertrophy, and diabetic cardiomyopathy (142, 143). SAN cells are rich in caveolin-3 protein (144). Studies have shown that caveolin-3 co-localizes with HCN4 channel and affects its function (145). The expression of caveolin-3 mutant modifies the gating properties of HCN4 channels by causing a rightward shift in the activation curve (146). Furthermore, when caveolae are disturbed in the SAN, β2-adrenergic receptor regulation of HCN4 channel was found to be lost (145). In spontaneously beating neonatal cardiac cells, the T78M mutation of the caveolin-3 gene significantly enhanced peak-to-peak AP variability linked to rightward shift of activation potential of HCN4 channels (147). In support of the vital role of Caveolin-3 in SAN function, Lang et al. (2016) found that in caveolin-3 knockout mice, heart rate fluctuation with altering periods of bradycardia-tachycardia rhythm was observed. Such change was linked to the disturbance of SAN function (144). In chronic STZ-induced diabetic rats, lower expression of caveolin-3 was detected (148, 149).

PKC-β2 is known to be overexpressed in the diabetic heart and contributes to cardiomyocyte hypertrophy in diabetes. Interestingly, impairment in caveolin-3 expression was found to be one of the underlying mechanisms for cardiac dysfunction that is linked to hyperglycemia-induced PKC-β2 activation (150). Therefore, it is expected that changes in the expression of caveolin-3 in any region in the heart may contribute to the pathogenesis of diabetic cardiomyopathy. However, data on the altered expression of caveolin-3 in the SAN of diabetic rats is scarce. In addition, α-actinin is another structural protein involved in maintaining cell shape and contractility. A significant decrease in the expression of α-actinin was observed throughout the heart regions but not in the diabetic SAN (118).

A hallmark of cell-to-cell coupling is the gap junction at the intercalated discs, forming macrochannels for effective transmission and propagation of the AP between cardiac cells. The expression and distribution of the different variants of connexins-Cx (the proteins forming gap junctions) is specific to each different area of the SAN (151). While Cx40, Cx45, and Cx46 are abundantly distributed in the central area of the SAN, Cx43 is almost non-existent in this tissue (12). The heterogeneity of the expression of these Gap junction proteins explains the distinctiveness of conduction through the SAN. Of interest, one of the striking remodeling features in diabetic cardiomyopathy is the persistently reduced transmission of the AP through gap junctions. In fact, the function of Cx43, which is predominantly expressed in the working myocardium, depends on tyrosine phosphorylation. Both the expression/distribution and phosphorylation of Cx43 are altered in diabetic hearts, leading to reduced impulse propagation which increases the risk for the development of fibrillation (152, 153). In SAN from diabetic animal models, the expression of Cx40, Cx43, and Cx45 is still controversial. Howarth et al. (2007) showed a moderate increase of these connexins in the SAN of the STZ-treated rats (154). However, Ferdous et al. (2016) reported an increase in the mRNA of Cx45 in the SAN of STZ-treated rats, without a significant change in the expression pattern of the Cx40 and Cx43 (107). The literature falls short on the implication of Cx40 and Cx45 in the electrical remodeling of the diabetic SAN, the slow conductance of the AP, and consequently cardiac rhythm. This warrants extensive investigation to fill this gap in the literature and to help stabilize cardiac rhythm in diabetic conditions.

4.4 Electrophysiological Effects of Anti-Diabetic Drugs on SAN Currents

While few studies indicate that anti-diabetic drugs significantly protect the cardiovascular system, other controversial reports conclude that anti-diabetic medicine is far from reversing the cardiac complications manifested in diabetic settings (155). For example, Metformin, a medicine used to treat T2DM, stimulates the 5′ adenosine monophosphate-activated protein kinase (AMPK) signaling pathway, which consequently stimulates the ATP-sensitive potassium channels (K_{ATP}) involved in the control of HR (156). In the same vein, the activation of AMPK contributes to the maintenance of the $I_{Ca,L}$, the $I_{Ca,L}$- triggered Ca^{2+} transients amplitude, the Ca^{2+} content, and promotes cell contraction (157).

Rosiglitazone, the thiazolidinedione class of anti-diabetic drugs, acts to inhibit K_{ATP} channels in the pancreatic β-cells (158). Inhibition of these channels by high levels of ATP causes membrane depolarization, Ca^{2+} influx through voltage-gated Ca^{2+} channels and Ca^{2+} -dependent secretion of insulin; thus inhibition of pancreatic K_{ATP} channels prevents insulin secretion (159). Conversely, the blockade of the cardiac isoform of the K_{ATP} channel ($K_{IR}6.2/SUR2A$) severely compromises the cardiac ability to cope with ischemic assaults (158, 160–162), implying that the K_{ATP} of SANCs would be tremendously altered in diabetic patients on Rosiglitazone treatment. However, existing studies do not provide confirmatory information on the role of anti-diabetic drugs on the AP of SANCs. This field warrants further investigations.

While insulin remains an ultimate treatment for a large group of diabetic patients, its effect on the electrophysiological properties of cardiac cells remains inexplicit. However, few studies highlighted an implication of insulin in the electrical

activity of cardiac myocytes. For example, in myocytes isolated from T1DM diabetic hearts, the main affected repolarizing current is the I_{to} (138). In an earlier report (1999), Shimoni and colleagues have shown that insulin treatment of isolated ventricular myocytes from STZ diabetic rats reverses the depression of ventricular K^+ currents (163). Moreover, insulin mediates its effect through insulin receptors and the cAMP-dependent PKA to stimulate $I_{Ca,L}$ in isolated rat ventricular myocytes in a dose-dependent and reversible manner (164). Interestingly, insulin may also play a role in both the "M" and "Ca^{2+}" clock systems by stimulating Ca^{2+}-ATPase activity at the SR and the SL, and by increasing the Na^+/Ca^{2+} exchange activity (164).

It is noticed that in insulin-resistant cardiac tissues, the normal rise in a calcium-independent sustained K^+ current is either reduced or eradicated (165). The addition of insulin to myocytes isolated from insulin-resistant rats, treated with metformin (an insulin-sensitizing drug), produced a very significant enhancement of sustained K^+ current (165). Thus, Metformin modulates the insulin resistance effect observed for cardiac K^+ current which implies that these changes may also occur at the SAN level. In addition, both acute and chronic insulin treatment improved sodium currents in the atrial muscle of T1DM Atika mice by promoting the electrical properties of the Nav1.5 channel and by increasing its expression. This stabilization effect of insulin on atrial fibrillation could probably be stretched on SAN tissues since they express the Nav1.5 channel, and since arrhythmic SANCs are a hallmark of diabetes in animal models (54, 166).

5 CONCLUSION AND FUTURE PERSPECTIVES

Despite its primordial role in generating the AP waves that drive cardiac contractions, the dynamics of the SAN in diabetic settings remain ill-defined. It is clear that hyperglycemia modulates the expression/function of the ion channels underlying the electrical properties of the SANCs. This is manifested by repression of the currents involved in the upstroke of the AP and the conduction of SAN tissues. Chronic anti-diabetes treatments (metformin, insulin, rosiglitazone) adversely affect the SAN and, consequently, cardiac function. This is in addition to the structural/functional changes that underscore diabetic cardiomyopathy (working myocardium and other parts of the conduction system, i.e., the atrioventricular node and Purkinje fibers). Although various animal models are now established to study diabetes, the literature falls short on the synergy of the SAN during this metabolic syndrome. This includes a gap in the knowledge on the structural remodeling of SAN in diabetes as well as the metabolic changes induced by diabetes in the SANC. This calls for more investigations focused on the molecular signature of diabetes-induced SAN dysfunction to build an informative platform that links the clinical aspect of SAN failure with diabetes, and to provide a safer therapeutic approach for this metabolic disorder of the cardiac pacemaker. The advent of live imaging and optical mapping provides unique tools to study the metabolic and electrical changes in human diabetic SANCs. An alternative and more attractive approach would be a targeted therapy (pharmacological or genetic) of the SAN in diabetic subjects to warrant normal pacemaker activity and typical cardiac function. The different modalities of diabetic SAN injuries showcased herein must be carefully considered in the field of biological SAN engineering to develop a diabetes-resistant SAN for patients with diabetes.

AUTHOR CONTRIBUTIONS

LTA and MN: Conceptualization of the manuscript. LTA, SC, EA, AAK, MN: Writing the original manuscript and editing. All authors contributed to the article and approved the submitted version.

REFERENCES

1. Monfredi O, Dobrzynski H, Mondal T, Boyett MR, Morris GM. The Anatomy and Physiology of the Sinoatrial Node–a Contemporary Review. *Pacing Clin Electrophysiol* (2010) 33(11):1392–406. doi: 10.1111/j.1540-8159.2010.02838.x
2. Dobrzynski H, Boyett MR, Anderson RH. New Insights into Pacemaker Activity: Promoting Understanding of Sick Sinus Syndrome. *Circulation* (2007) 115(14):1921–32. doi: 10.1161/CIRCULATIONAHA.106.616011
3. Keith A, Flack M. The Form and Nature of the Muscular Connections between the Primary Divisions of the Vertebrate Heart. *J Anat Physiol* (1907) 41(Pt 3):172–89.
4. Sanchez-Quintana D, Cabrera JA, Farre J, Climent V, Anderson RH, Ho SY. Sinus Node Revisited in the Era of Electroanatomical Mapping and Catheter Ablation. *Heart* (2005) 91(2):189–94. doi: 10.1136/hrt.2003.031542
5. Matsuyama TA, Inoue S, Kobayashi Y, Sakai T, Saito T, Katagiri T, et al. Anatomical Diversity and Age-Related Histological Changes in the Human Right Atrial Posterolateral Wall. *Europace* (2004) 6(4):307–15. doi: 10.1016/j.eupc.2004.03.011
6. Efimov IR, Fedorov VV, Joung B, Lin SF. Mapping Cardiac Pacemaker Circuits: Methodological Puzzles of the Sinoatrial Node Optical Mapping. *Circ Res* (2010) 106(2):255–71. doi: 10.1161/CIRCRESAHA.109.209841
7. Lakatta EG, Maltsev VA. Vinogradova TM. A Coupled System of Intracellular Ca2+ Clocks and Surface Membrane Voltage Clocks Controls the Timekeeping Mechanism of the Heart's Pacemaker. *Circ Res* (2010) 106(4):659–73. doi: 10.1161/CIRCRESAHA.109.206078
8. Aziz Q, Li Y, Tinker A. Potassium Channels in the Sinoatrial Node and Their Role in Heart Rate Control. *Channels (Austin)* (2018) 12(1):356–66. doi: 10.1080/19336950.2018.1532255
9. Verkerk AO, Wilders R, van Borren MM, Peters RJ, Broekhuis E, Lam K, et al. Pacemaker Current (I(F)) in the Human Sinoatrial Node. *Eur Heart J* (2007) 28(20):2472–8. doi: 10.1093/eurheartj/ehm339
10. Verheijck EE, van Ginneken AC, Wilders R, Bouman LN. Contribution of L-Type Ca2+ Current to Electrical Activity in Sinoatrial Nodal Myocytes of Rabbits. *Am J Physiol* (1999). doi: 10.1152/ajpheart.1999.276.3.H1064
11. Csepe TA, Zhao J, Hansen BJ, Li N, Sul LV, Lim P, et al. Human Sinoatrial Node Structure: 3d Microanatomy of Sinoatrial Conduction Pathways. *Prog Biophys Mol Biol* (2016) 120(1-3):164–78. doi: 10.1016/j.pbiomolbio.2015.12.011

12. Boyett MR, Honjo H, Kodama I. The Sinoatrial Node, a Heterogeneous Pacemaker Structure. *Cardiovasc Res* (2000) 47(4):658–87. doi: 10.1016/s0008-6363(00)00135-8
13. Bartos DC, Grandi E, Ripplinger CM. Ion Channels in the Heart. *Compr Physiol* (2015) 5(3):1423–64. doi: 10.1002/cphy.c140069
14. Busquet J, Fontan F, Anderson RH, Ho SY, Davies MJ. The Surgical Significance of the Atrial Branches of the Coronary Arteries. *Int J Cardiol* (1984) 6(2):223–36. doi: 10.1016/0167-5273(84)90357-7
15. Ramanathan L, Shetty P, Nayak SR, Krishnamurthy A, Chettiar GK, Chockalingam A. Origin of the Sinoatrial and Atrioventricular Nodal Arteries in South Indians: An Angiographic Study. *Arq Bras Cardiol* (2009) 92(5):314–9. doi: 10.1590/s0066-782x2009000500002
16. Saremi F, Abolhoda A, Ashikyan O, Milliken JC, Narula J, Gurudevan SV, et al. Arterial Supply to Sinuatrial and Atrioventricular Nodes: Imaging with Multidetector Ct. *Radiology* (2008) 246(1):99–107. doi: 10.1148/radiol.2461070030
17. Zhou B. Sinoatrial Node Pacemaker Cells: Cardiomyocyte- or Neuron-Like Cells? *Protein Cell* (2021) 12(7):518–9. doi: 10.1007/s13238-021-00827-w
18. Mackaay AJ, Op't Hof T, Bleeker WK, Jongsma HJ, Bouman LN. Interaction of Adrenaline and Acetylcholine on Cardiac Pacemaker Function. Functional Inhomogeneity of the Rabbit Sinus Node. *J Pharmacol Exp Ther* (1980) 214(2):417–22.
19. Unudurthi SD, Wolf RM, Hund TJ. Role of Sinoatrial Node Architecture in Maintaining a Balanced Source-Sink Relationship and Synchronous Cardiac Pacemaking. *Front Physiol* (2014) 5:446. doi: 10.3389/fphys.2014.00446
20. Balbi T, Ghimenton C, Pasquinelli G, Foroni L, Grillini M, Pierini G. Advancement in the Examination of the Human Cardiac Sinus Node: An Unexpected Architecture and a Novel Cell Type Could Interest the Forensic Science. *Am J Forensic Med Pathol* (2011) 32(2):112–8. doi: 10.1097/PAF.0b013e3181ce9f23
21. Sano T, Yamagishi S. Spread of Excitation from the Sinus Node. *Circ Res* (1965) 16:423–30. doi: 10.1161/01.res.16.5.423
22. Christoffels VM, Moorman AF. Development of the Cardiac Conduction System: Why Are Some Regions of the Heart More Arrhythmogenic Than Others? *Circ Arrhythm Electrophysiol* (2009) 2(2):195–207. doi: 10.1161/CIRCEP.108.829341
23. Yi T, Wong J, Feller E, Sink S, Taghli-Lamallem O, Wen J, et al. Electrophysiological Mapping of Embryonic Mouse Hearts: Mechanisms for Developmental Pacemaker Switch and Internodal Conduction Pathway. *J Cardiovasc Electrophysiol* (2012) 23(3):309–18. doi: 10.1111/j.1540-8167.2011.02191.x
24. Erokhina IL, Rumyantsev PP. Ultrastructure of DNA-Synthesizing and Mitotically Dividing Myocytes in Sinoatrial Node of Mouse Embryonal Heart. *J Mol Cell Cardiol* (1986) 18(12):1219–31. doi: 10.1016/s0022-2828(86)80426-6
25. Shiraishi I, Takamatsu T, Minamikawa T, Onouchi Z, Fujita S. Quantitative Histological Analysis of the Human Sinoatrial Node During Growth and Aging. *Circulation* (1992) 85(6):2176–84. doi: 10.1161/01.cir.85.6.2176
26. Thery C, Gosselin B, Lekieffre J, Warembourg H. Pathology of Sinoatrial Node. Correlations with Electrocardiographic Findings in 111 Patients. *Am Heart J* (1977) 93(6):735–40. doi: 10.1016/s0002-8703(77)80070-7
27. Rosenberg AA, Weiser-Bitoun I, Billman GE, Yaniv Y. Signatures of the Autonomic Nervous System and the Heart's Pacemaker Cells in Canine Electrocardiograms and Their Applications to Humans. *Sci Rep* (2020) 10(1):9971. doi: 10.1038/s41598-020-66709-z
28. Mangoni ME, Nargeot J. Genesis and Regulation of the Heart Automaticity. *Physiol Rev* (2008) 88(3):919–82. doi: 10.1152/physrev.00018.2007
29. MacDonald EA, Rose RA, Quinn TA. Neurohumoral Control of Sinoatrial Node Activity and Heart Rate: Insight from Experimental Models and Findings from Humans. *Front Physiol* (2020) 11:170. doi: 10.3389/fphys.2020.00170
30. Larsson PH. How Is the Heart Rate Regulated in the Sinoatrial Node? Another Piece to the Puzzle. *J Gen Physiol* (2010) 136(3):237–41.
31. Grimm M, Brown JH. Beta-Adrenergic Receptor Signaling in the Heart: Role of Camkii. *J Mol Cell Cardiol* (2010) 48(2):322–30. doi: 10.1016/j.yjmcc.2009.10.016
32. Behar J, Ganesan A, Zhang J, Yaniv Y. The Autonomic Nervous System Regulates the Heart Rate through Camp-Pka Dependent and Independent Coupled-Clock Pacemaker Cell Mechanisms. *Front Physiol* (2016) 7:419. doi: 10.3389/fphys.2016.00419
33. Vinogradova TM, Zhou YY, Bogdanov KY, Yang D, Kuschel M, Cheng H, et al. Sinoatrial Node Pacemaker Activity Requires Ca(2+)/Calmodulin-Dependent Protein Kinase Ii Activation. *Circ Res* (2000) 87(9):760–7. doi: 10.1161/01.res.87.9.760
34. Wahl-Schott C, Fenske S, Biel M. Hcn Channels: New Roles in Sinoatrial Node Function. *Curr Opin Pharmacol* (2014) 15:83–90. doi: 10.1016/j.coph.2013.12.005
35. Liao Z, Lockhead D, Larson ED, Proenza C. Phosphorylation and Modulation of Hyperpolarization-Activated Hcn4 Channels by Protein Kinase a in the Mouse Sinoatrial Node. *J Gen Physiol* (2010) 136(3):247–58. doi: 10.1085/jgp.201010488
36. Hennis K, Biel M, Wahl-Schott C, Fenske S. Beyond Pacemaking: Hcn Channels in Sinoatrial Node Function. *Prog Biophys Mol Biol* (2021) 166:51–60. doi: 10.1016/j.pbiomolbio.2021.03.004
37. Yaniv Y, Lakatta EG, Maltsev VA. From Two Competing Oscillators to One Coupled-Clock Pacemaker Cell System. *Front Physiol* (2015) 6:28. doi: 10.3389/fphys.2015.00028
38. Di Francesco D. A New Interpretation of the Pace-Maker Current in Calf Purkinje Fibres. *J Physiol* (1981) 314:359–76. doi: 10.1113/jphysiol.1981.sp013713
39. Hagiwara N, Irisawa H, Kameyama M. Contribution of Two Types of Calcium Currents to the Pacemaker Potentials of Rabbit Sino-Atrial Node Cells. *J Physiol* (1988) 395:233–53. doi: 10.1113/jphysiol.1988.sp016916
40. Marionneau C, Couette B, Liu J, Li H, Mangoni ME, Nargeot J, et al. Specific Pattern of Ionic Channel Gene Expression Associated with Pacemaker Activity in the Mouse Heart. *J Physiol* (2005) 562(Pt 1):223–34. doi: 10.1113/jphysiol.2004.074047
41. Sanders L, Rakovic S, Lowe M, Mattick PA, Terrar DA. Fundamental Importance of Na+-Ca2+ Exchange for the Pacemaking Mechanism in Guinea-Pig Sino-Atrial Node. *J Physiol* (2006) 571(Pt 3):639–49. doi: 10.1113/jphysiol.2005.100305
42. Shibasaki T. Conductance and Kinetics of Delayed Rectifier Potassium Channels in Nodal Cells of the Rabbit Heart. *J Physiol* (1987) 387:227–50. doi: 10.1113/jphysiol.1987.sp016571
43. Sanguinetti MC, Jurkiewicz NK. Two Components of Cardiac Delayed Rectifier K+ Current. Differential Sensitivity to Block by Class Iii Antiarrhythmic Agents. *J Gen Physiol* (1990) 96(1):195–215. doi: 10.1085/jgp.96.1.195
44. Rigg L, Heath BM, Cui Y, Terrar DA. Localisation and Functional Significance of Ryanodine Receptors During Beta-Adrenoceptor Stimulation in the Guinea-Pig Sino-Atrial Node. *Cardiovasc Res* (2000) 48(2):254–64. doi: 10.1016/s0008-6363(00)00153-x
45. Tsutsui K, Monfredi OJ, Sirenko-Tagirova SG, Maltseva LA, Bychkov R, Kim MS, et al. A Coupled-Clock System Drives the Automaticity of Human Sinoatrial Nodal Pacemaker Cells. *Sci Signal* (2018) 11(534):1–27. doi: 10.1126/scisignal.aap7608
46. Sirenko ST, Zahanich I, Li Y, Lukyanenko YO, Lyashkov AE, Ziman BD, et al. Phosphoprotein Phosphatase 1 but Not 2a Activity Modulates Coupled-Clock Mechanisms to Impact on Intrinsic Automaticity of Sinoatrial Nodal Pacemaker Cells. *Cells* (2021) 10(11):1–21. doi: 10.3390/cells10113106
47. Boles A, Kandimalla R, Reddy PH. Dynamics of Diabetes and Obesity: Epidemiological Perspective. *Biochim Biophys Acta Mol Basis Dis* (2017) 1863(5):1026–36. doi: 10.1016/j.bbadis.2017.01.016
48. Atlas ID. Diabetes around the World in 2021. In: *International Diabetes Federation 10th Edition*.
49. Pastore I, Bolla AM, Montefusco L, Lunati ME, Rossi A, Assi E, et al. The Impact of Diabetes Mellitus on Cardiovascular Risk Onset in Children and Adolescents. *Int J Mol Sci* (2020) 21(14):1–17. doi: 10.3390/ijms21144928
50. Tancredi M, Rosengren A, Svensson AM, Kosiborod M, Pivodic A, Gudbjornsdottir S, et al. Excess Mortality among Persons with Type 2 Diabetes. *N Engl J Med* (2015) 373(18):1720–32. doi: 10.1056/NEJMoa1504347
51. Assoumou HG, Pichot V, Barthelemy JC, Dauphinot V, Celle S, Gosse P, et al. Metabolic Syndrome and Short-Term and Long-Term Heart Rate Variability in Elderly Free of Clinical Cardiovascular Disease: The Proof Study. *Rejuvenation Res* (2010) 13(6):653–63. doi: 10.1089/rej.2010.1019

52. Lin YK, Chen YJ, Chen SA. Potential Atrial Arrhythmogenicity of Adipocytes: Implications for the Genesis of Atrial Fibrillation. *Med Hypotheses* (2010) 74(6):1026–9. doi: 10.1016/j.mehy.2010.01.004
53. Sornelli F, Fiore M, Chaldakov GN, Aloe L. Adipose Tissue-Derived Nerve Growth Factor and Brain-Derived Neurotrophic Factor: Results from Experimental Stress and Diabetes. *Gen Physiol Biophys* (2009) 28:179–83.
54. Soltysinska E, Speerschneider T, Winther SV, Thomsen MB. Sinoatrial Node Dysfunction Induces Cardiac Arrhythmias in Diabetic Mice. *Cardiovasc Diabetol* (2014) 13:122. doi: 10.1186/s12933-014-0122-y
55. Vinogradova TM, Bogdanov KY, Lakatta EG. Beta-Adrenergic Stimulation Modulates Ryanodine Receptor Ca(2+) Release During Diastolic Depolarization to Accelerate Pacemaker Activity in Rabbit Sinoatrial Nodal Cells. *Circ Res* (2002) 90(1):73–9. doi: 10.1161/hh0102.102271
56. Deng W, Bukiya AN, Rodriguez-Menchaca AA, Zhang Z, Baumgarten CM, Logothetis DE, et al. Hypercholesterolemia Induces up-Regulation of Kach Cardiac Currents*Via* a Mechanism Independent of Phosphatidylinositol 4,5-Bisphosphate and Gbetagamma. *J Biol Chem* (2012) 287(7):4925–35. doi: 10.1074/jbc.M111.306134
57. Singh JP, Larson MG, O'Donnell CJ, Wilson PF, Tsuji H, Lloyd-Jones DM, et al. Association of Hyperglycemia with Reduced Heart Rate Variability (the Framingham Heart Study). *Am J Cardiol* (2000) 86(3):309–12. doi: 10.1016/s0002-9149(00)00920-6
58. Liu Y, Jansen HJ, Krishnaswamy PS, Bogachev O, Rose RA. Impaired Regulation of Heart Rate and Sinoatrial Node Function by the Parasympathetic Nervous System in Type 2 Diabetic Mice. *Sci Rep* (2021) 11(1):12465. doi: 10.1038/s41598-021-91937-2
59. Bakkar NZ, Dwaib HS, Fares S, Eid AH, Al-Dhaheri Y, El-Yazbi AF. Cardiac Autonomic Neuropathy: A Progressive Consequence of Chronic Low-Grade Inflammation in Type 2 Diabetes and Related Metabolic Disorders. *Int J Mol Sci* (2020) 21(23):1–20. doi: 10.3390/ijms21239005
60. Vinik AI, Ziegler D. Diabetic Cardiovascular Autonomic Neuropathy. *Circulation* (2007) 115(3):387–97. doi: 10.1161/CIRCULATIONAHA.106.634949
61. Maser RE, Mitchell BD, Vinik AI, Freeman R. The Association between Cardiovascular Autonomic Neuropathy and Mortality in Individuals with Diabetes: A Meta-Analysis. *Diabetes Care* (2003) 26(6):1895–901. doi: 10.2337/diacare.26.6.1895
62. Kahn SE, Cooper ME, Del Prato S. Pathophysiology and Treatment of Type 2 Diabetes: Perspectives on the Past, Present, and Future. *Lancet* (2014) 383 (9922):1068–83. doi: 10.1016/S0140-6736(13)62154-6
63. Krishnaswamy PS, Egom EE, Moghtadaei M, Jansen HJ, Azer J, Bogachev O, et al. Altered Parasympathetic Nervous System Regulation of the Sinoatrial Node in Akita Diabetic Mice. *J Mol Cell Cardiol* (2015) 82:125–35. doi: 10.1016/j.yjmcc.2015.02.024
64. Park HJ, Zhang Y, Du C, Welzig CM, Madias C, Aronovitz MJ, et al. Role of Srebp-1 in the Development of Parasympathetic Dysfunction in the Hearts of Type 1 Diabetic Akita Mice. *Circ Res* (2009) 105(3):287–94. doi: 10.1161/CIRCRESAHA.109.193995
65. Cseh D, Climie RE, Offredo L, Guibout C, Thomas F, Zanoli L, et al. Type 2 Diabetes Mellitus Is Independently Associated with Decreased Neural Baroreflex Sensitivity: The Paris Prospective Study Iii. *Arterioscler Thromb Vasc Biol* (2020) 40(5):1420–8. doi: 10.1161/ATVBAHA.120.314102
66. Ruiz J, Monbaron D, Parati G, Perret S, Haesler E, Danzeisen C, et al. Diabetic Neuropathy Is a More Important Determinant of Baroreflex Sensitivity Than Carotid Elasticity in Type 2 Diabetes. *Hypertension* (2005) 46(1):162–7. doi: 10.1161/01.HYP.0000169053.14440.7d
67. Ziegler D, Zentai CP, Perz S, Rathmann W, Haastert B, Doring A, et al. Prediction of Mortality Using Measures of Cardiac Autonomic Dysfunction in the Diabetic and Nondiabetic Population: The Monica/Kora Augsburg Cohort Study. *Diabetes Care* (2008) 31(3):556–61. doi: 10.2337/dc07-1615
68. Ewing DJ, Martyn CN, Young RJ, Clarke BF. The Value of Cardiovascular Autonomic Function Tests: 10 Years Experience in Diabetes. *Diabetes Care* (1985) 8(5):491–8. doi: 10.2337/diacare.8.5.491
69. Boudet G, Walther G, Courteix D, Obert P, Lesourd B, Pereira B, et al. Paradoxical Dissociation between Heart Rate and Heart Rate Variability Following Different Modalities of Exercise in Individuals with Metabolic Syndrome: The Resolve Study. *Eur J Prev Cardiol* (2017) 24(3):281–96. doi: 10.1177/2047487316679523
70. Schroeder EB, Liao D, Chambless LE, Prineas RJ, Evans GW, Heiss G. Hypertension, Blood Pressure, and Heart Rate Variability: The Atherosclerosis Risk in Communities (Aric) Study. *Hypertension* (2003) 42 (6):1106–11. doi: 10.1161/01.HYP.0000100444.71069.73
71. Hufnagel C, Chambres P, Bertrand PR, Dutheil F. The Need for Objective Measures of Stress in Autism. *Front Psychol* (2017) 8:64. doi: 10.3389/fpsyg.2017.00064
72. Dutheil F, Chambres P, Hufnagel C, Auxiette C, Chausse P, Ghozi R, et al. 'Do Well B.': Design of Well Being Monitoring Systems. A Study Protocol for the Application in Autism. *BMJ Open* (2015) 5(2):e007716. doi: 10.1136/bmjopen-2015-007716
73. de Andrade PE, do Amaral JAT, Paiva LDS, Adami F, Raimudo JZ, Valenti VE, et al. Reduction of Heart Rate Variability in Hypertensive Elderly. *Blood Press* (2017) 26(6):350–8. doi: 10.1080/08037051.2017.1354285
74. Yadav RL, Yadav PK, Yadav LK, Agrawal K, Sah SK, Islam MN. Association between Obesity and Heart Rate Variability Indices: An Intuition toward Cardiac Autonomic Alteration - a Risk of Cvd. *Diabetes Metab Syndr Obes* (2017) 10:57–64. doi: 10.2147/DMSO.S123935
75. Karason K, Molgaard H, Wikstrand J, Sjostrom L. Heart Rate Variability in Obesity and the Effect of Weight Loss. *Am J Cardiol* (1999) 83(8):1242–7. doi: 10.1016/s0002-9149(99)00066-1
76. Solanki JD, Basida SD, Mehta HB, Panjwani SJ, Gadhavi BP. Comparative Study of Cardiac Autonomic Status by Heart Rate Variability between under-Treatment Normotensive and Hypertensive Known Type 2 Diabetics. *Indian Heart J* (2017) 69(1):52–6. doi: 10.1016/j.ihj.2016.07.013
77. Lotric MB, Stefanovska A, Stajer D, Urbancic-Rovan V. Spectral Components of Heart Rate Variability Determined by Wavelet Analysis. *Physiol Meas* (2000) 21(4):441–57. doi: 10.1088/0967-3334/21/4/302
78. Jaiswal M, Urbina EM, Wadwa RP, Talton JW, D'Agostino RBJr., Hamman RF, et al. Reduced Heart Rate Variability among Youth with Type 1 Diabetes: The Search Cvd Study. *Diabetes Care* (2013) 36(1):157–62. doi: 10.2337/dc12-0463
79. Shepard PD, Canavier CC, Levitan ES. Ether-a-Go-Go-Related Gene Potassium Channels: What's All the Buzz About? *Schizophr Bull* (2007) 33 (6):1263–9. doi: 10.1093/schbul/sbm106
80. Lomax AE, Rose RA, Giles WR. Electrophysiological Evidence for a Gradient of G Protein-Gated K+ Current in Adult Mouse Atria. *Br J Pharmacol* (2003) 140(3):576–84. doi: 10.1038/sj.bjp.0705474
81. Shui Z, Boyett MR, Zang WJ, Haga T, Kameyama K. Receptor Kinase-Dependent Desensitization of the Muscarinic K+ Current in Rat Atrial Cells. *J Physiol* (1995) 487(Pt 2):359–66. doi: 10.1113/jphysiol.1995.sp020885
82. Bender K, Wellner-Kienitz MC, Bosche LI, Rinne A, Beckmann C, Pott L. Acute Desensitization of Girk Current in Rat Atrial Myocytes Is Related to K+ Current Flow. *J Physiol* (2004) 561(Pt 2):471–83. doi: 10.1113/jphysiol.2004.072462
83. Cifelli C, Rose RA, Zhang H, Voigtlaender-Bolz J, Bolz SS, Backx PH, et al. Rgs4 Regulates Parasympathetic Signaling and Heart Rate Control in the Sinoatrial Node. *Circ Res* (2008) 103(5):527–35. doi: 10.1161/CIRCRESAHA.108.180984
84. Ishii M, Inanobe A, Kurachi Y. Pip3 Inhibition of Rgs Protein and Its Reversal by Ca2+/Calmodulin Mediate Voltage-Dependent Control of the G Protein Cycle in a Cardiac K+ Channel. *Proc Natl Acad Sci USA* (2002) 99 (7):4325–30. doi: 10.1073/pnas.072073399
85. Oudit GY, Sun H, Kerfant BG, Crackower MA, Penninger JM, Backx PH. The Role of Phosphoinositide-3 Kinase and Pten in Cardiovascular Physiology and Disease. *J Mol Cell Cardiol* (2004) 37(2):449–71. doi: 10.1016/j.yjmcc.2004.05.015
86. Bertrand L, Horman S, Beauloye C, Vanoverschelde JL. Insulin Signalling in the Heart. *Cardiovasc Res* (2008) 79(2):238–48. doi: 10.1093/cvr/cvn093
87. Swaminathan PD, Purohit A, Soni S, Voigt N, Singh MV, Glukhov AV, et al. Oxidized Camkii Causes Cardiac Sinus Node Dysfunction in Mice. *J Clin Invest* (2011) 121(8):3277–88. doi: 10.1172/JCI57833
88. Luo M, Guan X, Luczak ED, Lang D, Kutschke W, Gao Z, et al. Diabetes Increases Mortality after Myocardial Infarction by Oxidizing Camkii. *J Clin Invest* (2013) 123(3):1262–74. doi: 10.1172/JCI65268
89. Wu Y, Anderson ME. Camkii in Sinoatrial Node Physiology and Dysfunction. *Front Pharmacol* (2014) 5:48. doi: 10.3389/fphar.2014.00048

90. Volpe CMO, Villar-Delfino PH, Dos Anjos PMF, Nogueira-Machado JA. Cellular Death, Reactive Oxygen Species (Ros) and Diabetic Complications. *Cell Death Dis* (2018) 9(2):119. doi: 10.1038/s41419-017-0135-z
91. Vinogradova T, Tarasov K, Riordon D, Tarasova Y, Lakatta E. Normal Spontaneous Firing of Cardiac Pacemaker Cells Is Regulated by Basal Pkc Delta Activation. *Eur Heart J* (2020) 41.
92. Kondo H, Kira S, Oniki T, Gotoh K, Fukui A, Abe I, et al. Interleukin-10 Treatment Attenuates Sinus Node Dysfunction Caused by Streptozotocin-Induced Hyperglycaemia in Mice. *Cardiovasc Res* (2019) 115(1):57–70. doi: 10.1093/cvr/cvy162
93. Levelt E, Pavlides M, Banerjee R, Mahmod M, Kelly C, Sellwood J, et al. Ectopic and Visceral Fat Deposition in Lean and Obese Patients with Type 2 Diabetes. *J Am Coll Cardiol* (2016) 68(1):53–63. doi: 10.1016/j.jacc.2016.03.597
94. Yanni J, Tellez JO, Sutyagin PV, Boyett MR, Dobrzynski H. Structural Remodelling of the Sinoatrial Node in Obese Old Rats. *J Mol Cell Cardiol* (2010) 48(4):653–62. doi: 10.1016/j.yjmcc.2009.08.023
95. Grden M, Podgorska M, Szutowicz A, Pawelczyk T. Altered Expression of Adenosine Receptors in Heart of Diabetic Rat. *J Physiol Pharmacol* (2005) 56 (4):587–97.
96. Lou Q, Hansen BJ, Fedorenko O, Csepe TA, Kalyanasundaram A, Li N, et al. Upregulation of Adenosine A1 Receptors Facilitates Sinoatrial Node Dysfunction in Chronic Canine Heart Failure by Exacerbating Nodal Conduction Abnormalities Revealed by Novel Dual-Sided Intramural Optical Mapping. *Circulation* (2014) 130(4):315–24. doi: 10.1161/CIRCULATIONAHA.113.007086
97. Gallego M, Zayas-Arrabal J, Alquiza A, Apellaniz B, Casis O. Electrical Features of the Diabetic Myocardium. Arrhythmic and Cardiovascular Safety Considerations in Diabetes. *Front Pharmacol* (2021) 12:687256. doi: 10.3389/fphar.2021.687256
98. Siscovick DS, Sotoodehnia N, Rea TD, Raghunathan TE, Jouven X, Lemaitre RN. Type 2 Diabetes Mellitus and the Risk of Sudden Cardiac Arrest in the Community. *Rev Endocr Metab Disord* (2010) 11(1):53–9. doi: 10.1007/s11154-010-9133-5
99. Wasada T, Katsumori K, Hasumi S, Kasanuki H, Arii H, Saeki A, et al. Association of Sick Sinus Syndrome with Hyperinsulinemia and Insulin Resistance in Patients With Non-Insulin-Dependent Diabetes Mellitus: Report of Four Cases. *Intern Med* (1995) 34(12):1174–7. doi: 10.2169/internalmedicine.34.1174
100. Guzman E, Singh N, Khan IA, Niarchos AP, Verghese C, Saponieri C, et al. Left Bundle Branch Block in Type 2 Diabetes Mellitus: A Sign of Advanced Cardiovascular Involvement. *Ann Noninvasive Electrocardiol* (2004) 9 (4):362–5. doi: 10.1111/j.1542-474X.2004.94577.x
101. Movahed MR, Hashemzadeh M, Jamal MM. Increased Prevalence of Third-Degree Atrioventricular Block in Patients with Type II Diabetes Mellitus. *Chest* (2005) 128(4):2611–4. doi: 10.1378/chest.128.4.2611
102. Lychev VG, Klester EB, Plinokosova LA. Arrhythmia in Patients with Chronic Heart Insufficiency and Type 2 Diabetes Mellitus. *Klin Med (Mosk)* (2014) 92(3):38–42.
103. Huxley RR, Filion KB, Konety S, Alonso A. Meta-Analysis of Cohort and Case-Control Studies of Type 2 Diabetes Mellitus and Risk of Atrial Fibrillation. *Am J Cardiol* (2011) 108(1):56–62. doi: 10.1016/j.amjcard.2011.03.004
104. Hillis GS, Woodward M, Rodgers A, Chow CK, Li Q, Zoungas S, et al. Resting Heart Rate and the Risk of Death and Cardiovascular Complications in Patients with Type 2 Diabetes Mellitus. *Diabetologia* (2012) 55(5):1283–90. doi: 10.1007/s00125-012-2471-y
105. Movahed MR, Hashemzadeh M, Jamal MM. Increased Prevalence of Infectious Endocarditis in Patients With Type II Diabetes Mellitus. *J Diabetes Complications* (2007) 21(6):403–6. doi: 10.1016/j.jdiacomp.2007.07.003
106. Howarth FC, Jacobson M, Shafiullah M, Adeghate E. Long-Term Effects of Type 2 Diabetes Mellitus on Heart Rhythm in the Goto-Kakizaki Rat. *Exp Physiol* (2008) 93(3):362–9. doi: 10.1113/expphysiol.2007.040055
107. Ferdous Z, Qureshi MA, Jayaprakash P, Parekh K, John A, Oz M, et al. Different Profile of Mrna Expression in Sinoatrial Node from Streptozotocin-Induced Diabetic Rat. *PloS One* (2016) 11(4):e0153934. doi: 10.1371/journal.pone.0153934
108. Lengyel C, Virag L, Biro T, Jost N, Magyar J, Biliczki P, et al. Diabetes Mellitus Attenuates the Repolarization Reserve in Mammalian Heart. *Cardiovasc Res* (2007) 73(3):512–20. doi: 10.1016/j.cardiores.2006.11.010
109. Torres-Jacome J, Gallego M, Rodriguez-Robledo JM, Sanchez-Chapula JA, Casis O. Improvement of the Metabolic Status Recovers Cardiac Potassium Channel Synthesis in Experimental Diabetes. *Acta Physiol (Oxf)* (2013) 207 (3):447–59. doi: 10.1111/apha.12043
110. Huang X, Zhong N, Zhang H, Ma A, Yuan Z, Guo N. Reduced Expression of Hcn Channels in the Sinoatrial Node of Streptozotocin-Induced Diabetic Rats. *Can J Physiol Pharmacol* (2017) 95(5):586–94. doi: 10.1139/cjpp-2016-0418
111. Shinagawa Y, Satoh H, Noma A. The Sustained Inward Current and Inward Rectifier K+ Current in Pacemaker Cells Dissociated from Rat Sinoatrial Node. *J Physiol* (2000) 523 Pt 3:593–605. doi: 10.1111/j.1469-7793.2000.t01-2-00593.x
112. Nof E, Vysochek L, Meisel E, Burashnikov E, Antzelevitch C, Clatot J, et al. Mutations in Nav1.5 Reveal Calcium-Calmodulin Regulation of Sodium Channel. *Front Physiol* (2019) 10:700. doi: 10.3389/fphys.2019.00700
113. Lei M, Jones SA, Liu J, Lancaster MK, Fung SS, Dobrzynski H, et al. Requirement of Neuronal- and Cardiac-Type Sodium Channels for Murine Sinoatrial Node Pacemaking. *J Physiol* (2004) 559(Pt 3):835–48. doi: 10.1113/jphysiol.2004.068643
114. Protas L, Oren RV, Clancy CE, Robinson RB. Age-Dependent Changes in Na Current Magnitude and Ttx-Sensitivity in the Canine Sinoatrial Node. *J Mol Cell Cardiol* (2010) 48(1):172–80. doi: 10.1016/j.yjmcc.2009.07.028
115. Li N, Kalyanasundaram A, Hansen BJ, Artiga EJ, Sharma R, Abudulwahed SH, et al. Impaired Neuronal Sodium Channels Cause Intranodal Conduction Failure and Reentrant Arrhythmias in Human Sinoatrial Node. *Nat Commun* (2020) 11(1):512. doi: 10.1038/s41467-019-14039-8
116. Papadatos GA, Wallerstein PM, Head CE, Ratcliff R, Brady PA, Benndorf K, et al. Slowed Conduction and Ventricular Tachycardia after Targeted Disruption of the Cardiac Sodium Channel Gene Scn5a. *Proc Natl Acad Sci USA* (2002) 99(9):6210–5. doi: 10.1073/pnas.082121299
117. Stables CL, Musa H, Mitra A, Bhushal S, Deo M, Guerrero-Serna G, et al. Reduced Na(+) Current Density Underlies Impaired Propagation in the Diabetic Rabbit Ventricle. *J Mol Cell Cardiol* (2014) 69:24–31. doi: 10.1016/j.yjmcc.2013.12.031
118. Zhang Y, Wang Y, Yanni J, Qureshi MA, Logantha S, Kassab S, et al. Electrical Conduction System Remodeling in Streptozotocin-Induced Diabetes Mellitus Rat Heart. *Front Physiol* (2019) 10:826. doi: 10.3389/fphys.2019.00826
119. Giacco F, Brownlee M. Oxidative Stress and Diabetic Complications. *Circ Res* (2010) 107(9):1058–70. doi: 10.1161/CIRCRESAHA.110.223545
120. Liu M, Liu H, Dudley SCJr.. Reactive Oxygen Species Originating from Mitochondria Regulate the Cardiac Sodium Channel. *Circ Res* (2010) 107 (8):967–74. doi: 10.1161/CIRCRESAHA.110.220673
121. Chandler NJ, Greener ID, Tellez JO, Inada S, Musa H, Molenaar P, et al. Molecular Architecture of the Human Sinus Node: Insights into the Function of the Cardiac Pacemaker. *Circulation* (2009) 119(12):1562–75. doi: 10.1161/CIRCULATIONAHA.108.804369
122. Fenske S, Hennis K, Rotzer RD, Brox VF, Becirovic E, Scharr A, et al. Camp-Dependent Regulation of Hcn4 Controls the Tonic Entrainment Process in Sinoatrial Node Pacemaker Cells. *Nat Commun* (2020) 11(1):5555. doi: 10.1038/s41467-020-19304-9
123. Zagotta WN, Olivier NB, Black KD, Young EC, Olson R, Gouaux E. Structural Basis for Modulation and Agonist Specificity of Hcn Pacemaker Channels. *Nature* (2003) 425(6954):200–5. doi: 10.1038/nature01922
124. DiFrancesco D, Tortora P. Direct Activation of Cardiac Pacemaker Channels by Intracellular Cyclic Amp. *Nature* (1991) 351(6322):145–7. doi: 10.1038/351145a0
125. Herrmann S, Stieber J, Ludwig A. Pathophysiology of Hcn Channels. *Pflugers Arch* (2007) 454(4):517–22. doi: 10.1007/s00424-007-0224-4
126. Howarth FC, Qureshi MA, Jayaprakash P, Parekh K, Oz M, Dobrzynski H, et al. The Pattern of Mrna Expression Is Changed in Sinoatrial Node from Goto-Kakizaki Type 2 Diabetic Rat Heart. *J Diabetes Res* (2018) 2018:8454078. doi: 10.1155/2018/8454078
127. Grisanti LA. Diabetes and Arrhythmias: Pathophysiology, Mechanisms and Therapeutic Outcomes. *Front Physiol* (2018) 9:1669. doi: 10.3389/fphys.2018.01669

128. Iop L, Iliceto S, Civieri G, Tona F. Inherited and Acquired Rhythm Disturbances in Sick Sinus Syndrome, Brugada Syndrome, and Atrial Fibrillation: Lessons from Preclinical Modeling. *Cells* (2021) 10(11):1–52. doi: 10.3390/cells10113175
129. Yang B, Huang Y, Zhang H, Huang Y, Zhou HJ, Young L, et al. Mitochondrial Thioredoxin-2 Maintains Hcn4 Expression and Prevents Oxidative Stress-Mediated Sick Sinus Syndrome. *J Mol Cell Cardiol* (2020) 138:291–303. doi: 10.1016/j.yjmcc.2019.10.009
130. Li Y, Wang F, Zhang X, Qi Z, Tang M, Szeto C, et al. Beta-Adrenergic Stimulation Increases Cav3.1 Activity in Cardiac Myocytes through Protein Kinase A. *PloS One* (2012) 7(7):e39965. doi: 10.1371/journal.pone.0039965
131. Mesirca P, Torrente AG, Mangoni ME. T-Type Channels in the Sino-Atrial and Atrioventricular Pacemaker Mechanism. *Pflugers Arch* (2014) 466 (4):791–9. doi: 10.1007/s00424-014-1482-6
132. Mangoni ME, Traboulsie A, Leoni AL, Couette B, Marger L, Le Quang K, et al. Bradycardia and Slowing of the Atrioventricular Conduction in Mice Lacking Cav3.1/Alpha1g T-Type Calcium Channels. *Circ Res* (2006) 98 (11):1422–30. doi: 10.1161/01.RES.0000225862.14314.49
133. Salem KA, Qureshi MA, Sydorenko V, Parekh K, Jayaprakash P, Iqbal T, et al. Effects of Exercise Training on Excitation-Contraction Coupling and Related Mrna Expression in Hearts of Goto-Kakizaki Type 2 Diabetic Rats. *Mol Cell Biochem* (2013) 380(1-2):83–96. doi: 10.1007/s11010-013-1662-2
134. Howarth FC, Qureshi MA, Hassan Z, Isaev D, Parekh K, John A, et al. Contractility of Ventricular Myocytes Is Well Preserved Despite Altered Mechanisms of Ca2+ Transport and a Changing Pattern of Mrna in Aged Type 2 Zucker Diabetic Fatty Rat Heart. *Mol Cell Biochem* (2012) 361(1-2):267–80. doi: 10.1007/s11010-011-1112-y
135. Mangoni ME, Couette B, Bourinet E, Platzer J, Reimer D, Striessnig J, et al. Functional Role of L-Type Cav1.3 $Ca2^+$ Channels in Cardiac Pacemaker Activity. *Proc Natl Acad Sci USA* (2003) 100(9):5543–8. doi: 10.1073/pnas.0935295100
136. Torrente AG, Mesirca P, Neco P, Rizzetto R, Dubel S, Barrere C, et al. L-Type Cav1.3 Channels Regulate Ryanodine Receptor-Dependent $Ca2^+$ Release During Sino-Atrial Node Pacemaker Activity. *Cardiovasc Res* (2016) 109 (3):451–61. doi: 10.1093/cvr/cvw006
137. Striessnig J, Grabner M, Mitterdorfer J, Hering S, Sinnegger MJ, Glossmann H. Structural Basis of Drug Binding to L Ca2+ Channels. *Trends Pharmacol Sci* (1998) 19(3):108–15. doi: 10.1016/s0165-6147(98)01171-7
138. Ozturk N, Uslu S, Ozdemir S. Diabetes-Induced Changes in Cardiac Voltage-Gated Ion Channels. *World J Diabetes* (2021) 12(1):1–18. doi: 10.4239/wjd.v12.i1.1
139. Factor SM, Robinson TF, Dominitz R, Cho SH. Alterations of the Myocardial Skeletal Framework in Acute Myocardial Infarction with and without Ventricular Rupture. A Preliminary Report. *Am J Cardiovasc Pathol* (1987) 1(1):91–7.
140. Ward ML, Crossman DJ. Mechanisms Underlying the Impaired Contractility of Diabetic Cardiomyopathy. *World J Cardiol* (2014) 6 (7):577–84. doi: 10.4330/wjc.v6.i7.577
141. He M, Qiu J, Wang Y, Bai Y, Chen G. Caveolin-3 and Arrhythmias: Insights into the Molecular Mechanisms. *J Clin Med* (2022) 11(6):1–13. doi: 10.3390/jcm11061595
142. Parton RG. Caveolae: Structure, Function, and Relationship to Disease. *Annu Rev Cell Dev Biol* (2018) 34:111–36. doi: 10.1146/annurev-cellbio-100617-062737
143. Koga A, Oka N, Kikuchi T, Miyazaki H, Kato S, Imaizumi T. Adenovirus-Mediated Overexpression of Caveolin-3 Inhibits Rat Cardiomyocyte Hypertrophy. *Hypertension* (2003) 42(2):213–9. doi: 10.1161/01.HYP.0000082926.08268.5D
144. Lang D, Warden A, Balijepalli R, Kamp TJ, Glukhov AV. Loss of Caveolin-3 Disrupts Mouse Sinoatrial Node Pacemaking and Stimulates Atrial Arrhythmogenesis. *Circulation* (2016) 134:A15361. doi: 10.1161/circ.134.suppl_1.15361
145. Barbuti A, Terragni B, Brioschi C, DiFrancesco D. Localization of F-Channels to Caveolae Mediates Specific Beta2-Adrenergic Receptor Modulation of Rate in Sinoatrial Myocytes. *J Mol Cell Cardiol* (2007) 42 (1):71–8. doi: 10.1016/j.yjmcc.2006.09.018
146. Ye B, Balijepalli RC, Foell JD, Kroboth S, Ye Q, Luo YH, et al. Caveolin-3 Associates with and Affects the Function of Hyperpolarization-Activated Cyclic Nucleotide-Gated Channel 4. *Biochemistry* (2008) 47(47):12312–8.
147. Campostrini G, Bonzanni M, Lissoni A, Bazzini C, Milanesi R, Vezzoli E, et al. The Expression of the Rare Caveolin-3 Variant T78m Alters Cardiac Ion Channels Function and Membrane Excitability. *Cardiovasc Res* (2017) 113(10):1256–65. doi: 10.1093/cvr/cvx122
148. Penumathsa SV, Thirunavukkarasu M, Zhan L, Maulik G, Menon VP, Bagchi D, et al. Resveratrol Enhances Glut-4 Translocation to the Caveolar Lipid Raft Fractions through Ampk/Akt/Enos Signalling Pathway in Diabetic Myocardium. *J Cell Mol Med* (2008) 12(6A):2350–61. doi: 10.1111/j.1582-4934.2008.00251.x
149. Penumathsa SV, Thirunavukkarasu M, Samuel SM, Zhan L, Maulik G, Bagchi M, et al. Niacin Bound Chromium Treatment Induces Myocardial Glut-4 Translocation and Caveolar Interaction*Via* Akt, Ampk and Enos Phosphorylation in Streptozotocin Induced Diabetic Rats after Ischemia-Reperfusion Injury. *Biochim Biophys Acta* (2009) 1792(1):39–48. doi: 10.1016/j.bbadis.2008.10.018
150. Lei S, Li H, Xu J, Liu Y, Gao X, Wang J, et al. Hyperglycemia-Induced Protein Kinase C Beta2 Activation Induces Diastolic Cardiac Dysfunction in Diabetic Rats by Impairing Caveolin-3 Expression and Akt/Enos Signaling. *Diabetes* (2013) 62(7):2318–28. doi: 10.2337/db12-1391
151. Verheijck EE, van Kempen MJ, Veereschild M, Lurvink J, Jongsma HJ, Bouman LN. Electrophysiological Features of the Mouse Sinoatrial Node in Relation to Connexin Distribution. *Cardiovasc Res* (2001) 52(1):40–50. doi: 10.1016/s0008-6363(01)00364-9
152. Joshi MS, Mihm MJ, Cook AC, Schanbacher BL, Bauer JA. Alterations in Connexin 43 During Diabetic Cardiomyopathy: Competition of Tyrosine Nitration Versus Phosphorylation. *J Diabetes* (2015) 7(2):250–9. doi: 10.1111/1753-0407.12164
153. Mayama T, Matsumura K, Lin H, Ogawa K, Imanaga I. Remodelling of Cardiac Gap Junction Connexin 43 and Arrhythmogenesis. *Exp Clin Cardiol* (2007) 12(2):67–76.
154. Howarth FC, Nowotny N, Zilahi E, El Haj MA, Lei M. Altered Expression of Gap Junction Connexin Proteins May Partly Underlie Heart Rhythm Disturbances in the Streptozotocin-Induced Diabetic Rat Heart. *Mol Cell Biochem* (2007) 305(1-2):145–51. doi: 10.1007/s11010-007-9537-z
155. Brown NJ. Cardiovascular Effects of Antidiabetic Agents: Focus on Blood Pressure Effects of Incretin-Based Therapies. *J Am Soc Hypertens* (2012) 6 (3):163–8. doi: 10.1016/j.jash.2012.02.003
156. Nantsupawat T, Wongcharoen W, Chattipakorn SC, Chattipakorn N. Effects of Metformin on Atrial and Ventricular Arrhythmias: Evidence from Cell to Patient. *Cardiovasc Diabetol* (2020) 19(1):198. doi: 10.1186/s12933-020-01176-4
157. Harada M, Tadevosyan A, Qi X, Xiao J, Liu T, Voigt N, et al. Atrial Fibrillation Activates Amp-Dependent Protein Kinase and Its Regulation of Cellular Calcium Handling: Potential Role in Metabolic Adaptation and Prevention of Progression. *J Am Coll Cardiol* (2015) 66(1):47–58. doi: 10.1016/j.jacc.2015.04.056
158. Dart C. Selective Block of K(Atp) Channels: Why the Anti-Diabetic Sulphonylureas and Rosiglitazone Have More in Common Than We Thought. *Br J Pharmacol* (2012) 167(1):23–5. doi: 10.1111/j.1476-5381.2012.01990.x
159. Ashcroft FM, Gribble FM. Atp-Sensitive K+ Channels and Insulin Secretion: Their Role in Health and Disease. *Diabetologia* (1999) 42(8):903–19. doi: 10.1007/s001250051247
160. Lu L, Reiter MJ, Xu Y, Chicco A, Greyson CR, Schwartz GG. Thiazolidinedione Drugs Block Cardiac Katp Channels and May Increase Propensity for Ischaemic Ventricular Fibrillation in Pigs. *Diabetologia* (2008) 51(4):675–85. doi: 10.1007/s00125-008-0924-0
161. Yu L, Jin X, Yang Y, Cui N, Jiang C. Rosiglitazone Inhibits Vascular Katp Channels and Coronary Vasodilation Produced by Isoprenaline. *Br J Pharmacol* (2011) 164(8):2064–72. doi: 10.1111/j.1476-5381.2011.01539.x
162. Bonnet F, Scheen AJ. Impact of Glucose-Lowering Therapies on Risk of Stroke in Type 2 Diabetes. *Diabetes Metab* (2017) 43(4):299–313. doi: 10.1016/j.diabet.2017.04.004
163. Shimoni Y, Ewart HS, Severson D. Insulin Stimulation of Rat Ventricular K+ Currents Depends on the Integrity of the Cytoskeleton. *J Physiol* (1999) 514(Pt 3):735–45. doi: 10.1111/j.1469-7793.1999.735ad.x
164. Aulbach F, Simm A, Maier S, Langenfeld H, Walter U, Kersting U, et al. Insulin Stimulates the L-Type Ca2+ Current in Rat Cardiac

Myocytes. *Cardiovasc Res* (1999) 42(1):113–20. doi: 10.1016/s0008-6363(98)00307-1

165. Shimoni Y, Severson D, Ewart HS. Insulin Resistance and the Modulation of Rat Cardiac K(+) Currents. *Am J Physiol Heart Circ Physiol* (2000) 279(2): H639–49. doi: 10.1152/ajpheart.2000.279.2.H639
166. Polina I, Jansen HJ, Li T, Moghtadaei M, Bohne LJ, Liu Y, et al. Loss of Insulin Signaling May Contribute to Atrial Fibrillation and Atrial Electrical Remodeling in Type 1 Diabetes. *Proc Natl Acad Sci USA* (2020) 117 (14):7990–8000. doi: 10.1073/pnas.1914853117

Conflict of Interest: The authors declare that the research was conducted in the absence of any commercial or financial relationships that could be construed as a potential conflict of interest.

Publisher's Note: All claims expressed in this article are solely those of the authors and do not necessarily represent those of their affiliated organizations, or those of the publisher, the editors and the reviewers. Any product that may be evaluated in this article, or claim that may be made by its manufacturer, is not guaranteed or endorsed by the publisher.

frontiers | Frontiers in Endocrinology

TYPE Original Research
PUBLISHED 15 August 2022
DOI 10.3389/fendo.2022.933635

OPEN ACCESS

EDITED BY
Ying Xin,
Jilin University, China

REVIEWED BY
Kawsar Ahmed,
Mawlana Bhashani Science and Technology University, Bangladesh
Jinhui Liu,
Nanjing Medical University, China
Jin-Yu Sun,
Nanjing Medical University, China
Yao-Zong Guan,
Second Affiliated Hospital of Guangxi Medical University, China

*CORRESPONDENCE
Xinli Li
xinli3267@njmu.edu.cn

†These authors have contributed equally to this work

SPECIALTY SECTION
This article was submitted to Cardiovascular Endocrinology, a section of the journal Frontiers in Endocrinology

RECEIVED 01 May 2022
ACCEPTED 27 July 2022
PUBLISHED 15 August 2022

CITATION
Guo Q, Zhu Q, Zhang T, Qu Q, Cheang I, Liao S, Chen M, Zhu X, Shi M and Li X (2022) Integrated bioinformatic analysis reveals immune molecular markers and potential drugs for diabetic cardiomyopathy. *Front. Endocrinol.* 13:933635. doi: 10.3389/fendo.2022.933635

Integrated bioinformatic analysis reveals immune molecular markers and potential drugs for diabetic cardiomyopathy

Qixin Guo†, Qingqing Zhu†, Ting Zhang, Qiang Qu, Iokfai Cheang, Shengen Liao, Mengli Chen, Xu Zhu, Mengsha Shi and Xinli Li*

Department of Cardiology, The First Affiliated Hospital of Nanjing Medical University, Nanjing, China

Diabetic cardiomyopathy (DCM) is a pathophysiological condition induced by diabetes mellitus that often causes heart failure (HF). However, their mechanistic relationships remain unclear. This study aimed to identify immune gene signatures and molecular mechanisms of DCM. Microarray data from the Gene Expression Omnibus (GEO) database from patients with DCM were subjected to weighted gene co-expression network analysis (WGCNA) identify co-expression modules. Core expression modules were intersected with the immune gene database. We analyzed and mapped protein-protein interaction (PPI) networks using the STRING database and MCODE and filtering out 17 hub genes using cytoHubba software. Finally, potential transcriptional regulatory factors and therapeutic drugs were identified and molecular docking between gene targets and small molecules was performed. We identified five potential immune biomarkers: proteosome subunit beta type-8 (*PSMB8*), nuclear factor kappa B1 (*NFKB1*), albumin (*ALB*), endothelin 1 (*EDN1*), and estrogen receptor 1 (*ESR1*). Their expression levels in animal models were consistent with the changes observed in the datasets. *EDN1* showed significant differences in expression in both the dataset and the validation model by real-time quantitative PCR (qPCR) and Western blotting (WB). Subsequently, we confirmed that the potential transcription factors upstream of *EDN1* were PRDM5 and KLF4, as its expression was positively correlated with the expression of the two transcription factors. To repurpose known therapeutic drugs, a connectivity map (CMap) database was retrieved, and nine candidate compounds were identified. Finally, molecular docking simulations of the proteins encoded by the five genes with small-molecule drugs were performed. Our data suggest that *EDN1* may play a key role in the development of DCM and is a potential DCM biomarker.

KEYWORDS

diabetic cardiomyopathy, bioinformatics, molecular docking, potential drugs, diabetes mellitus, biomarker

Introduction

Diabetic cardiomyopathy (DCM) is defined as myocardial dysfunction that develops from complex pathophysiological mechanisms of diabetes in the absence of coronary artery disease (CAD) or hypertension (1). Currently, epidemiological studies have indicated a high incidence (19–26%) of heart failure (HF) in patients with diabetes mellitus (2), creating a heavy financial burden on both government and citizens (3).

However, due to the lack of early symptoms and signs, DCM was often ignored (4). Even in asymptomatic patients with well-controlled diabetes, up to 50% have been found to exhibit some degree of cardiac dysfunction (5). The current treatments for DCM have been traditional cardiac and anti-glycemic drugs, with no targeted therapies (6). Considering that there are no established diagnostic criteria and targeted therapeutics for DCM, the development of diagnostic biomarkers and the identification of therapeutic targets based on its molecular mechanism are of great clinical significance.

Multiple factors contribute to the pathophysiology of DCM, including systemic metabolic disorders, inappropriate activation of the renin-angiotensin-aldosterone system (RAAS), subcellular abnormalities, oxidative stress, inflammation, and dysfunctional immunomodulation (7). With immunological mechanisms contributing to the pathogenesis of HF, immunology has become a significant research topic. The Canakinumab Anti-inflammatory Thrombosis Outcome Study (CANTOS) trial has shown that inflammation is one of the main drivers of atherosclerosis (8). Further exploration of immunology was expected to expand our understanding of the fundamental mechanisms of DCM.

Numerous groups have performed comprehensive, microarray-based, genome-wide analyses. The use of bioinformatics methods and tools to identify disease signatures and drug targets is rapidly maturing. Despite these analyses, addressing DCM by immune-informatics approaches remains largely unexplored. In this study, we integrated bioinformatic analysis to identify immune molecular biomarkers and potential drugs for diabetic cardiomyopathy, further testing them using molecular docking and animal model validation.

Materials and methods

Dataset and differentially expressed genes (DEGs)

Raw microarray data from the dataset GSE4745, based on the platform GPL85, were downloaded from the GEO database. These data were converted to gene names and normalized, followed by removal of bias and variability from the dataset using the combat function in the surrogate variable analysis (sva) package. The analysis of digital gene expression using the R (edgeR) package was used to screen for DEGs between diabetic patients and healthy controls. The selection criteria were $|\log_2 FC| > 1$ and false discovery rate (FDR) < 0.05.

Immune infiltration analysis

The degrees of infiltration by 22 immune cell types were quantified by transcriptomic data using the CIBERSORT deconvolution algorithm. The cell types investigated included plasma cells, resting memory CD4+ T cells, CD8+ T cells, naïve CD4+ T cells, T follicular helper cells, regulatory T cells (Tregs), activated memory CD4+ T cells, gamma delta T cells, naïve B cells, memory B cells, monocytes, M0 macrophages, M1 macrophages, M2 macrophages, resting natural killer (NK) cells, activated NK cells, activated mast cells, eosinophils, neutrophils, resting dendritic cells, activated dendritic cells, and resting mast cells. The CIBERSORT data were visualized using R software.

WGCNA and ImmPort database of immune-related genes

WGCNA is an algorithm that finds co-expressed gene modules of high biological significance and explores the relationship between gene networks and diseases. We obtained approximately 5000 genes for further analysis based on P values < 0.05 and logFC > 0.05. The main processes were: (i) the hierarchical clustering (hclust) function was used for hclustanalysis; (ii) the Topological Overlap Matrix (TOM) was constructed using the pickSoftThreshold function to determine the optimal soft threshold; (iii) the expression profile of each module was summarized by module signature genes (ME); (iv) the relationship between ME and DCM was calculated using Pearson correlation analysis; (v) Gene Ontology (GO) annotation and KEGG pathway enrichment analysis were performed for these functional modules and (vi) genes from the immune database intersected with genes from the module.

Establishment of PPI network topology algorithm and hub node detection

PPIs are a target of cell biology research and a prerequisite for systems biology studies (9). Proteins were placed in PPI networks through interactions with another protein, suggesting its possible function(s). We constructed PPI networks from DEGs using the STRING (https://string-db.org/) repository to describe functional and physical interactions in DCM (10). Hub nodes were generally defined by highly interconnected nodes in large and complex PPI networks. Hub nodes were determined by

a degree topology algorithm using cytoHubba (http://apps.cytoscape.org/apps/cytohubba), a Cytoscape plug-in for Cytoscape software (11). PPI network was then analyzed using the MCODE plug-in with default parameters degree cutoff ≥2, node score cutoff ≥2, K-core ≥2 and max depth =100); finally, cytoHubba was used to identify hub genes.

Gene set enrichment analysis (GSEA) and potential transcription factors (TFs)

Gene sets with enrichment scores with a normalized P < 0.05, and an FDR of < 0.25, were considered significantly enriched. The University of California Santa Cruz (UCSC) sequence database was used to identify promoter sequences of target genes, followed by a search for potential TFs in the JASPAR database, a first screening step based on the direction and correlation level of transcription, and a second step using expression in the GEPIA database and clarification of its binding structural domain.

Potential therapeutic chemicals and their molecular docking to proteins

Genes of interest were imported into the clue.io platform to identify potentially useful small molecules (Supplementary Figure 1). There were three steps for molecular docking. First, the drug candidates were imported into the PubChem database to obtain their three-dimensional structures and minimize their energy using viaChem 3D. Second, target genes were imported into the Universal Protein Resource (UniProt) and Protein Databank (PDB) databases to obtain the highest-resolution receptor structures and perform dehydration, hydrogenation, and charge setting operations (using viaAutoDockTools and PyMOL software). Third, molecular linkage was performed using AutoDock Vina-1.5.7 software. Molecular docking simulations were used to gain insight into how these drugs bind to their targets. The binding energy between the ligand and receptor was calculated to predict affinities. A binding energy of less than 0 indicates higher affinity of binding between two molecules freely, corresponding to a smaller binding energy and a more stable binding conformation.

Establishment of a murine DCM model

Male C57BL/6 mice (4 weeks old, weight 18–20 g) (n = 24) were purchased from the Model Animal Research Center of Nanjing University. All mice were kept in specific-pathogen-free environment (temperature 25 ± 2°C, humidity 50 ± 5%) with a 12-h light–dark cycle. Normal control mice were fed standard rodent diet and DCM model mice were fed a high-fat diet (HFD; 60% calories as fat). After four weeks of feeding, control mice were intraperitoneally injected with citrate-phosphate buffer (pH 4.2, 0.1 mmol/L). Mice in the HFD group received an intraperitoneal injection of 30 mg/kg streptozotocin (STZ; Lot No. S0130) dissolved in the same citrate-phosphate buffer for seven consecutive days. One week after the completion of STZ injections, blood glucose levels were measured. Echocardiography was performed at the end of 16 weeks. The research protocol was approved by the Animal Ethics Committee of Nanjing Medical University (license number IACUC-1903016).

Echocardiography and statistical analysis

Mice were anesthetized with 1.5–2% isoflurane and transthoracic echocardiography was performed using a Vevo 2100 instrument (VisualSonics Inc., Toronto, Ontario, Canada). The following parameters were measured from M-mode images: left ventricular ejection fraction (EF%), left ventricular fractional shortening (FS%), early phase (E-wave), late phase (A-wave), and E/A ratio. Continuous variables in these data are expressed as means ± standard deviations, and categorical variables are expressed as frequencies with percentages. Comparisons between diabetic cardiomyopathy and non-diabetic cardiomyopathy groups were made using Welch's *t*-test, Student's *t*-test, or the Mann-Whitney U test, depending on whether the data met normality and chi-squaredness. All statistical analyses were conducted using R software (version 4.0.3). Two-sided P values < 0.05 were considered statistically significant.

Reverse transcription, quantitative real-time polymerase chain reaction (qRT-PCR), and western blotting (WB)

Myocardial tissues were treated with TRIzol reagent for total RNA extraction. The RNA was reverse-transcribed into complementary DNA (cDNA) after measuring the corresponding concentration. Finally, qRT-PCR was performed to verify expression levels. The procedure for PCR is shown below: in brief, samples were incubated at 95°C for 5 min, followed by 40 cycles at 95°C for 10 s, and finally at 60°C for 20 s. 18S levels were used to normalize mRNA expression levels. The primer sequences were as follows: 5'-CTGCCGTCTGAGTGTATCGC-3′ and 5′-GCTGGGGCTGAGGAAAGTG-3 for 18S, 5'-ATGGCGTTACTGGATCTGTGC-3' and 5'-GCGGAGAAACTGTAGTGTCCC-3' for Psmb8; 5'-GGGGCCTGCAAAGGTTATC-3' and 5'-TGCTGTTACGGTGCATACCC-3' for Nfkb1;

5'-CAAGAGTGAGATCGCCCATCG-3 and 5'-TTACTTCCTGCACTAATTTGGCA-3' for Alb; 5'-GAGCGCGTCGTACCGTATG-3 and 5'-ACTGACATCTAACTGCCTGGT-3' for Edn1; 5'-CCCGCCTTCTACAGGTCTAAT-3' and 5'-CTTTCTCGTTACTGCTGGACAG-3' for Esr1.

WB was performed as follows: (i) Cells were lysed at 4°C using RIPA buffer (P0013C, Beyotime, Shanghai, China) and the cell lysates were collected. (ii) Protein concentration was measured using a BCA protein assay kit and equal amounts of proteins were separated using 10% sodium dodecyl sulfate-polyacrylamide gel electrophoresis (SDS-PAGE) (Millipore, Billerica, MA, USA) and transferred onto polyvinylidene difluoride (PVDF) membranes. (iii) The membranes were blocked with 5% skim milk for 2 h at room temperature. The membranes were cut according to the molecular weight of the target protein based on the pre-stained protein ladder. Subsequently, membranes were incubated overnight at 4°C with primary antibody (Edn1,1:1000; Psmb8,1:1000; Alb,1:1000; Nfkb1,1:1000; Esr1,1:1000; Gapdh, 1:1000). (iv) The membrane strips were incubated with the secondary antibody for 2 h at room temperature. The intensity of the protein bands was observed using Labworks software (Bio-Rad, USA) and analyzed using ImageJ software.

Results

Research design

The flowchart is shown in Figure 1. In summary, hub DCM genes were identified from microarray data from the GEO database. DCM was associated with the infiltration of multiple immune cell types using the CIBERSORT test. Subsequently, WGCNA was performed to screen the core modules and identify intersections with the genes in the immune gene database.

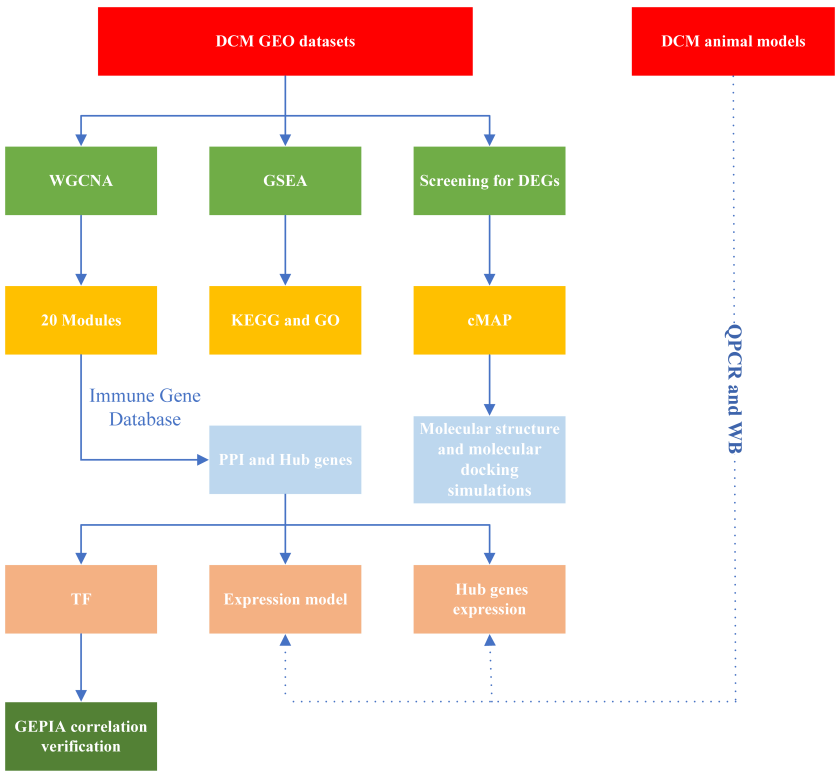

FIGURE 1
Study workflow. DCM, Diabetic cardiomyopathy; GEO, Gene Expression Omnibus; GO, Gene Ontology; PPI, protein-protein interaction; cMAP, Connectivity Map; KEGG, Kyoto Encyclopedia of Genes and Genomes; GSEA, Gene Set Enrichment Analysis; TF, transcription factors; DEGs, differentially expressed genes; WGCNA, Weight gene co-expression network analysis; GEPIA, Gene Expression Profiling Interactive Analysis; QPCR, quantitative real-time PCR; WB, Western blotting.

Potential drug molecules for core targets were searched as well as TFs regulating the transcription of the genes encoding them; the possibility of molecular structure docking and expression consistency was verified. Finally, qPCR was performed to verify the relationships between expression levels of the core DCM targets and clinical phenotypes in animal models.

DCM-related immune genes

The pickSoftThreshold parameter was calculated to set six as the optimal soft threshold. A dynamic cut tree with a merge cut height of 0.25 was used for module identification and module merging. The minimum number of genes in each network module was set to 30, producing 19 modules. The black module had the strongest correlation (correlation coefficient: 0.69, $P < 0.0001$) with DCM and was identified as the core module (Figure 2). There were significant differences in proportions of immune cells between groups and samples, with naïve B cells, plasma cells, resting NK cells, activated NK cells, and eosinophils with the most pronounced extents of DCM infiltration. The black module contained 248 genes, and the immune gene database contained 1793 genes, 22 of which were contained in both the immune database and the module (Figure 3).

A PPI network for module analysis and selection of hub genes

To investigate the interactions of DEGs associated with DCM occurrence and to obtain central genes, all DEGs were analyzed using STRING. Those with composite scores >0.7 suggested close associations between genes and were imported into Cytoscape for further analysis. In this network, there were 168 nodes and 527 edges; using MCODE, eight key modules were identified from the entire network (Supplementary Figure 2). The identified immune-related genes were further screened using cytoHubba, which produced five hub genes: *PSMB8, NFKB1, ALB, EDN1*, and *ESR1*. Figure 4 showed the density map of the dataset GSE4745. The density plots had a smooth distribution of points along the numerical axis. The peaks of the density plots are located at locations with the highest concentrations of points. Furthermore, we show the variation of target genes in the dataset across different groups.

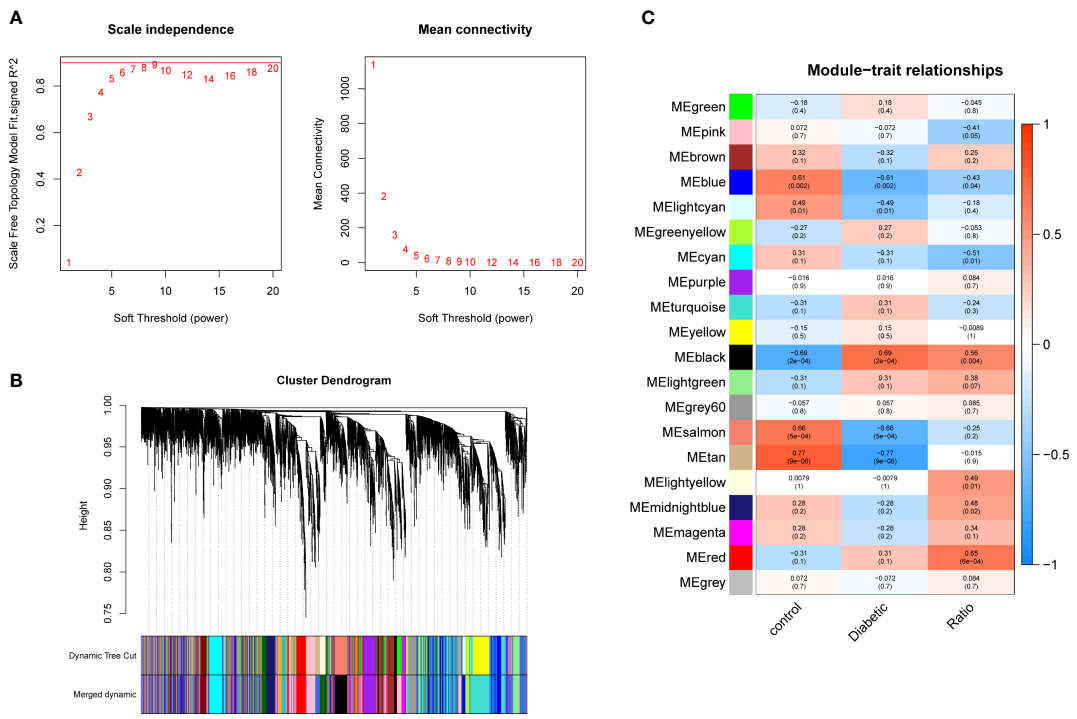

FIGURE 2
Gene co-expression modules. **(A)** Analysis of network topology for soft-thresholding powers. **(B)** Hierarchical cluster dendrogram of DCM-related genes based on one dissimilarity measure. **(C)** Module-phenotype associations.

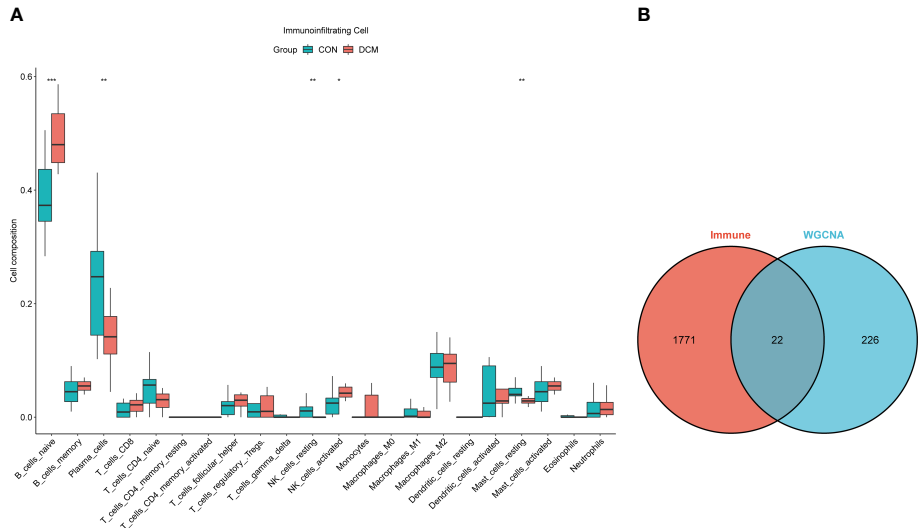

FIGURE 3
Immune infiltration analysis and intersection dataset. **(A)** Boxplot diagram of proportions of 22 types of immune cells. **(B)** Venn diagram of intersection of black modules and immune genes. * means p value <0.05; ** means p value <0.01; *** means p value <0.001.

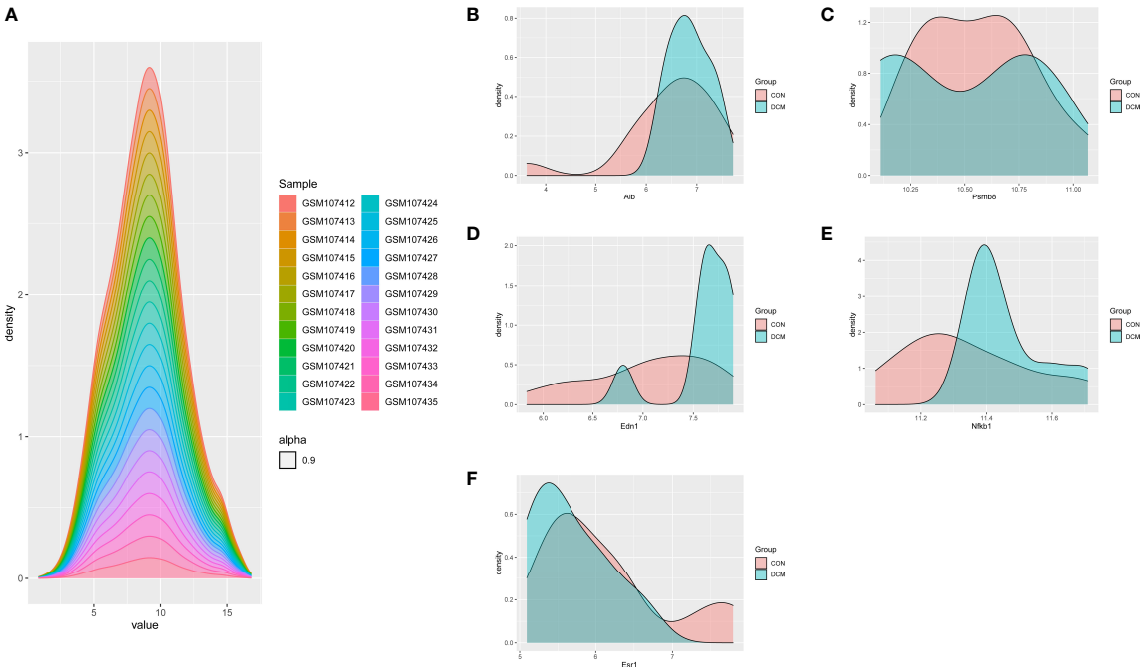

FIGURE 4
Density plots of the dataset GSE4745, showing a smooth distribution of the points along the numeric axis. The peaks of the density plot are at the locations with the highest concentration of points. **(A)** density plot of sample dataset. **(B–F)** Density plots of hub genes.

GO and KEGG enrichment analysis of modules and gene sets

The primary enrichments corresponding to the black module included small-molecule catabolic process, fatty acid metabolic process, ribonucleotide metabolic process, NADH metabolic process, response to hypoxia, and response to nutrient levels. Primary enrichments in the cell component (CC) included mitochondrial matrix, apical plasma membrane, cytosolic ribosome, and oxidoreductase complex. The primary enrichment in molecule function (MF) was thioester hydrolase activity. Primary enrichments in the KEGG pathway were valine, leucine, and isoleucine degradation; carbon metabolism; glutathione metabolism; and the PPAR signaling pathway (Supplementary Figure 3). GSEA showed that compared to control samples (screening based on |NES|>0.7,P < 0.05, and q < 0.25), the identified CC terms were complex with collagen trimers. The identified MF terms were thioester hydrolase activity, intracellular ligand-gated ion channel activity, and extracellular matrix structural constituents, conferring tensile strength. The identified reaction terms included mitochondrial fatty acid beta-oxidation, insulin processing, interferon alpha/beta signaling, collagen chain trimerization, and branched-chain amino acid catabolism. The identified pathways were linoleic acid metabolism, fatty acid elongation, unsaturated fatty acid biosynthesis, and chemical carcinogenesis (DNA adducts) (Figure 5).

Murine model of DCM

A total of 24 mice were included, 12 experimental and 12 controls. There was a statistically significant difference in E/A ratios between groups (1.20 ± 0.14 vs 1.42 ± 0.22; P = 0.006), indicating significant diastolic dysfunction. Moreover, EF (65.3 ± 4.4 vs 72.3 ± 5.4; P = 0.002) and FS (35.1 ± 3.0 vs 40.8 ± 4.5; P = 0.001) values for the experimental group were significantly smaller than those of the controls, indicative of systolic dysfunction. All echocardiography parameters measured are listed in Table 1.

qPCR validation of hub genes and TFs

Relative expression levels of the hub genes are shown in Figure 6. The difference in gene expression between the DCM and CON groups was consistent with the PCR results. No statistically significant differences were found in the expression of four genes (*Psmb8*, *Alb*, *Nfkb1*, and *Esr1*). Only the expression of *Edn1* in the DCM group was significantly higher than that in controls (P = 0.02). The model was also built to test its predictive ability for DCM, with an area under the curve (AUC) of 0.859 for the test set and 0.861 for the validation set, showing good sensitivity and specificity. The three most likely upstream TFs (PRDM5, GATA4, and KLF4) corresponding to EDN1 were predicted by JASPAR and imported into GEPIA for validation of

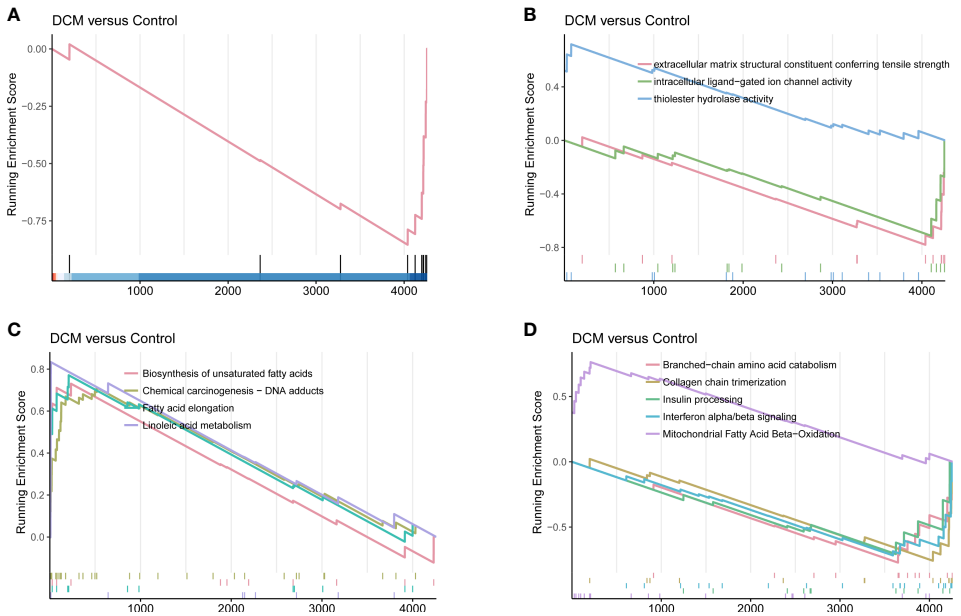

FIGURE 5
DCM-related gene set enrichment analysis. **(A)** Cell component. **(B)** Molecular function. **(C)** KEGG pathway. **(D)** Reactome.

10.3389/fendo.2022.933635

TABLE 1 Ultrasound in mice.

Group	DCM N = 12	CON N = 12	P	TOTAL N = 24
A, mm/s	609 ± 113	544 ± 72	0.105	577 ± 98
E, mm/s	722 ± 93	764 ± 95	0.284	743 ± 94
E/A	1.20 ± 0.14	1.42 ± 0.22	0.006	1.3 ± 0.2
Heart Rate, bpm	531 ± 78	550 ± 45	0.475	540 ± 63
Diameter;s, mm	2.34 ± 0.28	2.10 ± 0.28	0.045	2.2 ± 0.3
Diameter;d, mm	3.60 ± 0.27	3.53 ± 0.24	0.546	3.6 ± 0.25
Volume;s, ul	19.4 ± 6.1	14.9 ± 5.0	0.06	17.1 ± 5.9
Volume;d, ul	54.8 ± 10.0	52.6 ± 8.3	0.536	53.6 ± 9.1
Stroke Volume, ul	35.4 ± 4.4	37.6 ± 4.2	0.23	36.5 ± 4.4
Ejection Fraction, %	65.3 ± 4.4	72.3 ± 5.4	0.002	68.8 ± 6.0
Fractional Shortening, %	35.1 ± 3.0	40.8 ± 4.5	0.001	38.0 ± 4.7
Cardiac Output, ml/min	18.6 ± 2.7	20.6 ± 2.3	0.069	19.6 ± 2.7
LV Mass, mg	122.5 ± 12.0	134.2 ± 19.2	0.089	128.4 ± 16.7
LV Mass Cor, mg	98.0 ± 9.6	107.3 ± 15.3	0.089	102.7 ± 13.4
LVAW;s, mm	1.40 ± 0.14	1.61 ± 0.12	0.001	1.50 ± 0.16
LVAW;d, mm	0.97 ± 0.11	1.10 ± 0.09	0.004	1.03 ± 0.12
LVPW;s, mm	1.29 ± 0.12	1.40 ± 0.09	0.021	1.34 ± 0.11
LVPW;d, mm	0.90 ± 0.08	0.92 ± 0.08	0.524	0.91 ± 0.08

A, A peak; E, E peak; LV, left ventricle; LVAW, Left Ventricular Actual Weight; s, systole; d, diastole; LVPW, Left ventricular posterior wall.

gene and TFr expression correlation. Among them, PRDM5 and KLF4 expression was strongly correlated with EDN1 expression, with correlation coefficients of 0.55 ($P < 0.0001$) and 0.51 ($P < 0.0001$), respectively. The TF core binding thresholds are shown in Figure 7.

Validation of protein level expression

WB was used to detect changes in the expression of target proteins. Compared with that in the normal group, the expression level of Edn1, Alb, Psmb8 and Esr1 in the DCM group was significantly changed; however, the expression levels of Nfkb1 did not differ significantly. This result is consistent with the bioinformatics prediction results and the PCR results (Figure 8).

Candidate target docking and validation

Nine potential therapeutic molecules were identified from the CMap database: telomerase inhibitor IX, isoliquiritigenin, medrysone, benzoic acid, oxymetholone, sulforaphane, pevonedistat, epoxycholesterol, and 2-chloro-6-(1-piperazinyl) pyrazine (Table 2). Pevonedistat failed to bind to EDN1; the binding energies of the remaining candidates were -5.9, -5.3, -5.8, -3.2, -6.5, -2.3, -5.2, and -3.4 kcal/mol, respectively. The molecular docking is diagrammed in Figure 9.

While computational predictions usually require experimental verification, there were greater difficulties and limitations in practical implementation. Based on our experience from previous studies (12), we constructed receiver operator characteristic curve (ROC) curves corresponding to the components (active and inactive compounds) to be separated by virtual screening (Figure 10). Among them, medrysone, sulforaphane and 2-chloro-6-(1-piperazinyl)pyrazine were validated, corresponding to AUC of 0.848, 0.776, and 0.9, respectively.

Discussion

DCM is characterized by a feed-forward cycle of metabolic imbalance, HF, and multiple organ dysfunction (3). Hyperglycemia and other metabolic abnormalities that induce systemic inflammation activate the immune system play roles in the progression of DCM (13). The interactions of multiple innate and adaptive immune cell populations, as well as the immune response and its regulation, also play important roles. Currently, clinical treatment strategies for DCM focus on antifibrotic agents, anti-inflammatory agents, and antioxidants, in addition to controlling metabolic disorders (14, 15). Based on immunomodulation, we expected to find key targets in diabetic

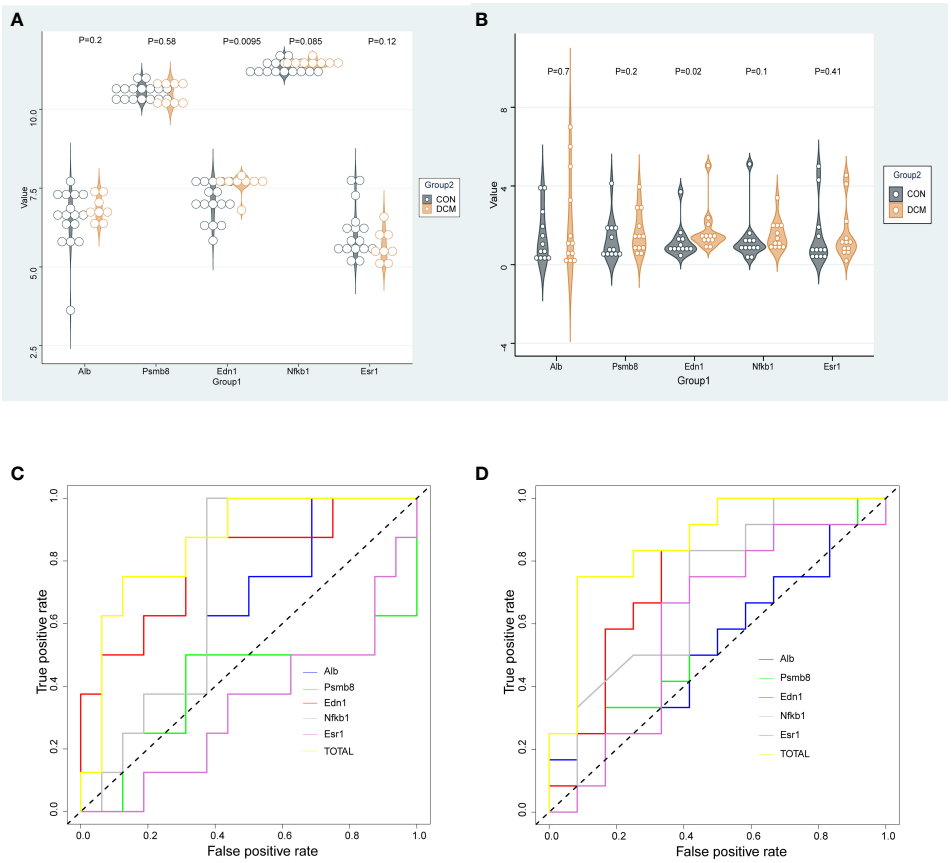

FIGURE 6
Gene expression and validation. **(A)** Dataset gene expression; **(B)** Murine DCM gene expression; **(C)** ROC for gene expression in dataset; **(D)** ROC curve for murine DCM gene expression.

cardiomyopathy to provide a highly sensitive and early method for diagnosis and targeted therapy.

A hostile environment of hyperglycemia, hyperlipidemia, hyperinsulinemia, and insulin resistance, underpinned by chronic systemic inflammation, activates the RAAS and maladaptive immune responses, changes the function of calcium, and regulates the release of cytokine in DCM (16, 17). GO function and pathway enrichment analyses showed that the products of the identified screened genes were located in the mitochondrial matrix, apical plasma membrane, cytosolic ribosome, and oxidoreductase complex; they are involved in the regulation of redox state, fatty acid metabolism, and nucleotide metabolism, which is consistent with the relevant literature. KEGG analysis showed that fatty acid synthesis and metabolism were important pathways associated with diabetic HF (18, 19). It is consistent with the reported results that diabetic cardiomyopathy is closely related to immunity (13, 20).

Through reanalysis of the GSE4745, we identified the black module as the most significant for diabetic HF with WGCNA and CIBERSORT algorithms, then identified five hub genes based on their degree values from the PPI network.: *PSMB8, NFKB1, ALB, EDN1*, and *ESR1*. Proteasome subunit beta 8) is a catalytic subunit involved in tumor infiltration and neuroinflammation (21, 22). Nuclear factor kappa B1 is a classic transcriptional regulator with multi-system involvement (23). Albumin acts as a carrier of fatty acids and a variety of enzymes, involved in the metabolism of endogenous and exogenous compounds. Hypoalbuminemia has also emerged as an independent prognosticator in many cardiovascular diseases (24, 25). *ESR1* encodes the estrogen receptor and ligand-activated TFs to regulate the estrogen signaling pathway, but its abundance in the heart is much less than that in the endometrium. It is usually relevant to the growth of galactophore tumors but has also been reported to be involved in impaired glycemic homeostasis (26). *EDN1*, located on human chromosome 6, encodes a pre-proprotein that generates a secreted peptide of the endothelin/sarafotoxin family that affects blood vessel contraction.

Identified and verified by RT-PCR in our study, the expression of *EDN1* was found to be of significantly higher

10.3389/fendo.2022.933635

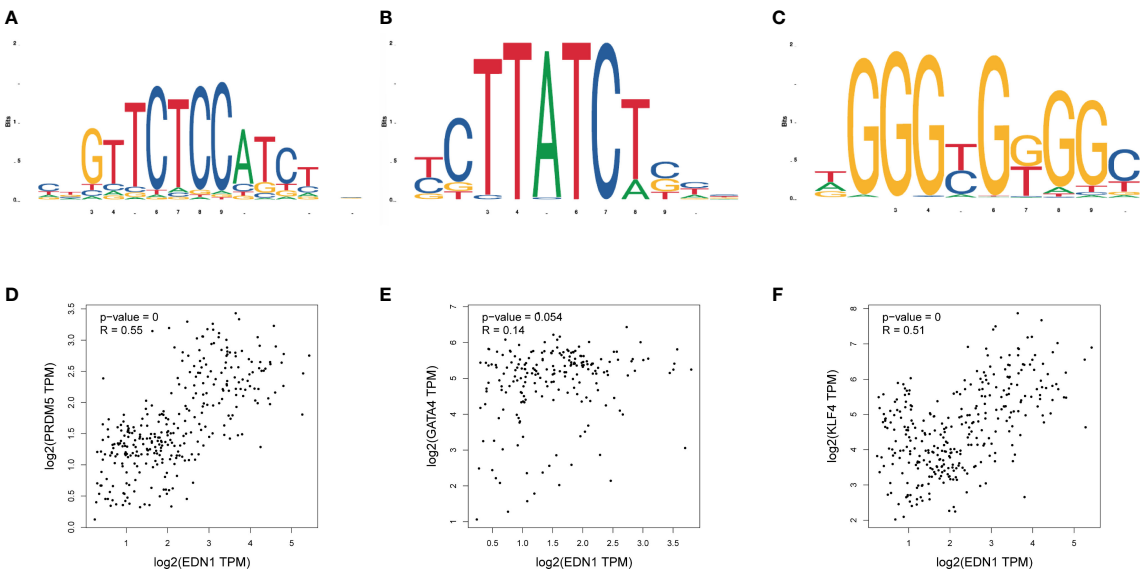

FIGURE 7
Binding sites of transcription factors and expression correlation verification. **(A)** Binding site of *Prdm5*; **(B)** Binding site of *Gata4*; **(C)** Binding site of *Klf4*; **(D)** Correlation between *Prdm5* and *Edn1* gene expression in myocardial tissue; **(E)** Correlation between *Gata4* and *Edn1* gene expression in myocardial tissue; **(F)** Correlation between *Klf4* and *Edn1* gene expression in myocardial tissue.

level in DCM than in normal samples. A separate GWAS suggested that phosphatase and actin regulator protein 1 (PHACTR1) and EDN1 (upstream of PHACTR1) are risk factors in five vascular diseases, including CAD, migraine, cervical artery dissection, fibromuscular dysplasia, and hypertension (27). Also, binding of both mineralocorticoid and glucocorticoid receptors to the endothelin 1 EDN1 hormone response elements plays an important role in the regulation of renal sodium transport and cardiovascular physiology (28). Case-control studies have shown that

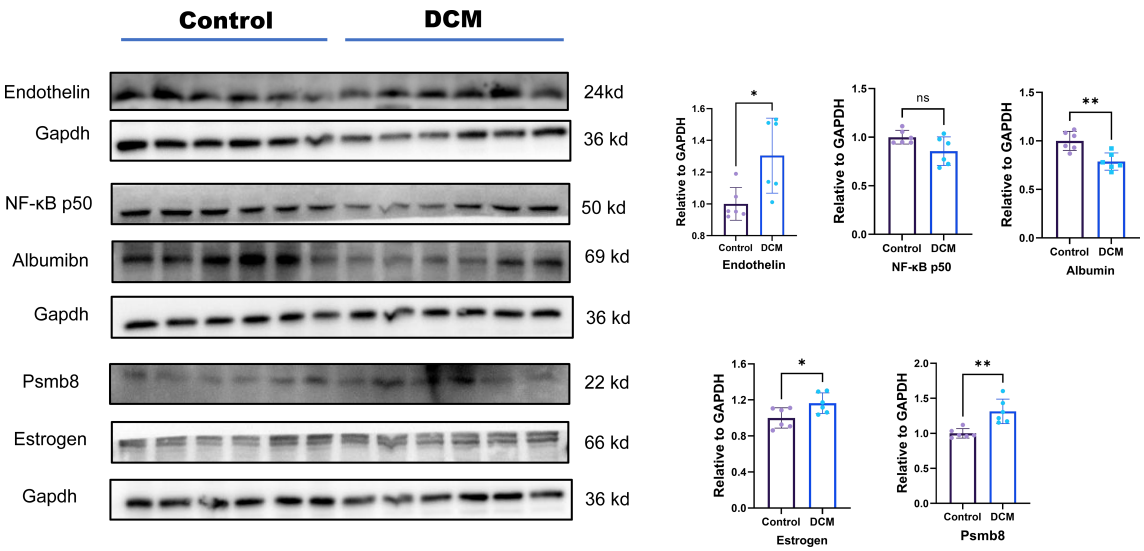

FIGURE 8
Protein level expression of hub genes. Ns means p value >0.05;* means p value <0.05; ** means p value <0.01; *** means p value <0.001.

10.3389/fendo.2022.933635

TABLE 2 Significant small molecule chemicals.

Name	Score	Description	Target	Canonical SMILES
Telomerase Inhibitor IX	96.29	Telomerase inhibitor	TERT	C1=CC(=CC(=C1)NC(=O)C2=C(C(=CC=C2)O)O)NC(=O)C3=C(C(=CC=C3)O)O
Isoliquiritigenin	93.6	Guanylate cyclase activator	AKR1B1, HRH2, SIRT1	C1=CC(=CC=C1C=CC(=O)C2=C(C=C(C=C2)O)O)O
Medrysone	90.81	Glucocorticoid receptor agonist	NR3C1	CC1CC2C3CCC(C3(CC(C2C4(C1=CC(=O)CC4)C)O)C)C(=O)C
Benzoic acid	87.7	Protein tyrosine kinase inhibitor	ABL1, EGFR	COC(=O)C1=CC=C(C=C1)NCC2=C(C=CC(=C2)O)O
Oxymetholone	86.26	Androgen receptor agonist	AR	CC12CCC3C(C1CCC2(C)O)CCC4C3(CC(=CO)C(=O)C4)C
Sulforaphane	86.22	Antineoplastic	NFE2L2	CS(=O)CCCCN=C=S
Pevonedistat	85.24	Nedd activating enzyme inhibitor	NAE1, UBA3	C1CC2=CC=CC=C2C1NC3=C4C=CN(C4=NC=N3)C5CC(C(C5)O)COS(=O)(=O)N
Epoxycholesterol	85.16	LXR agonist	NR1H2, NR1H3	CC(C)CCCC(C)C1CCC2C1(CCC3C2CC4C5(C3(CCC(C5)O)C)O4)C
2-Chloro-6-(1-piperazinyl) pyrazine	-93.16	Serotonin receptor agonist	HTR2A,HTR2B, HTR2C	C1CN(CCN1)C2=CN=CC(=N2)Cl

Canonical SMILE: Internationally recognized atomic structure. Target: Validated targets with activity.

PHACTR1/EDN1 is a risk factor for several vascular diseases, such as spontaneous coronary artery dissection (SCAD) (29). Some studies have suggested an association between the *EDN1* polymorphism and risk of atherosclerosis progression in great cardiac vessels and coronary arteries (30, 31). EDN1 has been implicated in the pathogenesis of microcirculation disturbances and may be critical for maintaining normal contractile function and preventing the myocardium from overstretching or even affecting blood pressure levels (32–34). Coronary microvascular dysfunction has been reported in patients with diabetes through quantitative myocardial contrast echocardiography and strain-rate imaging, as well as by adenosine stress cardiovascular magnetic resonance (CMR) (35, 36). Therefore, it is reasonable to hypothesize that EDN1 is a potential biomarker for HF induced by DCM.

We screened for potential therapeutics that can regulate the activity of TFs upstream of EDN1 to affect the pathophysiology of diabetic cardiomyopathy. Based on molecular docking, we identified telomerase inhibitor IX, isoliquiritigenin, medrysone, benzoic acid, Oxymetholone, sulforaphane,

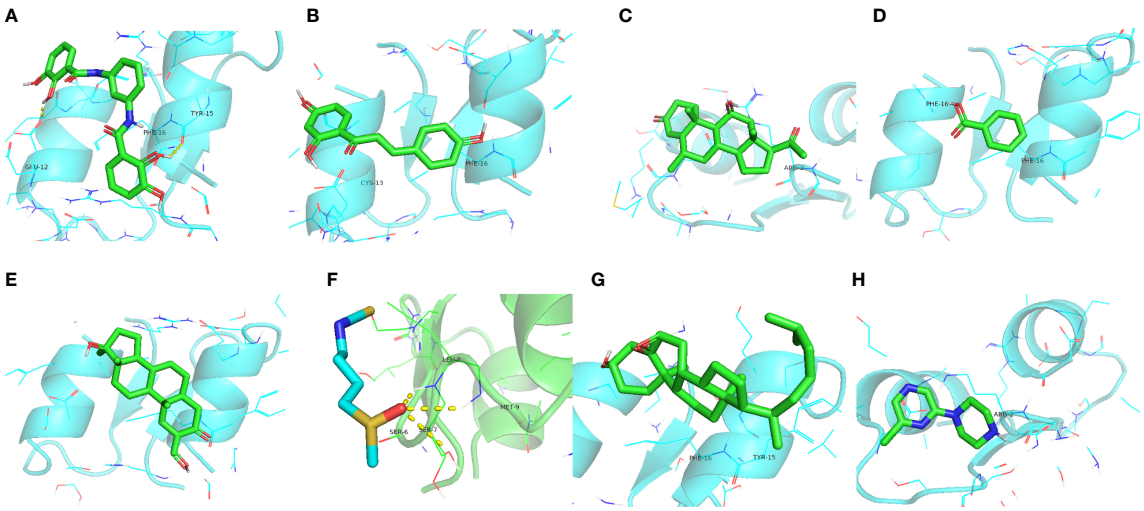

FIGURE 9
Molecular docking simulations. **(A)** EDN1 with telomerase inhibitor IX. **(B)** EDN1 with isoliquiritigenin. **(C)** EDN1 with medrysone. **(D)** EDN1 with benzoic acid. **(E)** EDN1 with oxymetholone. **(F)** EDN1 with sulforaphane. **(G)** EDN1 with epoxycholesterol. **(H)** 2-chloro-6-(1-piperazinyl)pyrazine.

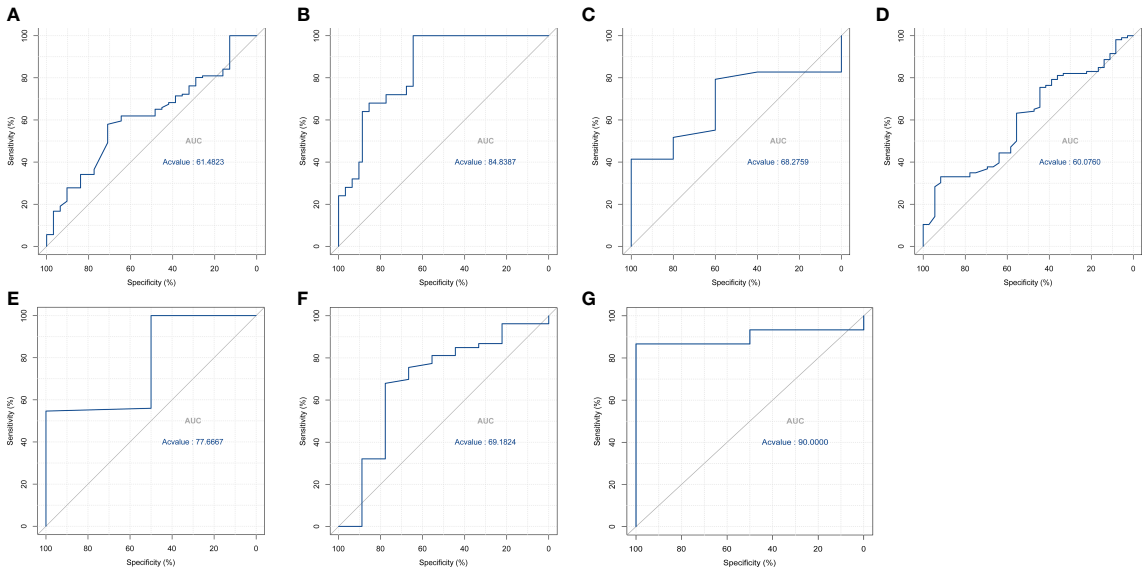

FIGURE 10
ROC curves of the virtual filter for **(A)** isoliquiritigenin; **(B)** medrysone; **(C)** benzoic acid; **(D)** oxymetholone; **(E)** sulforaphane; **(F)** pevonedistat; **(G)** 2-chloro-6-(1-piperazinyl)pyrazine.

epoxycholesterol, and 2-chloro-6-(1-piperazinyl)pyrazine. In other studies, it has been shown that telomerase inhibitor IX affects tumor inhibition (37). Isoliquiritigenin has neuroprotective and antioxidant activities, while inhibiting apoptosis by ameliorating the loss of mitochondrial membrane potential and the change of nuclear morphology (38). Medrysone suppresses the effects of multiple aspects of innate and adaptive immune responses (39). Benzoic acid has been shown to improve gut functions *via* regulating enzyme activity, redox status, immunity, and microbiota (40). Oxymetholone's anabolic properties have been studied for the treatment of damaged myocardium (41). Through the molecular target Nrf2 of Sulforaphane, it can exert a beneficial role by activating genes and molecules with antioxidant, anti-inflammatory, and anti-apoptotic properties (42). Epoxycholesterol can prevent foam cell formation in human SMCs and restore the elaboration of extracellular matrix (43). However, these molecular docking and network data require further validation by *in vivo* and *in vitro* experiments.

This study has two primary limitations. First, the verification of hub genes and their functions has only been performed in a murine model, but not in other animals or in human clinical trials. Second, experiments related to biological functions *in vivo* and *in vitro* require further study. In conclusion, in this study, we found *EDN1* to be a key gene in DCM, then predicted its regulatory TFs and identified potential therapeutic molecules. This suggests that *EDN1* has potential as a biomarker and therapeutic target for DCM.

Data availability statement

Publicly available datasets were analyzed in this study. This data can be found here: Gene Expression Omnibus (GEO), accession number, GSE4745.

Ethics statement

The animal study was reviewed and approved by Animal Ethics Committee of Nanjing Medical University (License number: IACUC-1903016).

Author contributions

XL provided the general direction of the project, while QG performed data extraction, statistical analysis and writing. QZ was responsible for the establishment of animal models and the testing of model data. TZ, IC, SL, MC, XZ, and MS provided their own suggestions for revision when writing was completed. All authors have read and approved the final version of the manuscript.

Funding

This research was supported by National Natural Science Foundation of China (grant number 2017YFC1700505).

Acknowledgments

The authors thank the patients and investigators who participated in GEO for providing the data and Jiajin Chen, Department of Biostatistics, School of Public Health, Nanjing Medical University, for statistical guidance.

Conflict of interest

The authors declare that the research was conducted in the absence of any commercial or financial relationships that could be construed as a potential conflict of interest.

The reviewers JS and JL declared a shared affiliation, with no collaboration, with the authors to the handling editor at the time of the review.

Publisher's note

Supplementary material

The Supplementary Material for this article can be found online at: https://www.frontiersin.org/articles/10.3389/fendo.2022.933635/full#supplementary-material

References

1. Cosentino F, Grant PJ, Aboyans V, Bailey CJ, Ceriello A, Delgado V, et al. ESC Guidelines on diabetes, pre-diabetes, and cardiovascular diseases developed in collaboration with the EASD. *Eur Heart J* (2020) 41(2):255–323. doi: 10.1093/eurheartj/ehz486

2. Jia G, Hill MA, Sowers JR. Diabetic cardiomyopathy: An update of mechanisms contributing to this clinical entity. *Circ Res* (2018) 122(4):624–38. doi: 10.1161/CIRCRESAHA.117.311586

3. Braunwald E. Diabetes, heart failure, and renal dysfunction: the vicious circles. *Prog Cardiovasc Dis* (2019) 62(4):298–302. doi: 10.1016/j.pcad.2019.07.003

4. Stanton AM, Vaduganathan M, Chang LS, Turchin A, Januzzi JLJr., Aroda VR. Asymptomatic diabetic cardiomyopathy: an underrecognized entity in type 2 diabetes. *Curr Diabetes Rep* (2021) 21(10):41. doi: 10.1007/s11892-021-01407-2

5. Ritchie RH, Abel ED. Basic mechanisms of diabetic heart disease. *Circ Res* (2020) 126(11):1501–25. doi: 10.1161/CIRCRESAHA.120.315913

6. Murtaza G, Virk HUH, Khalid M, Lavie CJ, Ventura H, Mukherjee D, et al. Diabetic cardiomyopathy - a comprehensive updated review. *Prog Cardiovasc Dis* (2019) 62(4):315–26. doi: 10.1016/j.pcad.2019.03.003

7. Jia G, Whaley-Connell A, Sowers JR. Diabetic cardiomyopathy: a hyperglycaemia- and insulin-resistance-induced heart disease. *Diabetologia* (2018) 61(1):21–8. doi: 10.1007/s00125-017-4390-4

8. Lutgens E, Atzler D, Döring Y, Duchene J, Steffens S, Weber C. Immunotherapy for cardiovascular disease. *Eur Heart J* (2019) 40(48):3937–46. doi: 10.1093/eurheartj/ehz283

9. Taz TA, Ahmed K, Paul BK, Al-Zahrani FA, Mahmud SMH, Moni MA. Identification of biomarkers and pathways for the SARS-CoV-2 infections that make complexities in pulmonary arterial hypertension patients. *Brief Bioinform* (2021) 22(2):1451–65. doi: 10.1093/bib/bbab026

10. Mahmud SMH, Al-Mustanjid M, Akter F, Rahman MS, Ahmed K, Rahman MH, et al. Bioinformatics and system biology approach to identify the influences of SARS-CoV-2 infections to idiopathic pulmonary fibrosis and chronic obstructive pulmonary disease patients. *Brief Bioinform* (2021) 22(5):bbab115. doi: 10.1093/bib/bbab115

11. Taz TA, Ahmed K, Paul BK, Kawsar M, Aktar N, Mahmud SMH, et al. Network-based identification genetic effect of SARS-CoV-2 infections to idiopathic pulmonary fibrosis (IPF) patients. *Brief Bioinform* (2021) 22(2):1254–66. doi: 10.1093/bib/bbaa235

12. Tanzir Mehedi S, Ahmed K, Bui FM, Rahaman M, Hossain I, Tonmoy TM, et al. MLBioIGE: integration and interplay of machine learning and bioinformatics approach to identify the genetic effect of SARS-COV-2 on idiopathic pulmonary fibrosis patients. *Biol Methods Protoc* (2022) 7(1):bpac013. doi: 10.1093/biomethods/bpac013

13. Tian CJ, Zhang JH, Liu J, Ma Z, Zhen Z. Ryanodine receptor and immune-related molecules in diabetic cardiomyopathy. *ESC Heart Fail* (2021) 8(4):2637–46. doi: 10.1002/ehf2.13431

14. Tan Y, Zhang Z, Zheng C, Wintergerst KA, Keller BB, Cai L. Mechanisms of diabetic cardiomyopathy and potential therapeutic strategies: preclinical and clinical evidence. *Nat Rev Cardiol* (2020) 17(9):585–607. doi: 10.1038/s41569-020-0339-2

15. Nishida K, Otsu K. Inflammation and metabolic cardiomyopathy. *Cardiovasc Res* (2017) 113(4):389–98. doi: 10.1093/cvr/cvx012

16. Jia G, DeMarco VG, Sowers JR. Insulin resistance and hyperinsulinaemia in diabetic cardiomyopathy. *Nat Rev Endocrinol* (2016) 12(3):144–53. doi: 10.1038/nrendo.2015.216

17. Kaur N, Guan Y, Raja R, Ruiz-Velasco A, Liu W. Mechanisms and therapeutic prospects of diabetic cardiomyopathy through the inflammatory response. *Front Physiol* (2021) 12:694864. doi: 10.3389/fphys.2021.694864

18. Birkenfeld AL, Jordan J, Dworak M, Merkel T, Burnstock G. Myocardial metabolism in heart failure: purinergic signalling and other metabolic concepts. *Pharmacol Ther* (2019) 194:132–44. doi: 10.1016/j.pharmthera.2018.08.015

19. Berthiaume JM, Kurdys JG, Muntean DM, Rosca MG. Mitochondrial NAD(+)/NADH redox state and diabetic cardiomyopathy. *Antioxid Redox Signal* (2019) 30(3):375–98. doi: 10.1089/ars.2017.7415

20. Sun Y, Ding S. NLRP3 inflammasome in diabetic cardiomyopathy and exercise intervention. *Int J Mol Sci* (2021) 22(24)13228. doi: 10.3390/ijms222413228

21. Chen D, Jin C, Dong X, Wen J, Xia E, Wang Q, et al. Pan-cancer analysis of the prognostic and immunological role of PSMB8. *Sci Rep* (2021) 11(1):20492. doi: 10.1038/s41598-021-99724-9

22. Guo T, Liu C, Yang C, Wu J, Su P, Chen J. Immunoproteasome subunit PSMB8 regulates microglia-mediated neuroinflammation upon manganese exposure by PERK signaling. *Food Chem Toxicol* (2022) 163:112951. doi: 10.1016/j.fct.2022.112951

23. Lorenzini T, Fliegauf M, Klammer N, Frede N, Proietti M, Bulashevska A, et al. Characterization of the clinical and immunologic phenotype and management of 157 individuals with 56 distinct heterozygous NFkB1 mutations. *J Allergy Clin Immunol* (2020) 146(4):901–11. doi: 10.1016/j.jaci.2019.11.051

24. De Simone G, di Masi A, Ascenzi P. Serum albumin: A multifaced enzyme. *Int J Mol Sci* (2021) 22(18) 10086. doi: 10.3390/ijms221810086

25. Arques S. Human serum albumin in cardiovascular diseases. *Eur J Intern Med* (2018) 52:8–12. doi: 10.1016/j.ejim.2018.04.014

26. Gregorio KCR, Laurindo CP, Machado UF. Estrogen and glycemic homeostasis: the fundamental role of nuclear estrogen receptors ESR1/ESR2 in glucose transporter GLUT4 regulation. *Cells* (2021) 10(1) 99. doi: 10.3390/cells10010099

27. Gupta RM, Hadaya J, Trehan A, Zekavat SM, Roselli C, Klarin D, et al. A genetic variant associated with five vascular diseases is a distal regulator of endothelin-1 gene expression. *Cell* (2017) 170(3):522–533.e15. doi: 10.1016/j.cell.2017.06.049

28. Stow LR, Gumz ML, Lynch IJ, Greenlee MM, Rudin A, Cain BD, et al. Aldosterone modulates steroid receptor binding to the endothelin-1 gene (edn1). *J Biol Chem* (2009) 284(44):30087–96. doi: 10.1074/jbc.M109.030718

29. Adlam D, Olson TM, Combaret N, Kovacic JC, Iismaa SE, Al-Hussaini A, et al. Association of the PHACTR1/EDN1 genetic locus with spontaneous coronary artery dissection. *J Am Coll Cardiol* (2019) 73(1):58–66. doi: 10.1016/j.jacc.2018.09.085

30. Vargas-Alarcon G, Vallejo M, Posadas-Romero C, Juarez-Rojas JG, Martinez-Rios MA, Peña-Duque MA, et al. The -974C>A (rs3087459) gene polymorphism in the endothelin gene (EDN1) is associated with risk of developing acute coronary syndrome in Mexican patients. *Gene* (2014) 542 (2):258–62. doi: 10.1016/j.gene.2013.09.003

31. Dubovyk YI, Oleshko TB, Harbuzova VY, Ataman AV. Positive association between EDN1 rs5370 (Lys198Asn) polymorphism and large artery stroke in a Ukrainian population. *Dis Markers* (2018) 2018:1695782. doi: 10.1155/2018/1695782

32. Hathaway CK, Grant R, Hagaman JR, Hiller S, Li F, Xu L, et al. Endothelin-1 critically influences cardiac function *via* superoxide-MMP9 cascade. *PNAS* (2015) 112(16):5141–6. doi: 10.1073/pnas.1504557112

33. Funalot B, Courbon D, Brousseau T, Poirier O, Berr C, Cambien F, et al. Genes encoding endothelin-converting enzyme-1 and endothelin-1 interact to influence blood pressure in women: the EVA study. *J Hypertens* (2004) 22(4):739–43. doi: 10.1097/00004872-200404000-00016

34. Ford TJ, Corcoran D, Padmanabhan S, Aman A, Rocchiccioli P, Good R, et al. Genetic dysregulation of endothelin-1 is implicated in coronary microvascular dysfunction. *Eur Heart J* (2020) 41(34):3239–52. doi: 10.1093/eurheartj/ehz915

35. Moir S, Hanekom L, Fang ZY, Haluska B, Wong C, Burgess M, et al. Relationship between myocardial perfusion and dysfunction in diabetic cardiomyopathy: a study of quantitative contrast echocardiography and strain rate imaging. *Heart (Br Card Soc)* (2006) 92(10):1414–9. doi: 10.1136/hrt.2005.079350

36. Levelt E, Rodgers CT, Clarke WT, Mahmod M, Ariga R, Francis JM, et al. Cardiac energetics, oxygenation, and perfusion during increased workload in patients with type 2 diabetes mellitus. *Eur Heart J* (2016) 37(46):3461–9. doi: 10.1093/eurheartj/ehv442

37. Li Y, Gu J, Ding Y, Gao H, Li Y, Sun Y, et al. A small molecule compound IX inhibits telomere and attenuates oncogenesis of drug-resistant leukemia cells. *FASEB J* (2020) 34(7):8843–57. doi: 10.1096/fj.201902651RR

38. Shi D, Yang J, Jiang Y, Wen L, Wang Z, Yang B. The antioxidant activity and neuroprotective mechanism of isoliquiritigenin. *Free Radic Biol Med* (2020) 152:207–15. doi: 10.1016/j.freeradbiomed.2020.03.016

39. Bano S, Wahab AT, Yousuf S, Jabeen A, Mesaik MA, Rahman AU, et al. New anti-inflammatory metabolites by microbial transformation of medrysone. *PloS One* (2016) 11(4):e0153951. doi: 10.1371/journal.pone.0153951

40. Mao X, Yang Q, Chen D, Yu B, He J. Benzoic acid used as food and feed additives can regulate gut functions. *BioMed Res Int* (2019) 2019:5721585. doi: 10.1155/2019/5721585

41. Pavlatos AM, Fultz O, Monberg MJ, Vootkur APharmd. Review of oxymetholone: a 17alpha-alkylated anabolic-androgenic steroid. *Clin Ther* (2001) 23(6):789–801. discussion 771. doi: 10.1016/S0149-2918(01)80070-9

42. Schepici G, Bramanti P, Mazzon E. Efficacy of sulforaphane in neurodegenerative diseases. *Int J Mol Sci* (2020) 21(22) 8637. doi: 10.3390/ijms21228637

43. Beyea MM, Reaume S, Sawyez CG, Edwards JY, O'Neil C, Hegele RA, et al. The oxysterol 24(s),25-epoxycholesterol attenuates human smooth muscle-derived foam cell formation *via* reduced low-density lipoprotein uptake and enhanced cholesterol efflux. *J Am Heart Assoc* (2012) 1(3):e000810. doi: 10.1161/JAHA.112.000810

frontiers | Frontiers in Endocrinology

TYPE Original Research
PUBLISHED 18 August 2022
DOI 10.3389/fendo.2022.953305

OPEN ACCESS

EDITED BY
Jamie Lynn Young,
University of Louisville, United States

REVIEWED BY
Andrew P Braun,
University of Calgary, Canada
Frank Christopher Howarth,
United Arab Emirates University,
United Arab Emirates

*CORRESPONDENCE
Yanfang Zheng
yfzheng@fjtcm.edu.cn
Mingqing Huang
hmq1115@126.com
Xian Zhou
p.zhou@westernsydney.edu.au

†These authors have contributed equally to this work and share first authorship

SPECIALTY SECTION
This article was submitted to Cardiovascular Endocrinology, a section of the journal Frontiers in Endocrinology

RECEIVED 26 May 2022
ACCEPTED 04 August 2022
PUBLISHED 18 August 2022

CITATION
Wang C, Sun Y, Liu W, Liu Y, Afzal S, Grover J, Chang D, Münch G, Li CG, Lin S, Chen J, Zhang Y, Cheng Z, Lin Y, Zheng Y, Huang M and Zhou X (2022) Protective effect of the curcumin-baicalein combination against macrovascular changes in diabetic angiopathy.
Front. Endocrinol. 13:953305.
doi: 10.3389/fendo.2022.953305

Protective effect of the curcumin-baicalein combination against macrovascular changes in diabetic angiopathy

Chenxiang Wang[1†], Yibin Sun[1†], Wenjing Liu[1†], Yang Liu[2], Sualiha Afzal[3], Jahnavi Grover[3], Dennis Chang[2], Gerald Münch[3], Chun Guang Li[2], Shiling Lin[1], Jianyu Chen[1], Yiping Zhang[4], Zaixing Cheng[1], Yanxiang Lin[1], Yanfang Zheng[1*], Mingqing Huang[1*] and Xian Zhou[2*]

[1]Fujian Key Laboratory of Chinese Materia Medica, College of Pharmacy, Fujian University of Traditional Chinese Medicine, Fuzhou, China, [2]NICM Health Research Institute, Western Sydney University, Westmead, NSW, Australia, [3]School of Medicine, Western Sydney University, Campbelltown, NSW, Australia, [4]Third Institute of Oceanography, Technical Innovation Center for Utilization of Marine Biological Resources, Ministry of Natural Resources, Xiamen, China

Endothelial dysfunction is an early pathological event in diabetic angiopathy which is the most common complication of diabetes. This study aims to investigate individual and combined actions of Curcumin (Cur) and Baicalein (Bai) in protecting vascular function. The cellular protective effects of Cur, Bai and Cur+Bai (1:1, *w/w*) were tested in H_2O_2 (2.5 mM) impaired EA. hy926 cells. Wistar rats were treated with vehicle control as the control group, Goto-Kakizaki rats (n=5 each group) were treated with vehicle control (model group), Cur (150 mg/kg), Bai (150 mg/kg), or Cur+Bai (75 mg/kg Cur + 75 mg/kg Bai, OG) for 4 weeks after a four-week high-fat diet to investigate the changes on blood vessel against diabetic angiopathy. Our results showed that Cur+Bai synergistically restored the endothelial cell survival and exhibited greater effects on lowering the fasting blood glucose and blood lipids in rats comparing to individual compounds. Cur+Bai repaired the blood vessel structure in the aortic arch and mid thoracic aorta. The network pharmacology analysis showed that Nrf2 and MAPK/JNK kinase were highly relevant to the multi-targeted action of Cur+Bai which has been confirmed in the *in vitro* and *in vivo* studies. In conclusion, Cur+Bai demonstrated an enhanced activity in attenuating endothelial dysfunction against oxidative damage and effectively protected vascular function in diabetic angiopathy rats.

KEYWORDS

curcumin, baicalein, endothelial dysfunction, diabetic angiopathy, synergy, network pharmacology, Nrf2-HO-1, MAPK/JNK

Introduction

As the major regulator of vascular homeostasis, the endothelium is an important locus to control vascular constriction and dilation (1). Endothelial dysfunction, characterised as a disrupted balance between vasodilation and vasoconstriction, is associated with many diseases including diabetes mellitus (DM), cardiovascular diseases and metabolic syndrome (2).

Endothelial injury occurs due to many risk factors including oxidative stress, inflammation, long-term hyperglycemia, insulin resistance, glucose and lipid metabolism disorders (3). In particular this process can result in the development of diabetic angiopathy, which is closely related to the mortality and morbidity arising from DM (4).

Hyperlipidemia is an independent risk factor of endothelial dysfunction. Chronic hyperglycemia and hyperlipidemia in DM both induce higher oxidative stress and inflammation in endothelium leading to excessive apoptosis and dysfunction of vascular endothelial cells. Cell damage increases the permeability of the endothelial layer, which promotes the invasion and accumulation of lipids in the blood vessel wall (5, 6). Additionally, immune cells such as monocytes are also recruited into the vascular endothelium due to inflammation, further contribute to the development of diabetic angiopathy.

Curcumin (Cur), the main natural polyphenol found in *Curcuma longa* L. species, has been demonstrated to markedly attenuate DM-induced endothelial dysfunction in animal studies (7, 8). The mechanism of Cur in protecting the endothelium have been investigated in the diabetic model. The benefit was mainly attributed to the inhibition of oxidative stress, as evidenced by decreased reactive oxygen species (ROS) (8), superoxide overproductions and increased heme oxygenase 1 (HO-1) activity (7). The efficacy of Cur in clinical trials remains inconclusive as it has been limited by poor bioavailability (low absorption and rapid excretion). Thus, research focus has been shifted to the modification of structure or the combined use of Cur with other biomolecules or phytochemicals to enhance its efficacy and bioavailability (9). For example, a Cur and vitamin C combination enhanced the effectiveness in protecting endothelial function, which was related to the strengthened antioxidant with hypoglycemic and hypolipidemic actions (10).

Baicalein (Bai) is a phytochemical isolated from the roots of *Scutellaria baicalensis* Georgi and *Scutellaria lateriflora* L. and possesses a multitude of pharmacological activities (11). It prevented the exaggerated constriction of blood vessels in the insulin-resistance rat model with macro-vascular impairment (12). It also inhibited high glucose-induced vascular inflammation in human umbilical vein endothelial cells (HUVECs) and mouse models (13). However, relatively high doses (100-150 mg/kg) of Bai were used in animal studies, restricting its further investigation in human clinical trials. The mechanism of action of Bai was associated with the upregulation of antioxidant nuclear factor erythroid 2–related factor 2 (Nrf2) mediated antioxidant pathway and downregulating Nuclear factor kappa B (NF-κB)-mediated inflammatory pathways (12, 13).

Chinese herbal medicines serve as an abundant source of drug discovery and development. The key mechanism of Chinese herbal medicines relies on the multi-component and multi-targeted action of the bioactive molecules. Thus, the optimal combination of selected bioactive molecules from Chinese herbal medicines may provide an attractive alternative or adjunct therapy in contrast to the single-entity, single-targeted pharmaceuticals (14). Network Pharmacology, a systems biology approach, can be applied to identify the bioactive molecules in the Chinse herbal medicines, and predict their targeted genes and signaling pathways (15). The development of mathematical models for synergistic interactions has enabled increasing research to determine synergy in natural products leading to novel combination therapies. Among them, combination index (CI) is one of the most popular models to determine the synergistic effect of two or more agents acting on a specific pharmacological target (i.e. receptor, gene, protein) in comparison to the action of each individual agent (16).

Based on the individual effects and associated mechanisms of Cur and Bai in protecting endothelium against diabetes, we speculated that Cur and Bai, when used as a combination, may interact synergistically leading to strengthened antioxidant activity and multi-targeted effects. This study aims to investigate the individual and combined effects of Cur and Bai against macrovascular changes in diabetic angiopathy by protecting the endothelium and their underpinning mechanisms via network pharmacology analysis, *in vitro* and *in vivo* investigations.

Materials and methods

Network construction and network analysis

To analyse the possible interaction of Cur and Bai against relevant disease targets, a network was constructed using the terms "endothelial dysfunction", "diabetic angiopathy" and "atherosclerosis and endothelial dysfunction". Briefly, the target disease condition (i.e. endothelial dysfunction)-related genes were obtained using the Online Mendelian Inheritance in Man (OMIM) Database (http://www.omim.org/), GeneCards Database (https://www.GeneCards.org/) and DisGeNET Database (http://www.disgenet.org/home/) by searching the key words "endothelial dysfunction". Duplicate targets were removed after collecting all the genes targets in the three databases. The 2-dimensional structures of Cur and Bai were obtained from PubChem (https://pubchem.ncbi.nlm.nih.gov/) and their individual structure was subjected to the PharmMapper (http://www.lilab-ecust.cn/pharmmapper/) to populate their relevant gene targets. Common gene targets by Cur and Bai and disease condition were input to Search Tool for the Retrieval of Interacting Genes/Proteins

(STRING, URL: https://string-db.org/4) to generate the protein-protein interaction (PPI) network. Disconnected nodes were hidden in the default setting of the network. Based on the constructed PPI network for each compound, we then investigated the associated Gene Ontology (GO) including biological process, cellular component and molecular function that represent gene product properties through the Database for Annotation, Visualization and Integrated Discovery (DAVID) online enrichment analysis database (https://david.ncifcrf.gov/home.jsp). We also explored the Kyoto Encyclopedia of Genes and Genomes (KEGG) pathways from DAVID. The top 5-15 targets in each function were selected and input to Bioinformatics (http://www.bioinformatics.com.cn/) to conduct the enrichment analysis of KEGG pathways and GO enrichment analysis, and the terms with a p-value less than 0.05 were filtered for the subsequent network construction. The overlapping gene targets were integrated and uploaded to Cytoscape (v.3.7.2) to construct the interactive network of "signaling pathway-gene target-drug". The most relevant gene targets and KEGG pathways for both Cur and Bai were shown in the final network. The workflow for the network pharmacology analysis is shown in Supplementary Material 1A.

H_2O_2 induced oxidative stress and drug treatments in endothelial cells

Human cardiovascular endothelial cell line (EA. hy926) was purchased from American Type Culture Collection (ATCC, USA, ATCC®CRL-2922™). Cells were cultured in DMEM/Ham's F12 (Lonza, Australia) supplemented with 10% fetal bovine serum (FBS, Sigma, Australia) and 100 U/mL of penicillin-streptomycin (Gibco BRL, Australia). The cells from passage 20 to 30 were grown in a 5% CO2-humidified incubator at 37°C until confluency for the bioassays. The reference compounds of curcumin (Cur, Cat.no. BP0421) and baicalein (Bai, Cat.no. BP0232) were purchased from Chengdu Biopurify (China) with their identities confirmed by the high-performance liquid chromatography and purity over 98% (Supplementary Material 2A, B). They were both dissolved in dimethyl sulfoxide (DMSO, Sigma, Australia) at 15 mg/mL. Cur+Bai combination was prepared by mixing Cur and Bai both at 15 mg/mL in DMSO at the ratio of 1:1, *w/w*. Then Cur, Bai and Cur+Bai were dissolved in serum-free DMEM to 15 µg/mL and diluted by 1:2 fold with the final concentration of DMSO at 0.1%.

We followed our previous published method (9, 17) to investigate the protective effects of Cur, Bai, and Cur+Bai on endothelial cells against the oxidative damage from hydrogen peroxide (H_2O_2). EA. hy926 cells (1×10^6 cells/mL) were seeded with DMEM/Ham's F12 supplemented with 10% FBS and 100 U/mL of penicillin-streptomycin in the 96 well Corning Costar plate (Sigma, Australia) overnight. The media was replaced with serum-free DMEM/Ham's F12, and the cells were incubated with serial diluted Cur, Bai, or Cur+Bai (0.43-15 µg/mL) for 1 h before the addition of H_2O_2 (Sigma-Aldrich, Australia) at 2.5 mM to induce the oxidative damage. Gallic acid acts as an antioxidant inhibiting oxidative species and enhance cell survival in the presence of H_2O_2 at low concentration (18–21). Thus, it has been used as comparison reference in our *in vitro* assays. EA. hy926 cells were co-incubated with 8.51 µg/mL (50 µM) gallic acid with a two-fold serial dilution 1 h prior to the stimulation of H_2O_2.

Cell viability assessment by Alamar Blue and caspase-3 assays

EA. hy926 cells were pre-treated with serial diluted Cur, Bai and Cur+Bai for 1 h, and stimulated with H_2O_2 (2.5 mM) overnight. The cell supernatant was then replaced with Alamar Blue (10 µg/mL) in phosphate buffered saline (PBS) for 2 h. The fluorescent absorbance of Alamar Blue was measured at 540 nm excitation and 590 nm emission using a microplate reader (BMG LABTECH FLUOstar OPTIMA, Mount Eliza, Victoria, Australia). The cells were lysed on ice for 10 min, and then subjected to a Caspase-3 assay kit (ABCAM, Australia, ab39401) for the measurement of cellular protein levels of caspase-3 following the protocol in Zhou et al. (9, 17). The absorbance was read on a microplate reader (BMG LABTECH FLUOstar Optima, Mount Eliza, Victoria, Australia) at a wavelength of 410 nm.

Intracellular oxidative status measurements by ROS expression

The intracellular level of oxidative stress with or without treatments was measured by ROS expression according to the protocol of cellular ROS assay kit (ABCAM, Australia, ab113851) cited in (9, 17). Briefly, EA. hy926 cells were stained with 2′,7′-dichlorofluorescin diacetate (DCFDA) (20 µM) at 100 µL per well for 45 min at 37°C in the dark. The plate's initial absorbance was recorded as A0 with an excitation at 455 nm and an emission at 535 nm in fluorescence mode. After washing with ice-cold PBS, the cells were treated with Cur, Bai, Cur+Bai at increasing concentrations (0.86–15 µg/mL) or tertbutyl hydroperoxide (TBHP, 50 µM, positive control) for 1 h followed by the stimulation of H_2O_2 for 30 min. The absorbance was measured again and recorded as A1. The fold change of ROS was calculated as A1 normalised to its corresponding A0 (A1/A0).

Intracellular oxidative status measurements by Nrf2 luciferase, superoxide dismutases and nicotinamide adenine dinucleotide enzymatic activities

The Nrf2-mediated pathway was investigated for the cyto-protection of Cur+Bai against oxidative stress. MCF7 AREc32 cells

were cultured in DMEM (10% FBS, 1% penicillin), which were donated by Professor Gerald Münch in School of Medicine, Western Sydney University. Cells were seeded in 96-well plates at a density of 1.0 ×106 cell/mL till confluency and then treated with 0.1% DMSO in serum-free media (blank control), increasing concentrations of Cur, Bai, Cur+Bai, and tertiary butylhydroquinone (TBHQ, positive control). The Nrf2 total luciferin was detected by luciferase assay with optimization (9). The luminescence was measured within 30 min at an excitation wavelength of 488 nm and an emission wavelength of 525 nm. The activation of Nrf2 was calculated by fold compared to the blank control.

For the superoxide dismutases (SOD) assays, EA. hy926 cells cultured in the T25 flasks (Sigma, Australia) were treated with 0.1% DMSO, Cur, Bai, or Cur+Bai at the concentrations of 3.25 and 7.50 μg/mL for 4 h, and the cells were harvested by the lysis buffer (0.1 M tris HCl, pH 7.4 containing 0.5% Triton X-100, 5 mM β-ME, 0.1 mg/mL PMSF) on ice for 10 min. The protein was collected by centrifugation at 14,000×*g* for 5 min at 4°C. The collected protein was then subjected to the measurement of SOD using the commercial kit from Sigma-Aldrich (Australia) according to the manufacturer's protocol (9).

For the nicotinamide adenine dinucleotide (NAD+) assay, EA. hy926 cells (1.0 × 106 cell/mL) were seeded on a 96-well plate (Sigma, Australia) overnight for 120 μL per well to allow confluency. The cells were then treated with media with 0.1% DMSO, Cur, Bai, or Cur+Bai at 7.5 μg/mL for 24 h. The total cellular NAD production was measured using the NAD+/NADH cell-based assay kit (Cayman, Australia) as cited in Zhou et al. (9).

High-fat diet induced hyperlipidaemia rats and drug intervention

Following the bioassays in endothelial cells, the effect of Cur+Bai against macrovascular changes in diabetic angiopathy was investigated in the spontaneous model of type 2 diabetes, the Goto–Kakizaki (GK) rat (22, 23).

All animal experiments were conducted with the approval of the Animal Care and Use Committee of Fujian University of Traditional Chinese Medicine (approval number: 2021068), and followed the Animal Research: Reporting of *In Vivo* Experiments (ARRIVE) guidelines and the National Institutes of Health guide for the care and use of Laboratory animals (NIH Publications No. 8023, revised 1978). Male Wistar rats and Goto-Kakizaki rats (12-week-old, 300 ± 20 g) were purchased from Cavens Biogle (Suzhou) Model Animal Research Ltd. Co. (Suzhou, no. SCXK-2018-0002). Animals were provided with food and water ad libitum under specific pathogen free conditions at the temperature of 24°C ± 1°C, with 12-h light/dark cycle and unlimited drinking water supply.

After 7 days of acclimation, Wistar rats were given normal diet and GK rats were given high-fat diet containing 10% refined lard, 1.5% cholesterol, 0.3% pig bile salts and 88.2% normal diet for 4 weeks (22). The changes of fasting blood glucose (FBG) and body weights were monitored once a week throughout the trial. After 4 weeks, the Wistar rats were allocated to the control group (n=5): oral gavage (OG, passage of a gavage needle into the esophagus) administered with 0.5% sodium carboxymethyl cellulose solution (CMC-Na) as the vehicle control; The GK rats were randomly allocated to four groups (1) The model group (n=5) rats were OG administered with 0.5% CMC-Na in 10 mL; (2) Cur treatment group (n=5) were OG administered with Cur (150 mg/kg) in 10 mL 0.5% CMC-Na; 3) Bai treatment group (n=5) were OG administered with Bai (150 mg/kg dissolved in 10 mL of 0.5% CMC-Na; 4) Cur+Bai treatment group (n=5) were OG administered with Cur+Bai (75 mg/kg Cur + 75 mg/kg Bai both dissolved in 10 mL of 0.5% CMC-Na). All the treatments were given for 4 weeks (24). CMC-Na was used to enhance the drug stability of Cur and Cur+Bai in the prepared suspensions (25). The treatments in each group were given at 9 AM once daily. At the end of treatment (week 8), the animals were fasted for 12 h and anesthesitised with 25% Ulatan (1.1 g/kg, IP injection) before the blood was collected from the abdominal aorta. The aortic arch and mid thoracic aorta were collected immediately. The serum samples were collected by centrifugation at 500 g for 10 min, and the supernatants were collected for analysis.

Body weight, fasted blood glucose test, blood lipid level and related oxidative and inflammatory biomarkers

The FBG and body weight were recorded once a week after the intervention (week 4-8). In preparation, the animals were fasted for 9 h before their tail blood was collected and tested using blood glucose test strips measured by the glucometer (Roche, USA). The FBG and body weight measurements at each time point were conducted three times for each animal, and the averaged value was recorded.

The blood lipid biomarkers including total cholesterol (TCHO), triglyceride (TG), non-esterified fatty acids (NEFA), low-density lipoprotein cholesterol (LDL-C) were measured using commercial kits (Nanjing Jiancheng Bioengineering Institute, China). The oxidative stress biomarkers including superoxide dismutase (SOD), myeloperoxidase (MPO), NAD +/NADPH levels were measured using commercial kits (Nanjing Jiancheng Bioengineering Institute, China). The inflammatory biomarker, tumor necrosis factor-α (TNF-α) was measured using ELISA kit (BOSTER Biological Technology co. ltd, China).

Hematoxylin and eosin staining and TUNEL staining of blood vessel

Pathological hematoxylin and eosin (H&E) staining was conducted following steps in previous studies (26, 27). Briefly, aortic arch and mid thoracic aorta blood vessel tissues were

collected, fixed with 4% paraformaldehyde, and dehydrated with ascending concentrations of ethanol. The tissues were cleaned with xylene I (100% ethanol and pure fresh xylene solution 1:1) and xylene II (pure fresh xylene) solutions for 40 min, respectively. The tissues were embedded in paraffin for 48 h and sectioned into 5 µm thickness. Each section was perfused in xylene I and II again for 10 min to remove the wax. Then the sectioned tissues were soaked in descending ethanol. Then they were stained with hematoxylin and eosin. These stained sections were sealed, mounted using Permount™ media, imaged and analysed using a light microscope. The dewaxed tissue was also subjected to the TUNEL staining with DAPI for blue staining of the nucleus and apoptotic cells stained with green fluorescence.

Western blot analysis

EA. hy926 cells and entire aorta wall tissues from rats were washed twice with ice-cold PBS. Whole cell protein lysates were prepared by a lysis buffer supplemented with protease inhibitor mixture (Cell Signaling Technology, USA) and quantified by the Pierce BCA protein kit (Thermo Fisher Scientific, Australia). Equal amounts of protein samples (10 mg/mL) from each group were subjected to sodium dodecyl sulfate polyacrylamide gel electrophoresis and the proteins were transferred to PVDF membranes (Thermo Fisher Scientific, Australia). After being blocked with 5% skim milk at room temperature for 1 h, the membranes were incubated with the following primary antibodies overnight at 4˚C: caspase-1 p20 (1:500, SantaCruz, sc-398715), NLRP3 (1:1000, Abcam, 263899), Nrf2 (1:1000, Cell Signaling Technologies, 86806S), HO-1 (1:1000, Cell Signaling Technologies, 12721S), eNOS (1:1000, Cell Signaling Technologies, 32027S), p-JNK (1:1000, Cell Signaling Technologies, 9255S), JNK (1:1000, Cell Signaling Technologies, 9252S), p-p38 (1:1000, Cell Signaling Technologies, 4511S) and p38 (1:1000, Cell Signaling Technologies, 8690S). β-actin and GAPDH were used as the internal controls (1:3000, Beijing TransGen, China, catalogue number: HC201 and HC301) in this study. Then, the blots were washed in PBST three times (three min at a time) and subsequently incubated with anti-rabbit or anti-mouse horseradish peroxidase-conjugated secondary antibody (Cell signaling Technologies, 7074s or Proteintech, SA000-1, USA) for 1.5 h. Two separate gels were used for the examination of the phosphorylated and total proteins. The images were taken by the ChemiDoc XRS plus imaging system (Bio-Rad, Hercules, CA). The intensity of the targeted bands was quantified by ImageJ software. The quantitative data was presented as the ratio of intensity of targeted protein to that of β-actin.

Synergy determination and statistical analysis

CompuSyn (Biosoft, US) was used to analyse the synergistic/antagonistic interaction between Cur and Bai based on the median-effect equation and isobologram analysis (16). The specific measurement for the combination index (CI) value represents the interaction level, where CI < 1, CI = 1, and CI > 1 suggest synergistic, additive, and antagonistic interaction, respectively. The calculation of CI values was based on Chou-Talalay method and determined by CompuSyn (28).

The values of concentrations and their corresponding responses of individual or combined Cur and Bai from the cell viability assay were input to the CompuSyn program. The CI-Fa (fraction affected level) curves were than generated with the CI and Fa values regarding the synergistic/antagonistic interactions. The CI-Fa curves show the dynamic changes of the interaction (based on CI values) with the different levels of Fa (cell viability).

All statistics comparisons were performed using GraphPad Version 9 (US). The significance was analysed by one-way analysis of variance (ANOVA) with Tukey's multiple comparisons test and Dunnett's test as post-hoc test, or unpaired t test. The data was expressed as mean ± standard deviation with at least three individual experiments ($n \geq 3$) or mean ± standard error of the mean (SEM) with n=5 rats per group. $P<0.05$ was considered statistically significant.

Results

Identification of common gene and KEGG targets by network construction and analysis

For endothelial dysfunction, GeneCards, DisGeNET and OMIM searches generated 1500, 716 and 185 gene targets, respectively. The pharmacological actions of Cur and Bai have been connected with 49 and 47 gene targets, respectively. After filtering, 20 and 22 common gene targets were screened for Cur and Bai against endothelial dysfunction. As shown in Supplementary Material 1B, the compound–candidate target (C-T) network was constructed for Cur and Bai against endothelial dysfunction which consisted of 291 edges 63 nodes. The key common gene targets included MAPK14, MAPK8, MAPK 10, NQO1, CDK2, ESR1, ESR2, F2, HSP90AA1, ADAM17 (degrees ranged from 12-23), with MAPK 14 ranked as the top gene (the highest degree).

We have listed the top 15 signaling pathways that were involved in the targets of Cur and Bai against endothelial dysfunction (Supplementary Material 1C, D). The top 3 signaling pathways of Cur are pathways in cancer, Foxo signaling pathway, and endocrine resistance (ranked by degree). The top three signaling pathways of Bai are Estrogen signaling pathway, Chemical carcinogenesis-receptor activation and Fluid shear stress and atherosclerosis. The top 3 targeted signaling pathways shared by both Cur and Bai against endothelial dysfunction were identified through the constructed network. These were Endocrine resistance (degree=32), Pathways in cancer (degree=19), and Fluid shear stress and atherosclerosis (degree=16). Among them, only the Fluid shear stress and

atherosclerosis pathway, is categorized in cardiovascular diseases; thus, particular attention was paid to this pathway as shown in Supplementary Material 1E. The top 10 KEGG pathways that are affected by both Cur and Bai are shown in Table 1.

This KEGG pathway map contains two major components (sub-pathways); the anti-atherogensis and pro-atherogensis pathway. In the anti-atherogensis pathway, Nrf2 has a central role as its translocation switches on the downstream functional responses against atherosclerosis including antioxidant, anti-inflammatory, vasodilatory, and anti-thrombotic actions. In the pro-atherogensis pathway, the phosphorylation of p38 and JNK induces the activation of transcription factor AP-1. It then leads to a serial cascades' response of inflammation, matric degeneration, and angiogenesis contributing to pro-atherogensis.

Further network pharmacology analysis for Cur and Bai against diabetic angiopathy and atherosclerosis/endothelial dysfunction was also constructed as shown in Supplementary Material 3, 4, respectively.

Synergistic effect of Cur+Bai on restoring cell viability of EA. hy926 cells

Following the results obtained from network pharmacology analysis, the individual and combined actions of Cur and Bai on EA. hy926 cells were explored to see if they exhibited the expected protective effect on endothelium against oxidative stress which is one of the risk factors in diabetic angiopathy. As shown in Figure 1A, H_2O_2 dose-dependently (0.31–10 mM) reduced the cell viability compared to the untreated cells (cells with media only, $p<0.0001$) assessed by the Alamar Blue assay. At 2.5 mM, H_2O_2 reduced the cell viability dramatically to 8.99 ± 1.11% only. Thus, this concentration of H_2O_2 was selected to establish the oxidative stress induced cell impairment model in EA. hy926 cells. As shown in Figure 1B, gallic acid restored the cell viability to 72.92 ± 8.54% at 2.12 μg/mL (12.46 μM) against the oxidative damage of H_2O_2.

In Figure 1B, the pretreatment with Bai significantly restored cell viability to 38.42 ± 5.80% at 15 μg/mL ($p<0.0001$), whereas Cur (0.47-15 μg/mL) showed a dose-dependent increasing trend of the cell viability but did not reach significance. Combinations of Cur+Bai showed a prominent effect in restoring cell viability in a dose-dependent manner. Particularly, Cur+Bai (3.75 – 15 μg/mL) showed significantly higher cell viabilities compared to that of the blank control ($p<0.05$), and the improvement was consistently higher than that of Cur or Bai alone ($p<0.05$). CI model in Figure 1C revealed a strong synergy (CI values< 0.53) in most concentration levels when Fa ranged from 0.1 to 0.97 (representing 10%-97% cell viability levels).

Following this, the activity of total intracellular caspase-3 enzymes was assessed to determine whether Cur+Bai reduced the apoptotic cells against the impairment from H_2O_2. As shown in Figure 1D, EA. hy926 cells incubated with H_2O_2 (2.5 mM) for 24 h caused a significant increase in caspase-3 activity measured at 24 h ($p<0.05$) compared to that of the blank control, indicating an elevated cell apoptotic level with the stimulation of H_2O_2. At concentration level of 7.5 μg/mL, the effect of Cur and Bai were insignificant, whereas Cur+Bai markedly reduced the caspase-3 level to a comparable level of blank control ($p<0.0001$). The reduction of caspase-3 by Cur+Bai was markedly greater than that of Cur or Bai (both $p<0.01$). At 15 μg/mL, all the treatments demonstrated a down-regulatory trend of caspase-3, with the lowest expression of caspase-3 protein by Cur+Bai ($p<0.001$) which was greater than that of Cur alone ($p<0.05$).

Cur+Bai increased Nrf2-regulated antioxidant response and downregulated MAPK-JNK pathway in EA. hy926 cells

Figure 2A shows that ROS increased by 14.21 ± 1.82 times in H_2O_2 (2.5 mM) stimulated EA. hy926 cells whereas non-treated cells only expressed 5.53 ± 0.32 fold of ROS. TBHP was used as a positive control which boosted the ROS level by 12.42 ± 0.32 fold. Treatment of Cur, Bai, and Cur+Bai significantly reduced the ROS fold change against H_2O_2 (2.5 mM) at 1.88–15 μg/mL (all $p<0.05$). Furthermore, Cur+Bai showed a significantly greater inhibition of ROS than that of Cur at 0.94 and 1.88 μg/mL ($p<0.001$) when compared at the same concentration level.

The activation of the Nrf2 activity by Cur+Bai was investigated to see if it was associated with the synergistic protective effect of Cur +Bai on endothelial cells against oxidative damage as indicated by the network pharmacology analysis. As shown in Figure 2B, Cur +Bai dose-dependently increased the Nrf2 luciferase with the maximum fold change of 28.48 ± 4.91 at 15 μg/mL, whereas the up-regulatory effect by Cur or Bai alone were insignificant. The positive control, TBHQ, increased Nrf2 expression by 12.76 ± 1.01 fold at 4.16 μg/mL (25 μM). We then analysed the induction of HO-1 protein by Cur, Bai, or Cur+Bai, as the downstream protein target regulated by Nrf2 (Figure 2C). Individual Cur and Bai at 15 μg/mL showed an increasing trend of HO-1 expression compared to that of untreated cells, however, the increase did not reach a significance level. Cur+Bai (15 μg/mL) increased the HO-1 protein expression by 1.81 ± 0.01 times with the greatest increase ($p<0.0001$) among three treatments.

The expressions of SOD and NAD+ were examined as Nrf2-HO-1 regulated antioxidant (co)enzymes (Figure 2D, E). Cur or Bai alone at 7.5 μg/mL showed an increasing trend of SOD activity, although it did not reach a statistical significance compared to that of untreated cells (blank). In contrast, Cur+Bai (7.5 μg/mL) significantly increased the SOD activity (89.84 ± 3.04% *vs.* blank 75.52 ± 6.23%, $p<0.0001$). The increase of SOD activity by Cur+Bai was significantly higher than that of Cur or Bai (both $p<0.001$). Similarly, Cur+Bai (7.5 μg/mL) significantly increased the total intracellular NAD production compared to that of the blank control (untreated cells) (64.20 ± 8.51 nM *vs.* blank 23.08 ± 3.63 nM, $p<0.01$). The increase of NAD by Cur+Bai (7.5

TABLE 1 KEGG pathways affected by both Cur and Bai against endothelial dysfunction.

Pathway	Category	P value
Pathways in cancer	Cancer: overview	0.0000000170229
Endocrine resistance	Drug resistance: antineoplastic	0.00000128102
Fluid shear stress and atherosclerosis	Cardiovascular disease	0.00000720725
Epithelial cell signaling in Helicobacter pylori infection	Infectious disease: bacterial	0.0000111191
Prolactin signaling pathway	Endocrine system	0.0000111191
Progesterone-mediated oocyte maturation	Endocrine system	0.0000494524
Lipid and atherosclerosis	Cardiovascular disease	0.0000595532
Relaxin signaling pathway	Endocrine system	0.00012373
Estrogen signaling pathway	Endocrine system	0.000160666

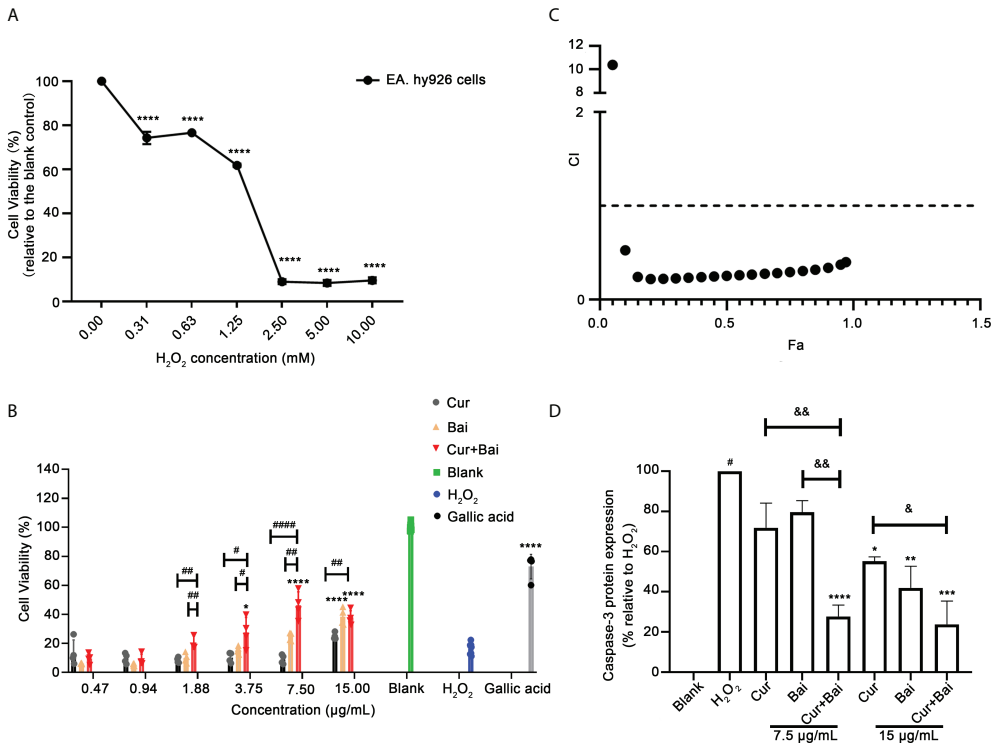

FIGURE 1
Synergistic activity of combined Cur and Bai in restoring H_2O_2 impaired cell viability in EA. hy926 cells assessed by Alamar Blue assays. **(A)** H_2O_2 dose-dependently reduced cell viability in EA. hy926 cells by Alamar Blue assay. **** p<0.0001 *vs.* H_2O_2 concentration = 0.00 mM in EA. hy926 cells. **(B)** Pretreatment of Cur, Bai, or Cur+Bai (1:1, *w/w*) restored the cell viability of EA. hy926 cells against the stimulation of H_2O_2 at 2.5 mM assessed by Alamar Blue assay. Gallic acid was used as a comparative reference. The effect of Cur+Bai in restoring the impaired cell viability was significantly greater than that of Cur or Bai at 1.62, 3.25, 7.50 and 15 μg/mL. *p<0.05, ****p<0.0001 *vs.* H_2O_2 only. $^{\#}p$<0.05, $^{\#\#}p$<0.01, $^{\#\#\#\#}p$<0.0001 *vs.* Cur or Bai individual treatment. **(C)** Synergistic interaction of Cur+Bai in restoring cell viability analysed by CI-Fa curve in EA. hy926 cells. Fa represents the cell viability, and CI<1 represents synergy whereas CI>1 represents antagonism. **(D)** Cur+Bai (7.5 and 15 μg/mL) exhibited an enhanced effect in inhibiting H_2O_2-induced caspase-3 protein expression in comparison to that of the individual compound. $^{\#}p$<0.05 *vs.* Blank (H_2O_2 = 0.00 mM), *p<0.05 *vs.* H_2O_2 (2.5 mM), $^{\&}p$<0.05, $^{\&\&}p$<0.01 *vs.* Cur or Bai at the same concentration level. Results were expressed as mean ± standard deviation for at least three individual experiments. The p values were obtained from one-way ANOVA analysis.. **p<0.01, ***p<0.001, ****p<0.0001.

μg/mL) was significantly higher than that of Cur (p<0.05) but comparable to that of Bai alone.

Western blot analysis was conducted to analyse the regulated phosphorylation of MAPKp38 and JNK by Cur+Bai, Cur or Bai. Our results in Figures 2F, G showed that the stimulation of H_2O_2 (2.5 mM) significantly upregulated the phosphorylation of MAPKp38 and JNK by 1.49 ± 0.29 and 17.31 ± 9.19 times, respectively compared to the blank control (both p<0.05). The

10.3389/fendo.2022.953305

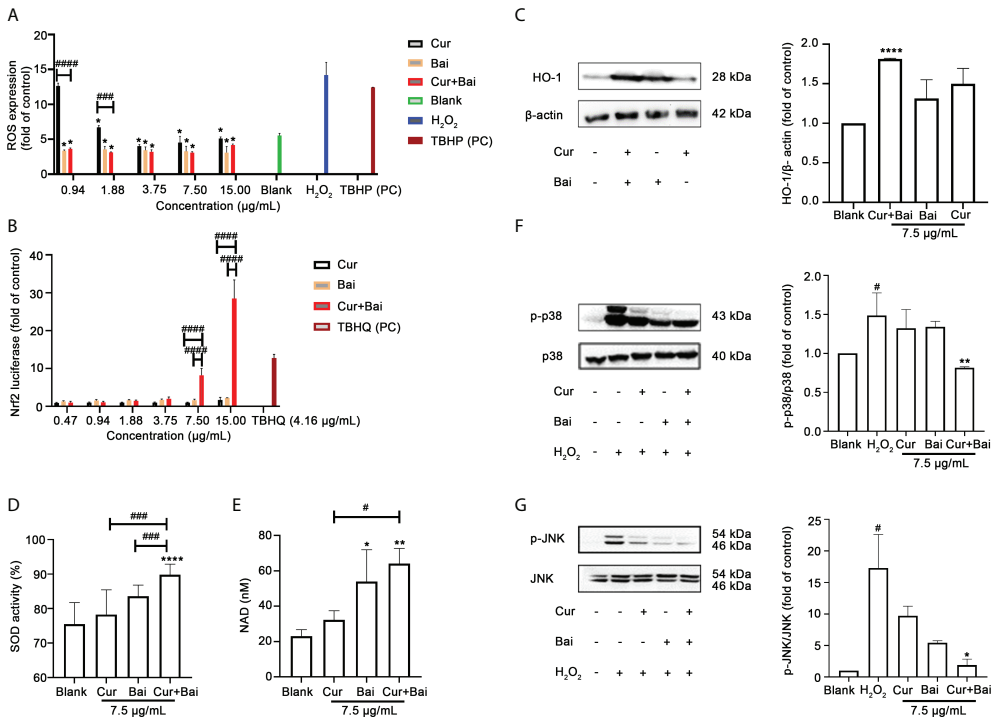

FIGURE 2
Cur+Bai attenuated H_2O_2-induced endothelial damage in EA. hy926 cells which may be associated with regulating Nrf2-HO-1 and MAPK pathways. **(A)** ROS expression in EA. hy926 cells pretreated with Cur, Bai or Cur+Bai with serial dilutions from 15 μg/mL and stimulated with H_2O_2 for 4 h. TBHP (50 μM) was used as the positive control. The ROS expression was presented as the fold change to the blank control (cells with media only). *p<0.05 *vs.* H_2O_2 only. $^{###}p$<0.001, $^{####}p$<0.0001 *vs.* Cur or Bai at the same concentration level. n=3 individual experiments. **(B)** Nrf2 luciferase under the treatment of Cur, Bai or Cur+Bai (0.47-15 μg/mL). The Nrf2 luciferase was presented as fold change to that of the blank control (cells with media only). TBHQ was used as the positive control. $^{####}p$<0.0001 *vs.* Cur or Bai at the same concentration level. n=3 individual experiments. **(C)** The up-regulatory activity of Cur+Bai on HO-1/beta-actin which was greater than that of Cur or Bai alone (7.5 μg/mL) as assessed by the Western blot analysis (n=3 individual experiments). ****p<0.0001 *vs.* blank. Cur+Bai increased cellular SOD **(D)** and NAD (nM) **(E)** productions. *p<0.05, **p<0.01 *vs.* blank; $^{#}p$<0.05, $^{###}p$<0.001 *vs.* Cur or Bai at the same concentration level (7.5 μg/mL). The error bars represent the standard deviation of measurements for over three samples in three separate assay runs (n = 3). **(F, G)** Cur+Bai (7.5 μg/mL) downregulated the phosphorylation of MAPKp38 and JNK as assessed by the Western blot analysis (n=3 individual experiments). $^{#}p$<0.05 *vs.* blank control. *p<0.05, **p<0.01 *vs.* H_2O_2. Results were expressed as mean ± standard deviation for at least three individual experiments. The p values were obtained from one-way ANOVA analysis.

treatment of Cur or Bai (7.5 μg/mL) did not show a significant inhibition of p-p38/p38 whereas Cur+Bai (7.5 μg/mL) significantly reduced the expression (p<0.01 *vs.* H_2O_2) to a comparable level of the blank control. Cur+Bai (7.5 μg/mL) also demonstrated a significant downregulation of p-JNK/JNK to 1.91 ± 0.61 fold change compared to that of H_2O_2 only (p<0.05), whereas the effects of Cur or Bai (7.5 μg/mL) were less remarkable.

Cur+Bai protected aortic blood vessels and decreased the blood lipid levels in diabetic rats

The individual and combined effects of Cur and Bai on endothelial and vascular function in GK rat model were investigated.

The changes in blood glucose level and body weight were monitored every week from week 4 to week 8. As shown in Figure 3A, the body weight in the control group remained at a similar level throughout the trial, with an average weight of 583.4 ± 37.6 g in week 4 to 591.0 ± 31.0 g in week 8. In comparison, the body weight in the GK rat model group was averaged at 367.8 ± 12.8 g in week 4 and 381.6 ± 11.0 g in week 8. The treatment of Cur, Bai or Cur+Bai did not show significant change of the body weight compared to the model group throughout the trial.

As shown in Figure 3B, the FBG level in the model group was constantly higher than that of the control group from week 4 (26.37 ± 6.65 *vs.* 4.92 ± 0.54 mmol/L, p<0.0001) to week 8 (26.42 ± 4.43 *vs.* 5.56 ± 0.34 mmol/L, p<0.0001). The treatment of Cur+Bai markedly reduced the FBG level starting from week 5 (13.30 ± 2.97 mmol/L), which was significantly lower than that of the model group (25.49 ± 9.28 mmol/L, p<0.05). Moreover, the FBG reducing effect of Cur+Bai was greater than that of Bai (25.85 ± 9.41 mmol/L, p<0.01) or Cur alone (21.91 ± 9.08 mmol/L, p<0.01)

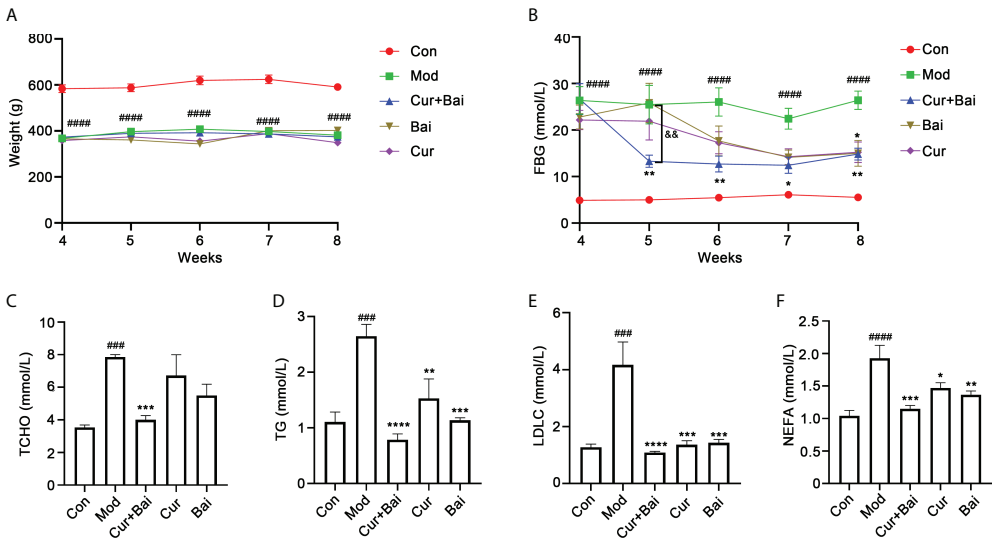

FIGURE 3
Cur+Bai effectively lowered the FBG and blood lipid levels in diabetic rats. **(A)** The body weights of diabetic model group were constantly lower than that of the control group (n=5 per group). The treatments of Cur+Bai, Cur or Bai did not change body weight from week 4 to week 8 compared to that of the diabetic model group. $^{\#\#\#\#}p<0.0001$ *vs.* control group. **(B)**. Cur+Bai, Cur and Bai time-dependently reversed the HFD-induced high FBG level (mmol/L) in diabetic group (n=5 per group) from week 4 to week 8. The FBG lowering effect in the Cur+Bai was greater than that of Cur or Bai group from week 5 to week 7. $^{\#\#\#\#}p<0.0001$ *vs.* Con at the same time point. $^{*}p<0.05$, $^{**}p<0.01$ *vs.* Mod at the same time point. $^{\&\&}p<0.01$, Cur+Bai *vs.* Bai compared at the same time point. The changes of blood lipid levels by Cur+Bai, Cur and Bai in the diabetic rats, including TCHO **(C)**, TG **(D)**, LDLC **(E)** and NEFA **(F)** with n=5 per group. $^{\#\#\#}p<0.001$, $^{\#\#\#\#}p<0.0001$ *vs.* Con at the same time point. $^{*}p<0.05$, $^{**}p<0.01$, $^{***}p<0.001$, $^{****}p<0.0001$ *vs.* Mod at the same time point. Results were expressed as mean ± SEM for five rats per group. The *p* values were obtained from one-way ANOVA analysis.

at week 5 which the individual effects were insignificant. The individual effects of Cur and Bai were not obvious until week 8 which reached a statistical significance with $p<0.05$. In contrast, Cur+Bai constantly lowered FBG level from week 6 to week 8 ($p<0.05$) with the FBG level ranging from 12.46 ± 3.91 to 14.86 ± 2.85 mmol/L.

The blood lipid levels were measured using the serum collected from the abdominal aorta. As shown in Figures 3C–F, the model group showed significantly higher levels of TCHO ($p<0.001$), TG ($p<0.001$), LDLC ($p<0.001$) and NEFA ($p<0.0001$) in comparison to that of the control group. Cur alone did not show a significant effect in lowering TCHO, but markedly reduced TG ($p<0.01$), LDL-C ($p<0.001$) and NEFA ($p<0.001$). Similarly, Bai was not effective in lowering TCHO, but significantly reduced TG ($p<0.001$), LDLC ($p<0.001$), NEFA ($p<0.01$). Remarkably, the treatments of Cur+Bai constantly showed significant effects in reducing their levels (all p values<0.001). Moreover, the greatest reductions were generally seen in Cur+Bai for all the tested blood lipids compared to that of Cur or Bai alone, although no significance difference was detected.

The pathological changes of blood vessels in the mid thoracic and aortic arch tissues by the treatment of Cur+Bai were monitored. As shown in Figure 4A, a smooth inner surface of the blood vessel was observed in the control group, whereas the model group showed a damaged inner surface of the blood vessel (indicated by a red arrow) and the presence of lipid droplets (adipose tissue, indicated by black arrows) in the middle layer of the blood vessel. The treatment of Cur+Bai showed a normal morphology of the blood vessel with a smooth surface of the inner layer and very few adipose tissues in the middle layer. Both the individual treatments of Cur and Bai showed smooth endothelium layer, however, adipose tissues were observed especially in the Cur-treated group. The statistical analysis showed a significantly higher percentage of aortic adipose tissue in the model group (13.01 ± 6.55%) compared to that of the control group (0.28 ± 0.31%, $p<0.001$). The treatments of Cur+Bai (0.36 ± 0.51%, $p<0.001$), Cur (3.40 ± 3.23%, $p<0.01$) and Bai (1.72 ± 1.56%, $p<0.01$) all significantly lowered the adipose tissue level compared to that of the model group. The lowest adipose tissue (%) was shown in the Cur+Bai treated group. In addition, as shown in Figure 4B, it was quite evident that the blood vessel wall was much thicker in the model group compared to that of the control group ($p<0.001$). The treatment with Cur+Bai ($p<0.001$), Cur ($p<0.01$) or Bai ($p<0.001$) all significantly reduced the blood wall thickness compared to that of the model group.

10.3389/fendo.2022.953305

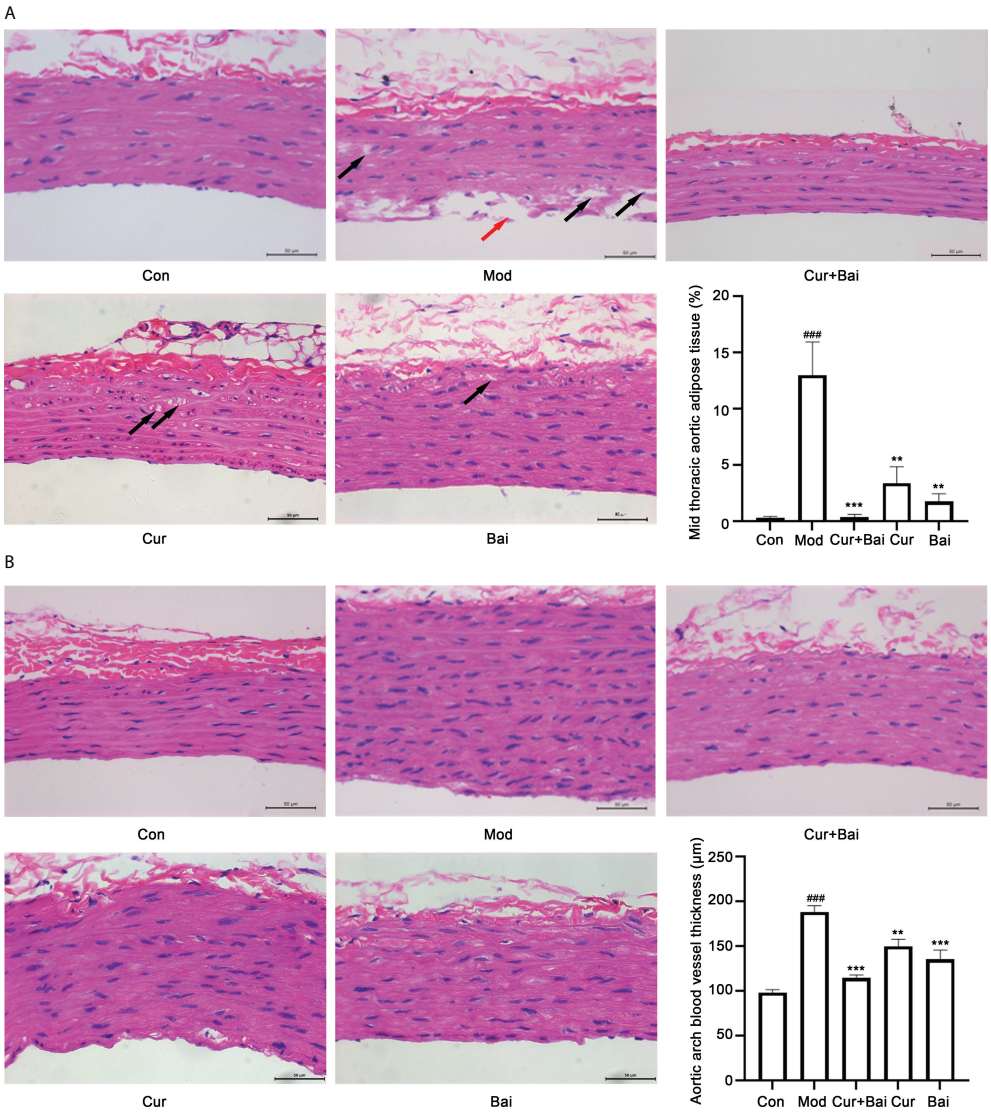

FIGURE 4
The treatments of Cur+Bai, Cur and Bai repaired the blood vessel morphology in both mid thoracic and aortic arch tissue in the diabetic rats. **(A)** Representative pathological staining of blood vessel tissue in the mid thoracic aorta in the control, model, Cur+Bai, Cur and Bai treated groups (n=5 per group). Scale bar = 50 um. Red arrow points to the injured inner surface of the blood vessel. Black arrows point to the adipose tissue in the middle layer of the blood vessel. The statistical analysis on the mid thoracic aorta adipose tissue (percentage) in five groups. Dynamic Med 6.0 microscopic image analysis system was used for the quantitative analysis of adipose tissue in the aorta. The adipose tissue in the aorta (%) was calculated as below: Aorta adipose tissue (%) = the sum of adipose tissue areas in the H&E staining area/total area of the blood vessel in the same H&E staining area* 100%. $^{###}p<0.001$ *vs.* Con group. $^{**}p<0.01$, $^{***}p<0.001$ *vs.* Mod group. **(B)** Representative pathological staining of blood vessel tissue in the aortic arch in the control, model, Cur+Bai, Cur and Bai treated groups (n=5 per group). Scale bar = 50 um. The statistical analysis on the thickness of the aortic arch blood vessel wall (μm) in five groups. $^{###}p<0.001$ *vs.* Con group. $^{**}p<0.01$, $^{***}p<0.001$ *vs.* Mod group. Results were expressed as mean ± SEM for five rats per group. The *p* values were obtained from one-way ANOVA analysis.

The effect of Cur+Bai in restoring cell survival in the blood vessels was examined by the TUNEL staining. Figures 5A, C revealed that there was obvious cell apoptosis in blood vessel (as highlighted by the green fluorescence) in both mid thoracic aorta and aortic arch. The statistical analysis in Figures 5B, D showed the significant higher TUNEL positive cells % in the model group in the mid thoracic aorta and aortic arch ($p<0.01$ and $p<0.001$). There were very few apoptotic cells in the Cur +Bai treated groups as evidenced by the weak green fluorescence and significantly lower TUNEL positive cells % (mid thoracic aorta: $p<0.01$ and aortic arch: $p<0.001$). Cur significantly reduced the TUNEL positive cells in the aortic arch ($p<0.05$), whereas Bai was insignificant in the aortic arch or mid thoracic aorta.

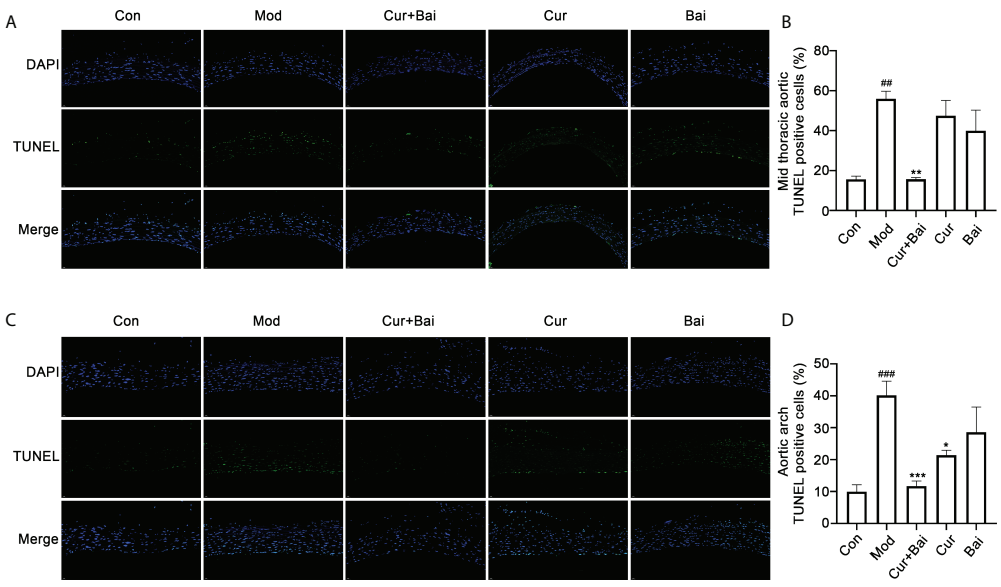

FIGURE 5
TUNEL staining for the mid thoracic and aortic arch blood vessel tissue in the control, model Cur+Bai, Cur and Bai treated groups. Represent TUNEL staining images of blood vessel in thorax **(A)** and heart **(B)**. Statistical analysis of the TUNEL positive cells in the mid thoracic **(C)** and aortic arch **(D)**. $^{\#\#}p<0.01$, $^{\#\#\#}p<0.001$ *vs.* control group. $^{*}p<0.05$, $^{**}p<0.01$, $^{***}p<0.001$ *vs.* model group. Results were expressed as mean ± SEM for five rats per group. The *p* values were obtained from one-way ANOVA analysis.

Cur+Bai increased the eNOS protein expression, protected aorta blood vessels in relation to Nrf2-regulated antioxidant enzymes and MAPK pathway

In diabetes, the expression of endothelial nitric oxide synthase (eNOS) is altered which leads to endothelial dysfunction and the progression of diabetic angiopathy (29). The changes in eNOS protein expression were examined by Western Blot analysis as shown in Figure 6A. The model group showed a significantly lower eNOS protein expression ($p<0.001$) compared to the control group, suggesting an impaired endothelial function in the diabetic animals. On the other hand, treated groups including Cur+Bai, Cur and Bai all significantly reversed the eNOS protein expressions ($p<0.05$), with Cur+Bai showed the highest expression of eNOS ($p<0.001$).

The Nrf2-mediated antioxidant defensive mechanism by Cur +Bai was investigated *in vivo*. As shown in Figures 6B, C, the protein levels of Nrf2 ($p<0.001$) and HO-1 ($p<0.01$) were significantly lower in the diabetic model group compared to that of the control group. The treatment of Cur+Bai significantly restored the Nrf2 ($p<0.001$) and HO-1 ($p<0.001$) protein expressions in comparison to that of the model group. Individual Cur and Bai also significantly increased the Nrf2 protein expression ($p<0.01$), however, they were insignificant in restoring the protein expression of HO-1. Following that, Cur+Bai significantly restored the expressions of SOD ($p<0.001$) and NAD +/NADH ($p<0.05$) compared to that of the model group (Figures 6D, E) which was consistent to that of the *in vitro* findings. Individual Cur and Bai significantly increased SOD expression ($p<0.001$) to the same extend as the Cur+Bai combination. Bai also increased the level of NAD+/NADH ($p<0.05$) whereas Cur did not show any significant effect. Cur +Bai significantly reduced the expression of MPO ($p<0.001$) compared to that of the model group (Figure 6F). The combined effect was comparable to that of Cur and Bai alone.

Since both the network pharmacology analysis and *in vitro* testing showed that p-p38 and p-JNK could be the key targets of Cur+Bai, these two protein targets were tested *in vivo*. As shown in Figures 7A, B, the phosphorylated p38 ($p<0.05$) and JNK ($p<0.001$) were significantly increased in the model group. In contrast, the treatment of Cur+Bai significantly lowered the expressions of p-p38 ($p<0.05$) and p-JNK ($p<0.0001$), suggesting that MAPKp38 and JNK still play a role in the action of Cur+Bai in protecting blood vessel and endothelium in diabetic animals. The downregulation of p-p38 by Cur+Bai was comparable to that of Bai alone ($p<0.05$ *vs.* model group), whereas Cur showed insignificant effect. Interestingly, Cur significantly reduced p-JNK ($p<0.0001$) which was similar to that of Cur+Bai, and Bai also showed a significant inhibition ($p<0.01$).

The reduced level of MPO led to the investigation of inflammatory markers in the blood vessel by Cur+Bai. As shown in Figure 7C, the level of TNF-α was significantly

10.3389/fendo.2022.953305

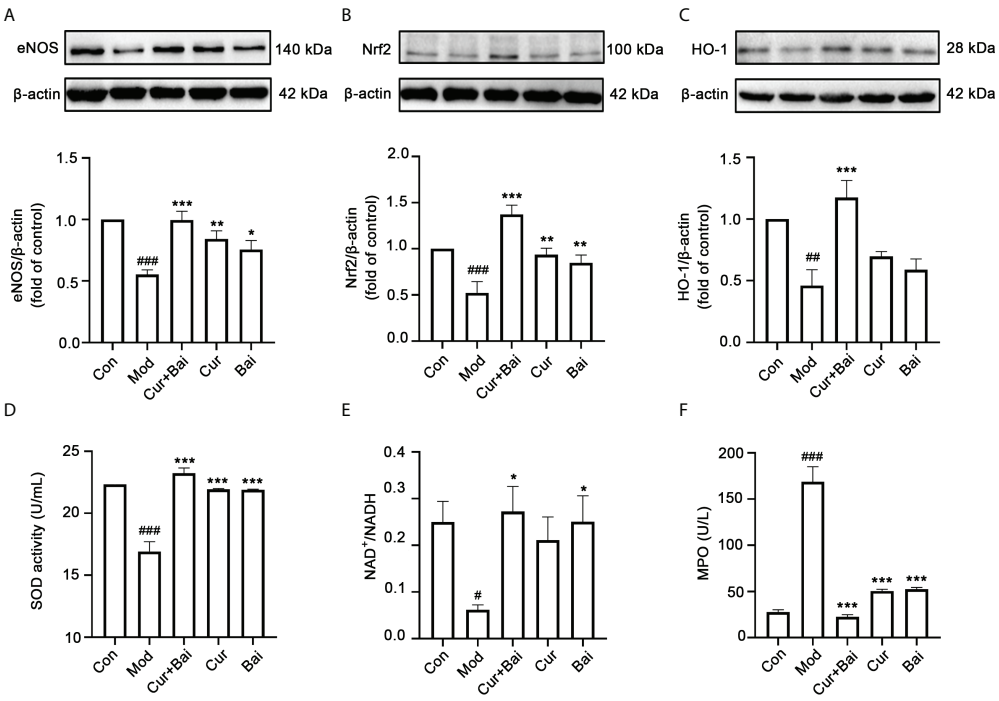

FIGURE 6
The treatment of Cur+Bai upregulated eNOS protein expression, Nrf2-HO-1 mediated antioxidant activity and downregulated MAPKp38-JNK pathway in the entire aorta wall in the diabetic rats. **(A)** Cur+Bai, Cur and Bai upregulated eNOS protein expression in diabetic rats as analysed by the Western blot analysis. n=3, $^{###}p<0.001$ *vs.* control group, $^{*}p<0.05$, $p<0.01$, $p<0.001$ *vs.* model group. **(B)** Cur+Bai, Cur and Bai upregulated Nrf2 protein expression in diabetic rats as analysed by the Western blot analysis. n=3, $^{###}p<0.001$ *vs.* control group, $^{**}p<0.01$, $^{***}p<0.01$ *vs.* model group. **(C)** Cur+Bai upregulated HO-1 protein expression in diabetic rats as analysed by the Western blot analysis. n=3, $^{##}p<0.01$ *vs.* control group, $^{***}p<0.001$ *vs.* model group. **(D)** Cur+Bai, Cur and Bai upregulated the SOD enzymatic activity (U/mL). n=5 per group, $^{###}p<0.001$ *vs.* control group, $^{***}p<0.001$ *vs.* model group. **(E)** Cur+Bai and Bai promoted the NAD+/NADPH ratio. n=5 per group, $^{#}p<0.05$ *vs.* control group, $^{*}p<0.05$ *vs.* model group. **(F)** Cur+Bai, Cur and Bai downregulated the MPO expression (U/mL) in the diabetic rats. n=5 per group, $^{#}p<0.05$ *vs.* control group, $^{*}p<0.05$ *vs.* model group. Results were expressed as mean ± SEM for five rats per group. The *p* values were obtained from one-way ANOVA analysis.

elevated in the model group ($p<0.001$) and the treatment of Cur +Bai significantly lowered the level ($p<0.01$) which was at a comparable level to that of the control group. Bai also significantly reduced TNF-α production ($p<0.01$), however, the effect from Cur was insignificant.

Discussions

Endothelial dysfunction is an early marker in the pathogenesis of vascular diseases (30). It also has a strong link with diabetic angiopathy which is the major complication of DM. Many risk factors of DM are involved in the development of endothelial dysfunction such as hyperglycaemia and hyperlipidaemia that cause oxidative stress and inflammation in endothelium. Cur and Bai are two nutraceuticals that have been individually demonstrated to protect the endothelium in DM through antioxidant and anti-inflammatory related pathways. The present study investigated the combined activity of Cur and Bai in rescuing endothelial survival against the impairment of H_2O_2 in EA. hy926 cells, and protecting blood vessels in aortic arch and mid thoracic aorta of diabetic rats. The detailed mechanisms of the Cur and Bai combination were elucidated through the network pharmacology analysis and partially validated by the *in vitro* and *in vivo* experimental investigations. To our knowledge, this is the first study that investigates the enhanced pharmacological activity of a Cur and Bai combination by in silico analysis, cellular assays and animal models.

The potent antioxidant activity of Cur has led to a few studies that investigated its individual effect in protecting the endothelium against a variety of impairments (31). A study from Sun etal. (32) suggested that the pretreatment of Cur (25 μM) partly inhibited the H_2O_2 induced oxidative stress, and attenuated H_2O_2-induced apoptosis index (9.67 ± 1.26% *vs.* 15.00 ± 1.77%, $p<0.05$) in HUVECs (32). Bai was shown to mitigate endothelial injury against radiation-induced enteritis and inhibit lipopolysaccharides-induced proinflammatory response and apoptosis in HUVECs (33, 34). Based on these previous

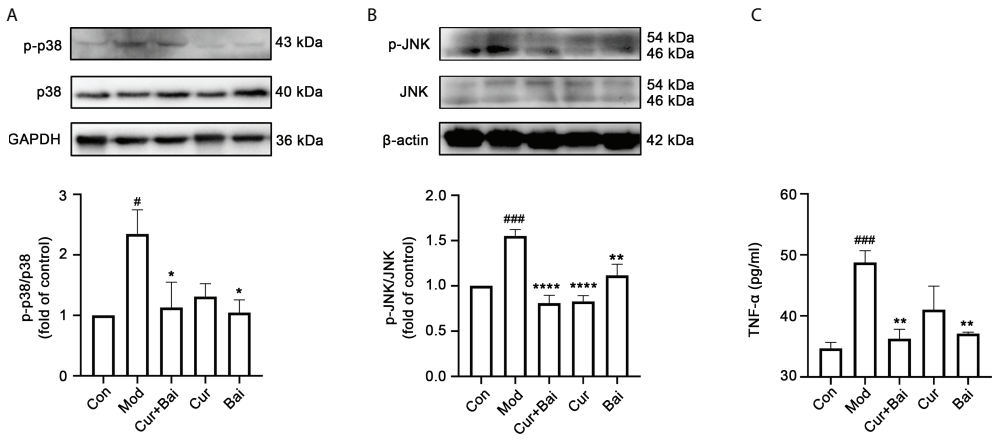

FIGURE 7
The treatment of Cur+Bai downregulated phosphorylated MAPKp38 and JNK, and reduced the production of TNF-α in the entire aorta wall in the diabetic rats. **(A)** Cur+Bai and Bai downregulated phosphorylated MAPKp38 expression in diabetic rats as analysed by the Western blot analysis. n=3, $^{\#}p<0.05$ *vs.* control group, $^{*}p<0.05$ *vs.* model group. **(B)** Cur+Bai, Cur and Bai downregulated phosphorylated JNK expression in diabetic rats as analysed by the Western blot analysis. n=3, $^{\#\#\#}p<0.001$ *vs.* control group, $^{**}p<0.01$, $^{****}p<0.0001$ *vs.* model group. **(C)** The treatment of Cur+Bai downregulated the TNF-α production expression in the diabetic rats. n=5, $^{\#\#\#}p<0.001$ *vs.* control group, $^{**}p<0.01$ *vs.* model group. Results were expressed as mean ± SEM for five rats per group. The *p* values were obtained from one-way ANOVA analysis.

studies, we tested the pharmacological activities of Cur, Bai and their combination using a generic and common endothelial injury model induced by H_2O_2. EA. hy926 cells are the human umbilical vein cell line which was established by fusing primary human umbilical vein cells with a thioguanine-resistant clone of A549 by exposure to polyethylene glycol (PEG). This cell line has been widely used in various studies on endothelial cells and blood vessel related research. Previous studies have demonstrated that EA. hy926 preserves similar characteristics with primary human endothelial cells, such as Human Aortic Endothelial Cells (HAEC) (35, 36). Exposure to hydrogen peroxide (H_2O_2) is widely used procedure to cause oxidative damage/stress in cellular models. The Fenton's reaction between H_2O_2 and Fe2+ ions generates the highly reactive OH radical and is thought to be the main mechanism for oxidative damage (37). Many studies have applied H_2O_2 to induce cell injury in EA. hy926 cells for the study of endothelial injury including our previously published studies (9, 17, 38). The individual treatments of Cur and Bai showed dose-dependent improvement of cell survival in EA. hy926 cells, which were in line with the previous studies. Remarkably, the Cur +Bai combination has demonstrated a synergistic activity in restoring cell viability in EA. hy926 cells. Cur+Bai also reduced apoptotic level shown by the caspase-3 protein expression.

Further investigation on Cur+Bai combination in restoring the entire macrovascular pathological changes was conducted in a diabetic rat model. Two previous *in vivo* studies demonstrated that pre-treatment of Cur (15 days orally, 200 mg/kg or 2 weeks of 200 to 400 mg/kg, P.O.) prevented the increase in oxidative stress, reduced the cell apoptosis level and repaired the endothelial function as observed in the aortic tissue against cyclosporin A (31) and methotrexate (39). Bai has also been demonstrated to inhibit high glucose induced vascular inflammation in mice (13) and STZ-induced diabetic retinopathy rats (40). In this study, Cur and Bai used alone significantly lowered the FBG level, and reduced the blood lipids levels including TG, LDLC and NEFA, compared to the diabetic model group. Remarkably, the effect of the Cur+Bai combination was the greatest among all treatments that showed the lowest levels of FBG and tested blood lipids. It is worth mentioning that the dosage of Cur and Bai in the individual treatment group (150 mg/kg) doubled the dosage of Cur and Bai in the combination group (75 mg/kg for each), but the Cur+Bai generally showed a comparable or even greater effect in lowering the blood lipid levels. We then focused on the effect of Cur+Bai in protecting morphology and function of blood vessel in the diabetic model. The Cur+Bai combination significantly restored the eNOS protein expression, suggesting a remarkable protective effect on endothelial function in the diabetic rats. The pathological staining showed that the Cur+Bai combination maintained the normal structure of the endothelium and reduced adipose tissue in comparison to that of the diabetic model group. Thus, the endothelial protective action of Cur+Bai may partially be attributed to its anti-hyperglycemic and anti-hyperlipidemic activities. The TUNEL staining showed a significantly lower level of cell loss in the Cur+Bai treatment group compared to that of the model group in the three layers of the blood vessel, indicating its protection of blood vessel against diabetic angiopathy *in vivo*. Taken together, the above-mentioned results supported the feasible use of Cur+Bai as an oral supplement treatment (once a day) for diabetic angiopathy with a short treatment duration to regulate the glucose metabolism and restore the blood vessel status and function in diabetic

angiopathy. The clinical dosage used in this study for Cur+Bai is estimated to be 1.5 g per 60 kg body weight, which is consisted of 0.75 g Cur and 0.75 g Bai. The clinical dosage used for Cur alone to improve the symptoms of diabetic microangiopathy is approximately 1 g per day for 4 weeks (41). In this case, if Cur is prepared in the Cur+Bai combination, a greater effect maybe reached with only half of the dosage. Further clinical trials are warranted to confirm the assumption.

Although there is an increasing number of studies that showed synergistic activity of phytochemicals (14), understanding the molecular mechanisms of synergy remains a challenge as it usually involves multi-faceted molecular targets. Previous studies have revealed the possible molecular mechanisms of Cur and Bai as individual compounds. Sun etal. (32) has linked the antioxidant action of Cur in protecting endothelium to the restored enzymatic activity of sirtuin 1 (SIRT1), which then upregulated the phosphorylation of eNOS and nitric oxide (32). The effect of Bai on diabetic-induced endothelial dysfunction was related to both antioxidant and anti-inflammatory activities (4, 13, 40). Bai was shown to inhibit the activation of nuclear factor (NF)-κB, the central signaling pathway of inflammation. In turn, it attenuated the vascular inflammatory response which is a critical event underlying the development of diabetic angiopathy (13).

In the present study, the molecular mechanisms of Cur and Bai, and their combination were investigated through a network pharmacology analysis. Our results revealed that (1) there are a number of overlapping genes and KEGG pathways (common targets) that are mediated by Cur and Bai against endothelial dysfunction, (2) top commonly targeted genes included MAPK 9, 10 and 14, and top targeted KEGG pathways included Pathways in cancer, Endocrine resistance and Fluid shear stress and atherosclerosis. The common gene targets and the KEGG pathway might be the key to explore the mechanisms of action of the Cur+Bai combination. The importance of the MAPK pathway was emphasized by the genes MAPK 8, MAPK10 and MAPK 14, which were all identified as common targets of Cur and Bai. The Nrf2 pathway was investigated due it is role as the essential antioxidant switcher to initiate the anti-atherosclerosis response in the Fluid sheer stress and atherosclerosis pathway. Additionally, MAPKp38 and JNK are essential protein kinases that participates in the pro-atherogenic response in the Fluid sheer stress and atherosclerosis pathway. Thereby these molecular targets are focused for the mechanistic study on Cur+Bai against diabetic angiopathy.

We demonstrated that the protective effect of the Cur+Bai combination in EA. hy926 cells was associated with Nrf2-HO-1 mediated antioxidant defense system. This was evidenced by significantly inhibited ROS level, magnified Nrf2 luciferase, upregulated HO-1 protein expressions as well as increased Phase II antioxidant enzymes including SOD and NAD enzymatic activities. Furthermore, the up-regulatory activities on Nrf2, HO-1 and phase II antioxidant enzymes by Cur+Bai were all significantly higher than that of Cur or Bai alone, which may help to explain the observed synergistic activity of Cur+Bai in restoring the impaired cell viability. Nrf2 is a master regulator of cellular resistance to oxidants which controls the basal and induced expression of an array of antioxidant response element-dependent genes (42). The induction of Nrf2 launches the expressions of Phase II antioxidant enzymes such as SOD and total NAD+ that directly detoxify ROS and thus reduce the level of oxidative stress (43–45). In fact, the results from our previous study demonstrated a synergistic activity of Cur and resveratrol in attenuating H_2O_2-induced endothelial oxidative damage and apoptosis, and the synergistic mechanism was associated with further strengthened upregulation of Nrf2-HO-1 mediated antioxidant pathway (9). Thus, it was speculated that this finding could be used to identify novel synergistic combination. Indeed, our present study showed that Cur interacted with Bai synergistically which might be partially related to the further upregulated Nrf2-HO-1 pathway. This finding underpins our previous finding that synergy may occur through the strengthening of the Nrf2-HO-1 pathway.

The prediction of network pharmacology on the synergistic mechanism of the Cur and Bai combination has been partially confirmed by our experimental investigation on the protein kinases of MAPKp38 and JNK. Our *in vitro* investigation showed that the phosphorylated p38 and JNK increased significantly by the stimulation of H_2O_2, which are key regulators in oxidative stress and inflammatory response in endothelial apoptosis (46, 47). The Cur+Bai combination significantly downregulated the protein kinase of p38 and JNK which the effect was greater than Cur or Bai alone. This finding supported the synergistic action of Cur+Bai in reducing cell apoptosis in EA. hy926 cells. In addition, the downregulation of p38 and JNK by Cur+Bai in diabetic rats may contribute to its observed protective effect on blood vessel. These experimental findings partially confirmed our network pharmacology results, although additional molecular targets and their crosstalk may also be involved, warranting further investigation and validation. Our results showed that the Cur+Bai combination also effectively reduced the level of TNF-α in the blood vessel tissue, the production of which is associated with the Fluid shear stress and atherosclerosis KEGG pathway and pathological progression of diabetic angiopathy (48).

Extrapolation of the results from cellular-based *in vitro* study to that of an *in vivo* investigation still present a great challenge. Some pharmacokinetics processes such as absorption, distribution, metabolism and elimination need to be taken into account when the efficacy of a phytochemical in a whole organism is concerned. Cur has been confirmed to exhibit very poor oral bioavailability (around 1%) (49) which rendered undetectable or extremely low amount in blood (50). Orally administered curcumin is transformed into dihydrocurcumin and tetrahydrocurcumin within one hour, and then largely converted into glucuronide and glucuronide/sulfate conjugates

(51). Thus, the observed effect of Cur in the diabetic rats may be attributed to the functional role of these metabolites. Tetrahydrocurcumin, the main metabolite of Cur in the blood circulation, was shown to suppress oxidative stress (52), and improved vascular dysfunction, arterial stiffness, and hypertension associated with cadmium exposure in mice (53). The effect of glucuronide and glucuronide/sulfate conjugates in protecting vascular function against oxidative stress is unknown. Oral Bai also undergoes a fast and extensive phase II metabolism with a negligible absorption in rats (54, 55). Bai via oral administration was mainly transformed into its conjugated metabolites, glucuronides/sulfates of baicalein (75.7%) (56) including baicalin which were extensively circulating in the plasma (57, 58) (54). Baicalin is shown to repair the blood vessel function in aorta in diabetic mice, due to a mechanism associated with Nrf2 signaling (4). Thus, the observed effect of Bai in this study may at least partly be attributable to the action of baicalin. Thereby, the underlying mechanism of the combined action of Cur+Bai in restoring on macrovascular changes may rely on the action of their metabolites. The next step can be the pharmacokinetic study of Cur+Bai in the diabetic rats and determination of the ratio of their metabolites, followed by the study of the interaction of their metabolites.

At present, there is no robust statistical analysis method available to quantify synergy in a combination at one dosage level. Thus the "synergy" in this study was based on statistical comparison between the individual treatments to that of the combined treatments (i.e. t-test or one-way analysis of variance). There are several other limitations of the study. The secondary cell line, EA. hy926 cells were used to investigate the protective effect of the Cur+Bai combination in endothelial cells, rather than using the primary aortic endothelial cells, which does not fully inform the effects of Cur+Bai on native endothelium in aortic blood vessels. The effect of Cur+Bai observed in the animal study was only based on male animals, but not on female's counterparts. The quantified phenotype changes in the endothelium following *in vivo* treatment were limited in this study. Due to the absence of pharmacokinetic data, there remains challenge to investigate the Cur+Bai combination as a therapeutic agent in the management of diabetic angiopathy.

Conclusions

The presented study suggested that Cur and Bai interacted synergistically in restoring cell survival in H_2O_2 impaired EA. hy926 cells. The combined treatment of Cur and Bai reduced FBG and blood lipids levels including TCHO, TG, LDLC and NEFA in diabetic GK rats. The Cur+Bai combination protected the endothelium function, maintained the blood vessel wall and reduced the adipose tissue in both aortic arch and mid thoracic aorta blood vessels.

The mechanisms associated with the synergistic interactions of Cur and Bai were investigated by the network pharmacology analysis. MAPK gene targets and Fluid sheer stress and atherosclerosis pathway were analysed to be the key common targets of Bai and Cur against endothelial dysfunction. Our *in vitro* results revealed that the Cur+Bai combination reduced ROS fold change and upregulated Nrf2, HO-1, SOD, and NAD regulators. It also markedly downregulated the phosphorylation of MAPKp38 and JNK against the stimulation of H_2O_2. In diabetic rats, the Cur+Bai combination upregulated the protein expressions of Nrf2 and HO-1, as well as increased the enzymatic activities of SOD, NAD+/NADPH, and decreased the enzymatic level of MPO. Furthermore, it inhibited the protein kinases of p38 and JNK. Cur and Bai also significantly reduced the level of TNF-α in the blood vessel tissue.

Altogether, our results demonstrated that the Cur+Bai combination significantly attenuated endothelial injury against oxidative damage in endothelial cells and effectively protected blood vessel in diabetic rats via regulating Nrf2-HO-1 mediated antioxidant defensive system and MAPK pathways. Our findings may help develop novel combination therapies with multi-targeted actions for mitigating endothelial dysfunction in diabetic angiopathy against hyperglycaemia, hyperlipidaemia and oxidative damage.

Data availability statement

The original contributions presented in the study are included in the article/Supplementary Material. Further inquiries can be directed to the corresponding authors.

Ethics statement

The animal study was reviewed and approved by the Animal Care and Use Committee of Fujian University of Traditional Chinese Medicine.

Author contributions

Conceptualization, XZ and YFZ; methodology, CW, YS and WL; software, SL, YLu, JG and XZ; validation, JC, CL and DC; formal analysis, YPZ, ZC and YXL; investigation, CW, YS, WL, SA and XZ; resources, CL, YFZ, and MH; data curation, JC., ZC, YXL and YPZ; writing original draft preparation, CW and XZ; writing review and editing, XZ, YFZ, DC, CL and GM; visualization, XZ and YFZ; supervision, YFZ, XZ and MH; project administration, XZ, YFZ and MH; funding acquisition, XZ, YFZ and MH. All authors contributed to the article and approved the submitted version.

Funding

This project is supported by the ICON (Improving Cardiovascular Outcome Network) Early Career Researchers Program awarded to XZ from the South Western Sydney Local Health District. The project is also funded by the National Natural Science Foundation of China (81973437, 81703909), the Fujian Provincial Marine Economic Development Special Fund Project (FJHJF-L-2021-4), the Collaborative Innovation Platform Project of Fuxiaquan National Innovation Demonstration Zone (2021FX02). XZ is supported by the Research Support Program Fellowship, Western Sydney University.

Acknowledgments

We thank to Mr John Truong for his kind support.

Conflict of interest

The authors declare that the research was conducted in the absence of any commercial or financial relationships that could be construed as a potential conflict of interest.

As a medical research institute, NICM Health Research Institute receives re-search grants and donations from foundations, universities, government agencies, individuals and industry. Sponsors and donors also provide untied funding for work to advance the vision and mission of the Institute.

Publisher's note

All claims expressed in this article are solely those of the authors and do not necessarily represent those of their affiliated organizations, or those of the publisher, the editors and the reviewers. Any product that may be evaluated in this article, or claim that may be made by its manufacturer, is not guaranteed or endorsed by the publisher.

Supplementary material

The Supplementary Material for this article can be found online at: https://www.frontiersin.org/articles/10.3389/fendo.2022.953305/full#supplementary-material

References

1. Stehouwer CD, Lambert J, Donker A, van Hinsbergh VW. Endothelial dysfunction and pathogenesis of diabetic angiopathy. *Cardiovasc Res* (1997) 34:55–68. doi: 10.1016/s0008-6363(96)00272-6

2. Xu S, Ilyas I, Little PJ, Li H, Kamato D, Zheng X, et al. Endothelial dysfunction in atherosclerotic cardiovascular diseases and beyond: from mechanism to pharmacotherapies. *Pharmacol Rev* (2021) 73:924–67. doi: 10.1124/pharmrev.120.000096

3. Xu F, Liu Y, Zhu X, Li S, Shi X, Li Z, et al. Protective effects and mechanisms of vaccarin on vascular endothelial dysfunction in diabetic angiopathy. *Int J Mol Sci* (2019) 20:4587. doi: 10.3390/ijms20184587

4. Chen G, Chen X, Niu C, Huang X, An N, Sun J, et al. Baicalin alleviates hyperglycemia-induced endothelial impairment *via* Nrf2. *J Endocrinol* (2019) 240:81–98. doi: 10.1530/JOE-18-0457

5. Ansar S, Koska J, Reaven PD. Postprandial hyperlipidemia, endothelial dysfunction and cardiovascular risk: focus on incretins. *Cardiovasc Diabetol* (2011) 10:1–11. doi: 10.1186/1475-2840-10-61

6. Ding X, Yao W, Zhu J, Mu K, Zhang J, Zhang j.-a. resveratrol attenuates high glucose-induced vascular endothelial cell injury by activating the E2F3 pathway. *Biomed Res Int* (2020) 2020:6173618. doi: 10.1155/2020/6173618

7. Fang XD, Yang F, Zhu L, Shen YL, Wang LL, Chen YY. Curcumin ameliorates high glucose-induced acute vascular endothelial dysfunction in rat thoracic aorta. *Clin Exp Pharmacol Physiol* . (2009) 36:1177–82. doi: 10.1111/j.1440-1681.2009.05210.x

8. Wongeakin N, Bhattarakosol P, Patumraj S. Molecular mechanisms of curcumin on diabetes-induced endothelial dysfunctions: Txnip, ICAM-1, and NOX2 expressions. *BioMed Res Int* (2014) 2014:161346. doi: 10.1155/2014/161346

9. Zhou X, Afzal S, Zheng Y-F, Münch G, Li CG. Synergistic protective effect of curcumin and resveratrol against oxidative stress in endothelial EAhy926 cells. *Evid Based Complement Alternat Med* (2021) 2021:2661025. doi: 10.1155/2021/2661025

10. Patumraj S, Wongeakin N, Sridulyakul P, Jariyapongskul A, Futrakul N, Bunnag S. Combined effects of curcumin and vitamin c to protect endothelial dysfunction in the iris tissue of STZ-induced diabetic rats. *Clin Hemorheol Microcirc* (2006) 35:481–9.

11. Huang Y, Tsang S-Y, Yao X, Chen Z-Y. Biological properties of baicalein in cardiovascular system. *Cardiovasc Hematol Disord* (2005) 5:177–84. doi: 10.2174/1568006043586206

12. El-Bassossy HM, Hassan NA, Mahmoud MF, Fahmy A. Baicalein protects against hypertension associated with diabetes: effect on vascular reactivity and stiffness. *Phytomedicine.* (2014) 21:1742–5. doi: 10.1016/j.phymed.2014.08.012

13. Ku S-K, Bae J-S. Baicalin, baicalein and wogonin inhibits high glucose-induced vascular inflammation *in vitro* and *in vivo*. *BMB Rep* (2015) 48:519. doi: 10.5483/bmbrep.2015.48.9.017

14. Zhou X, Seto SW, Chang D, Kiat H, Razmovski-Naumovski V, Chan K, et al. Synergistic effects of Chinese herbal medicine: a comprehensive review of methodology and current research. *Front Pharmacol* (2016) 7:201. doi: 10.3389/fphar.2016.00201

15. Casas AI, Hassan AA, Larsen SJ, Gomez-Rangel V, Elbatreek M, Kleikers PW, et al. From single drug targets to synergistic network pharmacology in ischemic stroke. *PNAS.* (2019) 116:7129–36. doi: 10.1073/pnas.1820799116

16. Chou T-C. The combination index (CI< 1) as the definition of synergism and of synergy claims. *Synergy.* (2018) 7:49–50. doi: 10.1096/fasebj.2022.36.S1.0R290

17. Zhou X, Razmovski-Naumovski V, Kam A, Chang D, Li CG, Chan K, et al. Synergistic study of a danshen (Salvia miltiorrhizae radix et rhizoma) and sanqi (Notoginseng radix et rhizoma) combination on cell survival in EA. hy926 cells. *BMC Complement Altern Med* (2019) 19:1–13. doi: 10.1186/s12906-019-2458-z

18. Chen CH, Liu TZ, Chen CH, Wong CH, Chen CH, Lu FJ, et al. The efficacy of protective effects of tannic acid, gallic acid, ellagic acid, and propyl gallate against hydrogen peroxide-induced oxidative stress and DNA damages in IMR-90 cells. *Mol Nutr Food Res* (2007) 51:962–8. doi: 10.1002/mnfr.200600230

19. Jia Z, Anandh Babu PV, Chen W, Sun X. Natural products targeting on oxidative stress and inflammation: mechanisms, therapies, and safety assessment. *Oxid Med Cell Longev* (2018) 2018:6576093. doi: 10.1155/2018/6576093

20. Kam A, Li KM, Razmovski-Naumovski V, Nammi S, Chan K, Li GQ. Gallic Acid protects against endothelial injury by restoring the depletion of DNA methyltransferase 1 and inhibiting proteasome activities. *Int J Cardiol* (2014) 171:231–42. doi: 10.1016/j.ijcard.2013.12.020

21. Serrano J, Cipak A, Boada J, Gonzalo H, Cacabelos D, Cassanye A, et al. Double-edged sword behaviour of gallic acid and its interaction with peroxidases in human microvascular endothelial cell culture (HMEC-1). antioxidant and pro-oxidant effects. *Acta Biochim Pol* (2010) 57:193–8. doi: 10.18388/abp.2010_2394

22. Ergul A, Elgebaly MM, Middlemore M-L, Li W, Elewa H, Switzer JA, et al. Increased hemorrhagic transformation and altered infarct size and localization

after experimental stroke in a rat model type 2 diabetes. *BMC Neurol* (2007) 7:1–7. doi: 10.1186/1471-2377-7-33

23. Hachana S, Pouliot M, Couture R, Vaucher E. Diabetes-induced inflammation and vascular alterations in the goto–kakizaki rat retina. *Curr Eye Res* (2020) 45:965–74. doi: 10.1080/02713683.2020.1712730

24. Tsai I-J, Chen C-W, Tsai S-Y, Wang P-Y, Owaga E, Hsieh R-H. Curcumin supplementation ameliorated vascular dysfunction and improved antioxidant status in rats fed a high-sucrose, high-fat diet. *Appl Physiol Nutr Metab* (2018) 43:669–76. doi: 10.1139/apnm-2017-0670

25. Xu D-H, Wang S, Jin J, Mei X-T, Xu S-B. Dissolution and absorption researches of curcumin in solid dispersions with. *Asian J Pharm* (2006) 6:343–9.

26. Liu J, Jin Y, Li H, Yu J, Gong T, Gao X, et al. Probiotics exert protective effect against sepsis-induced cognitive impairment by reversing gut microbiota abnormalities. *J Agric Food Chem* (2020) 68:14874–83. doi: 10.1021/acs.jafc.0c06332

27. Zheng Y, Zhou X, Wang C, Zhang J, Chang D, Liu W, et al. Effect of tanshinone IIA on gut microbiome in diabetes-induced cognitive impairment. *Front Pharmacol* (2022) 13:890444. doi: 10.3389/fphar.2022.890444

28. Chou T-C. Drug combination studies and their synergy quantification using the chou-talalay method. *Cancer Res* (2010) 70:440–6. doi: 10.1158/0008-5472.CAN-09-1947

29. Yang Y-M, Huang A, Kaley G, Sun D. eNOS uncoupling and endothelial dysfunction in aged vessels. *Am J Physiol Heart Circ Physiol* (2009) 297:H1829–36. doi: 10.1152/ajpheart.00230.2009

30. Endemann DH, Schiffrin EL. Endothelial dysfunction. *J Am Soc Nephrol.* (2004) 15:1983–92. doi: 10.1097/01.ASN.0000132474.50966.DA

31. Sagiroglu T, Kanter M, Yagci MA, Sezer A, Erboga M. Protective effect of curcumin on cyclosporin a-induced endothelial dysfunction, antioxidant capacity, and oxidative damage. *Toxicol Ind Health* (2014) 30:316–27. doi: 10.1177/0748233712456065

32. Sun Y, Hu X, Hu G, Xu C, Jiang H. Curcumin attenuates hydrogen peroxide-induced premature senescence *via* the activation of SIRT1 in human umbilical vein endothelial cells. *Biol Pharm Bull* (2015) 38:1134–41. doi: 10.1248/bpb.b15-00012

33. Jang H, Lee J, Park S, Kim JS, Shim S, Lee SB, et al. Baicalein mitigates radiation-induced enteritis by improving endothelial dysfunction. *Front Pharmacol* (2019) 10:892. doi: 10.3389/fphar.2019.00892

34. Wan CX, Xu M, Huang SH, Wu QQ, Yuan Y, Deng W, et al. Baicalein protects against endothelial cell injury by inhibiting the TLR4/NF–κB signaling pathway. *Mol Med Rep* (2018) 17:3085–91. doi: 10.3892/mmr.2017.8266

35. Ahn K, Pan S, Beningo K, Hupe D. A permanent human cell line (EA. hy926) preserves the characteristics of endothelin converting enzyme from primary human umbilical vein endothelial cells. *Life Sci* (1995) 56:2331–41. doi: 10.1016/0024-3205(95)00227-w

36. Thornhill M, Li J, Haskard D. Leucocyte endothelial cell adhesion: a study comparing human umbilical vein endothelial cells and the endothelial cell line EA-hy-926. *Scand J Immunol* (1993) 38:279–86. doi: 10.1111/j.1365-3083.1993.tb01726.x

37. Ransy C, Vaz C, Lombès A, Bouillaud F. Use of H_2O_2 to cause oxidative stress, the catalase issue. *Int J Mol Sci* (2020) 21:9149. doi: 10.3390/ijms21239149

38. Seto SW, Chang D, Ko WM, Zhou X, Kiat H, Bensoussan A, et al. Sailuotong prevents hydrogen peroxide (H_2O_2)-induced injury in EA. hy926 cells. *Int J Mol Sci* (2017) 18:95. doi: 10.3390/ijms18010095

39. Sankrityayan H, Majumdar AS. Curcumin and folic acid abrogated methotrexate induced vascular endothelial dysfunction. *Can J Physiol Pharmacol* (2016) 94:89–96. doi: 10.1139/cjpp-2015-0156

40. Yang L-p, Sun H-l, Wu L-m, Guo X-j, Dou H-l, Tso MO, et al. Baicalein reduces inflammatory process in a rodent model of diabetic retinopathy. *IOVS.* (2009) 50:2319–27. doi: 10.1167/iovs.08-2642

41. Gupta SC, Patchva S, Aggarwal BB. Therapeutic roles of curcumin: lessons learned from clinical trials. *AAPS J* (2013) 15:195–218. doi: 10.1208/s12248-012-9432-8

42. Ma Q. Role of nrf2 in oxidative stress and toxicity. *Annu Rev Pharmacol Toxicol* (2013) 53:401–26. doi: 10.1146/annurev-pharmtox-011112-140320

43. Dinkova-Kostova AT, Abramov AY. The emerging role of Nrf2 in mitochondrial function. *Free Radic Biol Med* (2015) 88:179–88. doi: 10.1016/j.freeradbiomed.2015.04.036

44. Matzinger M, Fischhuber K, Heiss EH. Activation of Nrf2 signaling by natural products-can it alleviate diabetes? *Biotechnol Adv* (2018) 36:1738–67. doi: 10.1016/j.biotechadv.2017.12.015

45. Wei C-C, Kong Y-Y, Li G-Q, Guan Y-F, Wang P, Miao C-Y. Nicotinamide mononucleotide attenuates brain injury after intracerebral hemorrhage by activating Nrf2/HO-1 signaling pathway. *Sci Rep* (2017) 7:1–13. doi: 10.1038/s41598-017-00851-z

46. Wu Y, Wang F, Fan L, Zhang W, Wang T, Du Y, et al. Baicalin alleviates atherosclerosis by relieving oxidative stress and inflammatory responses *via* inactivating the NF-κB and p38 MAPK signaling pathways. *BioMed Pharmacother.* (2018) 97:1673–9. doi: 10.1016/j.biopha.2017.12.024

47. Zhou P, Lu S, Luo Y, Wang S, Yang K, Zhai Y, et al. Attenuation of TNF-α-induced inflammatory injury in endothelial cells by ginsenoside Rb1 *via* inhibiting NF-κB, JNK and p38 signaling pathways. *Front Pharmacol* (2017) 8:464. doi: 10.3389/fphar.2017.00464

48. Vlassara H, Cai W, Crandall J, Goldberg T, Oberstein R, Dardaine V, et al. Inflammatory mediators are induced by dietary glycotoxins, a major risk factor for diabetic angiopathy. *Proc Natl Acad Sci USA* (2002) 99:15596–601. doi: 10.1073/pnas.242407999

49. Prasad S, Tyagi AK, Aggarwal BB. Recent developments in delivery, bioavailability, absorption and metabolism of curcumin: the golden pigment from golden spice. *Cancer Res Treat* (2014) 46:2–18. doi: 10.4143/crt.2014.46.1.2

50. Lopresti AL. The problem of curcumin and its bioavailability: could its gastrointestinal influence contribute to its overall health-enhancing effects? *Adv Nutr* (2018) 9:41–50. doi: 10.1093/advances/nmx011

51. Pandey A, Chaturvedi M, Mishra S, Kumar P, Somvanshi P, Chaturvedi R. Reductive metabolites of curcumin and their therapeutic effects. *Heliyon.* (2020) 6:e05469. doi: 10.1016/j.heliyon.2020.e05469

52. Okada K, Wangpoengtrakul C, Tanaka T, Toyokuni S, Uchida K, Osawa T. Curcumin and especially tetrahydrocurcumin ameliorate oxidative stress-induced renal injury in mice. *J Nutr* (2001) 131:2090–5. doi: 10.1093/jn/131.8.2090

53. Sangartit W, Kukongviriyapan U, Donpunha W, Pakdeechote P, Kukongviriyapan V, Surawattanawan P, et al. Tetrahydrocurcumin protects against cadmium-induced hypertension, raised arterial stiffness and vascular remodeling in mice. *PloS One* (2014) 9:e114908. doi: 10.1371/journal.pone.0114908

54. Lai MY, Hsiu SL, Tsai SY, Hou YC, Chao PDL. Comparison of metabolic pharmacokinetics of baicalin and baicalein in rats. *J Pharm Pharmacol* (2003) 55:205–9. doi: 10.1211/002235702522

55. Li L, Gao H, Lou K, Luo H, Hao S, Yuan J, et al. Safety, tolerability, and pharmacokinetics of oral baicalein tablets in healthy Chinese subjects: A single-center, randomized, double-blind, placebo-controlled multiple-ascending-dose study. *Clin Transl Sci* (2021) 14:2017–24. doi: 10.1111/cts.13063

56. Xu P, Zhou H, Li Y-Z, Yuan Z-W, Liu C-X, Liu L, et al. Baicalein enhances the oral bioavailability and hepatoprotective effects of silybin through the inhibition of efflux transporters BCRP and MRP2. *Front Pharmacol* (2018) 9:1115. doi: 10.3389/fphar.2018.01115

57. Chen H, Gao Y, Wu J, Chen Y, Chen B, Hu J, et al. Exploring therapeutic potentials of baicalin and its aglycone baicalein for hematological malignancies. *Cancer Lett* (2014) 354:5–11. doi: 10.1016/j.canlet.2014.08.003

58. Srinivas N. Baicalin, an emerging multi-therapeutic agent: pharmacodynamics, pharmacokinetics, and considerations from drug development perspectives. *Xenobiotica.* (2010) 40:357–67. doi: 10.3109/00498251003663724

frontiers | Frontiers in Endocrinology

TYPE Original Research
PUBLISHED 05 September 2022
DOI 10.3389/fendo.2022.978520

OPEN ACCESS

EDITED BY
Lu Cai,
University of Louisville, United States

REVIEWED BY
Wei Han,
Beijing Anzhen Hospital, Capital Medical University, China
Shengkai Yan,
Zunyi Medical University, China

*CORRESPONDENCE
Jun Dong
jun_dong@263.net
Wenxiang Chen
wxchen@nccl.org.cn

SPECIALTY SECTION
This article was submitted to Cardiovascular Endocrinology, a section of the journal Frontiers in Endocrinology

RECEIVED 26 June 2022
ACCEPTED 18 August 2022
PUBLISHED 05 September 2022

CITATION
Yang R, Zhang W, Wang X, Wang S, Zhou Q, Li H, Mu H, Yu X, Ji F, Dong J and Chen W (2022) Nonlinear association of 1, 5-anhydroglucitol with the prevalence and severity of coronary artery disease in chinese patients undergoing coronary angiography.
Front. Endocrinol. 13:978520.
doi: 10.3389/fendo.2022.978520

Nonlinear association of 1,5-anhydroglucitol with the prevalence and severity of coronary artery disease in chinese patients undergoing coronary angiography

Ruiyue Yang[1], Wenduo Zhang[2], Xinyue Wang[2], Siming Wang[1], Qi Zhou[1], Hongxia Li[1], Hongna Mu[1], Xue Yu[2], Fusui Ji[2], Jun Dong[1*] and Wenxiang Chen[1,3*]

[1]The Key Laboratory of Geriatrics, Beijing Institute of Geriatrics, Institute of Geriatric Medicine, Chinese Academy of Medical Sciences, Beijing Hospital/National Center of Gerontology of National Health Commission, Beijing, China, [2]Department of Cardiology, Beijing Hospital, National Center of Gerontology; Institute of Geriatric Medicine, Chinese Academy of Medical Sciences, Beijing, China, [3]National Center for Clinical Laboratories, Institute of Geriatric Medicine, Chinese Academy of Medical Sciences, Beijing Hospital/National Center of Gerontology, Beijing, China

Background: Postprandial hyperglycemia plays an important role in the pathogenesis of coronary artery disease (CAD). The aim of this study is to determine the associations of 1,5-Anhydroglucitol (1,5-AG), which reflects circulating glucose fluctuations, with the prevalence of CAD and CAD severity in coronary angiography defined Chinese patients.

Methods: 2970 Chinese patients undergoing coronary angiography were enrolled. Baseline demographics and medical history data was recorded. Serum 1,5-AG levels and biochemical parameters were measured. Baseline characteristics were compared across 1,5-AG categories in diabetes (DM) and non-DM groups. Logistic regression analysis was performed to evaluate the associations of 1,5-AG with the prevalence and severity of CAD.

Results: Lower 1,5-AG was significantly associated with higher Gensini scores in both DM and non-DM groups. Logistic regression analysis demonstrated that the associations of low 1,5-AG with the prevalence of CAD, elevated Gensini score and severe CAD robustly dose-response increased from undiagnosed DM with 1,5-AG ≥ 14μg/mL to DM with 1,5-AG < 14μg/mL even after adjusting for fasting blood glucose (FBG) or Hemoglobin A1c (HbA_{1c}). The associations were more significant in persons with DM. Significant modification effect of DM on the relationship of 1,5-AG with elevated Gensini score was found. In addition, nonlinear relationship and threshold effects of 1,5-AG with CAD and severity were observed.

Conclusion: Low 1,5-AG is significantly and independently associated with CAD and CAD severity in Chinese patients undergoing coronary angiography. Measurement of 1,5-AG is useful to differentiate subjects with extensive glucose fluctuations and high CAD risks, especially in DM patients.

Clinical Trial Registration: ClinicalTrials.gov, identifier NCT03072797.

KEYWORDS

1,5-anhydroglucitol, hemoglobin a1c, diabetes, coronary artery diseases, genuine score

Introduction

Atherosclerotic coronary artery disease (CAD) is among the leading cause of mortality and morbidity and puts an enormous economic burden worldwide (1). There are multiple risk factors for CAD such as smoking, obesity, hypertension, hyperglycemia and dyslipidemia (2). Early identification and intervention of the risk factors are effective measures to the prevention and treatment of CAD. Type 2 diabetes mellitus (DM) is considered to be an important risk factor in the development of CAD (3). Therefore, intensive blood glucose control is critical to reduce the mortality and morbidity of CAD in DM patients. Hemoglobin A1c (HbA1c), which reflects glycemic exposure over the past 2–3 months, is the standard measure used for diagnosis of diabetes as well as the clinical monitoring of glucose control (4). However, in patients with established DM, intensive intervention for glycemic control guided by HbA1c values did not improve the risk of macro-vascular complications and survival prognosis (5, 6). Previous studies have shown that postprandial hyperglycemia and glycemic variability are risk factors, independent of average glycemic level, for cardiovascular complications in people with DM (7, 8). A growing body of literature suggests that 1,5-Anhydroglucitol (1,5-AG) may provide a useful complement to HbA1c measurements (9), especially when short-term glycemic variability may not be reflected in traditional glycemia markers.

1,5-AG is a dietary monosaccharide, a naturally occurring 1-deoxy form of glucose, that is typically present at high but stable concentrations in the blood in normal glycemic status (10). Serum concentrations of 1,5-AG is adjusted by urinary excretion in the kidneys. Most 1,5-AG, which is filtered in glomerulus is reabsorbed at a specific fructose-mannose active transporter in the renal tubule, with a small amount, corresponding to dietary intake, excreted in the urine (11). The reabsorption is competitively inhibited by glucose. Therefore, the serum 1,5-AG level rapidly decreases when serum glucose level exceeds the threshold of urine glucose excretion (160-180 mg/dL), even when very short-lasting episodes appear. Previous studies have demonstrated that 1,5-AG level is negatively correlated with HbA1c and fasting blood glucose (FBG) and is a useful marker to identify well controlled, exclusively based on HbA1c levels DM patients with transient hyperglycaemia (12, 13).

In community-based studies, low 1,5-AG level is associated with the prevalence of CAD and also has predictive value for CAD events and mortality, in both DM and non-DM populations (9, 14). However, it is unclear if 1,5-AG is associated with CAD and CAD severity in high risk subjects and if 1,5-AG adds prognostic value to HbA1c, especially in Chinese populations. CAD severity can be evaluated by the Gensini score system which reflect the complexity and extent of CAD based on the artery morphology, coronary anatomy, and severity of stenosis in lesions (15, 16). Therefore, the present study was designed to determine the independent associations of 1,5-AG with the prevalence of CAD and CAD severity evaluated by Gensini score in Chinese patients underwent coronary angiography.

Abbreviations: CAD, coronary artery disease; DM, type2 diabetes mellitus; HTN, hypertension; PCI, percutaneous artery interventions; HbA1c, hemoglobin A1c; FBG, fasting blood glucose; 1,5-AG, 1,5-anhydroglucitol; TC, total cholesterol; TG, triglycerides; HDL-C, high-density lipoprotein cholesterol; LDL-C, low-density lipoprotein cholesterol; CREA, creatinine; UA, uric acid; eGFR, estimated glomerular filtration rate; BMI, body mass index; SBP, systolic blood pressure; DBP, diastolic blood pressure; IQR, interquartile ranges; ORs, Odds ratios; CIs, confidence intervals.

Materials and methods

Study population

From Mar, 2017 to 2020, 2970 consecutive patients undergoing coronary angiography in Beijing Hospital were enrolled in this study, in which 2945 subjects were measured serum 1,5-AG concentrations. The exclusion criteria were: (1) patients who had severe congenital heart disease, severe cardiac insufficiency, primary pulmonary hypertension, hepatic and renal

dysfunction; (2) patients who were receiving chemotherapy or radiotherapy, pregnant or nursing; (3) patients who were alcohol or drug abuser, or with mental illness under treatment. Baseline demographics and medical history information, including height, weight, blood pressure, lifestyle, and history of DM, hypertension (HTN), stroke, and premature CAD were surveyed by trained doctors during hospitalization. Patients with HTN, DM and dyslipidemia include those who have already been diagnosed with these diseases at enrolment and those newly diagnosed during hospitalization according to current guidelines. Before coronary angiography, fasting blood samples were taken into common vacutainer tubes and serum was separated by centrifugation. Serum samples were aliquoted into 2mL vials and stored at -80°C until analysis. This study was approved by the Ethics Committee of Beijing Hospital (2016BJYYEC-121-02) and the written informed consent was obtained from each patient.

Coronary angiography

Coronary angiographies were performed by experienced cardiologists using standard techniques in all study patients. All targeted coronary lesions of the patients were analyzed by the built-in QCA software of the Allura Xper FD20 Angiography System (Philips Healthcare, Netherlands). According to the classification of the American Heart Association Grading Committee, coronary arteries were divided into 15 segments. Coronary artery segments were carefully selected by cardiologists on the basis of smooth luminal borders and the absence of stenosis. All of the coronary arteries were injected and at least two views of the right coronary arteries and four views of the left coronary arteries were evaluated. The existence of CAD was analyzed by two experienced interventional cardiologists and was defined as the presence of one or more coronary arteries with 50% or more stenosis in the main epicardial coronary arteries. In the event of a disagreement, the opinion of a third observer was required, and the final decision was made by consensus of all three observers. To test the extent and severity of ischemia caused by the lesion, the Gensini scores (15, 16) were calculated in 2047 patients who did not have previous percutaneous artery interventions (PCI). Each lesion was assigned a score according to the percentage of stenosis, and multiplied by the coefficient defined for each major coronary artery and segment. The Gensini score of each patient was obtained by summing up the results. Subjects with Gensini scores of the top tertiles were referred as severe CAD.

Measurement of 1,5-AG and other variables

Serum 1,5-AG was measured by KingMed Diagnostics using Pyranose oxidase assay kit from Beijing Strong Biotechnologies, Inc. on a Roche Modular 702 system. Serum samples were thawed and mixed at room temperature. 1,5-AG concentration was measured according to the manufacturer's instructions. FBG, HbA1c, total cholesterol (TC), triglycerides (TG), high-density lipoprotein cholesterol (HDL-C), low-density lipoprotein cholesterol (LDL-C), creatinine (CREA), uric acid (UA) and estimated glomerular filtration rate (eGFR) were measured at the clinical laboratory of Beijing Hospital by using assay kits from Sekisui Medical Technologies (Osaka, Japan) on a Hitachi 7180 chemistry analyzer. Two quality control materials, prepared by mixed fresh serum samples, were analyzed with patient samples in each run in 1,5-AG assays to monitor the performance of the measurements. The average inter- assay CV was below 2%. Previous studies have shown this 1,5-AG assay to be highly reliable even in long-term stored samples (17). In the 2945 subjects measured, 100 samples had 1,5-AG concentration below the limit of detection, on this occasion, the lowest measured concentration was inputted.

Statistical analysis

Data were presented as percentages or medians and interquartile ranges (IQR). Baseline characteristics of the study population were compared across categories of 1,5-AG (≥14 μg/mL, <14μg/mL) in subjects with and without diagnosed DM. We used the Chi-squared test or Fisher exact test for categorical variables and the Kruskal-Wallis test for continuous variables. Correlations between 1,5-AG and conventional CAD risk factors were analyzed by Spearman nonparametric test.

To analyze the associations of 1,5-AG with the incidence of CAD and CAD severity defined by Gensini scores, multivariable logistic regression or linear regression analysis were performed. We divided the subjects with and without diabetes into two groups based on a cut point of 14 μg/mL. Those without diagnosed diabetes and 1,5-AG≥14 μg/mL served as the common reference group. Odds ratios (ORs) for CAD versus non-CAD, high versus low Gensini scores, or regression coefficients β for Gensini score, and the corresponding 95% confidence intervals (CIs) were evaluated. Potential confounding variables, including age, gender, current smoking, obesity or overweight, hypertension, dyslipidemia, stroke, family history of premature CAD, statin use, and FBG or $HbA_{1C,}$ were controlled in the regression models.

We used restricted cubic splines with five knots located at the 5th, 27.5th, 50th, 72.5th, and 95th percentiles and centered at the 14 μg/mL to explore whether there is a non-linear relationship between 1,5-AG and incident CAD and severity. Besides, two-piecewise linear regression model was also used to further explain the non-linearity and examine the threshold effect of the 1,5-AG on CAD and severity using a smoothing function. In the model, the threshold level (i.e.,turning point) was determined using trial and error, including selection of turning points along a pre-defined interval and then choosing

the turning point that gave the maximum model likelihood. We also conducted a log likelihood ratio test to examine the statistical significance.

In addition, the subgroup analyses and interaction tests were performed using stratified binary logistic regression model or linear regression. In order to further examine the robustness of associations between 1,5-AG and incident CAD and severity, we performed several sensitivity analyses: additionally adjusting for the serum concentrations of other biochemical parameters, including TC, TG, HDL-C, LDL-C, UA, Crea and eGFR; excluding participants with 1,5-AG below the limit of detection; using 1,5-AG concentration as a continuous independent variable instead of the category variable with a cutoff for 1,5-AG of ≥ 14 μg/mL, respectively.

The analyses were performed using SPSS 26.0 (Windows SPSS, Inc.) and R packages (http://www.r-project.org). All reported *P* values were two-tailed, *P* value<0.05 was considered significant.

Results

Characteristics of the study participants

At baseline, participants were a mean of 65 years old, 62.4% males and 49.6% had a diagnosed DM. The participants were classified into two groups of undiagnosed and diagnosed DM, the baseline characteristics by 1,5-AG categories (≥14 μg/mL, <14 μg/mL) within the two groups and among four subgroups were compared. As shown in Table 1, in patients with diagnosed DM (n=1462), 57.7% had 1,5-AG concentration <14mg/mL, while in patients without DM (n=1483), only 7.8% had low 1,5-AG levels (<14 μg/mL). In both diagnosed and undiagnosed DM, subjects with 1,5-AG <14 μg/mL had significantly higher FBG and HbA1C levels compared to those with 1,5-AG ≥14 mg/mL. The percent of coronary angiography defined CAD, as well as Gensini scores, were also higher in low 1,5-AG (< 14 μg/mL) subjects compared to those with higher 1,5-AG (≥ 14 μg/mL). In addition, age, BMI, SBP, percent of BMI ≥ 24 kg/m^2, HTN, DM, dyslipidemia, and statin use all significantly increased among subgroups (*P* values for trend <0.05). FBG, HbA1C, coronary angiography defined CAD, and Gensini scores were also significantly increased from undiagnosed DM to diagnosed DM and across different 1,5-AG categories (*P* values for trend <0.05).

Correlations between 1,5-AG and conventional CAD risk factors

Spearman correlations between 1,5-AG and other CAD risk factors were presented in Table 2. In subjects without a diagnosis of DM, serum 1,5-AG levels were significantly negatively correlated with age, BMI (*P*<0.001) and SBP (*P*<0.05), and positively correlated with UA (*P*<0.001) and eGFR (*P*<0.05). In subjects with a diagnosed DM, 1,5-AG was found to be negatively correlated with SBP (*P*<0.01) and eGFR (*P*<0.001), and positively correlated with TC (*P*<0.05), HDL-C, Crea and UA (*P*<0.001). In all the patients including both with and without DM, serum 1,5-AG was significantly negatively associated with age, BMI, SBP, and TG (*P*<0.001), and positively associated with TC (*P*<0.01) and HDL-C (*P*<0.001) levels. In addition, serum 1,5-AG was significantly negatively associated with Gensini scores in all subjects (*P*<0.001) and subjects with DM (*P*<0.01), but no association was found in subjects without DM. The weak associations found between 1,5-AG and TC were probably caused by the use of statins.

Multivariable analysis between categories of 1,5-AG with CAD, gensini scores and severe CAD

The associations between 1,5-AG and the presence of CAD, the Gensini scores, as well as CAD severity (high vs low Gensini score), were analyzed by the multivariable analysis in subjects with and without diagnosed DM, with those no diagnosed DM and 1,5-AG ≥14 μg/mL served as the common reference group. As shown in Table 3, the associations significantly increased, in a dose-response manner, from undiagnosed DM with 1,5-AG ≥ 14μg/mL and < 14μg/mL to DM with 1,5-AG ≥ 14μg/mL and < 14μg/mL in order (*P* values for trend <0.01). The highest ORs for the prevalence of CAD, elevated Gensini scores and severe CAD were found in subjects with diagnosed DM and 1,5-AG < 14 μg/mL after adjusting for age, gender, and other CAD risk factors (Model 1& 2). The associations were attenuated but remained significant after adjustment for FBG (Model 3) and HbA_{1C} (Model 4).

In subjects with diagnosed DM, compared with 1,5-AG ≥ 14 μg/mL, subjects with 1,5-AG < 14 μg/mL had more significant associations with the prevalent CAD, elevated Gensini scores and severe CAD in Model 1 &2 (*P*<0.05). The association remained significant after additional adjustment for FBG (Model 3) but not HbA1c (Model 4). However, in subjects without DM, compared with 1,5-AG ≥ 14 μg/mL, 1,5-AG < 14 μg/mL had no associations with the prevalence of CAD and elevated Gensini scores. Weak associations were found between 1,5-AG < 14 μg/mL and severe CAD in Model 2. The associations were no longer significant after further adjusting for FBG (Model 3) or HbA_{1C} (Model 4). These results indicated that, in the categorical analyses, the associations of low 1,5-AG (< 14 μg/mL) with the prevalent CAD, elevated Gensini scores and CAD severity were largely confined to persons with

10.3389/fendo.2022.978520

TABLE 1 Characteristics of the study participants by categories of 1,5-anhydroglucitol (1,5-AG) at baseline in subjects with and without diagnosed diabetes.

		No diagnosed diabetes, n =1483		Diagnosed diabetes, n =1462	
	Total	1,5-AG ≥ 14 μg/mL	1,5-AG < 14 μg/mL	1,5-AG ≥ 14 μg/mL	1,5-AG < 14 μg/mL
N	2945	1367	116	619	843
*1,5-AG, μg/mL	20.8 (10.1, 30.2)	28.1 (21.8, 35.2)	10.1 (7.5, 12.2) #	23.5 (18.5, 30.5)	5.9 (3.5, 9.4) #
1,5-AG, μg/mL, range	1.0, 99.3	14.0, 99.3	1.0, 13.99	14.0, 80.6	1.0, 13.99
*FBG, mmol/L	5.9 (5.1, 7.5)	5.2 (4.9, 5.8)	5.5 (5.0, 6.1) #	7.4 (6.0, 8.6)	7.9 (6.4, 10.0) #
*HbA1C, %	6.2 (5.8, 7.1)	5.8 (5.5, 6.0)	6.0 (5.6, 6.2) #	6.3 (5.9, 6.8)	7.6 (6.8, 8.6) #
*Age, y	65.0 (58.0, 74.0)	64.0 (57.0, 73.0)	69.0 (61.0, 77.8) #	67.0 (60.0, 74.0)	66.0 (58.0, 76.0)
Male, %	62.4	62.9	59.5	64.5	60.7
*BMI, kg/m^2	25.4 (23.4, 27.7)	25.1, (23.2, 27.3)	25.7 (23.8, 28.7) #	25.8 (23.9, 27.9)	25.5 (23.5, 28.0)
*BMI ≥ 24 kg/m^2, %	67.9	65.2	73.7	74.1	70.0
*SBP, mmHg	135.0 (123.0, 149.0)	133.0 (121.0, 146.0)	134.5 (123.0, 150.8)	136.0 (124.0, 150.0)	139.0 (127.0, 151.0) #
DBP, mmHg	79.0 (70.0, 85.0)	79.0 (71.0, 85.0)	79.5 (70.3, 86.8)	78.0 (70.0, 85.0)	78.0 (70.0, 85.0)
*TC, mmol/L	3.8 (3.2, 4.5)	3.9 (3.3, 4.5)	3.7 (3.2, 4.6)	3.8 (3.2, 4.5)	3.7 (3.2, 4.4)
*TG, mmol/L	1.3 (0.9, 1.8)	1.2 (0.9, 1.7)	1.2 (0.9, 1.7)	1.3 (1.0, 1.8)	1.3 (1.0, 1.9)
*HDL-C, mmol/L	1.0 (0.9, 1.2)	1.1 (0.9, 1.3)	1.0 (0.8, 1.2)	1.0 (0.9, 1.2)	1.0 (0.9, 1.1) #
LDL-C, mmol/L	2.3 (1.8, 2.8)	2.3 (1.8, 2.9)	2.3 (1.8, 2.9)	2.3 (1.8, 2.9)	2.2 (1.7, 2.8)
Crea, μmol/L	70.0 (60.0, 81.0)	70.0 (60.0, 80.0)	72.0 (62.0, 81.0)	71.0 (60.0, 83.0)	69.0 (57.0, 80.0) #
*UA, μmol/L	320.0 (266.0, 379.0)	327.0 (270.0, 390.0)	305.0 (251.5, 382.5)	333.0 (280.0, 384.0)	300.5 (254.0, 354.0) #
eGFR, mL/min per 1.73 m^2	95.5 (81.6, 110.3)	95.8 (83.1, 109.2)	91.9 (77.9, 104.7) #	93.3 (78.7, 109.1)	97.6 (80.3, 114.4) #
Current smoker, %	31.8	32.1	32.5	30.4	32.7
*Hypertension, %	60.7	66.4	73.5	73.8	74.3
*Diabetes, %	49.6	0	0	100	100
*Dyslipidemia, %	44.1	41.5	38.8	45.5	48.7
History of stroke, %	10.7	10.2	10.3	9.9	12.0
Family history of premature CAD, %	7.7	8.2	4.5	8.6	7.3
*Take statins continuously over 1 year, %	25.3	22.4	19.0 #	27.6	29.2
*Coronary angiography defined CAD, %	78.6	70.2	77.6	83.8	88.5 #
*Gensini score	12.0 (2.0, 37.5)	6.0 (1.0, 24.5)	9.5 (2.8, 29.5) #	18.3 (4.0, 45.5)	24.0 (6.0, 53.0) #

CAD, coronary artery disease; BMI, body mass index; SBP, Systolic blood pressure; DBP, Diastolic blood pressure; FBG, fasting blood glucose; TC-total cholesterol; TG- triglyceride; HDL-C, high density lipoprotein cholesterol; LDL-C, low density lipoprotein cholesterol; Crea, creatinine; UA, uric acid; eGFR, estimated glomerular filtration rate
Data are median (interquartile range) for continuous variables, or percentage for categorical variables. * P values for trend <0.05 among four groups. Significant differences (# P<0.05) compared with groups of 1,5-AG ≥ 14 μg/mL in no diagnosis of diabetes or diagnosed diabetes, respectively

diagnosed DM. In sensitivity analyses, associations of 1,5-AG with CAD, elevated Gensini scores and severe CAD remained essentially unchanged after further adjustment for other biochemical parameters, including TC, TG, HDL-C, LDL-C, UA, Crea and eGFR (Supplementary Table 1). Similar associations were observed when restricting the analyses to participants with 1,5-AG levels above the limit of detection (n=2845) (Supplementary Table 1) and using 1,5-AG concentration as a continuous independent variable instead of the category variable with a cutoff of 1,5-AG ≥ 14 μg/mL. (Figure 1, Supplementary Figure 1).

Analysis of nonlinear relationship between 1,5-AG and incident CAD and severity

The restricted cubic splines were used to flexibly model and visualize the distribution of 1,5-AG and its relation with CAD, elevated Gensini scores and CAD severity. As shown in the histograms (Figure 1), the distributions of 1,5-AG was substantially different in subjects with and without a diagnosis of DM. In subjects without DM, the distribution of 1,5-AG is roughly normal (light gray bars), however, in persons with

10.3389/fendo.2022.978520

TABLE 2 Spearman correlation (r) of 1,5-AG with other clinical parameters.

	All	No diagnosed diabetes	Diagnosed diabetes
Age	-0.061***	-0.093***	0.055*
FBG	-0.404***	-0.084**	-0.179***
HbA1C	-0.672***	-0.196***	-0.686***
BMI	-0.072***	-0.089***	0.004
SBP	-0.110***	-0.062*	-0.076**
DBP	0.006	-0.026	-0.010
TC	0.052**	-0.016	0.055*
TG	-0.067***	-0.015	-0.032
HDL-C	0.138***	-0.008	0.130***
LDL-C	0.037	-0.006	0.034
Crea	0.044*	0.006	0.108***
UA	0.158***	0.103***	0.226***
eGFR	-0.024	0.053*	-0.120***
Gensini score	-0.185***	-0.015	-0.093**

*p< 0.05, **p< 0.01, ***p< 0.001

TABLE 3 Adjusted β/OR (95% CI) and p-value of baseline diabetes-specific categories of 1,5-AG with prevalent coronary angiography defined CAD, Gensini score and severe CAD.

	Model 1	Model 2	Model 3	Model 4
Prevalent coronary angiography defined CAD				
No diagnosed diabetes				
1,5-AG ≥ 14 μg/mL	1.00 (reference)	1.00 (reference)	1.00 (reference)	1.00 (reference)
1,5-AG < 14 μg/mL	1.377 (0.864, 2.195), 0.178	1.597 (0.963, 2.648), 0.070	1.441 (0.861, 2.410), 0.164	1.130 (0.595, 2.146), 0.708
Diagnosed diabetes				
1,5-AG ≥ 14 μg/mL	2.087 (1.625, 2.681), <0.001	1.993 (1.539, 2.581), <0.001	1.271 (0.942, 1.714), 0.117	1.603 (1.164, 2.206), 0.004
1,5-AG < 14 μg/mL	*3.318 (2.591, 4.249), <0.001	*3.192 (2.467, 4.131), <0.001	*1.766 (1.284, 2.430), <0.001	1.641 (1.103, 2.440), 0.014
P for trend	<0.001	<0.001	<0.001	0.002
Gensini score				
No diagnosed diabetes				
1,5-AG ≥ 14 μg/mL	0 (reference)	0 (reference)	0 (reference)	0 (reference)
1,5-AG < 14 μg/mL	3.508 (-3.729, 10.746) 0.342	4.382 (-2.946, 11.709), 0.241	3.737 (-3.614, 11.087), 0.319	-1.077 (-10.696, 8.543), 0.826
Diagnosed diabetes				
1,5-AG ≥ 14 μg/mL	10.906 (7.244, 14.568), <0.001	10.848 (7.141, 14.554), <0.001	5.322 (1.132, 9.511), 0.013	9.069 (4.442, 13.696), <0.001
1,5-AG < 14 μg/mL	*18.008 (14.640, 21.377), <0.001	*17.476 (14.060, 20.893), <0.001	9.350 (4.981, 13.719), <0.001	9.700 (4.181, 15.220), <0.001
P for trend	<0.001	<0.001	<0.001	<0.001
Prevalent severe CAD				
No diagnosed diabetes				
1,5-AG ≥ 14 μg/mL	1.00 (reference)	1.00 (reference)	1.00 (reference)	1.00 (reference)
1,5-AG < 14 μg/mL	1.771 (0.974, 3.223), 0.061	*1.974 (1.044, 3.734) 0.036	1.681 (0.877, 3.225), 0.118	1.388 (0.603, 3.196), 0.441
Diagnosed diabetes				
1,5-AG ≥ 14 μg/mL	2.756 (2.018, 3.765), <0.001	2.751 (1.979, 3.825), <0.001	1.313 (0.885, 1.948), 0.176	2.308 (1.528, 3.484), <0.001
1,5-AG < 14 μg/mL	*5.060 (3.760, 6.811), <0.001	*5.164 (3.777, 7.059), <0.001	*1.933 (1.285, 2.908), 0.002	2.555 (1.569, 4.161), <0.001
P for trend	<0.001	<0.001	0.002	<0.001

ORs, odds ratios; CI, Confidence Intervals; CAD, coronary artery disease; SD, standard deviation

Model 1: age and gender. Model 2: variables in model 2 plus current smoker, obesity or overweight, hypertension, dyslipidemia, stroke, family history of premature CAD and statin use. Model 3: variables in model 2 plus FBG (mmol/L). Model4: variables in model 2 plus HbA_{1C} (%). P values for overall trend were calculated by modeling the category medians as a continuous variable. Significant differences (* P<0.05) between 1,5-AG categories within diabetes group (no diagnosis of diabetes or diagnosed diabetes)

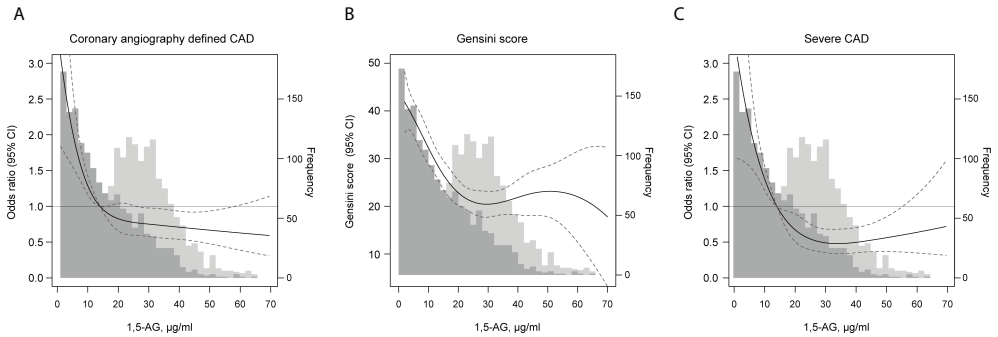

FIGURE 1
Adjusted associations of serum 1,5-AG levels with **(A)** coronary angiography defined CAD, **(B)** Gensini scores and **(C)** severe CAD in the BHAS study, N = 2945. 1,5-AG was modeled using restricted cubic splines (solid line) with knots at the 5th, 27.5th, 50th, 72.5th, and 95th percentiles. The concentration of 1,5-AG of 14 μg/mL was used as the reference point for **(A)** and **(C)**. 95% CIs are shown with the dashed lines. Models are adjusted for age, gender, current smoker, obesity or overweight, diabetes, hypertension, dyslipidemia, stroke and family history of premature CAD. Frequency histograms are shown for persons without diabetes (light gray bars) and for persons with diabetes (dark gray bars).

diagnosed DM, the distribution of 1,5-AG was non-normal and highly right skewed (black bars). When modeled with restricted cubic splines, the lowest level of 1,5-AG tended to be associated with the highest risk of incident CAD, elevated Gensini scores and severe CAD when adjusted for age, gender, current smoker, obesity or overweight, diabetes, hypertension, dyslipidemia, stroke, family history of premature CAD and statin use. The association was not linear across the entire distribution, we observed a threshold effect, with apparent dose-response associations at lower levels but little evidence of associations at higher levels. In Table 4, by using the two-piece wise linear regression model, the turning point of 1,5-AG was calculated as 14.0 μg/mL for prevalent CAD. Therefore, on the left of the turning point, the adjusted ORs (95%CI) were 0.420 (0.263, 0.670) (P <0.001), indicating significant associations with CAD. However, on the right of the turning point, the adjusted associations were not significant. Compared with the linear model, the differences found were statistically significant (P for log likelihood ratio tests were <0.001). Interestingly, the turning points for the Gensini scores and severe CAD were 29.7 μg/mL and 28.8 μg/mL respectively, which were much higher than that of CAD.

Stratified analysis of the associations between 1,5-AG with CAD, gensini scores and CAD severity

In order to examine the robust associations of 1,5-AG with CAD, associations between 1,5-AG levels and the incidence of

TABLE 4 Threshold effect analysis of 1,5-AG (per 1-SD increment) on coronary angiography defined CAD, Gensini score and the severity of CAD.

	Crude β/OR (95% CI) *p*-value	*Adjusted β/OR (95% CI) *p*-value
CAD		
1,5-AG < 14.0 μg/mL	0.296 (0.197, 0.445), <0.001	0.420 (0.263, 0.670), <0.001
1,5-AG ≥14.0 μg/mL	0.875 (0.776, 0.986), 0.029	0.969 (0.847, 1.108), 0.644
P for log likelihood ratio test	<0.001	0.002
Gensini score		
1,5-AG < 29.7 μg/mL	-9.018 (-11.240, -6.796), <0.001	-4.674 (-7.189, -2.159), <0.001
1,5-AG ≥ 29.7 μg/mL	2.189 (-1.335, 5.713) 0.2235	1.963 (-1.415, 5.340), 0.255
P for log likelihood ratio test	<0.001	0.008
Severe CAD		
1,5-AG < 28.8 μg/mL	0.433 (0.360, 0.520), <0.001	0.589 (0.464, 0.746), <0.001
1,5-AG ≥ 28.8 μg/mL	1.224 (0.962, 1.558), 0.100	1.221 (0.935, 1.595), 0.143
P for log likelihood ratio test	<0.001	<0.001

Crude: no adjustment
*Adjusted for age, gender, current smoker, obesity or overweight, diabetes, hypertension, dyslipidemia, stroke and family history of premature CAD

CAD, the Gensini scores and CAD severity were respectively analyzed in different subgroups, such as different age, gender, BMI (<24kg/m^2, ≥24kg/m^2), smoking status, hypertension, dyslipidemia, and with or without diagnosed DM, stroke, and family history of premature CAD. Interactions between 1,5-AG and these factors on the distribution of CAD, Gensini scores and severe CAD were also analyzed. As shown in Supplementary Figure 1, the results suggested that when 1,5-AG was used as continuous variables, each SD increase was associated with 15% decrease of prevalent CAD, 2 point lower of Gensini scores and 18% decrease of severe CAD. The associations were apparently more significant in persons with diagnosed DM compared with non-DM. These results were similar with those when 1,5-AG was modeled as a categorical variable (Table 3). However, only the interaction by DM for Gensini score was observed (*P* for interaction =0.029, Supplementary Figure 1B). Although the ORs (95% CI) for CAD and severe CAD were different in DM and non-DM patients [0.771 (0.650-0.914) vs 0.919 (0.799-1.057) for CAD, and 0.716 (0.580-0.884) vs 0.909 (0.751-1.100) for severe CAD], no significant effect modification by DM was found (*P* for interaction > 0.05). We did not observe interactions by age, sex, BMI, current smoker, dyslipidemia, stroke and family history of premature CAD for the presence of CAD, Gensini score and CAD severity (all *P* for interaction > 0.05).

Discussion

In the present study, we analyzed the associations between serum 1,5-AG with the prevalence of CAD and CAD severity as assessed by the Gensini score system in Chinese patients underwent coronary angiography. The results showed that low concentrations of 1,5-AG were independently associated with the prevalence of CAD, elevated Gensini scores and severe CAD after adjusting for age, gender and other CAD risk factors. More significant associations remain in DM patients after further adjusting for FBG or HbA_{1C}. Nonlinear relationship and threshold effects of 1,5-AG were found for prevalent CAD, elevated Gensini scores, and CAD burden, with the 1,5-AG turning points of 14.0μg/mL, 29.7μg/mL, and 28.8 μg/mL respectively.

DM is a disorder of impaired glucose homeostasis and is one of the important risk factors for cardiovascular diseases, including CAD and related mortality. Recent epidemiological, clinical and experimental data have suggested that effective controlling of blood glucose in the nonfasting state, especially the postprandial period, can reduce the risk of macroangiopathic complications of diabetes (7, 8, 18). Evaluating glycemic control is currently based on the self-monitoring of blood glucose and clinical testing for HbA1c, which is a surrogate biochemical marker of the average glycemia level over the previous 2-3 months (4). Although HbA1c provides a valuable, standardized and evidence-based parameter that is relevant for clinical decision making, there are circumstances that HbA1c levels are insufficient to predict the risk of adverse outcomes (19–21). Moreover, it was well established previously that although postprandial glycaemia can influence HbA1c concentration, glycated haemoglobin is not sensitive for short-lasting, transient hyperglycaemia (22). 1,5-AG is an emerging glycometabolic marker that complements HbA1c in terms of short-term glycemic control, postprandial hyperglycemia and glucose fluctuation (9, 10, 12–14). Serum 1,5-AG concentration is found to be relatively stable in normalglycemia state and rapidly falls reflecting not only chronic, but also short-lasting hyperglycaemic episodes. Therefore, measurement of 1,5-AG is important to identify transient hyperglycaemia and related CAD risks in DM patients and non-DM individuals.

Previous studies have reported that 1,5-AG levels are associated with vascular endothelial dysfunction (23), oxidative stress (24), carotid atherosclerosis (25, 26) and the prevalence of CAD (9, 27). In one previous prospective study of approximately 2000 persons in Japan, 1,5-AG at baseline was significantly associated with incident cardiovascular events during 11 years of follow-up (28). In the ARIC study, a community-based prospective cohort study, low 1,5-AG was associated with subclinical cardiovascular disease, cardiovascular outcomes and mortality in persons with a history of DM (14). However, the relationship of 1,5-AG with CAD or CAD events were not consistent in the population without diagnosis of DM (14, 29–31). The associations between 1,5AG and CAD were also studied in patients undergoing coronary angiography (32, 33), and found that the 1,5-AG levels were independently associated with CAD, and serum 1,5-AG value predicts CAD related adverse events even in non-DM patients without CAD. However, these studies had a relatively strict exclusion criteria and small number of participates which may have limited representations. In addition, whether the association between 1,5-AG and CAD is modified by DM is not clear. In the current study, the relationship of 1,5-AG with the prevalent CAD, Gensini scores, and CAD severity were analyzed in Chinese subjects undergoing coronary angiography in both DM and non-DM patients.

We first analyzed the baseline characteristics in diagnosed DM and non-DM by low (<14 μg/mL) and high (≥14 μg/mL) 1,5-AG categories. In both diagnosed and undiagnosed DM, lower 1,5-AG was associated with not only significantly higher FBG and HbA1C levels, but also higher Gensini scores. These results were in accordance with the previous reports (34, 35). Multivariable analysis showed that the associations robustly

dose-reponse increased from undiagnosed DM with 1,5-AG ≥ 14μg/mL to DM with 1,5-AG < 14μg/mL even after adjusting for FBG or HbA_{1c}. The associations of low concentrations of 1,5-AG with CAD, elevated Gensini score and severe CAD were more significant in persons with diagnosed DM. However, only significant modification effect of DM on the relationship of 1,5-AG with elevated Gensini score was found. These results suggested that measurement of serum 1,5-AG value may be useful for not only evaluation of glucose control but also CAD risk assessment in high risk populations, especially in DM patients.

Different values have been reported for blood 1,5-AG concentrations depending on the racial/ethnic groups, being higher in Asians and Africans compared to Caucasians (36, 37). In the previous study, 1,5-AG concentration of 10.0 μg/mL (14, 29, 32, 38) and 14.0 μg/mL (28, 31, 39) have been used as the cut-off values for defining exposure to hyperglycemia, potentially representing a subset of the population with higher post-prandial glycemic peaks. In our study, 57.7% of the subjects with diagnosed DM had 1,5-AG<14.0 μg/mL, and in subjects without DM, 92.2% had 1,5-AG>14.0μg/mL. These results were in accordance with the reports of Dr. Yamanouchi (40), in which 14 μg/mL was recommended as the normal lower limit of 1,5-AG levels. When modeled with restricted cubic splines, our results demonstrated that the lowest level of 1,5-AG was associated with the highest prevalence of CAD, elevated Gensini scores and sever CAD. In addition, the association was not linear across the entire distribution, in which a threshold effect was found. By using the two- piecewise linear regression model, the turning points of 1,5-AG for CAD, high Gensini scores, and severe CAD were calculated. The results suggested that, the linear associations between 1,5-AG and CAD was largely confined in 1,5-AG<14μg/mL. However, the turning points of 1,5-AG for high Gensini scores (29.7 μg/mL) and severe CAD (28.8 μg/mL) were much higher. These results indicate that, for prevention of the occurrence and development of atherosclerosis, more strict control of glycemic fluctuations are needed.

We recognize that our study has some limitations. First, this results are based on a single baseline measurement of 1,5-AG and lack of information on 2-h postprandial glucose. Second, owing to the observational nature of the study, we are also not able to completely rule out the possibility of residual confoundings. Third, since this study was a baseline data of our BHAS, the obtained results require further confirmation in future prospective analysis.

Conclusion

This study demonstrated that low 1,5-AG levels were independently associated with the prevalence of CAD and the severity of the disease evaluated by Gensini scores, in diagnosed DM patients, even after adjusting for FBG or HbA_{1C}. The relationship of 1,5-AG with CAD and severity were not linear with threshold effects existed. Our study added to the evidence regarding the value of 1,5-AG as an effective glycometabolic marker that complements HbA1c in terms of glucose fluctuation and CAD risk assessment in persons with DM. Additional studies are needed to understand its possible utility as a tool for diabetes management in primary and secondary prevention of CAD.

Data availability statement

The data analyzed in this study is subject to the following licenses/restrictions: The data that support the findings of this study are available from the corresponding author upon reasonable request. Requests to access these datasets should be directed to Jun Dong, jun_dong@263.net.

Ethics statement

The studies involving human participants were reviewed and approved by The Ethics Committee of Beijing Hospital (2016BJYYEC-121-02). The patients/participants provided their written informed consent to participate in this study.

Author contributions

JD, WC, XY and FJ were responsible for the study design and execution. WZ, XW, XY finished the coronary angiography procedures and clinical data collection. SW, HM and HL finished all the laboratory measurements and data collection. RY and QZ performed the data analysis. RY and JD wrote the main manuscript. WC edited the manuscript. All authors contributed to the article and approved the submitted version.

Funding

This work was supported by the CAMS Innovation Fund for Medical Sciences (No. 2021-I2M-1-050), the National Key R&D Program of China (2020YFC2008304), and Beijing Natural Science Foundation (No.7222156).

Acknowledgments

The authors thank Ms. Mo Wang and Yueming Tang for preparing the patient samples.

Conflict of interest

The authors declare that the research was conducted in the absence of any commercial or financial relationships that could be construed as a potential conflict of interest.

Publisher's note

All claims expressed in this article are solely those of the authors and do not necessarily represent those of their affiliated organizations, or those of the publisher, the editors and the reviewers. Any product that may be evaluated in this article, or claim that may be made by its manufacturer, is not guaranteed or endorsed by the publisher.

Supplementary material

The Supplementary Material for this article can be found online at: https://www.frontiersin.org/articles/10.3389/fendo.2022.978520/full#supplementary-material

References

1. Laslett LJ, Alagona PJr, Clark BA3rd, Drozda JPJr, Saldivar F, Wilson SR, et al. The worldwide environment of cardiovascular disease: Prevalence, diagnosis, therapy, and policy issues: a report from the American college of cardiology. *J Am Coll Cardiol* (2012) 60(25 Suppl):S1–49. doi: 10.1016/j.jacc.2012.11.002

2. Gilstrap LG, Wang TJ. Biomarkers and cardiovascular risk assessment for primary prevention: an update. *Clin Chem* (2012) 58(1):72–82. doi: 10.1373/clinchem.2011.165712

3. Stephens JW, Ambler G, Vallance P, Betteridge DJ, Humphries SE, Hurel SJ. Cardiovascular risk and diabetes. are the methods of risk prediction satisfactory? *Eur J Cardiovasc Prev Rehabil.* (2004) 11(6):521–8. doi: 10.1097/01.hjr.0000136418.47640.bc

4. American Diabetes Association. 2. classification and diagnosis of diabetes: Standards of medical care in diabetes-2020. *Diabetes Care* (2020) 43(Suppl 1):S14–31. doi: 10.2337/dc20-S002

5. ADVANCE Collaborative Group, Patel A, MacMahon S, Chalmers J, Neal B, Billot L, et al. Intensive blood glucose control and vascular outcomes in patients with type 2 diabetes. *N Engl J Med* (2008) 358(24):2560–72. doi: 10.1056/NEJMoa0802987

6. Duckworth W, Abraira C, Moritz T, Reda D, Emanuele N, Reaven PD, et al. Glucose control and vascular complications in veterans with type 2 diabetes. *N Engl J Med* (2009) 360(2):129–39. doi: 10.1056/NEJMoa0808431

7. Kuroda M, Shinke T, Sakaguchi K, Otake H, Takaya T, Hirota Y, et al. Association between daily glucose fluctuation and coronary plaque properties in patients receiving adequate lipid-lowering therapy assessed by continuous glucose monitoring and optical coherence tomography. *Cardiovasc Diabetol* (2015) 14:78. doi: 10.1186/s12933-015-0236-x

8. Kuroda M, Shinke T, Sakaguchi K, Otake H, Takaya T, Hirota Y, et al. Effect of daily glucose fluctuation on coronary plaque vulnerability in patients pre-treated with lipid-lowering therapy: A prospective observational study. *JACC Cardiovasc Interv.* (2015) 8(6):800–11. doi: 10.1016/j.jcin.2014.11.025

9. Ikeda N, Hiroi Y. Cardiovascular disease and 1,5-anhydro-d-glucitol. *Glob Health Med* (2019) 1(2):83–7. doi: 10.35772/ghm.2019.01031

10. Yamanouchi T, Tachibana Y, Akanuma H, Minoda S, Shinohara T, Moromizato H, et al. Origin and disposal of 1,5-anhydroglucitol, a major polyol in the human body. *Am J Physiol* (1992) 263: E268–73. doi: 10.1152/ajpendo.1992.263.2.E268

11. Yamanouchi T, Shinohara T, Ogata N, Tachibana Y, Akaoka I, Miyashita H. Common reabsorption system of 1,5-anhydro-D-glucitol, fructose, and mannose in rat renal tubule. *Biochim Biophys Acta* (1996) 1291(1):89–95. doi: 10.1016/0304-4165(96)00050-5

12. Dungan KM. 1,5-anhydroglucitol (GlycoMark) as a marker of short-term glycemic control and glycemic excursions. *Expert Rev Mol Diagn.* (2008) 8(1):9–19. doi: 10.1586/14737159.8.1.9

13. Krhač M, Lovrenčić MV. Update on biomarkers of glycemic control. *World J Diabetes* (2019) 10(1):1–15. doi: 10.4239/wjd.v10.i1.1

14. Selvin E, Rawlings A, Lutsey P, Maruthur N, Pankow JS, Steffes M, et al. Association of 1,5-anhydroglucitol with cardiovascular disease and mortality. *Diabetes* (2016) 65(1):201–8. doi: 10.2337/db15-0607

15. Gensini GG. A more meaningful scoring system for determining the severity of coronary heart disease. *Am J Cardiol* (1983) 51(3):606. doi: 10.1016/s0002-9149(83)80105-2

16. Sinning C, Lillpopp L, Appelbaum S, Ojeda F, Zeller T, Schnabel R, et al. Angiographic score assessment improves cardiovascular risk prediction: The clinical value of SYNTAX and gensini application. *Clin Res Cardiol* (2013) 102(7):495–503. doi: 10.1007/s00392-013-0555-4

17. Selvin E, Rynders GP, Steffes MW. Comparison of two assays for serum 1,5-anhydroglucitol. *Clin Chim Acta* (2011) 412(9-10):793–5. doi: 10.1016/j.cca.2011.01.007

18. Kataoka S, Gohbara M, Iwahashi N, Sakamaki K, Nakachi T, Akiyama E, et al. Glycemic variability on continuous glucose monitoring system predicts rapid progression of non-culprit lesions in patients with acute coronary syndrome. *Circ J* (2015) 79(10):2246–54. doi: 10.1253/circj.CJ-15-0496

19. Little RR, Rohlfing CL. The long and winding road to optimal HbA1c measurement. *Clin Chim Acta* (2013) 418:63–71. doi: 10.1016/j.cca.2012.12.026

20. Wright LA, Hirsch IB. Metrics beyond hemoglobin A1C in diabetes management: Time in range, hypoglycemia, and other parameters. *Diabetes Technol Ther* (2017) 19:S16–26. doi: 10.1089/dia.2017.0029

21. Bonora E, Calcaterra F, Lombardi S, Bonfante N, Formentini G, Bonadonna RC, et al. Plasma glucose levels throughout the day and HbA(1c) interrelationships in type 2 diabetes: Implications for treatment and monitoring of metabolic control. *Diabetes Care* (2001) 24(12):2023–9. doi: 10.2337/diacare.24.12.2023

22. Juraschek SP, Steffes MW, Selvin E. Associations of alternative markers of glycemia with hemoglobin A(1c) and fasting glucose. *Clin Chem* (2012) 58(12):1648–55. doi: 10.1373/clinchem.2012.188367

23. Torimoto K, Okada Y, Mori H, Tanaka Y. Low levels of 1,5-anhydro-D-glucitol are associated with vascular endothelial dysfunction in type 2 diabetes. *Cardiovasc Diabetol* (2014) 13:99. doi: 10.1186/1475-2840-13-99

24. Kohata Y, Ohara M, Nagaike H, Fujikawa T, Osaka N, Goto S, et al. Association of hemoglobin A1c, 1,5-Anhydro-D-Glucitol and glycated albumin with oxidative stress in type 2 diabetes mellitus patients: A cross-sectional study. *Diabetes Ther* (2020) 11(3):655–65. doi: 10.1007/s13300-020-00772-7

25. Sato T, Kameyama T, Inoue H. Association of reduced levels of serum 1,5-anhydro-d-glucitol with carotid atherosclerosis in patients with type 2 diabetes. *J Diabetes Complications* (2014) 28(3):348–52. doi: 10.1016/j.jdiacomp.2014.01.004

26. Liang M, McEvoy JW, Chen Y, Sharrett AR, Selvin E. Association of a biomarker of glucose peaks, 1,5-anhydroglucitol, with subclinical cardiovascular disease. *Diabetes Care* (2016) 39(10):1752–9. doi: 10.2337/dc16-0840

27. Fujiwara T, Yoshida M, Yamada H, Tsukui T, Nakamura T, Sakakura K, et al. Lower 1,5-anhydroglucitol is associated with denovo coronary artery disease in patients at high cardiovascular risk. *Heart Vessels* (2015) 30(4):469–76. doi: 10.1007/s00380-014-0502-y

28. Watanabe M, Kokubo Y, Higashiyama A, Ono Y, Miyamoto Y, Okamura T. Serum 1,5-anhydro-D-glucitol levels predict first-ever cardiovascular disease: An 11-year population-based cohort study in Japan, the suita study. *Atherosclerosis* (2011) 216(2):477–83. doi: 10.1016/j.atherosclerosis.2011.02.033

29. Warren B, Lee AK, Ballantyne CM, Hoogeveen RC, Pankow JS, Grams ME, et al. Associations of 1,5-anhydroglucitol and 2-hour glucose with major clinical outcomes in the atherosclerosis risk in communities (ARIC) study. *J Appl Lab Med* (2020) 5(6):1296–306. doi: 10.1093/jalm/jfaa066

30. Ouchi S, Shimada K, Miyazaki T, Takahashi S, Sugita Y, Shimizu M, et al. Low 1,5-anhydroglucitol levels are associated with long-term cardiac mortality in acute coronary syndrome patients with hemoglobin A1c levels less than 7.0. *Cardiovasc Diabetol* (2017) 16(1):151. doi: 10.1186/s12933-017-0636-1

31. Ikeda N, Hara H, Hiroi Y. Ability of 1,5-anhydro-d-glucitol values to predict coronary artery disease in a non-diabetic population. *Int Heart J* (2015) 56(6):587–91. doi: 10.1536/ihj.15-177

32. Ikeda N, Hara H, Hiroi Y, Nakamura M. Impact of serum 1,5-anhydro-d-glucitol level on prediction of major adverse cardiac and cerebrovascular events in non-diabetic patients without coronary artery disease. *Atherosclerosis* (2016) 253:1–6. doi: 10.1016/j.atherosclerosis.2016.08.016

33. Fujiwara T, Yoshida M, Yamada H, Tsukui T, Nakamura T, Sakakura K, et al. Lower 1,5-anhydroglucitol is associated with denovo coronary artery disease in patients at high cardiovascular risk. *Heart Vessels* (2015) 30(4):469–76. doi: 10.1007/s00380-014-0502-y

34. Dworacka M, Winiarska H. The application of plasma 1,5-anhydro-D-glucitol for monitoring type 2 diabetic patients. *Dis Markers* (2005) 21(3):127–32. doi: 10.1155/2005/251068

35. Ma C, Sheng J, Liu Z, Guo M. Excretion rates of 1,5-anhydro-D-glucitol, uric acid and microalbuminuria as glycemic control indexes in patients with type 2 diabetes. *Sci Rep* (2017) 7:44291. doi: 10.1038/srep44291

36. Herman WH, Dungan KM, Wolffenbuttel BH, Buse JB, Fahrbach JL, Jiang H, et al. Racial and ethnic differences in mean plasma glucose, hemoglobin A1c, and 1,5-anhydroglucitol in over 2000 patients with type 2 diabetes. *J Clin Endocrinol Metab* (2009) 94(5):1689–94. doi: 10.1210/jc.2008-1940

37. Selvin E, Warren B, He X, Sacks DB, Saenger AK. Establishment of community-based reference intervals for fructosamine, glycated albumin, and 1,5-anhydroglucitol. *Clin Chem* (2018) 64(5):843–50. doi: 10.1373/clinchem.2017.285742

38. Selvin E, Rawlings AM, Grams M, Klein R, Steffes M, Coresh J. Association of 1,5-anhydroglucitol with diabetes and microvascular conditions. *Clin Chem* (2014) 60(11):1409–18. doi: 10.1373/clinchem.2014.229427

39. Wada H, Dohi T, Miyauchi K, Takahashi N, Endo H, Kato Y, et al. Impact of serum 1,5-anhydro-D-glucitol level on the prediction of severe coronary artery calcification: an intravascular ultrasound study. *Cardiovasc Diabetol* (2019) 18 (1):69. doi: 10.1186/s12933-019-0878-1

40. Yamanouchi T, Akanuma Y, Toyota T, Kuzuya T, Kawai T, Kawazu S, et al. Comparison of 1,5-anhydroglucitol, HbA1c, and fructosamine for detection of diabetes mellitus. *Diabetes* (1991) 40(1):52–7. doi: 10.2337/diab.40.1.52

frontiers | Frontiers in Endocrinology

TYPE Review
PUBLISHED 15 September 2022
DOI 10.3389/fendo.2022.983713

OPEN ACCESS

EDITED BY
Ying Xin,
Jilin University, China

REVIEWED BY
Yi Tan,
University of Louisville, United States
Xiaozhen Dai,
Chengdu Medical College, China

*CORRESPONDENCE
Ling-Bo Qian
bioqian@163.com
Chi Xiao
xcier@163.com

SPECIALTY SECTION
This article was submitted to Cardiovascular Endocrinology, a section of the journal Frontiers in Endocrinology

RECEIVED 01 July 2022
ACCEPTED 16 August 2022
PUBLISHED 15 September 2022

CITATION
Chen M-Y, Meng X-F, Han Y-P, Yan J-L, Xiao C and Qian L-B (2022) Profile of crosstalk between glucose and lipid metabolic disturbance and diabetic cardiomyopathy: Inflammation and oxidative stress. *Front. Endocrinol.* 13:983713. doi: 10.3389/fendo.2022.983713

Profile of crosstalk between glucose and lipid metabolic disturbance and diabetic cardiomyopathy: Inflammation and oxidative stress

Meng-Yuan Chen, Xiang-Fei Meng, Yu-Peng Han, Jia-Lin Yan, Chi Xiao* and Ling-Bo Qian*

School of Basic Medical Sciences & Forensic Medicine, Hangzhou Medical College, Hangzhou, China

In recent years, the risk, such as hypertension, obesity and diabetes mellitus, of cardiovascular diseases has been increasing explosively with the development of living conditions and the expansion of social psychological pressure. The disturbance of glucose and lipid metabolism contributes to both collapse of myocardial structure and cardiac dysfunction, which ultimately leads to diabetic cardiomyopathy. The pathogenesis of diabetic cardiomyopathy is multifactorial, including inflammatory cascade activation, oxidative/nitrative stress, and the following impaired Ca^{2+} handling induced by insulin resistance/hyperinsulinemia, hyperglycemia, hyperlipidemia in diabetes. Some key alterations of cellular signaling network, such as translocation of CD36 to sarcolemma, activation of NLRP3 inflammasome, up-regulation of AGE/RAGE system, and disequilibrium of micro-RNA, mediate diabetic oxidative stress/inflammation related myocardial remodeling and ventricular dysfunction in the context of glucose and lipid metabolic disturbance. Here, we summarized the detailed oxidative stress/inflammation network by which the abnormality of glucose and lipid metabolism facilitates diabetic cardiomyopathy.

KEYWORDS

disturbance of glucose metabolism, inflammation, oxidative stress, disturbance of lipid metabolism, diabetic cardiomyopathy

1 Introduction

There are three major nutrients, including carbohydrates, fats and proteins, for human body's metabolism. The monosaccharide, especially glucose, hydrolyzed from carbohydrates provide indispensable energy for cellular function and survival. Diabetes mellitus is characterized by dysregulation of insulin pathway and insulin resistance leading to the disorder of carbohydrate metabolism and hyperglycemia. Microvascular and macrovascular abnormalities, resulting in diabetic retinopathy, nephropathy, neuropathy and cardiomyopathy, are primary causes of high disability and mortality in diabetes (1, 2). Diabetic cardiomyopathy (DCM) is confirmed to be inseparably related to the abnormal myocardial energy metabolism (3). With the development of diabetes, the inhibition of glucose utilization is accompanied with the increase of fatty acid β-oxidation to satisfy the cellular energy requirement (4). Lots of cellular signaling transduction pathways associating with inflammatory response and oxidative stress are abnormally regulated in the diabetic heart and cardiomyocyte because of the disturbance of glucose and lipid metabolism, which is involved in the development of cardiac hypertrophy, fibrosis and heart failure (5, 6). Here, we summarized the crosstalk between the abnormality of glucose and lipid metabolism and DCM focusing on oxidative stress and inflammation.

Abbreviations: AR, Aldose reductase; AGEs, Advanced glycation end-products; AMPK, AMP-activated protein kinase; ASC, Apoptosis-associated speck-like protein containing a caspase recruitment domain; CD36, Cluster of differentiation 36; DAG, Diacylglycerol; DCM, Diabetic cardiomyopathy; ECM, Extracellular matrix; eNOS, Endothelial nitric oxide synthase; ER, Endoplasmic reticulum; FAO, Fatty acid oxidation; F-6-P, Fructose 6-phosphate; FOXO1, Forkhead box protein O1; Glucosamine-6-P, Glucosamine-6-phosphate; GFAT, Glutamine-fructose-6-phosphate amidotransferase; GLUTs, Glucose transporters; GSH, Reduced glutathione; GSSH, Oxidized glutathione; IKK, IκB kinase; LCFA, Long-chain fatty acids; mPTP, Mitochondrial permeability transition pore; NAD^+, Oxidized form of nicotinamide adenine dinucleotide; NADPH, Reduced form of nicotinamide adenine dinucleotide phosphate; NF-κB, Nuclear factor κ-light-chain-enhancer of activated B cells; NLRP3, Nucleotide-binding domain, leucine-rich-containing family, pyrin domain containing 3; O_2^-, Superoxide anion; O-GlcNAcylation, O-linked N-acetylglucosamine glycosylation; oxLDL, Oxidized low-density lipoprotein; PAMPs, Pathogen-associated molecular patterns; PKC, Protein kinase C; PPAR, Peroxisome proliferator-activated receptor; RAGE, Receptor for AGE; ROS, Reactive oxygen species; T1DM, Type 1 diabetes mellitus; TLR4, Toll-like receptor 4; UDP-GlcNAc, UDP-N-acetylglucosamine.

2 What is diabetic cardiomyopathy

It has been estimated in IDF Diabetes Atlas (the 10th edition) that the global number of diabetes in the age of 20-79 was 537 million in 2021 (an increase of 16% compared with that in 2019), which has been projected to reach 643 million by 2030, and more than 6.7 million adults have died (about 12.2% of global death) due to diabetes and diabetic complications in 2021 (http://diabetesatlas.org/atlas/tenth-edition/). Such a high prevalence of diabetes and a hug number of diabetes-related death confirm that diabetes is one of the fastest growing global health emergencies in the 21st century. Despite the different pathophysiology of type 1 diabetes mellitus (T1DM) and T2DM, chronic systemic hyperglycemia and the disorder of glucose and lipid metabolism ultimately result in severe complications, such as blindness, kidney failure, cardiomyopathy, stroke, and lower limb amputation (2). The cardiovascular system is one of the most vulnerable targets of diabetes and suffers from endothelial dysfunction, atherosclerosis, cardiomyopathy, and even heart failure, which accounts for the major cause of morbidity and mortality in diabetic patients (7). Diabetes confers about a two-fold excess risk for cardiovascular disease independently from other conventional risk factors (8) and three-fold higher cardiovascular mortality had been reported in diabetic subjects by the Framingham Heart Study (4, 9). DCM is defined as a chronic metabolic heart disease in the absence of congenital heart disease, coronary artery disease, cardiac valve disease, or hypertension and is one of the major causes of the mortality in diabetic patients (10, 11). The typical manifest of DCM includes cardiac remodeling (hypertrophy and fibrosis) and dysfunction (12). Left ventricular diastolic dysfunction is one of the earliest characteristics of the diabetic heart and systolic dysfunction, even heart failure, develop at a later stage of DCM independent of hypertension and ischemic coronary artery disease (4, 12, 13).

3 Metabolic disorder in the diabetic heart

Although the normal adult heart can use a variety of energy substrates, such as glucose, lactate, fatty acids, ketones, and amino acids for the continuous requirement of energy, but it primarily utilizes long-chain fatty acids (LCFA) to supply 50%-70% of energy (4, 14). Chronic alterations of myocardial substrate preference, which begins from the early stage of diabetes, can contribute to DCM. As shown in Figure 1, the decrease in utilization of glucose owing to insulin resistance promotes fatty acid β-oxidation to supply 90%-100% of energy associated with the translocation of cluster of differentiation 36 (CD36), a fatty acid transporter, into the sarcolemma and enhanced LCFA uptake in the cardiomyocyte, meanwhile leads

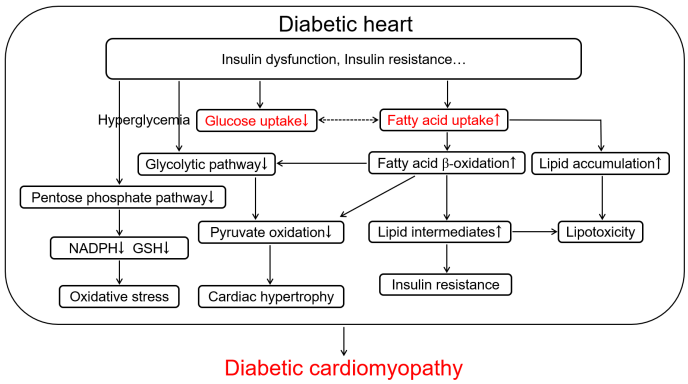

FIGURE 1
The scheme of glucose and lipid metabolism disorder in the diabetic heart contributing to diabetic cardiomyopathy. Diabetes-induced insulin dysfunction and insulin resistance cause the increase in fatty acid uptake characterized by up-regulation of fatty acid β-oxidation and lipid accumulation and the decrease in glucose uptake accompanying with hyperglycemia and down-regulation of pentose phosphate pathway and glycolytic pathway in the cardiomyocyte. Up-regulation of fatty acid β-oxidation further promotes the inhibition of glycolytic pathway and pyruvate oxidation, and increases lipid intermediates and lipotoxicity. These metabolic alterations in diabetes ultimately cause oxidative stress, further insulin resistance, and cardiac hypertrophy, which aggravates the development of diabetic cardiomyopathy. NADPH, reduced form of nicotinamide adenine dinucleotide phosphate; GSH, reduced glutathione.

to the lipotoxic cardiomyopathy in diabetes (14–16). Irreversible hyperglycemia and over-use of fatty acid β-oxidation, as forerunners in diabetes (13), break the cellular homeostasis of oxidation-reduction reaction and provoke cardiac inflammatory response, characterized by the over-production of reactive oxygen species (ROS) and pro-inflammatory factors, which contributes to the development of DCM, including ventricular remodeling, hypertrophy, myocardial stiffness, cardiac dysfunction, and heart failure (4, 13, 17). The impaired myocardial structure and function both contribute to further abnormalities of glucose and lipid metabolism in the diabetic heart, generating a positive feedback loop to exacerbate the cardiac injury in diabetes, which can not be ignored in the development of DCM (3, 18–20). Thus, rectifying metabolic disorder in the diabetic patient has been clinically accepted to attenuate cardiovascular complications.

3.1 Glycometabolism disorder and DCM

Hyperglycemia is an independent risk factor for DCM (5). The membrane glucose transporters (GLUTs) are responsible for the uptake of glucose into the cardiomyocyte. The shortage of insulin signaling or insulin resistance results in the internalization of GLUT4 and a marked down-regulation of membrane GLUT4 (Figure 2), which finally leads to the decreased glucose uptake in cells and hyperglycemia (21, 22) and compensatory increased LCFA uptake to break the equilibrium of myocardial energy metabolism in diabetes (5). Chronic hyperglycemia induces complicated alterations, including activation of sorbitol and hexosamine pathways, the increase of advanced glycation end-products (AGEs) and receptors for AGEs (RAGEs), and the explosion of ROS and proinflammatory factors, to result in cardiac remodeling and dysfunction in diabetes (Figure 2) (5, 13, 23).

3.1.1 Up-regulation of sorbitol pathway

With the development of diabetes, aldose reductase (AR), a rate-limiting enzyme in sorbitol pathway, is up-regulated to convert glucose into sorbitol at the expense of reduced form of nicotinamide adenine dinucleotide phosphate (NADPH). Sorbitol is, in turn, converted into fructose by sorbitol dehydrogenase at the expense of oxidized form of nicotinamide adenine dinucleotide (NAD^+) (Figure 2A) (24–26). Fructose can be further metabolized into fructose 3-phosphate and 3-deoxyglucosone, two potent nonenzymatic glycation agents, to augment the formation of AGEs, resulting in ROS production (25). Because NADPH is required for the shift of oxidized glutathione (GSSH) to reduced glutathione (GSH), an endogenous antioxidant, the consumption of NADPH by sorbitol pathway up-regulated by chronic hyperglycemia breaks the cellular antioxidant capacity (Figure 2A) (27). Thus the increase in intracellular sorbitol produced by sorbitol pathway has been identified as a biomarker of oxidative stress. Besides, the up-regulation of sorbitol pathway aberrant increases the activation of protein kinase C (PKC) (2). Accumulation of intracellular sorbitol causes hyperosmotic stress and the decreased activity of Na^+-K^+-ATPase (2, 23). An increase in cytosolic NADH/NAD^+ triggers mitochondrial dependent ROS formation (27). All these alterations induced by the

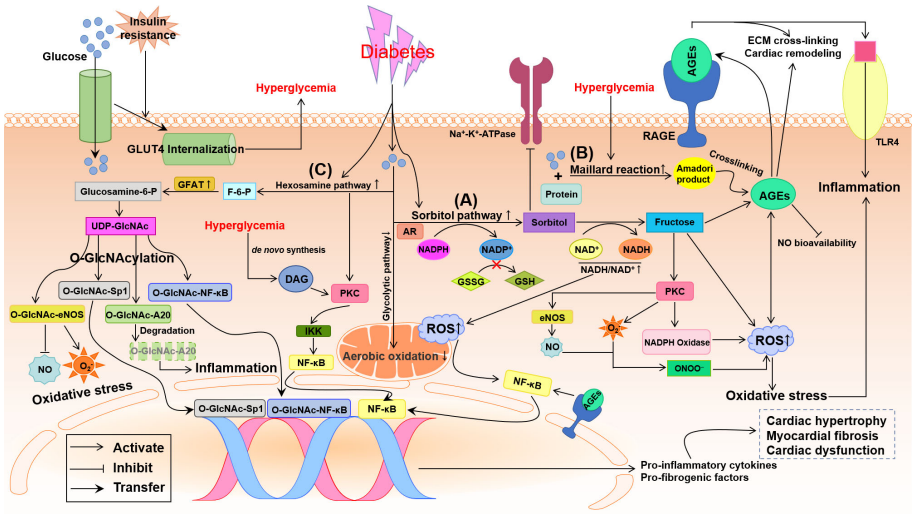

FIGURE 2
Potential pathways by which glycometabolism disorder damages the diabetic heart. Insulin resistance promotes the internalization of glucose transporter 4 (GLUT4) that means the decrease of transmembrane GLUT4 to inhibit glucose uptake in the diabetic cardiomyocyte. Oxidative stress and inflammation induced by the disturbance of glycometabolism involve the activation of three major pathways: sorbitol pathway, advanced glycation end-products (AGEs)/receptor of AGE (RAGE) and hexosamine pathway. **(A)** Up-regulation of sorbitol pathway augments oxidative stress through decreasing the reduced glutathione (GSH) and increasing reactive oxygen species (ROS), which causes nuclear factor κ-light-chain-enhancer of activated B cells (NF-κB)-induced inflammation. **(B)** Hyperglycemia boosts the formation AGEs and activates the AGE/RAGE system, which results in extracellular matrix (ECM) cross-linking, cardiac remodeling, nitric oxide (NO) inactivation and oxidative stress. **(C)** Up-regulation of hexosamine biosynthesis in diabetes leads to O-linked N-acetylglucosamine glycosylation (O-GlcNAcylation) modification of proteins, producing O-GlcNAc-A20, endothelial NO synthase (eNOS), Sp1 and NF-κB. O-GlcNAcylation of A20 accelerates its ubiquitination and proteasomal degradation resulting in inflammation. O-GlcNAcylation of Sp1 and NF-κB activate the transcriptional function to up-regulate pro-inflammatory and pro-fibrogenic factors. O-GlcNAc-eNOS decreases NO formation while increases superoxide anion (O^{2-}) production. In addition, hyperglycemia may also activate protein kinase C (PKC), directly through de novo synthesis of diacylglycerol (DAG) and indirectly through increased flux of sorbitol pathway and hexosamine pathway, to promote inflammation and oxidative stress. All these glycometabolism disorders result in cardiac remodeling and dysfunction in diabetes. AR, aldose reductase; F-6-P, fructose 6-phosphate; GFAT, glutamine-fructose-6-phosphate amidotransferase; Glucosamine-6-P, glucosamine-6-phosphate; GSSH, oxidized glutathione; IKK, IκB kinase; NADH/NAD$^+$, reduced/oxidized form of nicotinamide adenine dinucleotide; NADP$^+$, nicotinamide adenine dinucleotide phosphate; NADPH, reduced form of NADP$^+$; ONOO$^-$, peroxynitrite; TLR4, toll-like receptor 4; UDP-GlcNAc, UDP-N-acetylglucosamine.

up-regulation of sorbitol pathway in diabetes augments oxidative stress and leads to diabetic cardiovascular complications (Figure 2A).

3.1.2 Accumulation of AGEs

The AGEs formation is closely related to hyperglycemia and involves the development of diabetic cardiovascular complications (28, 29). Under long-standing hyperglycemia, reducing sugars such as glucose and fructose non-enzymatically binds with amino-acid residues in proteins, lipids and nucleic acids to form Schiff bases and Amadori products, the so-called Maillard reaction (Figure 2B), resulting in the accumulation of AGEs (30). The connective tissue matrix and membrane are prime targets of advanced glycation, by which high concentrations of AGEs are accumulated in cardiac tissues characterized by extracellular matrix (ECM) cross-linking (4) and myocardial stiffness (31). Formation of AGEs also produces excess ROS, which positively promotes the surges of AGEs, and reduces the bioavailability of NO leading to oxidative stress. AGEs activate RAGE to amply the inflammatory response by modulating nuclear factor κ-light-chain-enhancer of activated B cells (NF-κB) signaling and toll-like receptor 4 (TLR4) pathway (Figure 2B) (5, 31). These changes jointly promote myocardial fibrosis and diastolic dysfunction in diabetes. The interaction of AGE with a pattern recognition receptor termed RAGE affects numerous cell signal pathways related to inflammation and oxidative stress (31). Blocking RAGE signaling or knockdown RAGE gene has been demonstrated to alleviate cardiac hypertrophy and fibrosis and prevent the diabetic heart from systolic and diastolic dysfunction (32, 33).

3.1.3 Up-regulation of hexosamine biosynthesis

Under physiological conditions, only 2%-5% of the total glucose is metabolized through the hexosamine pathway (2, 27). When exposed to persistent hyperglycemia, the hexosamine pathway and the rate-limiting enzyme, glutamine-fructose-6-phosphate amidotransferase (GFAT), are both over activated to

convert glucose into excessive fructose 6-phosphate (F-6-P), glucosamine-6-phosphate and finally into UDP-N-acetylglucosamine (UDP-GlcNAc) (Figure 2C) (34). UDP-GlcNAc can donate N-acetylglucosamine to serine or threonine residues of target proteins within the nucleus and cytosol forming O-linked glycoproteins of proteins, which is called post-translational modification of proteins by single O-linked N-acetylglucosamine glycosylation (O-GlcNAcylation) (2, 34). The increased O-GlcNAcylation modification of proteins was found to alter gene expression in the diabetic heart and to be associated with DCM (2, 23, 35, 36). Abnormally elevated O-GlcNAc modification of endothelial nitric oxide synthase (eNOS) at Ser1177 deactivates eNOS and inhibits NO production (37), which impairs vasodilation, ECM remodeling and angiogenesis (Figure 2C). Importantly, several transcription factors, such as NF-κB (37, 38) and Sp1 (Figure 2C) (39), can be directly/indirectly activated by hyperglycemia-induced O-GlcNAcylation leading to the up-regulation of pro-inflammatory factors, including TGF-β, TNF-α and PAI-1, and down-regulation of SERCA2a leading to abnormal intracellular Ca^{2+} transient (38–40). Hyperglycemia clears anti-inflammatory and atheroprotective protein A20 *via* O-GlcNAcylation-dependent ubiquitination and proteasomal degradation (Figure 2C), which may be key to the cardiovascular system (37, 41).

3.2 Lipid metabolism disorder and DCM

Early in diabetes, abnormal glycometabolism grants the increase in fatty acid β-oxidation to compensate for a shortage of energy in the diabetic heart, which reduces mitochondrial oxidative capacity, and cardiac efficiency characterized by low ratio of myocardial ATP production/oxygen consumption and high mitochondria-derived superoxide anion (O_2^-) (42). As shown in Figure 3, the high fatty acid β-oxidation is accompanied with violent intracellular accumulation of toxic lipid metabolites, which precipitates DCM through multiple mechanisms including excessive generation of ROS, endoplasmic reticulum (ER) stress, and mitochondrial remodeling (43). Numerous studies using transgenic animal models have shown that up-regulation of myocardial fatty acid transporters such as CD36 and fatty acid transport protein 1 contribute to high fatty acid intake and lipotoxicity in the cardiomyocyte, which finally exacerbates the development of DCM (13, 44, 45).

3.2.1 Up-regulation of CD36

The LCFA transporter CD36, also named as scavenger receptor B2, has been evidenced to take oxidized low-density lipoproteins (oxLDLs) and phospholipids into myocytes and

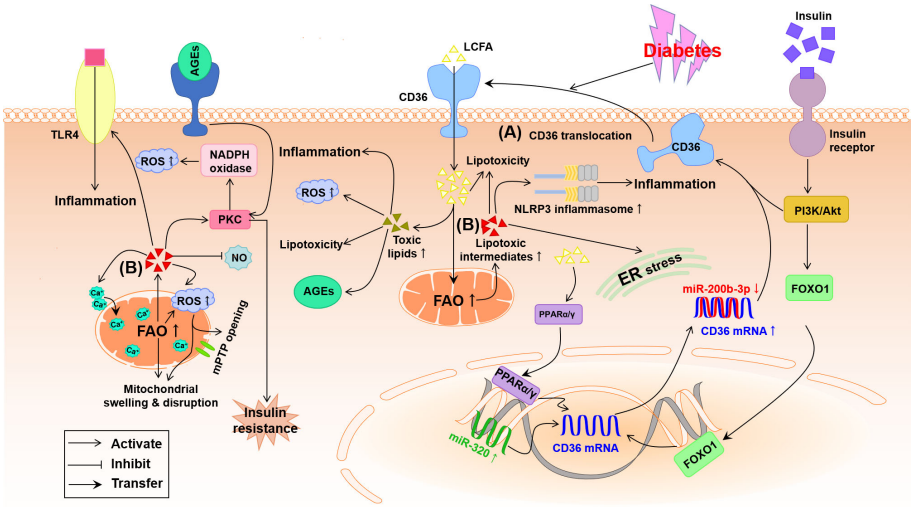

FIGURE 3
Potential pathways by which lipid metabolism disorder damages the diabetic heart. **(A)** Under diabetes conditions, the expression of cardiac PPARα/γ and FOXO1 is increased meanwhile miR-200b-3p is decreased and miR-320 is increased, which helps to up-regulation of CD36 causing the increase in LCFA uptake. **(B)** Abnormal FAO and accumulation of lipotoxic intermediates in the diabetic cardiomyocyte trigger oxidative stress, inflammation and ER stress. Furthermore, accumulation of lipotoxic intermediates in the diabetic cardiomyocyte increases mitochondrial uncoupling and impairment of mitochondria Ca^{2+} handing, leading to mitochondrial swelling and disruption through the opening of mitochondrial permeability transition pore (mPTP). AGEs, advanced glycation end-products; Akt, protein kinase B; CD36, cluster of differentiation 36; ER, endoplasmic reticulum; FAO, fatty acid oxidation; FOXO1, forkhead box protein O1; LCFA, long-chain fatty acid; NLRP3, nucleotide-binding domain, leucine-rich-containing family, pyrin domain containing 3; NO, nitric oxide; PI3K, phosphoinositide 3-kinase; PKC, protein kinase C; PPARα/γ, peroxisome proliferator-activated receptor α/γ; ROS, reactive oxygen species; TLR4, toll-like receptor 4.

lipocytes of rodents and humans, and up to 70% of total fatty acids into cardiomyocytes (46, 47). The up-regulation of CD36 has been evidenced on the sarcolemma of cardiomyocytes in diabetic mice and patients with DCM, which is owing to both high membrane translocation and high expression of CD36 triggered by hyperinsulinemia, hyperglycemia and hyperlipidemia during the development of diabetes (5, 48). As suggested in Figure 3, high insulin at the beginning of diabetes up-regulates CD36 mRNA expression by activating the transcription factor forkhead box protein O1 (FOXO1) and strongly transports CD36 to sarcolemma by activating the PI3K-Akt pathway while chronic high glucose and high triglyceride (TG) in the advanced stage of diabetes further facilitate CD36 expression and sarcolemma distribution (48, 49). The recent study indicates that up-regulated nuclear micro-RNA (miR)-320 and down-regulated miR-200b-3p induced by diabetes directly promote CD36 transcription and translation, respectively, thus further promoting the sarcolemma distribution of CD36 (Figure 3) (48). At the same time, excessive intracellular fatty acid accumulation and β-oxidation and high oxLDL uptake due to the increased sarcolemma distribution of CD36 produce a great deal of ROS, which can advance inflammation and insulin resistance to worsen DCM (4, 49–51). The cardiac impairment induced by the high level of CD36 has been further confirmed by the fact that absence of CD36 inhibited the accumulation of cardiac lipotoxicity whereas improved the cellular utilization of glucose ultimately rescuing DCM (52, 53). Therefore, the increased CD36 during DCM in turn aggravates the heart injury. In addition, the transcription factor peroxisome proliferator-activated receptor (PPAR), a class of ligand activated nuclear receptor including PPARα, PPARβ/δ and PPARγ, is activated by CD36-induced high intracellular LCFA, which up-regulates the transcription and sarcolemma distribution of CD36 to irritate fatty acids uptake and lipotoxicity in the diabetic myocardium through a positive feed-back (Figure 3A) (13, 54).

3.2.2 Lipid accumulation-mediated myocardial injury

In the diabetic heart, insulin-dependent glucose intake is impaired while cardiac fatty acid influx and accumulation of lipids and lipotoxic intermediates are increased, resulting in cardiac lipotoxicity to play a causal role in the development of DCM (10, 13). Aberrant accumulation of lipids in diabetes usually leads to cardiovascular complications including DCM and heart failure (47). Excessive accumulation of lipids can facilitate numerous pathological processes linked to the development of DCM including mitochondrial dysfunction, ER stress, inflammation, and apoptosis (47, 55). The increase in myocardial fats especially TG (the other forms of LCFA) may exert deleterious effect on the left ventricular mass and diastolic function (56), which has been demonstrated in both ob/ob and db/db mice (57, 58). Furthermore, a constant myocardial influx of LCFA far exceeds cellular metabolic utilization, and the normal process of fatty acid β-oxidation is collapsed to generate plenty of mitochondrial derived ROS, which destroys cellular structure and function and promotes the process of DCM.

3.2.3 Lipotoxic intermediates-mediated myocardial injury

Intramyocardial accumulation of lipotoxic intermediates, such as ceramide, diacylglycerol (DAG) and fatty acyl-CoAs, caused by lipid metabolism disorder creates a lipotoxic microenvironment in the heart, that likely renders much of the cardiac injuries in diabetes (47). As indicated in Figure 3B, these lipotoxic intermediates have been identified to activate some serine/threonine kinases including PKC and TLR4-mediated innate immunity, causing plenty of proinflammatory cytokines, oxidative stress, apoptosis and hypertrophy in the diabetic heart (47, 59, 60). Briefly, ceramide, the precursor of sphingolipids, stimulates the assembly of the nucleotide-binding domain, leucine-rich-containing family, pyrin domain containing 3 (NLRP3) inflammasome, ER stress, insulin resistance, and myocardial death (Figure 3B) (60, 61). DAG can activate PKC to trigger insulin resistance, the release of ROS and dilated lipotoxic cardiomyopathy. In addition, both DAG and ceramides probably inhibit the production of NO, which is responsible for cardiovascular endothelial dysfunction in diabetes (Figure 3B) (49). The increase of LCFA uptake exceeds the limited oxidation capacity in the diabetic heart, which causes the overproduction of fatty acyl-CoAs that associated with cardiac lipotoxicity (62). The high fatty acid oxidation (FAO) and excess fatty acyl-CoAs may activate PKCθ leading to insulin resistance and impaired glucose metabolism ultimately metabolic disorder leading to DCM (Figure 3B) (63, 64).

3.3 Common downstream pathway and miRNA interference

3.3.1 PKC

PKC, a family of serine-threonine kinases composed of at least 12 isoforms, can phosphorylate target proteins and is essential for cell proliferation and differentiation in a tissue- and isoform-dependent manner (18, 65). Long-standing hyperglycemia-induced activation of PKC, through predominately a *de novo* synthesis of DAG, has been confirmed to thicken basement membrane, reduce blood flow and deposit ECM in the heart from both diabetic rodents and patients, which renders the development of DCM from cardiac inflammation, hypertrophy, fibrosis and diastolic dysfunction to heart failure (62, 66–69).

Besides DAG, hyperglycemia may also activate PKC indirectly through increased flux of sorbitol pathway, increased flux of hexosamine pathway (Figure 2), and activated renin-angiotensin-aldosterone system, all of which result in the accumulation of pro-inflammatory cytokines and ROS in DCM (6, 34). PKC-induced overproduction of ROS mainly depends on the activation of NADPH oxidase (Figures 2, 3), which has been verified by the fact that treatment with the inhibitor of PKC reduced NADPH oxidase-produced ROS and rescued the heart from DCM (70–72). In addition, PKC can up-regulate eNOS to produce peroxynitrite ($ONOO^-$), a potent ROS, under the reaction of NO with O_2^-, which results in a decreased bioavailability of NO and an increased oxidative stress in the diabetic vasculature (Figure 2) (73). Furthermore, PKC can activate NF-κB *via* IκB kinase (IKK)-dependent inactivation of inhibitor of NF-κB to up-regulate proinflammatory factors (Figure 2) (74, 75). The role of PKC in the development of DCM has been verified by several studies that high oxidative stress and inflammation triggered by activation of PKCθ and $PKC\beta_2$ is essential to the diabetic cardiac hypertrophy and fibrosis (76–78).

3.3.2 AMPK

AMP-activated protein kinase (AMPK) is an evolutionarily conserved serine-threonine kinase which regulates cellular energy homeostasis and coordinates multiple pathological processes, such as diabetes, cancer, cardiac hypertrophy and other chronic diseases (79, 80). Substantial evidence suggests that activating AMPK may be key to the function and survival of the diabetic cardiovascular system by balancing the utilization of intracellular energy substrates (such as glycolysis, TG synthesis and FAO) (80, 81), suppressing NLPR3 inflammasome-related inflammation and NADPH oxidase-related oxidative stress, and modulating autophagy and ER stress (82–88). In view of this, AMPK, for example, pharmacologically activated by metformin (80, 81, 86), appears to be a potential target for treating DCM.

3.3.3 miRNAs

MiRNAs are a group of short (22~25 nucleotides), single-stranded and highly conserved RNAs and commonly act as post-transcriptional inhibitors of gene expression (89). A variety of miRNAs, including miR-1, miR-152, miR-187, miR-208a, miR-802, miR-126 and so on, have identified to modulate insulin production, energy metabolism (89, 90), and oxidative stress (89) resulting in DCM characterized by hypertrophy (89, 91), fibrosis (92) and heart failure (93–97). Recent studies have shown that miR-21 is abundantly expressed in the diabetic hearts (98–100), which accounts for the high oxidative stress and inflammation-related DCM probably through the insufficient activation of nuclear factor-E2 related factor 2 signaling pathway (100) and sprouty homolog 1/extracellular signal-regulated kinase/mammalian target of rapamycin (SPRY1/ERK/mTOR) pathway (99). The expression of miRNAs, such as miR-146a and miR-221, is disturbed to induce an enhancement of oxidative stress and inflammation response, which is acknowledged to promote the development of DCM. Several studies have showed that the significantly down-regulated miR-146a induced by longstanding hyperglycemia not only causes the overexpression of pro-inflammatory factors (IL-6, TNF-α and IL-1β) and NF-κB (101–103) but also generates excess ROS *via* NADPH oxidase 4 pathway, which impairs the diabetic cardiovascular system (101).

4 Inflammatory response and oxidative stress in DCM

Metabolic disturbance in the context of diabetes is associated with inflammation characterized by the excessive release of pro-inflammatory cytokines and activation of inflammatory cascade response (104). Pro-inflammatory cytokines, especially TNF-α, can lead to cardiac remodeling and dysfunction in the progression of diabetes. TNF-α inhibits tyrosine phosphorylation of insulin receptor substrate-1 aggravating insulin resistance and increases ventricular hypertrophy and vascular permeability leading to heart failure in diabetes (105). Inflammation and oxidative stress are closely interlinked (Figure 4). Both inflammatory response and overproduction of ROS/reactive nitrogen species (RNS) induced by metabolic disturbance in diabetes trigger NF-κB transcription and translocation to further arise pro-inflammatory cytokines and ROS/RNS, forming a vicious cycle of diabetic complications (106). Hyperglycemia and the increase of FAO produce excessive ROS/RNS to modify and blunt endogenous antioxidant defense systems, leading to deadly cell abnormalities such as mitochondrial membrane potential disruption (107), DNA double-strand break (27), and ER stress in diabetes (108). Eliminating pro-inflammatory factors and ROS/RNS is involved in the protection of correcting metabolic disturbance against DCM, which has been demonstrated by the curative effect of statins and active compounds in medicinal plants in diabetic heart diseases (109, 110).

4.1 Inflammation in DCM

A chronic inflammatory response clearly persists in diabetes through deadly activating the innate immune system to damage the heart (20, 111). Some early-responding pro-inflammatory immune cells, like M1-polarized macrophages, lymphocytes and neutrophils, secrete IL-6, IL-18, TNF-α, IL-1β to attack vascular smooth muscle cells, fibroblasts and cardiomyocytes impairing cellular energy metabolism and cause cardiovascular dysfunction (112, 113). TLR4 can be activated by the excess free fatty acid and pathogen-associated molecular patterns (PAMPs) to induce the synthesis of pro-inflammatory cytokines, meanwhile the activation of NF-κB by TLR4 also amplify the inflammatory response and pathological alterations

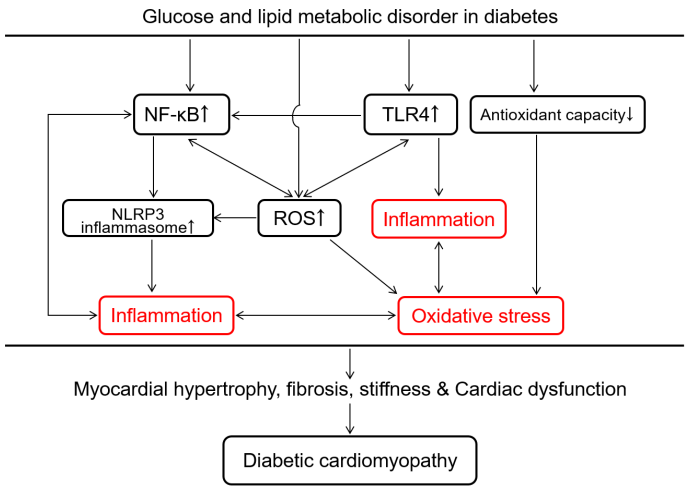

FIGURE 4
Overview of intracellular inflammation and oxidative stress interaction in response to glucose and lipid metabolic disorder in the development of diabetic cardiomyopathy. Glucose and lipid metabolic disorder in diabetes promotes cardiac inflammation *via* TLR4-mediated innate immunity, the surge of reactive oxygen species (ROS) and NF-κB-induced activation of NLRP3 inflammasome. The decrease in the antioxidant capacity and the increase in ROS production induced by the metabolic disorder both accelerate oxidative stress in the diabetic heart. Inflammation and oxidative stress promote each other to cause myocardial hypertrophy, fibrosis, stiffness and cardiac dysfunction, which is a potentially vicious cycle in the development of diabetic cardiomyopathy. NF-κB, nuclear factor κ-light-chain-enhancer of activated B cells; NLRP3, nucleotide-binding domain, leucine-rich-containing family, pyrin domain containing 3; TLR4, toll-like receptor 4.

(Figure 4) (114). This up-regulation of TLR4-mediated inflammation has been found in the diabetic heart (115) and repression of TLR4 benefits to lower lipid accumulation and to ameliorate cardiac function in diabetes (13, 116). Additionally, NLRP3 inflammasome, assembled by NLRP3, caspase-1, and apoptosis-associated speck-like protein containing a caspase recruitment domain (ASC), has been considered as another inflammatory participant in the ventricular remodeling and dysfunction of cardiac disease such as acute myocardial infarction, DCM and heart failure (117–119). The deleterious effect of activating NLRP3 inflammasome in DCM includes inflammation, fibrosis, pyroptosis and apoptosis (119–122). In addition to DAMPs/PAMPs (119, 123, 124), the increased fatty acids (122, 125), lipid intermediates (122), glucose (119), ROS (37, 119) are also the positive regulator to boost NLRP3 inflammasome in DCM. Once exposed to diabetic or other nociceptive stimuli, the auto-oligomerization of NLRP3 inflammasome is rapidly initiated by connecting NLRP3 proteins with ASC through both PYD domains (119). The NLRP3-ASC complex recruits pro-caspase-1 to form NLRP3 inflammasome *via* CARD domain interaction (122). Subsequently, pro-caspase-1 is cleaved into activated caspase-1, which promotes the secretion of IL-1β and IL-18 leading to a novel cell death named pyroptosis (123, 126). NLRP3 inflammasome plays a vital role in the progression of inevitable cardiac fibrosis and collagen deposition *via* suppressing MAPK signaling pathway and the production of cAMP and in myocardial fibroblasts (127–129). Given such destructive effect, NLRP3 inflammasome is probably a new target for the treatment of DCM.

4.2 Oxidative stress in DCM

ROS are primarily produced by mitochondrial respiratory chain as an electron leakage due to the impairing electron transport in hyperglycemia (130). NADPH oxidase is another prominent source of ROS in diabetes (27, 131). The decline of endogenous antioxidant capacity by inactivating antioxidants (such as GSH and vitamin E) and/or down-regulating antioxidant enzymes (such as superoxide dismutase, peroxidase and catalase) is also involved in the oxidative stress to develop DCM (Figure 4) (2, 27, 71, 130). Excess ROS can break DNA double-strand and oxidize proteins, by which glyceraldehyde 3-phosphate dehydrogenase, a key glycolytic enzyme in the glycolysis process, is down-regulated leading to the inhibition of glycolysis and accumulation of glycolytic intermediates (37). High glucose powerfully hampers the pentose phosphate pathway *via* inhibiting its rate-limiting enzyme glucose-6-phosphate dehydrogenase, to decrease the production of NADPH and GSH resulting in a lower antioxidant defense with a higher ROS production in endothelial cells and cardiomyocytes (Figure 1) (132, 133). The excessive ROS in diabetes can modify the structure of lipids named lipid peroxidation such as formation of malondialdehyde, 4-hydroxynonenam and oxLDL. These oxidized lipids commonly enhance pro-inflammatory response and participate diabetic

cardiovascular complications including atherosclerosis and DCM (50, 51). Hence, oxidative stress represents a major force in the development of diabetic inflammation and probably an important target in the treatment of DCM accompanied by disproportionate inflammation (Figure 4).

5 Conclusion

A variety of studies have confirmed that glucose and lipid metabolic disturbance plays a central role in the development of DCM through vicious oxidative stress and inflammatory response pathways. The polyol pathway, hexosamine biosynthesis, PCK activation, sarcolemmal translocation of CD36, up-regulation of AGE/RAGE system, and disequilibrium of micro-RNA are involved in the metabolic disturbance, all of which contribute to the enhancement of diabetic oxidative stress and inflammation finally resulting in DCM. Although several dependable first-line drugs targeting glucose/lipid metabolism such as metformin, thiazolidinediones and sodium-glucose transporter-2 inhibitors alleviate hyperglycemia, the exact effect of these agents on DCM still needs to be further explored in the diabetic animal model and patient.

Author contributions

M-YC wrote the manuscript. M-YC, X-FM, Y-PH, J-LY, CX, and L-BQ designed the figures and edited the manuscript. CX and L-BQ supervised the writing. All authors contributed to the article and approved the submitted version.

Funding

This work was supported by National Natural Science Foundation of China (81772035), Natural Science Foundation of Zhejiang Province (LQ20H150001), and Program of Cultivating Zhejiang Provincial High-level Personnel in Health (Innovative Talent in 2021).

Conflict of interest

The authors declare that the research was conducted in the absence of any commercial or financial relationships that could be construed as a potential conflict of interest.

Publisher's note

References

1. Marshall SM, Flyvbjerg A. Prevention and early detection of vascular complications of diabetes. *BMJ (Clin Res ed)* (2006) 333:475–80. doi: 10.1136/bmj.38922.650521.80

2. Forbes JM, Cooper ME. Mechanisms of diabetic complications. *Physiol Rev* (2013) 93:137–88. doi: 10.1152/physrev.00045.2011

3. Stanley WC, Lopaschuk GD, McCormack JG. Regulation of energy substrate metabolism in the diabetic heart. *Cardiovasc Res* (1997) 34:25–33. doi: 10.1016/s0008-6363(97)00047-3

4. Evangelista I, Nuti R, Picchioni T, Dotta F, Palazzuoli A. Molecular dysfunction and phenotypic derangement in diabetic cardiomyopathy. *Int J Mol Sci* (2019) 20:3264. doi: 10.3390/ijms20133264

5. Jia G, Adam WC, Sowers JR. Diabetic cardiomyopathy: A hyperglycaemia- and insulin-resistance-induced heart disease. *Diabetologia* (2018) 61:21–8. doi: 10.1007/s00125-017-4390-4

6. Jia G, Hill MA, Sowers JR. Diabetic cardiomyopathy: An update of mechanisms contributing to this clinical entity. *Circ Res* (2018) 122:624–38. doi: 10.1161/CIRCRESAHA.117.311586

7. Zheng Y, Ley SH, Hu FB. Global aetiology and epidemiology of type 2 diabetes mellitus and its complications. *Nat Rev Endocrinol* (2018) 14:88–98. doi: 10.1038/nrendo.2017.151

8. Sarwar N, Gao P, Seshasai SRK, Gobin R, Kaptoge S, Di Angelantonio E, et al. Diabetes mellitus, fasting blood glucose concentration, and risk of vascular disease: A collaborative meta-analysis of 102 prospective studies. *Lancet (Lond Engl)* (2010) 375:2215–22. doi: 10.1016/S0140-6736(10)60484-9

9. Mahmood SS, Levy D, Vasan RS, Wang TJ. The Framingham Heart Study and the epidemiology of cardiovascular disease: A historical perspective. *Lancet (Lond Engl)* (2014) 383:999–1008. doi: 10.1016/S0140-6736(13)61752-3

10. Bugger H, Abel ED. Molecular mechanisms of diabetic cardiomyopathy. *Diabetologia* (2014) 57:660–71. doi: 10.1007/s00125-014-3171-6

11. Dillmann WH. Diabetic cardiomyopathy. *Circ Res* (2019) 124:1160–2. doi: 10.1161/CIRCRESAHA.118.314665

12. Tate M, Grieve DJ, Ritchie RH. Are targeted therapies for diabetic cardiomyopathy on the horizon? *Clin Sci (London Engl 1979)* (2017) 131:897–915. doi: 10.1042/CS20160491

13. Tan Y, Zhang Z, Zheng C, Wintergerst KA, Keller BB, Cai L. Mechanisms of diabetic cardiomyopathy and potential therapeutic strategies: Preclinical and clinical evidence. *Nat Rev Cardiol* (2020) 17:585–607. doi: 10.1038/s41569-020-0339-2

14. Yan J, Young ME, Cui L, Lopaschuk GD, Liao R, Tian R. Increased glucose uptake and oxidation in mouse hearts prevent high fatty acid oxidation but cause cardiac dysfunction in diet-induced obesity. *Circulation* (2009) 119:2818–28. doi: 10.1161/CIRCULATIONAHA.108.832915

15. Lopaschuk GD, Ussher JR, Folmes CDL, Jaswal JS, Stanley WC. Myocardial fatty acid metabolism in health and disease. *Physiol Rev* (2010) 90:207–58. doi: 10.1152/physrev.00015.2009

16. Cai L, Kang YJ. Oxidative stress and diabetic cardiomyopathy: A brief review. *Cardiovasc Toxicol* (2001) 1:181–93. doi: 10.1385/ct:1:3:181

17. Aneja A, Tang WHW, Bansilal S, Garcia MJ, Farkouh ME. Diabetic cardiomyopathy: Insights into pathogenesis, diagnostic challenges, and

therapeutic options. *Am J Med* (2008) 121:748–57. doi: 10.1016/j.amjmed.2008.03.046

18. Faria A, Persaud SJ. Cardiac oxidative stress in diabetes: Mechanisms and therapeutic potential. *Pharmacol Ther* (2017) 172:50–62. doi: 10.1016/j.pharmthera.2016.11.013

19. Birse RT, Bodmer R. Lipotoxicity and cardiac dysfunction in mammals and drosophila. *Crit Rev Biochem Mol Biol* (2011) 46:376–85. doi: 10.3109/10409238.2011.599830

20. Donath MY, Dinarello CA, Mandrup-Poulsen T. Targeting innate immune mediators in type 1 and type 2 diabetes. *Nat Rev Immunol* (2019) 19:734–46. doi: 10.1038/s41577-019-0213-9

21. Saw EL, Pearson JT, Schwenke DO, Munasinghe PE, Tsuchimochi H, Rawal S, et al. Activation of the cardiac non-neuronal cholinergic system prevents the development of diabetes-associated cardiovascular complications. *Cardiovasc Diabetol* (2021) 20:50. doi: 10.1186/s12933-021-01231-8

22. Begum N, Draznin B. Effect of streptozotocin-induced diabetes on GLUT-4 phosphorylation in rat adipocytes. *J Clin Invest* (1992) 90:1254–62. doi: 10.1172/JCI115988

23. Brownlee M. Biochemistry and molecular cell biology of diabetic complications. *Nature* (2001) 414:813–20. doi: 10.1038/414813a

24. Gabbay KH. The sorbitol pathway and the complications of diabetes. *New Engl J Med* (1973) 288:831–6. doi: 10.1056/NEJM197304192881609

25. Tang WH, Martin KA, Hwa J. Aldose reductase, oxidative stress, and diabetic mellitus. *Front Pharmacol* (2012) 3:87. doi: 10.3389/fphar.2012.00087

26. Obrosova IG. Increased sorbitol pathway activity generates oxidative stress in tissue sites for diabetic complications. *Antioxid Redox Signaling* (2005) 7:1543–52. doi: 10.1089/ars.2005.7.1543

27. Papachristoforou E, Lambadiari V, Maratou E, Makrilakis K. Association of glycemic indices (hyperglycemia, glucose variability, and hypoglycemia) with oxidative stress and diabetic complications. *J Diabetes Res* (2020) 2020:7489795. doi: 10.1155/2020/7489795

28. Goldin A, Beckman JA, Schmidt AM, Creager MA. Advanced glycation end products: Sparking the development of diabetic vascular injury. *Circulation* (2006) 114:597–605. doi: 10.1161/CIRCULATIONAHA.106.621854

29. Giacco F, Brownlee M. Oxidative stress and diabetic complications. *Circ Res* (2010) 107:1058–70. doi: 10.1161/CIRCRESAHA.110.223545

30. Singh R, Barden A, Mori T, Beilin L. Advanced glycation end-products: A review. *Diabetologia* (2001) 44:129–46. doi: 10.1007/s001250051591

31. Frati G, Schirone L, Chimenti I, Yee D, Biondi-Zoccai G, Volpe M, et al. An overview of the inflammatory signalling mechanisms in the myocardium underlying the development of diabetic cardiomyopathy. *Cardiovasc Res* (2017) 113:378–88. doi: 10.1093/cvr/cvx011

32. Ma H, Li SY, Xu P, Babcock SA, Dolence EK, Brownlee M, et al. Advanced glycation endproduct (AGE) accumulation and AGE receptor (RAGE) up-regulation contribute to the onset of diabetic cardiomyopathy. *J Cell Mol Med* (2009) 13:1751–64. doi: 10.1111/j.1582-4934.2008.00547.x

33. Nielsen JM, Kristiansen SB, Nørregaard R, Andersen CL, Denner L, Nielsen TT, et al. Blockage of receptor for advanced glycation end products prevents development of cardiac dysfunction in db/db type 2 diabetic mice. *Eur J Heart Fail* (2009) 11:638–47. doi: 10.1093/eurjhf/hfp070

34. Chiu CJ, Taylor A. Dietary hyperglycemia, glycemic index and metabolic retinal diseases. *Prog retin eye Res* (2011) 30:18–53. doi: 10.1016/j.preteyeres.2010.09.001

35. Kenny HC, Abel ED. Heart failure in type 2 diabetes mellitus. *Circ Res* (2019) 124:121–41. doi: 10.1161/CIRCRESAHA.118.311371

36. Hu Y, Belke D, Suarez J, Swanson E, Clark R, Hoshijima M, et al. Adenovirus-mediated overexpression of O-GlcNAcase improves contractile function in the diabetic heart. *Circ Res* (2005) 96:1006–13. doi: 10.1161/01.RES.0000165478.06813.58

37. Shah MS, Brownlee M. Molecular and cellular mechanisms of cardiovascular disorders in diabetes. *Circ Res* (2016) 118:1808–29. doi: 10.1161/CIRCRESAHA.116.306923

38. Yang WH, Park SY, Nam HW, Kim DH, Kang JG, Kang ES, et al. NFkappaB activation is associated with its O-GlcNAcylation state under hyperglycemic conditions. *Proc Natl Acad Sci USA* (2008) 105:17345–50. doi: 10.1073/pnas.0806198105

39. Du XL, Edelstein D, Rossetti L, Fantus IG, Goldberg H, Ziyadeh F, et al. Hyperglycemia-induced mitochondrial superoxide overproduction activates the hexosamine pathway and induces plasminogen activator inhibitor-1 expression by increasing Sp1 glycosylation. *Proc Natl Acad Sci USA* (2000) 97:12222–6. doi: 10.1073/pnas.97.22.12222

40. Fricovsky ES, Suarez J, Ihm SH, Scott BT, Suarez Ramirez JA, Banerjee I, et al. Excess protein O-GlcNAcylation and the progression of diabetic cardiomyopathy. *Am J Physiol Regul Integr Comp Physiol* (2012) 303:R689–R99. doi: 10.1152/ajpregu.00548.2011

41. Shrikhande GV, Scali ST, da Silva CG, Damrauer SM, Csizmadia E, Putheti P, et al. O-glycosylation regulates ubiquitination and degradation of the anti-inflammatory protein A20 to accelerate atherosclerosis in diabetic ApoE-null mice. *PLoS One* (2010) 5:e14240. doi: 10.1371/journal.pone.0014240

42. Kim JA, Wei Y, Sowers JR. Role of mitochondrial dysfunction in insulin resistance. *Circ Res* (2008) 102:401–14. doi: 10.1161/CIRCRESAHA.107.165472

43. Riehle C, Bauersachs J. Of mice and men: Models and mechanisms of diabetic cardiomyopathy. *Basic Res Cardiol* (2018) 114:2. doi: 10.1007/s00395-018-0711-0

44. Chiu HC, Kovacs A, Blanton RM, Han X, Courtois M, Weinheimer CJ, et al. Transgenic expression of fatty acid transport protein 1 in the heart causes lipotoxic cardiomyopathy. *Circ Res* (2005) 96:225–33. doi: 10.1161/01.RES.0000154079.20681.B9

45. Park TS, Hu Y, Noh HL, Drosatos K, Okajima K, Buchanan J, et al. Ceramide is a cardiotoxin in lipotoxic cardiomyopathy. *J Lipid Res* (2008) 49:2101–12. doi: 10.1194/jlr.M800147-JLR200

46. Pepino MY, Kuda O, Samovski D, Abumrad NA. Structure-function of CD36 and importance of fatty acid signal transduction in fat metabolism. *Annu Rev Nutr* (2014) 34:281–303. doi: 10.1146/annurev-nutr-071812-161220

47. Ritchie RH, Zerenturk EJ, Prakoso D, Calkin AC. Lipid metabolism and its implications for type 1 diabetes-associated cardiomyopathy. *J Mol Endocrinol* (2017) 58:R225–R40. doi: 10.1530/JME-16-0249

48. Shu H, Peng Y, Hang W, Nie J, Zhou N, Wang DW. The role of CD36 in cardiovascular disease. *Cardiovasc Res* (2022) 118:115–29. doi: 10.1093/cvr/cvaa319

49. Zhang X, Fan J, Li H, Chen C, Wang Y. CD36 signaling in diabetic cardiomyopathy. *Aging Dis* (2021) 12:826–40. doi: 10.14336/AD.2020.1217

50. Nègre Salvayre A, Augé N, Camaré C, Bacchetti T, Ferretti G, Salvayre R. Dual signaling evoked by oxidized LDLs in vascular cells. *Free Radical Biol Med* (2017) 106:118–33. doi: 10.1016/j.freeradbiomed.2017.02.006

51. Farhangkhoee H, Khan ZA, Barbin Y, Chakrabarti S. Glucose-induced up-regulation of CD36 mediates oxidative stress and microvascular endothelial cell dysfunction. *Diabetologia* (2005) 48:1401–10. doi: 10.1007/s00125-005-1801-8

52. Yang J, Sambandam N, Han X, Gross RW, Courtois M, Kovacs A, et al. CD36 deficiency rescues lipotoxic cardiomyopathy. *Circ Res* (2007) 100:1208–17. doi: 10.1161/01.RES.0000264104.25265.b6

53. Nagendran J, Pulinilkunnil T, Kienesberger PC, Sung MM, Fung D, Febbraio M, et al. Cardiomyocyte-specific ablation of CD36 improves post-ischemic functional recovery. *J Mol Cell Cardiol* (2013) 63:180–8. doi: 10.1016/j.yjmcc.2013.07.020

54. Febbraio M, Hajjar DP, Silverstein RL. CD36: A class B scavenger receptor involved in angiogenesis, atherosclerosis, inflammation, and lipid metabolism. *J Clin Invest* (2001) 108:785–91. doi: 10.1172/JCI14006

55. Wang J, Song Y, Wang Q, Kralik PM, Epstein PN. Causes and characteristics of diabetic cardiomyopathy. *Rev Diabetes Stud* (2006) 3:108–17. doi: 10.1900/RDS.2006.3.108

56. Rijzewijk LJ, van der Meer RW, Smit JWA, Diamant M, Bax JJ, Hammer S, et al. Myocardial steatosis is an independent predictor of diastolic dysfunction in type 2 diabetes mellitus. *J Am Coll Cardiol* (2008) 52:1793–9. doi: 10.1016/j.jacc.2008.07.062

57. Christoffersen C, Bollano E, Lindegaard MLS, Bartels ED, Goetze JP, Andersen CB, et al. Cardiac lipid accumulation associated with diastolic dysfunction in obese mice. *Endocrinology* (2003) 144:3483–90. doi: 10.1210/en.2003-0242

58. Demarco VG, Ford DA, Henriksen EJ, Aroor AR, Johnson MS, Habibi J, et al. Obesity-related alterations in cardiac lipid profile and nondipping blood pressure pattern during transition to diastolic dysfunction in male db/db mice. *Endocrinology* (2013) 154:159–71. doi: 10.1210/en.2012-1835

59. Shi H, Kokoeva MV, Inouye K, Tzameli I, Yin H, Flier JS. TLR4 links innate immunity and fatty acid-induced insulin resistance. *J Clin Invest* (2006) 116:3015–25. doi: 10.1172/JCI28898

60. Chaurasia B, Summers SA. Ceramides-lipotoxic inducers of metabolic disorders. *Trends Endocrinol Metab* (2015) 26:538–50. doi: 10.1016/j.tem.2015.07.006

61. Kolwicz SC, Purohit S, Tian R. Cardiac metabolism and its interactions with contraction, growth, and survival of cardiomyocytes. *Circ Res* (2013) 113:603–16. doi: 10.1161/CIRCRESAHA.113.302095

62. D'Souza K, Nzirorera C, Kienesberger PC. Lipid metabolism and signaling in cardiac lipotoxicity. *Biochim Biophys Acta* (2016) 1861:1513–24. doi: 10.1016/j.bbalip.2016.02.016

63. Park S-Y, Kim H-J, Wang S, Higashimori T, Dong J, Kim Y-J, et al. Hormone-sensitive lipase knockout mice have increased hepatic insulin

sensitivity and are protected from short-term diet-induced insulin resistance in skeletal muscle and heart. *Am J Physiol Endocrinol Metab* (2005) 289:E30–E9. doi: 10.1152/ajpendo.00251.2004

64. Shulman GI. Cellular mechanisms of insulin resistance. *J Clin Invest* (2000) 106:171–6. doi: 10.1172/JCI10583

65. Drosatos K, Schulze PC. Cardiac lipotoxicity: Molecular pathways and therapeutic implications. *Curr Heart fail Rep* (2013) 10:109–21. doi: 10.1007/s11897-013-0133-0

66. Wakasaki H, Koya D, Schoen FJ, Jirousek MR, Ways DK, Hoit BD, et al. Targeted overexpression of protein kinase C beta2 isoform in myocardium causes cardiomyopathy. *Proc Natl Acad Sci USA* (1997) 94:9320–5. doi: 10.1073/pnas.94.17.9320

67. Farhangkhoee H, Khan ZA, Kaur H, Xin X, Chen S, Chakrabarti S. Vascular endothelial dysfunction in diabetic cardiomyopathy: Pathogenesis and potential treatment targets. *Pharmacol Ther* (2006) 111:384–99. doi: 10.1016/j.pharmthera.2005.10.008

68. Steinberg SF. Structural basis of protein kinase C isoform function. *Physiol Rev* (2008) 88:1341–78. doi: 10.1152/physrev.00034.2007

69. Das Evcimen N, King GL. The role of protein kinase C activation and the vascular complications of diabetes. *Pharmacol Res* (2007) 55:498–510. doi: 10.1016/j.phrs.2007.04.016

70. Guzik TJ, Mussa S, Gastaldi D, Sadowski J, Ratnatunga C, Pillai R, et al. Mechanisms of increased vascular superoxide production in human diabetes mellitus: Role of NAD(P)H oxidase and endothelial nitric oxide synthase. *Circulation* (2002) 105:1656–62. doi: 10.1161/01.cir.0000012748.58444.08

71. Inoguchi T, Sonta T, Tsubouchi H, Etoh T, Kakimoto M, Sonoda N, et al. Protein kinase C-dependent increase in reactive oxygen species (ROS) production in vascular tissues of diabetes: Role of vascular NAD(P)H oxidase. *J Am Soc Nephrol JASN* (2003) 14:S227–S32. doi: 10.1097/01.asn.0000077407.90309.65

72. Liu Y, Lei S, Gao X, Mao X, Wang T, Wong GT, et al. PKCβ inhibition with ruboxistaurin reduces oxidative stress and attenuates left ventricular hypertrophy and dysfunction in rats with streptozotocin-induced diabetes. *Clin Sci (London Engl 1979)* (2012) 122:161–73. doi: 10.1042/CS20110176

73. Cosentino F, Eto M, De Paolis P, van der Loo B, Bachschmid M, Ullrich V, et al. High glucose causes upregulation of cyclooxygenase-2 and alters prostanoid profile in human endothelial cells: Role of protein kinase C and reactive oxygen species. *Circulation* (2003) 107:1017–23. doi: 10.1161/01.cir.0000051367.92927.07

74. Min W, Bin ZW, Quan ZB, Hui ZJ, Sheng FG. The signal transduction pathway of PKC/NF-kappa B/c-fos may be involved in the influence of high glucose on the cardiomyocytes of neonatal rats. *Cardiovasc Diabetol* (2009) 8:8. doi: 10.1186/1475-2840-8-8

75. Wang M, Zhang W-B, Zhu J-H, Fu G-S, Zhou B-Q. Breviscapine ameliorates hypertrophy of cardiomyocytes induced by high glucose in diabetic rats *via* the PKC signaling pathway. *Acta Pharmacol Sin* (2009) 30:1081–91. doi: 10.1038/aps.2009.95

76. Lim JY, Park SJ, Hwang HY, Park EJ, Nam JH, Kim J, et al. TGF-beta1 induces cardiac hypertrophic responses *via* PKC-dependent ATF-2 activation. *J Mol Cell Cardiol* (2005) 39:627–36. doi: 10.1016/j.yjmcc.2005.06.016

77. Li Z, Abdullah CS, Jin ZQ. Inhibition of PKC-Θ preserves cardiac function and reduces fibrosis in streptozotocin-induced diabetic cardiomyopathy. *Br J Pharmacol* (2014) 171:2913–24. doi: 10.1111/bph.12621

78. Xia Z, Kuo KH, Nagareddy PR, Wang F, Guo Z, Guo T, et al. N-acetylcysteine attenuates PKCbeta2 overexpression and myocardial hypertrophy in streptozotocin-induced diabetic rats. *Cardiovasc Res* (2007) 73:770–82. doi: 10.1016/j.cardiores.2006.11.033

79. Qi D, Young LH. AMPK: Energy sensor and survival mechanism in the ischemic heart. *Trends Endocrinol Metab* (2015) 26:422–9. doi: 10.1016/j.tem.2015.05.010

80. Dolinsky VW, Dyck JRB. Role of AMP-activated protein kinase in healthy and diseased hearts. *Am J Physiol Heart Circ Physiol* (2006) 291:H2557–H69. doi: 10.1152/ajpheart.00329.2006

81. Ko HJ, Zhang Z, Jung DY, Jun JY, Ma Z, Jones KE, et al. Nutrient stress activates inflammation and reduces glucose metabolism by suppressing AMP-activated protein kinase in the heart. *Diabetes* (2009) 58:2536–46. doi: 10.2337/db08-1361

82. Xie Z, He C, Zou M-H. AMP-activated protein kinase modulates cardiac autophagy in diabetic cardiomyopathy. *Autophagy* (2011) 7:1254–5. doi: 10.4161/auto.7.10.16740

83. Zou M-H, Xie Z. Regulation of interplay between autophagy and apoptosis in the diabetic heart: New role of AMPK. *Autophagy* (2013) 9:624–5. doi: 10.4161/auto.23577

84. Li L, Chen X, Su C, Wang Q, Li R, Jiao W, et al. Si-Miao-Yong-An decoction preserves cardiac function and regulates GLC/AMPK/NF-κB and GLC/PPARα/PGC-1α pathways in diabetic mice. *Biomed Pharmacother* (2020) 132:110817. doi: 10.1016/j.biopha.2020.110817

85. Ma Z-G, Yuan Y-P, Xu S-C, Wei W-Y, Xu C-R, Zhang X, et al. CTRP3 attenuates cardiac dysfunction, inflammation, oxidative stress and cell death in diabetic cardiomyopathy in rats. *Diabetologia* (2017) 60:1126–37. doi: 10.1007/s00125-017-4232-4

86. Jeon S-M. Regulation and function of AMPK in physiology and diseases. *Exp Mol Med* (2016) 48:e245. doi: 10.1038/emm.2016.81

87. Song J, Li J, Hou F, Wang X, Liu B. Mangiferin inhibits endoplasmic reticulum stress-associated thioredoxin-interacting protein/NLRP3 inflammasome activation with regulation of AMPK in endothelial cells. *Metabolism* (2015) 64:428–37. doi: 10.1016/j.metabol.2014.11.008

88. Wang S, Zhang M, Liang B, Xu J, Xie Z, Liu C, et al. AMPKalpha2 deletion causes aberrant expression and activation of NAD(P)H oxidase and consequent endothelial dysfunction *in vivo*: Role of 26S proteasomes. *Circ Res* (2010) 106:1117–28. doi: 10.1161/CIRCRESAHA.109.212530

89. Fan B, Luk AOY, Chan JCN, Ma RCW. MicroRNA and diabetic complications: A clinical perspective. *Antioxid Redox Signal* (2018) 29:1041–63. doi: 10.1089/ars.2017.7318

90. Agbu P, Carthew RW. MicroRNA-mediated regulation of glucose and lipid metabolism. *Nat Rev Mol Cell Biol* (2021) 22:425–38. doi: 10.1038/s41580-021-00354-w

91. Rawal S, Manning P, Katare R. Cardiovascular MicroRNAs: As modulators and diagnostic biomarkers of diabetic heart disease. *Cardiovasc Diabetol* (2014) 13:44. doi: 10.1186/1475-2840-13-44

92. He X, Kuang G, Wu Y, Ou C. Emerging roles of exosomal miRNAs in diabetes mellitus. *Clin Trans Med* (2021) 11:e468. doi: 10.1002/ctm2.468

93. Zhang F, Ma D, Zhao W, Wang D, Liu T, Liu Y, et al. Obesity-induced overexpression of miR-802 impairs insulin transcription and secretion. *Nat Commun* (2020) 11:1822. doi: 10.1038/s41467-020-15529-w

94. Locke JM, da Silva Xavier G, Dawe HR, Rutter GA, Harries LW. Increased expression of miR-187 in human islets from individuals with type 2 diabetes is associated with reduced glucose-stimulated insulin secretion. *Diabetologia* (2014) 57:122–8. doi: 10.1007/s00125-013-3089-4

95. Ofori JK, Salunkhe VA, Bagge A, Vishnu N, Nagao M, Mulder H, et al. Elevated miR-130a/miR-130b/miR-152 expression reduces intracellular ATP levels in the pancreatic beta cell. *Sci Rep* (2017) 7:44986. doi: 10.1038/srep44986

96. Li Q, Song XW, Zou J, Wang GK, Kremneva E, Li XQ, et al. Attenuation of microRNA-1 derepresses the cytoskeleton regulatory protein twinfilin-1 to provoke cardiac hypertrophy. *J Cell Sci* (2010) 123:2444–52. doi: 10.1242/jcs.067165

97. Rawal S, Nagesh PT, Coffey S, Van Hout I, Galvin IF, Bunton RW, et al. Early dysregulation of cardiac-specific microRNA-208a is linked to maladaptive cardiac remodelling in diabetic myocardium. *Cardiovasc Diabetol* (2019) 18:13. doi: 10.1186/s12933-019-0814-4

98. Surina S, Fontanella RA, Scisciola L, Marfella R, Paolisso G, Barbieri M. MiR-21 in human cardiomyopathies. *Front Cardiovasc Med* (2021) 8:767064. doi: 10.3389/fcvm.2021.767064

99. Li X, Meng C, Han F, Yang J, Wang J, Zhu Y, et al. Vildagliptin attenuates myocardial dysfunction and restores autophagy *via* miR-21/SPRY1/ERK in diabetic mice heart. *Front Pharmacol* (2021) 12:634365. doi: 10.3389/fphar.2021.634365

100. Gao L, Liu Y, Guo S, Xiao L, Wu L, Wang Z, et al. LAZ3 protects cardiac remodeling in diabetic cardiomyopathy *via* regulating miR-21/PPARa signaling. *Biochim Biophys Acta Mol basis Dis* (2018) 1864:3322–38. doi: 10.1016/j.bbadis.2018.07.019

101. Wang HJ, Huang YL, Shih YY, Wu HY, Peng CT, Lo WY. microRNA-146a decreases high glucose/thrombin-induced endothelial inflammation by inhibiting NAPDH oxidase 4 expression. *Mediators Inflammation* (2014) 2014:379537. doi: 10.1155/2014/379537

102. Balasubramanyam M, Aravind S, Gokulakrishnan K, Prabu P, Sathishkumar C, Ranjani H, et al. Impaired miR-146a expression links subclinical inflammation and insulin resistance in type 2 diabetes. *Mol Cell Biochem* (2011) 351:197–205. doi: 10.1007/s11010-011-0727-3

103. Feng B, Chen S, Gordon AD, Chakrabarti S. MiR-146a mediates inflammatory changes and fibrosis in the heart in diabetes. *J Mol Cell Cardiol* (2017) 105:70–6. doi: 10.1016/j.yjmcc.2017.03.002

104. Wellen KE, Hotamisligil GS. Inflammation, stress, and diabetes. *J Clin Invest* (2005) 115:1111–9. doi: 10.1172/JCI25102

105. Calle MC, Fernandez ML. Inflammation and type 2 diabetes. *Diabetes Metab* (2012) 38:183–91. doi: 10.1016/j.diabet.2011.11.006

106. Zhang J, Wang X, Vikash V, Ye Q, Wu D, Liu Y, et al. ROS and ROS-mediated cellular signaling. *Oxid Med Cell Longevity* (2016) 2016:4350965. doi: 10.1155/2016/4350965

107. Kc S, Cárcamo JM, Golde DW. Vitamin C enters mitochondria *via* facilitative glucose transporter 1 (Glut1) and confers mitochondrial protection against oxidative injury. *FASEB J* (2005) 19:1657–67. doi: 10.1096/fj.05-4107com

108. Borradaile NM, Han X, Harp JD, Gale SE, Ory DS, Schaffer JE. Disruption of endoplasmic reticulum structure and integrity in lipotoxic cell death. *J Lipid Res* (2006) 47:2726–37. doi: 10.1194/jlr.M600299-JLR200

109. Al Rasheed NM, Al Rasheed NM, Hasan IH, Al Amin MA, Al Ajmi HN, Mohamad RA, et al. Simvastatin ameliorates diabetic cardiomyopathy by attenuating oxidative stress and inflammation in rats. *Oxid Med Cell Longevity* (2017) 2017:1092015. doi: 10.1155/2017/1092015

110. Xiao C, Xia ML, Wang J, Zhou XR, Lou YY, Tang LH, et al. Luteolin attenuates cardiac ischemia/reperfusion injury in diabetic rats by modulating Nrf2 antioxidative function. *Oxid Med Cell Longevity* (2019) 2019:2719252. doi: 10.1155/2019/2719252

111. Xu M, Liu PP, Li H. Innate immune signaling and its role in metabolic and cardiovascular diseases. *Physiol Rev* (2019) 99:893–948. doi: 10.1152/physrev.00065.2017

112. Saltiel AR, Olefsky JM. Inflammatory mechanisms linking obesity and metabolic disease. *J Clin Invest* (2017) 127:1–4. doi: 10.1172/JCI92035

113. Monnerat G, Alarcón ML, Vasconcellos LR, Hochman Mendez C, Brasil G, Bassani RA, et al. Author correction: Macrophage-dependent IL-1β production induces cardiac arrhythmias in diabetic mice. *Nat Commun* (2021) 12:7261. doi: 10.1038/s41467-021-27508-w

114. Rogero MM, Calder PC. Obesity, inflammation, toll-like receptor 4 and fatty acids. *Nutrients* (2018) 10:432. doi: 10.3390/nu10040432

115. Chiang CJ, Tsai BCK, Lu TL, Chao YP, Day CH, Ho TJ, et al. Diabetes-induced cardiomyopathy is ameliorated by heat-killed Lactobacillus reuteri GMNL-263 in diabetic rats *via* the repression of the toll-like receptor 4 pathway. *Eur J Nutr* (2021) 60:3211–23. doi: 10.1007/s00394-020-02474-z

116. Dong B, Qi D, Yang L, Huang Y, Xiao X, Tai N, et al. TLR4 regulates cardiac lipid accumulation and diabetic heart disease in the nonobese diabetic mouse model of type 1 diabetes. *Am J Physiol Heart Circ Physiol* (2012) 303:H732–H42. doi: 10.1152/ajpheart.00948.2011

117. Abbate A, Toldo S, Marchetti C, Kron J, Van Tassell BW, Dinarello CA. Interleukin-1 and the inflammasome as therapeutic targets in cardiovascular disease. *Circ Res* (2020) 126:1260–80. doi: 10.1161/CIRCRESAHA.120.315937

118. Toldo S, Abbate A. The NLRP3 inflammasome in acute myocardial infarction. *Nat Rev Cardiol* (2018) 15:203–14. doi: 10.1038/nrcardio.2017.161

119. Luo B, Huang F, Liu Y, Liang Y, Wei Z, Ke H, et al. NLRP3 inflammasome as a molecular marker in diabetic cardiomyopathy. *Front Physiol* (2017) 8:519. doi: 10.3389/fphys.2017.00519

120. Yang F, Qin Y, Wang Y, Meng S, Xian H, Che H, et al. Metformin inhibits the NLRP3 inflammasome *via* AMPK/mTOR-dependent effects in diabetic cardiomyopathy. *Int J Biol Sci* (2019) 15:1010–9. doi: 10.7150/ijbs.29680

121. Fender AC, Kleeschulte S, Stolte S, Leineweber K, Kamler M, Bode J, et al. Thrombin receptor PAR4 drives canonical NLRP3 inflammasome signaling in the heart. *Basic Res Cardiol* (2020) 115:10. doi: 10.1007/s00395-019-0771-9

122. Sharma A, Tate M, Mathew G, Vince JE, Ritchie RH, de Haan JB. Oxidative stress and NLRP3-inflammasome activity as significant drivers of diabetic cardiovascular complications: Therapeutic implications. *Front Physiol* (2018) 9:114. doi: 10.3389/fphys.2018.00114

123. Sharma BR, Kanneganti TD. NLRP3 inflammasome in cancer and metabolic diseases. *Nat Immunol* (2021) 22:550–9. doi: 10.1038/s41590-021-00886-5

124. Strowig T, Henao Mejia J, Elinav E, Flavell R. Inflammasomes in health and disease. *Nature* (2012) 481:278–86. doi: 10.1038/nature10759

125. Vandanmagsar B, Youm YH, Ravussin A, Galgani JE, Stadler K, Mynatt RL, et al. The NLRP3 inflammasome instigates obesity-induced inflammation and insulin resistance. *Nat Med* (2011) 17:179–88. doi: 10.1038/nm.2279

126. Wen H, Ting JPY, O'Neill LAJ. A role for the NLRP3 inflammasome in metabolic diseases–did Warburg miss inflammation? *Nat Immunol* (2012) 13:352–7. doi: 10.1038/ni.2228

127. Pinar AA, Scott TE, Huuskes BM, Tapia Cáceres FE, Kemp-Harper BK, Samuel CS. Targeting the NLRP3 inflammasome to treat cardiovascular fibrosis. *Pharmacol Ther* (2020) 209:107511. doi: 10.1016/j.pharmthera.2020.107511

128. Zhang X, Fu Y, Li H, Shen L, Chang Q, Pan L, et al. H3 relaxin inhibits the collagen synthesis *via* ROS- and P2X7R-mediated NLRP3 inflammasome activation in cardiac fibroblasts under high glucose. *J Cell Mol Med* (2018) 22:1816–25. doi: 10.1111/jcmm.13464

129. Shao BZ, Xu ZQ, Han BZ, Su DF, Liu C. NLRP3 inflammasome and its inhibitors: A review. *Front Pharmacol* (2015) 6:262. doi: 10.3389/fphar.2015.00262

130. Karam BS, Chavez Moreno A, Koh W, Akar JG, Akar FG. Oxidative stress and inflammation as central mediators of atrial fibrillation in obesity and diabetes. *Cardiovasc Diabetol* (2017) 16:120. doi: 10.1186/s12933-017-0604-9

131. Zhang Y, Murugesan P, Huang K, Cai H. NADPH oxidases and oxidase crosstalk in cardiovascular diseases: Novel therapeutic targets. *Nat Rev Cardiol* (2020) 17:170–94. doi: 10.1038/s41569-019-0260-8

132. Leverve XM, Guigas B, Detaille D, Batandier C, Koceir EA, Chauvin C, et al. Mitochondrial metabolism and type-2 diabetes: A specific target of metformin. *Diabetes Metab* (2003) 29:6S88–94. doi: 10.1016/s1262-3636(03)72792-x

133. González Domínguez Á, Visiedo F, Domínguez Riscart J, Ruiz Mateos B, Saez Benito A, Lechuga Sancho AM, et al. Blunted reducing power generation in erythrocytes contributes to oxidative stress in prepubertal obese children with insulin resistance. *Antioxid (Basel Switzerland)* (2021) 10:244. doi: 10.3390/antiox10020244

frontiers | Frontiers in Endocrinology

TYPE Original Research
PUBLISHED 16 September 2022
DOI 10.3389/fendo.2022.981100

OPEN ACCESS

EDITED BY
Lu Cai,
University of Louisville, United States

REVIEWED BY
Liu Kun,
Second People's Hospital of Hunan Province, China
Hegang Li,
Qingdao Agricultural University, China

*CORRESPONDENCE
Rui Liu
liur@jlu.edu.cn

†These authors have contributed equally to this work

SPECIALTY SECTION
This article was submitted to Cardiovascular Endocrinology, a section of the journal Frontiers in Endocrinology

RECEIVED 29 June 2022
ACCEPTED 26 August 2022
PUBLISHED 16 September 2022

CITATION
Yu T, Xu B, Bao M, Gao Y, Zhang Q, Zhang X and Liu R (2022) Identification of potential biomarkers and pathways associated with carotid atherosclerotic plaques in type 2 diabetes mellitus: A transcriptomics study.
Front. Endocrinol. 13:981100.
doi: 10.3389/fendo.2022.981100

Identification of potential biomarkers and pathways associated with carotid atherosclerotic plaques in type 2 diabetes mellitus: A transcriptomics study

Tian Yu[1,2†], Baofeng Xu[3,4†], Meihua Bao[4†], Yuanyuan Gao[1,2], Qiujuan Zhang[1], Xuejiao Zhang[2] and Rui Liu[1,4*]

[1]Department of Very Important People (VIP) Unit, China-Japan Union Hospital of Jilin University, Changchun, China, [2]Department of Endocrinology, China-Japan Union Hospital of Jilin University, Changchun, China, [3]Department of Stroke Center, First Hospital of Jilin University, Changchun, China, [4]School of Stomatology, Changsha Medical University, Changsha, China

Type 2 diabetes mellitus (T2DM) affects the formation of carotid atherosclerotic plaques (CAPs) and patients are prone to plaque instability. It is crucial to clarify transcriptomics profiles and identify biomarkers related to the progression of T2DM complicated by CAPs. Ten human CAP samples were obtained, and whole transcriptome sequencing (RNA-seq) was performed. Samples were divided into two groups: diabetes mellitus (DM) versus non-DM groups and unstable versus stable groups. The Limma package in R was used to identify lncRNAs, circRNAs, and mRNAs. Gene Ontology (GO) annotation and Kyoto Encyclopedia of Genes and Genomes (KEGG) pathway analyses, protein-protein interaction (PPI) network creation, and module generation were performed for differentially expressed mRNAs. Cytoscape was used to create a transcription factor (TF)-mRNA regulatory network, lncRNA/circRNA-mRNA co-expression network, and a competitive endogenous RNA (ceRNA) network. The GSE118481 dataset and RT-qPCR were used to verify potential mRNAs.The regulatory network was constructed based on the verified core genes and the relationships were extracted from the above network. In total, 180 differentially expressed lncRNAs, 343 circRNAs, and 1092 mRNAs were identified in the DM versus non-DM group; 240 differentially expressed lncRNAs, 390 circRNAs, and 677 mRNAs were identified in the unstable versus stable group. Five circRNAs, 14 lncRNAs, and 171 mRNAs that were common among all four groups changed in the same direction. GO/KEGG functional enrichment analysis showed that 171 mRNAs were mainly related to biological processes, such as immune responses, inflammatory responses, and cell adhesion. Five circRNAs, 14 lncRNAs, 46 miRNAs, and 54 mRNAs in the ceRNA network formed a regulatory relationship. C22orf34—hsa-miR-6785-5p—RAB37, hsacirc_013887—hsa-miR-6785-5p/hsa-miR-4763-5p/hsa-miR-30b-3p—RAB37, MIR4435-1HG—hsa-miR-30b-3p—RAB37, and GAS5—hsa-miR-30b-

3p—RAB37 may be potential RNA regulatory pathways. Seven upregulated mRNAs were verified using the GSE118481 dataset and RT-qPCR. The regulatory network included seven mRNAs, five circRNAs, six lncRNAs, and 14 TFs. We propose five circRNAs (hsacirc_028744, hsacirc_037219, hsacirc_006308, hsacirc_013887, and hsacirc_045622), six lncRNAs (EPB41L4A-AS1, LINC00969, GAS5, MIR4435-1HG, MIR503HG, and SNHG16), and seven mRNAs (RAB37, CCR7, CD3D, TRAT1, VWF, ICAM2, and TMEM244) as potential biomarkers related to the progression of T2DM complicated with CAP. The constructed ceRNA network has important implications for potential RNA regulatory pathways.

KEYWORDS

type 2 diabetes mellitus, carotid atherosclerosis, transcriptome, biomarker, pathways, stable plaque, unstable plaque

Introduction

Type 2 diabetes mellitus (T2DM) is a group of metabolic diseases that are mainly caused by chronic hyperglycemia due to multiple causes. Long-term progression can lead to atherosclerotic cardiovascular disease (ASCVD), which is the main cause of death in T2DM patients (1). When atherosclerosis (AS) occurs, a series of pathological changes, including fibro-lipopathy and foam cell necrosis, occur on the arterial wall and lead to plaque formation (2, 3). Cervical plaque formation is one of the main causes of stroke (4). The American Heart Association classifies carotid atherosclerotic plaques (CAPs) histologically into stable and unstable plaques (5). The formation and progression of unstable CAPs lead to more dangerous ischemic stroke events (6).

Patients with T2DM are more likely to form unstable plaques, and the probability of stroke is twice that of those without T2DM (7). Thus, increased vulnerability to CAP development in T2DM patients may be due to aggravated inflammation (8, 9), increased neovascularization (8), promotion of liponuclear expansion (10, 11), growing numbers of plaques (12), and other mechanisms. Clinically, it is of great significance to identify the stability of CAPs in T2DM patients as early as possible and to actively prevent the formation of unstable plaques. Unfortunately, plaque stability cannot be determined histologically despite the increasing number of methods to detect the development of CAPs in T2DM patients. Earlier bioinformatics studies have reported that T2DM alters CAP gene expression (13), but this has not been further confirmed with transcriptomics. Consequently, key biomarkers for T2DM complicated by CAP progression are currently unavailable.

In our study, after a carotid endarterectomy, CAPs were sampled for histological classification and high-throughput sequencing. Using bioinformatics analysis, we determined the corresponding biomarkers at the transcriptome level that indicate the stability of CAPs in T2DM patients. Additionally, the pathogenesis of the disease was explored and treatment targets are discussed.

Materials and methods

Data source

Samples were collected from 10 patients with CAPs at the First Hospital of Jilin University (Changchun, Jilin, from July 2019 to November 2019). The procedure was approved by the Ethics Committee of the First Hospital of Jilin University (No. 2019-272), and written informed consent was obtained from each participant. The processes of tissue classification, storage, transportation, RNA extraction, library preparation, RNA sequencing, and identification of mRNA, lncRNA, and circRNA spectra are consistent with our previously published research (14). Similarly, the transcriptome data PRJNA752896 from this study can be found in the NCBI database (https://submit.ncbi.nlm.nih.gov/subs/bioproject/).

We used "atherosclerotic plaque" and "type 2 diabetes" as keywords to search for relevant information in GEO (http://www.ncbi.nlm.nih.gov/geo) (15). The GSE118481 dataset satisfied our research conditions. This dataset included 16 samples of non-T2DM with CAPs (six asymptomatic and 10 symptomatic) and eight samples of T2DM with CAPs (six asymptomatic and two symptomatic). See Supplementary Figure 1 for a flowchart.

Distribution and comparative analysis of expression abundance among samples

A variety of methods were used to evaluate the correlations among 10 samples, using the cor function in R version 3.6.1 (https://stat.ethz.ch/R-manual/R-devel/library/stats/html/cor.html) to calculate the Pearson's correlation coefficient (PCC) between every two samples. The closer the correlation coefficient is to 1, the higher the similarity of expression patterns between samples (16), using version 1.7.8 of the psych package (https://cran.r-project.org/web/packages/psych/index.html) in R to perform principal component analysis (PCA) based on expression abundance on all samples to view the distribution among samples.

Screening of significantly differentially expressed RNAs and enrichment analysis of mRNAs

The Limma package (version 3.32.5) (17) (http://bioconductor.org/packages/release/bioc/html/limma.html) in R was used to screen RNAs (including lncRNA, circRNA, and mRNA) with a significant difference between the two comparison groups. FDR less than 0.05 and |log2FC|>0.5 were selected as the threshold criteria for screening significant differences. For the significantly differentially expressed RNAs screened from the two groups, the heatmap package (version1.0.8) (18) (https://cran.rproject.org/web/packages/pheatmap/index.html) in R was used to create a two-way hierarchical clustering heatmap.

Subsequently, the sets of significantly differentially expressed lncRNAs, circRNAs, and mRNAs screened from the two comparison groups of DM versus non-DM and unstable versus stable were compared, and the common RNAs of the two comparison groups were obtained. Next, the directions of the significant differences were investigated, and those that differed in the same direction among the common RNAs were retained as the target objects of future research. The mRNAs in the retained RNAs were enriched and analyzed based on Gene Ontology (GO) and Kyoto Encyclopedia of Genes and Genomes (KEGG) (19) using the DAVID (version 6.8) (20, 21) online analysis tool (https://david.ncifcrf.gov/), and a p-value less than 0.05 was selected as the screening significance threshold for correlations. The GO terms include biological process (BP), cellular component (CC), and molecular function (MF) (22).

Construction of protein-protein interaction (PPI) network

The STRING database (version11.0) (23) (http://string-db.org/) was used to search the interactive relationships between the proteins at the intersection of significantly differently expressed gene products retained in the two comparison groups. The interaction network was constructed, and then a visual representation was generated using Cytoscape (version 3.9.0) (24)(http://www.cytoscape.org/). The centrality of the gene nodes in the network was calculated using the plug-in CentiScaPe (version 2.2) (25) (http://apps.cytoscape.org/apps/centiscape) of Cytoscape. The three most common methods for measuring node centrality are degree centrality (DC), closeness centrality (CC), and betweenness centrality (BC). Next, the important gene nodes were screened by the centrality parameter, and the closely connected genes in the network were obtained. Then, the module identification plug-in MCODE (version1.4.2) in Cytoscape was used to partition and identify the network modules (parameters: degree cutoff=2, node score cutoff=0.2, k-core=2). Another plug-in, BINGO (version 2.44; http://apps.cytoscape.org/apps/bingo; FDR<0.05) (26), was used to divide and annotate the functional modules.

Construction of transcription factors (TFs)-differentially expressed gene regulatory network

The Translational Regulatory Relationships Unraveled by Sentence-based Text Mining (TRRUST) database (27) (https://www.grnpedia.org/trrust/) establishes the transcriptional regulation relationship of TFs based on literature mining. We uploaded the genes with significant differential expression at the intersection screened by the two comparison groups to the database and selected TFs with regulatory connection relationships with the genes with significant differential expression at the intersection. Next, according to the relationship between TFs and regulatory genes, a regulatory network was constructed and visually displayed using Cytoscape (24).

Construction of co-expression network of circRNA-mRNA and lncRNA-mRNA

For the significantly differentially expressed lncRNAs, circRNAs, and mRNAs screened from the two comparison groups, the PCC (28) between the expression levels of circRNA-mRNA and lncRNA-mRNA was calculated using the cor.test function in R. Connection pairs with a p-value less than 0.05 were screened, and co-expression networks of circRNA-mRNA and lncRNA-mRNA were constructed. The networks were visualized using Cytoscape (24).

Construction of competitive endogenous RNA(ceRNA) network

To construct lncRNA/circRNA-miRNA relationships, the sequences of all human miRNAs were downloaded from

miRBase (https://www.mirbase.org/), and then the sequences of significantly differentially expressed lncRNAs and circRNAs were extracted and retained by the two comparison groups from the RNA-seq data. Subsequently, the miRanda localization tool (29) (http://cbio.mskcc.org/miRNA2003/miranda.html) was used to predict the binding relationships of lncRNA-miRNA and circRNAs-miRNA (miRanda alignment parameter settings: gap extend=0, score threshold =100, energy threshold =-20, % matched seq threshold =80%).

For the construction of miRNA-mRNA relationships, the miRNAs linked to lncRNAs and circRNAs in the previous step were searched and the target genes they regulated were identified using the miRwalk3.0 database (30)(http://mirwalk.umm.uni-heidelberg.de/). Further, the significantly differentially expressed mRNAs screened from the two comparison groups were mapped to the target genes to identify the significantly differentially expressed mRNAs that were regulated.

To construct a ceRNA network, the lncRNA/circRNA-miRNA-mRNA regulatory network was formed after integration based on the relationships between lncRNA/circRNA-miRNA and miRNA-mRNA. The generated network was visualized using Cytoscape (24).

Public database validation analysis

The gene expression profile data in the GSE118481 dateset were downloaded from the GEO database, which included 24 CAP tissue samples. Further, all samples were divided into two comparison groups according to source information: DM versus non-DM and stable versus unstable. The same Limma algorithm and screening threshold (FDR is less than 0.05, |log2FC|>0.5) were used, and mRNAs with significant differential expression in the two comparison groups were screened. Next, we compared the mRNAs screened from the two comparison groups in the RNA-seq data, selected the overlapping sections, and visualized the mRNA expression levels of the overlapping sections in the RNA-seq data and GEO data.

Reverse-Transcription quantitative polymerase chain reaction (RT-qPCR) validation

We used seven unstable CAPs with DM and seven stable CAPs without DM for liquid nitrogen grinding and Trizol reagent (Invitrogen, Carlsbad, California, USA) extraction to obtain total RNA. After concentration and quality evaluation by microplate reader, total RNA was reverse transcribed to cDNA using the RevertAid First Strand cDNA Synthesis Kit (Thermo Scientific, Waltham, Massachusetts, USA). Then, the cDNA samples were mixed with FastStart Universal SYBR Green Master (Rox) (Roche, Mannheim, Germany) and injected into an Eppendorf AG 22331 Hamburg PCR Thermal Cycler. β-Actin was used as the internal control. Primer sequences are listed in Supplementary Table 1. All samples were run in triplicate, and the results were analyzed using the 2 (−ΔΔCt) method.

Construction of regulatory network where important factors are located

The overlapping mRNAs obtained in the previous step, were combined with the PPI network, TF-mRNA regulatory network, lncRNA/circRNA-mRNA co-expression network, and the ceRNA regulatory network previously constructed. Then, the overlapping mRNAs were extracted to jointly build a comprehensive network.

Statistical analyses

GraphPad Prism was used to draw graphics and perform statistical analysis of RT-qPCR data using the Wilcoxon rank sum test. Other statistical analyses were performed using R software. T-tests were used to compare differences in expression between the groups. The expression level of mRNAs is presented as the mean ± SD. $p < 0.05$ was considered statistically significant.

Results

Distribution and comparative analysis of expression abundance

The PCCs between samples with different RNAs expression levels were distributed above 0.6. PCA analysis was performed based on expression abundance. The results showed that the correlation between gene expression levels was very high, the sample distribution was relatively clustered, and there was no discrete type (Figure 1).

Identification of differentially expressed RNAs

Statistics on the number and types of significantly differentially expressed RNAs were screened according to the two comparison groups and the common RNAs following comparison are shown in Supplementary Table 2. Among them, 180 lncRNAs, 343 circRNAs, and 677 mRNAs were differentially expressed between the DM versus non-DM groups, and 240 lncRNAs, 390 circRNAs, and 677 mRNAs were differentially expressed between the unstable versus stable

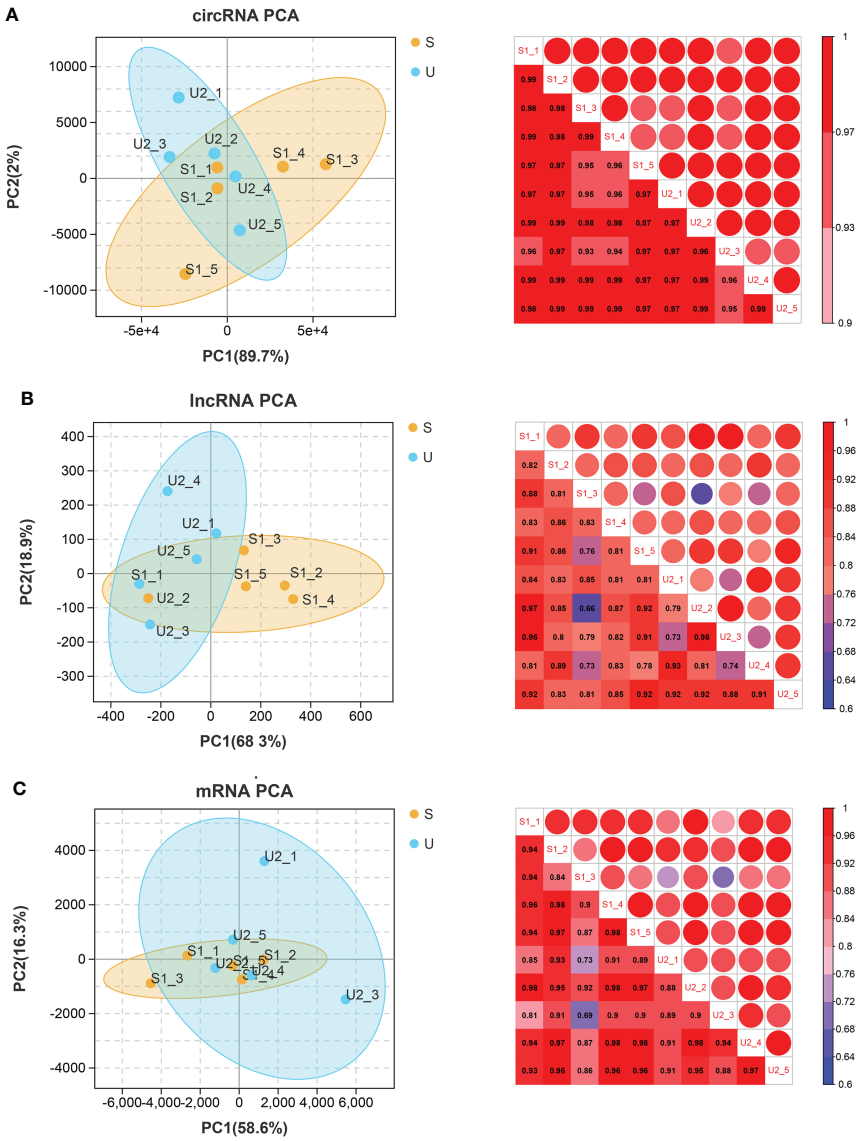

FIGURE 1
circRNA **(A)**, lncRNA **(B)**, and mRNA **(C)**. Left: PCA map of samples based on expression abundance. X, Y, and Z axes represent PC1, 2, and 3 respectively. Dots of different colors represent samples of different groups (S represents the stable group and U represents the unstable group); Right: heatmap of correlation between two samples based on expression abundance. The change of color from cold color to hot color indicates the relationship of the correlation coefficient between samples from small to large, the horizontal and vertical axes represent the name of samples, and the numbers in each grid represent the value of correlation coefficient.

groups. After investigating the direction of the significant differences of overlapping RNAs in the two comparison groups, five circRNAs (three downregulated and two upregulated), 14 lncRNAs (five downregulated and nine upregulated), and 171 mRNAs (80 downregulated and 91 upregulated) had the same significant difference directions in the two comparison groups. Figure 2A shows volcano plots depicting the significantly differentially expressed RNAs and whether they were up- or downregulated. Heatmaps of the expression level of each of the top 10 RNAs that were up- and downregulated among the significantly differentially expressed RNAs are shown in Figure 2B.

Function and pathway enrichment analysis of differentially expressed mRNAs

We screened 22 BPs, nine CCs, seven MFs, and 14 KEGG signaling pathways (Supplementary Table 3); the columnar

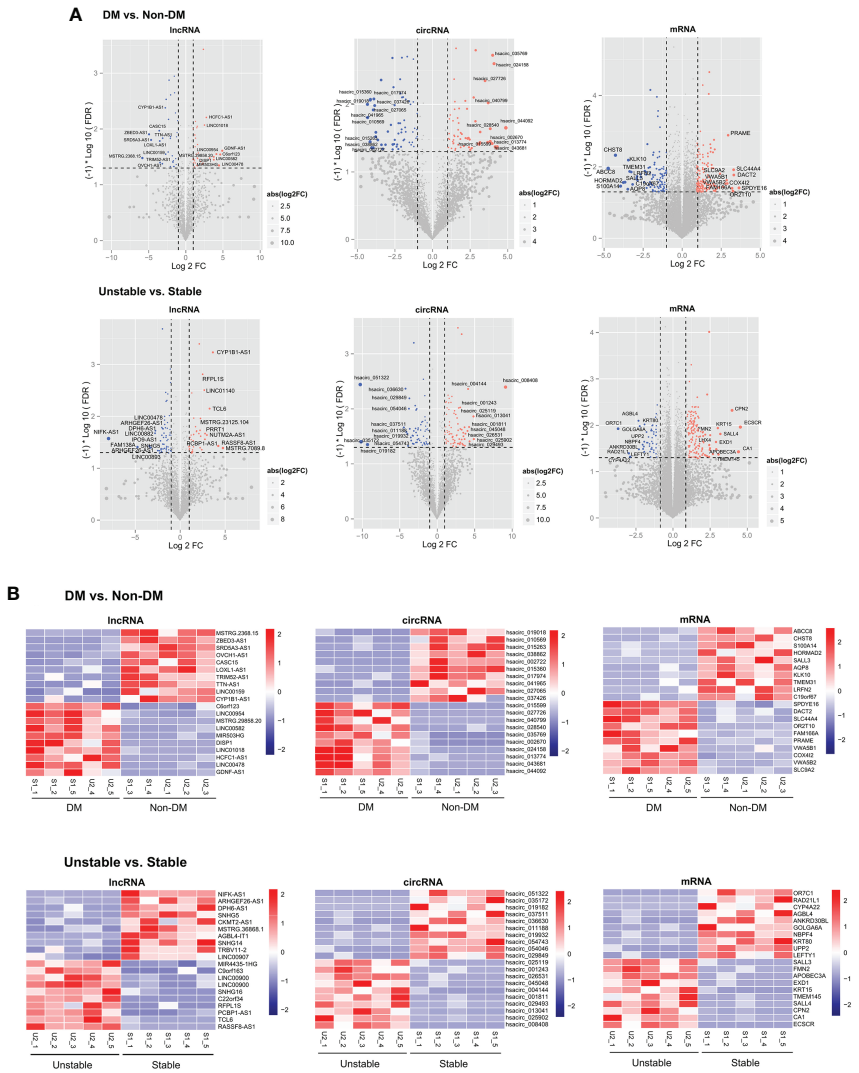

FIGURE 2
(A) The DM versus non-DM and unstable versus stable comparison groups volcano plot. The blue and red dots respectively indicated significantly downregulated and upregulated RNAs, the horizontal dotted line indicated FDR<0.05, and the two red vertical dotted lines indicated |log2FC|>0.5. The top 10 RNAs are marked. **(B)** Heat map of the expression levels of the top 10 RNAs in DM versus non-DM and unstable versus stable groups.

figure is shown in Figure 3. The results showed that BPs and KEGG pathways of 171 mRNAs were significantly enriched in positive regulation of T cell receptor signaling pathway, regulation of immune response, lymphocyte chemotaxis, T cell differentiation, T cell costimulation, inflammatory response, cell adhesion molecules (CAMs), chemokine signaling pathway, focal adhesion, adherens junction, and NF-kappa B signaling pathways, which are involved in immune responses, cell adhesion, and inflammatory reactions. Additionally, the type I interferon signaling pathway and epithelial to mesenchymal transition are considered to be related to the progression of AS (31, 32), and regulation of phosphatidylinositol 3-kinase signaling is considered to be related to insulin resistance and AS (33). MFs were significantly enriched in phosphotyrosine binding, actin filament binding, CCR chemokine receptor binding, iodide transmembrane transporter activity, extracellular matrix structural constituent, 2'-5'-oligoadenylate synthetase activity, and structural constituent of muscle. CCs were significantly enriched in the integral component of plasma membrane, Ndc80 complex, extracellular matrix, extracellular region, sarcolemma, integral component of membrane, adherens junction, and immunological synapse.

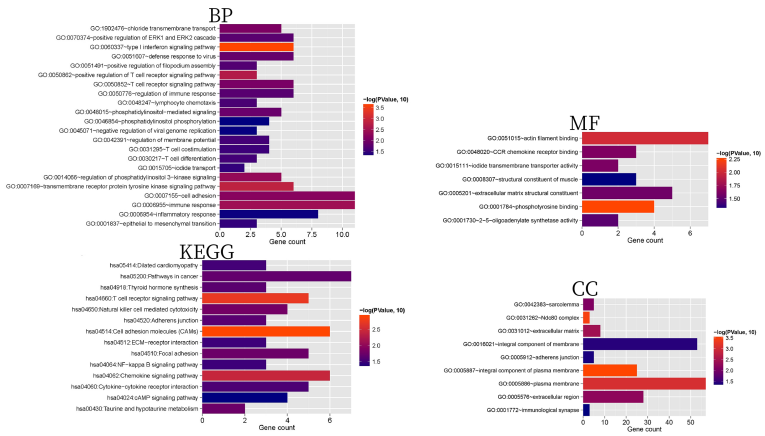

FIGURE 3
BP, CC, MF, and KEGG histograms related to 171 mRNAs with significant differential expression. The horizontal axis represents the number of genes, the vertical axis represents the significantly related items, and the color represents the correlation. The closer to red, the higher the significance.

Construction of a PPI network of differentially expressed mRNAs, regulatory relationship with TFs, co-expression network with differentially expressed circRNAs, and differentially expressed lncRNAs

A total of 697 pairs of interaction links were obtained using the STRING database to construct an interaction network. As shown in Figure 4A, the network contained 154 gene nodes. The important connecting genes in the network were screened and sorted from high to low according to the degree of nodes; the top 20 are displayed in Supplementary Table 4. The top 20 genes were LONRF2, CTNNA3, VWF, LCK, CCR7, LEF1, CD3D, GIMAP8, OASL, RIMS4, GIMAP5, HLA-B, LINGO1, ZAP70, CD40LG, CD5, TRAT1, ACTN2, HAPLN2, and DUSP26.

The PPI network was divided into four modules (Figure 4B). After GO annotation, we obtained BP, MF, and CC which were significantly related to each module. Among the BPs, modules 1, 2, 3, and 4 were significantly related to lymphocyte activation, extracellular structure organization, RNA catabolic process, and nuclear division, respectively. Among the MFs, they were each involved in one of the armadillo repeat domain binding, neurotransmitter receptor activity, transcription cofactor activity, and protein domain-specific binding processes. Among the CCs, they were involved in the cell surface, extracellular matrix, and nucleus. All the significantly relevant GO annotations for each module are listed in Supplementary Table 5.

A total of 88 TF-mRNA regulatory junction pairs were screened. Based on the relationships between TFs and regulatory genes, a regulatory network was constructed (Figure 4C). We also compared all TFs in the TRRUST database with 171 target mRNAs and obtained four intersections (Dlx4, Gli1, LEF1, and hoxd1).

A total of 516 and 450 connecting pairs were screened from circRNA-mRNAs and lncRNA-mRNAs, respectively, to construct the co-expression network of circRNA-mRNAs and lncRNAs-mRNAs (Figures 4D, E).

Construction of ceRNA network

A total of 260 circRNAs-miRNA, 612 lncRNA-miRNA, and 131 miRNA-mRNA linkage pairs were obtained. Based on these regulatory relationships, a ceRNA regulatory network integrating the circRNA/lncRNA-miRNA regulatory axis was constructed (Figure 5). The network included five circRNAs, 13 lncRNAs, 46 miRNAs, and 54 mRNAs.

GSE118481 dataset and RT-qPCR validation analysis

A total of 690 and 1118 significantly differentially expressed genes meeting the threshold requirements were screened in the DM versus non-DM and symptomatic versus asymptomatic groups, respectively. A total of 136 overlapping regions were screened in both groups (Figure 6A). Then, the direction of significant differences in overlapping genes in the two comparison groups was investigated. A total of 94 significantly differentially expressed genes with the same direction of difference were obtained.

After comparing these 94 genes with 171 mRNAs screened from the two comparison groups of RNA-seq data (Figure 6B), a total of 16 overlapping genes were obtained, of which seven

FIGURE 4
(A) PPI network of significantly differentially expressed genes. The red and blue nodes represent the genes that are significantly upregulated and downregulated, respectively, in the two comparison groups. **(B)** Interaction network module diagram. The red and blue nodes represent the genes that are significantly upregulated and downregulated, respectively, in the two comparison groups. **(C)** TF-differential gene regulatory network. The yellow square and circle represent TFs and significantly differentially expressed genes, respectively, and the red and blue nodes represent the genes that are significantly upregulated and downregulated, respectively, in the two comparison groups. **(D)** circRNAs-miRNA co-expression network, red and blue represent the RNAs that are significantly upregulated and downregulated, respectively, in the two comparison groups, and round and diamond represent mRNAs and circRNAs, respectively; The blue and gray lines indicate significant negative and positive correlations, respectively. **(E)** lncRNA-miRNA co-expression network, red and blue represent the RNAs that are significantly upregulated and downregulated, respectively, in the two comparison groups, and round and square respectively represent mRNAs and lncRNAs; The blue and gray lines indicate significant negative and positive correlations, respectively.

genes were in the same direction of difference in the RNA-seq data and GSE118481 data (CCR7, CD3D, ICAM2, TMEM244, TRAT1, VWF, and RAB37). Column charts of the expression levels of the seven genes in different data are shown in Figures 6C, D.

RT-qPCR verified that CCR7 ($p < 0.05$), CD3D ($p < 0.05$), ICAM2 ($p < 0.05$), TMEM244 ($p < 0.01$), TRAT1 ($p < 0.01$), VWF ($p < 0.05$), and RAB37 ($p < 0.05$) were upregulated in the DM with unstable CAP group compared with the non-DM with stable CAP group (Figure 7).

Construction of a regulatory network where the seven mRNAs are located

Crucial factors related to seven mRNAs were extracted from the PPI network, TF-mRNA regulatory network, lncRNA/circRNAs-mRNA co-expression network, and the ceRNA regulatory network previously constructed. Supplementary Table 6 shows the connection relationships used to build a comprehensive network where the overlapping important mRNAs are located (Figure 8). The important factors included

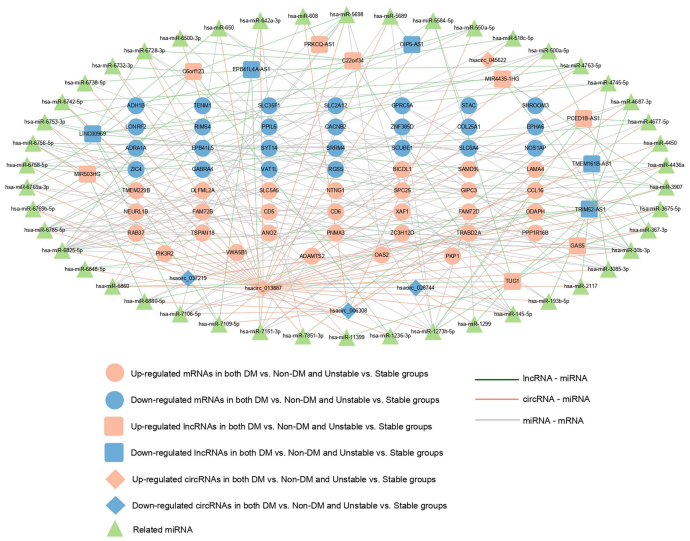

FIGURE 5
ceRNA regulatory network: red and blue represent the RNAs that are significantly upregulated and downregulated, respectively, in the two comparison groups. Round, diamond, and square respectively represent mRNAs, circRNAs, and lncRNAs, and green triangle represents the related miRNAs. Blue, red, and gray represent lncRNA- miRNA, circRNAs-miRNA, and miRNA-mRNA connections, respectively.

in the network were as follows: five circRNAs (hsacirc_028744, hsacirc_037219, hsacirc_006308, hsacirc_013887, and hsacirc_045622), six lncRNAs (EPB41L4A-AS1, LINC00969, GAS5, MIR4435-1HG, MIR503HG, and SNHG16), and seven mRNAs (RAB37, CCR7, CD3D, TRAT1, VWF, ICAM2, and TMEM244). Among them, TFs including ERG, ETS1, ETS2, GATA6, NFIC, NFIL3, NFKB1, POU2F1, POU2F1, RELA, and YY1 are involved in the regulation of the gene VWF; TFs including EPAS1, HIF1A, KLF2, NFKB1, RELA, and TRERF1 are involved in the regulation of the gene CCR7; and the TF of ERG is involved in the regulation of the gene ICAM2. In addition, C22orf34 can act as a ceRNA to compete with RAB37 through hsa-miR-6785-5p, hsacirc_013887 can compete with RAB37 through hsa-miR-6785-5p, hsa-miR-4763-5p, hsa-miR-30b-3p, MIR4435-1HG can compete with RAB37 through hsa-miR-30b-3p, and GAS5 can compete with RAB37 through hsa-miR-30b-3p. These six circRNA/lncRNA-miRNA-mRNAs may be key regulatory axes in the ceRNA network.

Discussion

Patients with T2DM are more likely to face CAP-related complications than those without T2DM (7). These T2DM patients are also more likely to develop unstable AS plaques, resulting in more serious cardiovascular events (34). Therefore, it is crucial to identify the T2DM complicated by unstable CAP earlier in clinical practice. Further, mechanisms underlying disease progression need to be elucidated along with identification of corresponding therapeutic targets.

By comparing the genes expressed in human T2DM patients with unstable CAP samples and non-T2DM patients with stable CAP samples, we identified a total of 171 target mRNAs with significant differential expression, of which 91 were upregulated and 80 were downregulated. By applying GO annotation and KEGG pathway analyses, we noticed that most of the enriched items were related to immune responses, cell adhesion, and inflammatory responses, which is consistent with published studies (3, 35–40). Further analyses indicated that AS formation cannot be separated from the adhesion and migration of monocytes, inflammatory cells, inflammatory mediators, and cytokines in the arterial wall (3). The enrichment results also showed that the plaque formation process of T2DM with unstable CAP also involves a similar pathogenesis. T2DM exacerbates the direct effect of inflammation on AS (35), and the immune response also plays an important role in the progression of AS (36, 37). Adaptive and innate immunity play an important role in the progression of T2DM (38, 39), and hyperglycemia promotes AS progression by regulating the adaptive immunity of macrophages (40). The microenvironment of AS plaques is very complex, where both inflammatory and immune responses are involved and play an important role (41–43). Considering that immune cell infiltration plays a key role in CAP development (44, 45) and that hyperglycemia alters the plaque environment, it is surprising that the role of immune cell infiltration in the progression of CAP under hyperglycemia remains unexplored.

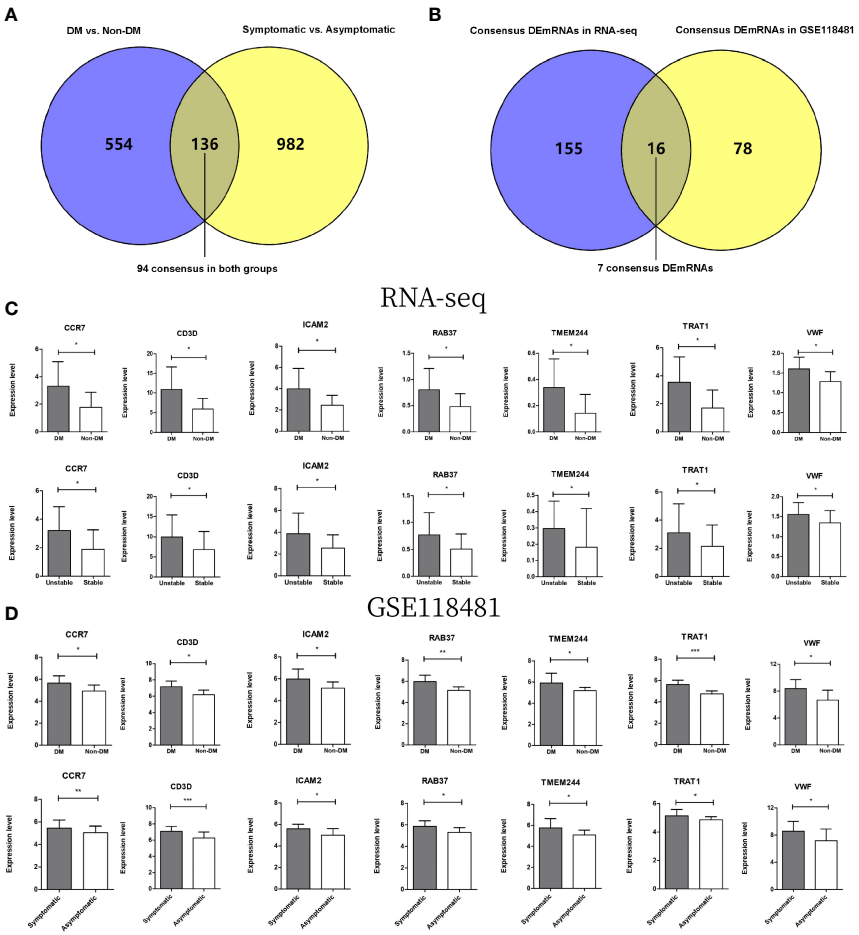

FIGURE 6
(A) Wayne diagram for comparison of significantly differentially expressed genes in DMs versus non-DM and symptomatic versus asymptomatic groups in GSE118481 datasets. **(B)** Wayne diagram comparing overlapping genes in DM versus non-DM and stable versus unstable groups with target mRNA in RNA-seq data results. **(C)** The expression levels of 7 genes were distributed in two comparison groups in the RNA-seq data. **(D)** The expression levels of 7 genes were distributed in two comparison groups in the GSE118481 dataset. * indicates $p<0.05$, * * indicates $p<0.01$, * * * indicates $p<0.001$.

Future research should address this issue. Furthermore, research on the CAP microenvironment and the emergence of corresponding therapeutic targets provide a new research direction for the therapies of T2DM complicated with CAP (42, 43, 46, 47).

We identified seven potential mRNAs, five circRNAs, and six lncRNAs using comprehensive bioinformatic methods. These genes and non-coding RNAs may serve as biomarkers for CAP progression in T2DM. Among them, CCR7, ICAM2, VWF, and RAB37 have been reported to be associated with T2DM or ASCVD-related diseases (48–60). Our study is the first to demonstrate that CD3D, TRAT1, and TMEEM244 are also associated with CAP progression in T2DM. Additionally, for non-coding RNA, we constructed a ceRNA regulatory network to further explore the progression mechanism of T2DM complicated with CAP.

The C-C motif chemokine receptor 7 (CCR7) was one of the major differentially expressed genes obtained by comparing T2DM patients with unstable CAP samples and non-T2DM patients with stable CAP. CCR7 is expressed by B cells, mature dendritic cells (DC), and several T cell subsets including immature, regulatory, and central memory T cells (61). Notably, CCR7 has been identified as a marker for AS progression (51). Similarly, CCR7 has been identified as a differentially expressed gene in non-DM and DM islet samples, indicating that CCR7 may play an important role in the pathogenesis of T2DM (52). Chemokines are a large family of proteins that regulate immune cell transport. They play a key role in guiding the movement and activity of leukocytes during homeostasis, immune surveillance, and inflammation. CC-chemokine ligand 19 (CCL19) and CC-chemokine ligand 21 (CCL21), are CCR7 ligands (61). Adaptive immunity is involved

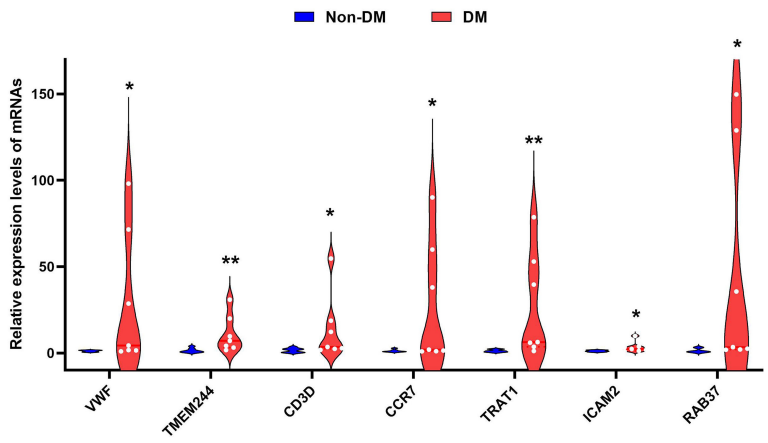

FIGURE 7
Violin diagram of RT-qPCR results for seven genes. * indicates $p < 0.05$, ** indicates $p < 0.01$.

in the pathogenesis of AS, and the chemokines CCL19 and CCL21 are involved in lymphocyte homing in atherosclerotic lesions (48). A few studies have noticed elevated plasma levels of CCL19 and CCL21 in ApoE-/- mice with AS lesions, human CAP, and patients with coronary artery disease (49). Further, while the levels of CCL19 and CCL21 in the plasma in atherosclerotic lesions have been noticed, both these molecules are reported to be upregulated in carotid AS (50). Overall, a large number of studies have probed the role of chemokines and chemokine receptors in the development of AS (48) and by now the importance of chemokines in AS treatment is widely accepted (53). In view of this evidence, we believe that CCR7 is an important biomarker for the progression of T2DM complicated by CAP and plays an important role in identifying relevant targets for the treatment of the disease.

Intercellular adhesion molecule-2 (ICAM-2) was another differentially expressed gene obtained by comparison between T2DM patients with unstable CAP samples and non-T2DM

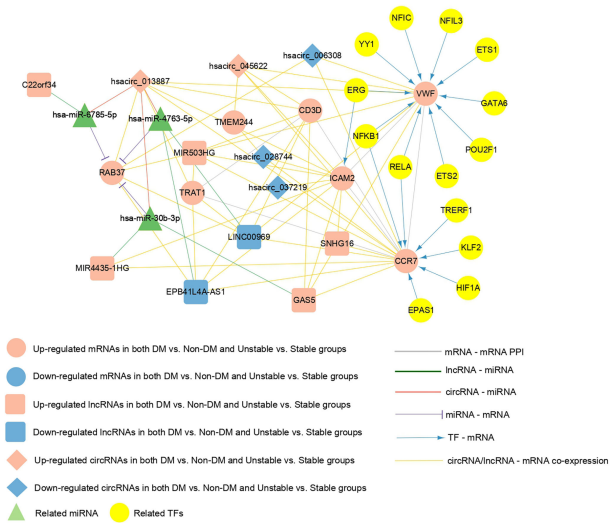

FIGURE 8
The comprehensive network of important overlapping genes. Red and blue represent the RNAs that are significantly upregulated and downregulated, respectively, in the two comparison groups. Circles, diamonds, and squares represent mRNAs, circRNAs, and lncRNAs, respectively, green triangles represent related miRNAs, and yellow circles represent TFs. Grey lines indicate an interaction connection. Green, red, and purple line respectively indicate lncRNA-miRNA, circRNA-miRNA, and miRNA- mRNA connections. Blue lines indicate TF-mRNA connections, and yellow lines indicate circRNA/lncRNA-mRNA co-expression associations.

patients with stable CAP. The protein encoded by this gene is a member of the intercellular adhesion molecule (ICAM) family. Numerous studies have shown that cell adhesion molecules (CAM) play a crucial role in AS initiation and progression (54, 55). ICAM-1 is widely recognized as the driver of the inflammatory response (62). One study has shown that ICAM-1 and ICAM-2 are involved in every step of neutrophil extravasation (56). A recent meta-analysis showed that elevated circulating CAM levels increased the risk of T2DM in a dose-dependent manner (57). Therefore, we suggest that ICAM-2 likely plays an important role in the progression of CAP-complicated T2DM.

Along with ICAM-2, the von Willebrand factor (VWF) was listed as another differentially expressed gene. VWF encodes a glycoprotein that is involved in hemostasis. VWF is engaged in primary hemostasis and coagulation processes, where it acts as a carrier for blood clotting factor VIII, prevents degradation of the factor by protein C, and significantly increases its plasma half-life (58). VWF plays a crucial role in platelet adhesion at sites of vascular injury. It mediates the initial progression of thrombosis at endothelial injury sites through specific interactions with the subendothelial collagen and platelet receptors (63, 64). Earlier studies have reported that VWF can be used as a procoagulant biomarker to predict the risk of cardiovascular and renal complications in diabetic patients (58). A meta-analysis characterized the prognostic value of VWF for ASCVD complications in T2DM patients by comparing plasma VWF levels in T2DM patients with and without coronary artery disease (59). In our study, VWF expression was significantly upregulated in T2DM patients with unstable CAP. Therefore, VWF has potential to be considered as an important biomarker of CAP progression in T2DM.

RAB37, a member of the RAS oncogene family, encodes a protein. Bioinformatics analysis has shown that RAB37 is differentially expressed in Alzheimer's disease (65). Further, a proteomic study reported that the RAB37 protein is related to insulin secretory granules, which are responsible for the storage and secretion of insulin (60). In addition, RAB37 is expressed in human islets and β-cell lines and is involved in the regulation of insulin secretion (66). These studies indicate that RAB37 is associated with T2DM, and our study concurs with this evidence and indicates that RAB37 may play a role in T2DM with CAP at the same time.

The protein encoded by the CD3D gene is a part of the T-cell receptor (TCR)/CD3 complex and participates in T-cell development and signal transduction (67). It exists on the surface of T lymphocytes and plays an important role in the adaptive immune response.A bioinformatis study on the progression of rheumatoid arthritis has shown that CD3D is a potential key mediator and diagnostic marker (68). TRAT 1 stabilizes the TCR/CD3 complex on the surface of T cells. CD3D and TRAT1 are closely related to T cells, and studies have shown that T cells are involved in the pathogenesis of AS and T2DM (37, 69). TMEM244 is a protein-coding gene. Studies have shown that this gene may be used as a marker of Sézary syndrome and other T-cell lymphomas (70). Therefore, it is necessary to consider that the three genes identified for the first time in our study may participate in the progression of T2DM complicated with CAP through an immune response.

The ceRNA hypothesis has revealed a new mechanism for RNA interactions that suggests biological processes can be regulated by an intrinsic mechanism (71). Many bioinformatics studies have constructed AS- or T2DM-related ceRNA regulatory networks using the ceRNA hypothesis (72–74). In this study, a circRNA/lncRNA-miRNA-mRNA regulatory network with CAP progression in T2DM was constructed for the first time, including five circRNAs,13 lncRNAs, 46 miRNAs, and 54 mRNA. Our results suggest that multiple regulatory axes in ceRNA networks may play key roles in the pathogenesis of the disease. We propose that C22orf34—hsa-miR-6785-5p—RAB37, hsacirc_ 013887—hsa-miR-6785-5p/hsa-miR-4763-5p/hsa-miR-30b-3p-RAB37, MIR4435-1HG—hsa-miR-30b-3p—RAB37, and GAS5—hsa-miR-30b-3p—RAB37 are potential RNA regulatory pathways that regulate disease progression.

Previous studies have assessed the role of RNAs that are associated with T2DM and CAP progression (75, 76). However, only a few studies (13), including this study, have explored the progression of T2DM with CAP using advanced bioinformatic methods. While our results provide useful insights into the role of certain genes and RNAs in the progression of T2DM with CAP, our study also has a few limitations. First, there are few public databases that met the purpose of this study. Consequently, the sample size of RNA-seq in our study was small, and further research should be carried out using larger samples. Second, the diagnostic efficacy of some central genes and non-coding RNAs described in our study needs to be verified by clinical data. Finally, the ceRNA regulatory network based on bioinformatics prediction must be verified using molecular methods. In conclusion, the results of our study show that some potentially important genes, non-coding RNAs, pathways, and ceRNA regulatory networks are associated with the progression of T2DM with CAP. Based on these results, we predict that these observations will aid future studies involved in diagnosis, pathogenesis, and potential targeted therapy of T2DM with CAP.

Data availability statement

Publicly available datasets were analyzed in this study. This data can be found here: https://www.ncbi.nlm.nih.gov/sra/

PRJNA752896; https://www.ncbi.nlm.nih.gov/geo/query/acc.cgi?acc=GSE118481.

Ethics statement

The studies involving human participants were reviewed and approved by the Ethics Committee of the First Hospital of Jilin University. The patients/participants provided their written informed consent to participate in this study.

Author contributions

TY, MB, and BX were involved in data collection, data analysis, and article writing. RL designed the project and was responsible for article revisions. YG and QZ were involved in constructing the figures. XZ and TY were responsible for completing RT-qPCR. All authors contributed to the article and approved the submitted version.

Funding

This work was supported by grants from the National Natural Science Foundation of China (81900739), Department of Science and Technology of Jilin Province (20210204217YY), Interdisciplinary Innovation Project of the First Hospital of Jilin University (JDYYJCHX2020014), and Scientific Research Project of the Jilin Provincial Department of Education (JJKH20211162KJ,3D5212598430).

Acknowledgments

We would like to thank all patients and participants who contributed to this study. In addition, the scientific research center of China-Japan Union Hospital of Jilin University provided support for the RT-qPCR experiment.

Conflict of interest

The authors declare that the research was conducted in the absence of any commercial or financial relationships that could be construed as potential conflict of interest.

Publisher's note

Supplementary material

The Supplementary Material for this article can be found online at: https://www.frontiersin.org/articles/10.3389/fendo.2022.981100/full#supplementary-material

References

1. Zheng Y, Ley SH, Hu FB. Global aetiology and epidemiology of type 2 diabetes mellitus and its complications. *Nat Rev Endocrinol* (2018) 14(2):88–98. doi: 10.1038/nrendo.2017.151

2. Libby P, Buring JE, Badimon L, Hansson GK, Deanfield J, Bittencourt MS, et al. Atherosclerosis. *Nat Rev Dis Primers* (2019) 5(1):56. doi: 10.1038/s41572-019-0106-z

3. Geovanini GR, Libby P. Atherosclerosis and inflammation: Overview and updates. *Clin Sci (Lond)* (2018) 132(12):1243–52. doi: 10.1042/CS20180306

4. Ooi YC, Gonzalez NR. Management of extracranial carotid artery disease. *Cardiol Clin* (2015) 33(1):1–35. doi: 10.1016/j.ccl.2014.09.001

5. Stary HC. Natural history and histological classification of atherosclerotic lesions: An update. *Arterioscler Thromb Vasc Biol* (2000) 20(5):1177–8. doi: 10.1161/01.atv.20.5.1177

6. Spagnoli LG, Mauriello A, Sangiorgi G, Fratoni S, Bonanno E, Schwartz RS, et al. Extracranial thrombotically active carotid plaque as a risk factor for ischemic stroke. *JAMA* (2004) 292(15):1845–52. doi: 10.1001/jama.292.15.1845

7. Sarwar N, Gao P, Seshasai SR, Gobin R, Kaptoge S, Di Angelantonio E, et al. Diabetes mellitus, fasting blood glucose concentration, and risk of vascular disease: A collaborative meta-analysis of 102 prospective studies. *Lancet* (2010) 375 (9733):2215–22. doi: 10.1016/s0140-6736(10)60484-9

8. Moreno PR, Fuster V. New aspects in the pathogenesis of diabetic atherothrombosis. *J Am Coll Cardiol* (2004) 44(12):2293–300. doi: 10.1016/j.jacc.2004.07.060

9. Burke AP, Kolodgie FD, Zieske A, Fowler DR, Weber DK, Varghese PJ, et al. Morphologic findings of coronary atherosclerotic plaques in diabetics: A postmortem study. *Arterioscler Thromb Vasc Biol* (2004) 24(7):1266–71. doi: 10.1161/01.ATV.0000131783.74034.97

10. Kato K, Yonetsu T, Kim SJ, Xing L, Lee H, McNulty I, et al. Comparison of nonculprit coronary plaque characteristics between patients with and without diabetes: A 3-vessel optical coherence tomography study. *JACC Cardiovasc Interv* (2012) 5(11):1150–8. doi: 10.1016/j.jcin.2012.06.019

11. Sun B, Li X, Liu X, Ge X, Lu Q, Zhao X, et al. Association between carotid plaque characteristics and acute cerebral infarction determined by mri in patients with type 2 diabetes mellitus. *Cardiovasc Diabetol* (2017) 16(1):111. doi: 10.1186/s12933-017-0592-9

12. Li X, Sun B, Wang L, Zhang J, Zhang J, Zhao Z, et al. Association of type 2 diabetes mellitus and glycemic control with intracranial plaque characteristics in patients with acute ischemic stroke. *J Magn Reson Imaging* (2021) 54(2):655–66. doi: 10.1002/jmri.27614

13. Li YY, Zhang S, Wang H, Zhang SX, Xu T, Chen SW, et al. Identification of crucial genes and pathways associated with atherosclerotic plaque in diabetic patients. *Pharmgenomics Pers Med* (2021) 14:211–20. doi: 10.2147/PGPM.S281705

14. Bao MH, Zhang RQ, Huang XS, Zhou J, Guo Z, Xu BF, et al. Transcriptomic and proteomic profiling of human stable and unstable carotid atherosclerotic plaques. *Front Genet* (2021) 12:755507. doi: 10.3389/fgene.2021.755507

15. Barrett T, Wilhite SE, Ledoux P, Evangelista C, Kim IF, Tomashevsky M, et al. Ncbi geo: Archive for functional genomics data sets–update. *Nucleic Acids Res* (2013) 41(Database issue):D991–5. doi: 10.1093/nar/gks1193

16. Chen G, Li Y, Su Y, Zhou L, Zhang H, Shen Q, et al. Identification of candidate genes for necrotizing enterocolitis based on microarray data. *Gene* (2018) 661:152–9. doi: 10.1016/j.gene.2018.03.088

17. Ritchie ME, Phipson B, Wu D, Hu Y, Law CW, Shi W, et al. Limma powers differential expression analyses for rna-sequencing and microarray studies. *Nucleic Acids Res* (2015) 43(7):e47. doi: 10.1093/nar/gkv007

18. Wang L, Cao C, Ma Q, Zeng Q, Wang H, Cheng Z, et al. Rna-seq analyses of multiple meristems of soybean: Novel and alternative transcripts, evolutionary and functional implications. *BMC Plant Biol* (2014) 14:169. doi: 10.1186/1471-2229-14-169

19. Kanehisa M, Goto S. Kegg: Kyoto encyclopedia of genes and genomes. *Nucleic Acids Res* (2000) 28(1):27–30. doi: 10.1093/nar/28.1.27

20. Huang DW, Sherman BT, Lempicki RA. Systematic and integrative analysis of Large gene lists using David bioinformatics resources. *Nat Protoc* (2009) 4 (1):44–57. doi: 10.1038/nprot.2008.211

21. Huang da W, Sherman BT, Lempicki RA. Bioinformatics enrichment tools: Paths toward the comprehensive functional analysis of Large gene lists. *Nucleic Acids Res* (2009) 37(1):1–13. doi: 10.1093/nar/gkn923

22. Consortium GO. The gene ontology (Go) project in 2006. *Nucleic Acids Res* (2006) 34(Database issue):D322–6. doi: 10.1093/nar/gkj021

23. Szklarczyk D, Gable AL, Nastou KC, Lyon D, Kirsch R, Pyysalo S, et al. The string database in 2021: Customizable protein-protein networks, and functional characterization of user-uploaded Gene/Measurement sets. *Nucleic Acids Res* (2021) 49(D1):D605–D12. doi: 10.1093/nar/gkaa1074

24. Shannon P, Markiel A, Ozier O, Baliga NS, Wang JT, Ramage D, et al. Cytoscape: A software environment for integrated models of biomolecular interaction networks. *Genome Res* (2003) 13(11):2498–504. doi: 10.1101/gr.1239303

25. Scardoni G, Petterlini M, Laudanna C. Analyzing biological network parameters with centiscape. *Bioinformatics* (2009) 25(21):2857–9. doi: 10.1093/bioinformatics/btp517

26. Maere S, Heymans K, Kuiper M. Bingo: A cytoscape plugin to assess overrepresentation of gene ontology categories in biological networks. *Bioinformatics* (2005) 21(16):3448–9. doi: 10.1093/bioinformatics/bti551

27. Han H, Cho JW, Lee S, Yun A, Kim H, Bae D, et al. Trrust V2: An expanded reference database of human and mouse transcriptional regulatory interactions. *Nucleic Acids Res* (2018) 46(D1):D380–D6. doi: 10.1093/nar/gkx1013

28. Zou KH, Tuncali K, Silverman SG. Correlation and simple linear regression. *Radiology* (2003) 227(3):617–22. doi: 10.1148/radiol.2273011499

29. Betel D, Koppal A, Agius P, Sander C, Leslie C. Comprehensive modeling of microrna targets predicts functional non-conserved and non-canonical sites. *Genome Biol* (2010) 11(8):R90. doi: 10.1186/gb-2010-11-8-r90

30. Hemmat N, Mokhtarzadeh A, Aghazadeh M, Jadidi-Niaragh F, Baradaran B, Baghi HB. Role of micrornas in epidermal growth factor receptor signaling pathway in cervical cancer. *Mol Biol Rep* (2020) 47(6):4553–68. doi: 10.1007/s11033-020-05494-4

31. Chen HJ, Tas SW, de Winther MPJ. Type-I interferons in atherosclerosis. *J Exp Med* (2020) 217(1):e20190459. doi: 10.1084/jem.20190459

32. Wesseling M, Sakkers TR, de Jager SCA, Pasterkamp G, Goumans MJ. The morphological and molecular mechanisms of Epithelial/Endothelial-to-Mesenchymal transition and its involvement in atherosclerosis. *Vascul Pharmacol* (2018) 106:1–8. doi: 10.1016/j.vph.2018.02.006

33. Nigro J, Osman N, Dart AM, Little PJ. Insulin resistance and atherosclerosis. *Endocr Rev* (2006) 27(3):242–59. doi: 10.1210/er.2005-0007

34. Einarson TR, Acs A, Ludwig C, Panton UH. Prevalence of cardiovascular disease in type 2 diabetes: A systematic literature review of scientific evidence from across the world in 2007-2017. *Cardiovasc Diabetol* (2018) 17(1):83. doi: 10.1186/s12933-018-0728-6

35. Ray A, Huisman MV, Tamsma JT, van Asten J, Bingen BO, Broeders EA, et al. The role of inflammation on atherosclerosis, intermediate and clinical cardiovascular endpoints in type 2 diabetes mellitus. *Eur J Intern Med* (2009) 20 (3):253–60. doi: 10.1016/j.ejim.2008.07.008

36. Ma SD, Mussbacher M, Galkina EV. Functional role of b cells in atherosclerosis. *Cells* (2021) 10(2):270. doi: 10.3390/cells10020270

37. Saigusa R, Winkels H. Ley K. *T Cell Subsets Functions Atherosclerosis. Nat Rev Cardiol* (2020) 17(7):387–401. doi: 10.1038/s41569-020-0352-5

38. Zhou T, Hu Z, Yang S, Sun L, Yu Z, Wang G. Role of adaptive and innate immunity in type 2 diabetes mellitus. *J Diabetes Res* (2018) 2018:7457269. doi: 10.1155/2018/7457269

39. SantaCruz-Calvo S, Bharath L, Pugh G, SantaCruz-Calvo L, Lenin RR, Lutshumba J, et al. Adaptive immune cells shape obesity-associated type 2 diabetes mellitus and less prominent comorbidities. *Nat Rev Endocrinol* (2022) 18(1):23–42. doi: 10.1038/s41574-021-00575-1

40. Edgar L, Akbar N, Braithwaite AT, Krausgruber T, Gallart-Ayala H, Bailey J, et al. Hyperglycemia induces trained immunity in macrophages and their precursors and promotes atherosclerosis. *Circulation* (2021) 144(12):961–82. doi: 10.1161/CIRCULATIONAHA.120.046464

41. Wu MY, Li CJ, Hou MF, Chu PY. New insights into the role of inflammation in the pathogenesis of atherosclerosis. *Int J Mol Sci* (2017) 18(10):2034. doi: 10.3390/ijms18102034

42. Herrero-Fernandez B, Gomez-Bris R, Somovilla-Crespo B, Gonzalez-Granado JM. Immunobiology of atherosclerosis: A complex net of interactions. *Int J Mol Sci* (2019) 20(21):5293. doi: 10.3390/ijms20215293

43. Ketelhuth DFJ, Lutgens E, Bäck M, Binder CJ, Van den Bossche J, Daniel C, et al. Immunometabolism and atherosclerosis: Perspectives and clinical significance: A position paper from the working group on atherosclerosis and vascular biology of the European society of cardiology. *Cardiovasc Res* (2019) 115 (9):1385–92. doi: 10.1093/cvr/cvz166

44. Tan L, Xu Q, Shi R, Zhang G. Bioinformatics analysis reveals the landscape of immune cell infiltration and immune-related pathways participating in the progression of carotid atherosclerotic plaques. *Artif Cells Nanomed Biotechnol* (2021) 49(1):96–107. doi: 10.1080/21691401.2021.1873798

45. Li S, Zhang Q, Huang Z, Tao W, Zeng C, Yan L, et al. Comprehensive analysis of immunocyte infiltration and the key genes associated with intraplaque hemorrhage in carotid atherosclerotic plaques. *Int Immunopharmacol* (2022) 106:108633. doi: 10.1016/j.intimp.2022.108633

46. Koelwyn GJ, Corr EM, Erbay E, Moore KJ. Regulation of macrophage immunometabolism in atherosclerosis. *Nat Immunol* (2018) 19(6):526–37. doi: 10.1038/s41590-018-0113-3

47. Shen Y, Xu LR, Tang X, Lin CP, Yan D, Xue S, et al. Identification of potential therapeutic targets for atherosclerosis by analysing the gene signature related to different immune cells and immune regulators in atheromatous plaques. *BMC Med Genomics* (2021) 14(1):145. doi: 10.1186/s12920-021-00991-2

48. Li J, Ley K. Lymphocyte migration into atherosclerotic plaque. *Arterioscler Thromb Vasc Biol* (2015) 35(1):40–9. doi: 10.1161/atvbaha.114.303227

49. Damås JK, Smith C, Øie E, Fevang B, Halvorsen B, Waehre T, et al. Enhanced expression of the homeostatic chemokines Ccl19 and Ccl21 in clinical and experimental atherosclerosis: Possible pathogenic role in plaque destabilization. *Arterioscler Thromb Vasc Biol* (2007) 27(3):614–20. doi: 10.1161/01.ATV.0000255581.38523.7c

50. Halvorsen B, Dahl TB, Smedbakken LM, Singh A, Michelsen AE, Skjelland M, et al. Increased levels of Ccr7 ligands in carotid atherosclerosis: Different effects in macrophages and smooth muscle cells. *Cardiovasc Res* (2014) 102(1):148–56. doi: 10.1093/cvr/cvu036

51. Hueso M, Mallén A, Casas Á, Guiteras J, Sbraga F, Blasco-Lucas A, et al. Integrated Mirna/Mrna counter-expression analysis highlights oxidative stress-related genes Ccr7 and Foxo1 as blood markers of coronary arterial disease. *Int J Mol Sci* (2020) 21(6):1943. doi: 10.3390/ijms21061943

52. Cui Y, Chen W, Chi J, Wang L. Differential expression network analysis for diabetes mellitus type 2 based on expressed level of islet cells. *Ann Endocrinol (Paris)* (2016) 77(1):22–9. doi: 10.1016/j.ando.2015.11.002

53. Koenen RR, Weber C. Chemokines: Established and novel targets in atherosclerosis. *EMBO Mol Med* (2011) 3(12):713–25. doi: 10.1002/emmm.201100183

54. Ling S, Nheu L, Komesaroff PA. Cell adhesion molecules as pharmaceutical target in atherosclerosis. *Mini Rev Med Chem* (2012) 12(2):175–83. doi: 10.2174/138955712798995057

55. Chi Z, Melendez AJ. Role of cell adhesion molecules and immune-cell migration in the initiation, onset and development of atherosclerosis. *Cell Adh Migr* (2007) 1(4):171–5. doi: 10.4161/cam.1.4.5321

56. Lyck R, Enzmann G. The physiological roles of icam-1 and icam-2 in neutrophil migration into tissues. *Curr Opin Hematol* (2015) 22(1):53–9. doi: 10.1097/moh.0000000000000103

57. Qiu S, Cai X, Liu J, Yang B, Zügel M, Steinacker JM, et al. Association between circulating cell adhesion molecules and risk of type 2 diabetes: A meta-analysis. *Atherosclerosis* (2019) 287:147–54. doi: 10.1016/j.atherosclerosis.2019.06.908

58. Domingueti CP, Dusse LM, Carvalho M, de Sousa LP, Gomes KB, Fernandes AP. Diabetes mellitus: The linkage between oxidative stress, inflammation, hypercoagulability and vascular complications. *J Diabetes Complications* (2016) 30(4):738–45. doi: 10.1016/j.jdiacomp.2015.12.018

59. Peng X, Wang X, Fan M, Zhao J, Lin L, Liu J. Plasma levels of Von willebrand factor in type 2 diabetes patients with and without cardiovascular diseases: A meta-analysis. *Diabetes Metab Res Rev* (2020) 36(1):e3193. doi: 10.1002/dmrr.3193

60. Brunner Y, Couté Y, Iezzi M, Foti M, Fukuda M, Hochstrasser DF, et al. Proteomics analysis of insulin secretory granules. *Mol Cell Proteomics* (2007) 6 (6):1007–17. doi: 10.1074/mcp.M600443-MCP200

61. Forster R, Davalos-Misslitz AC, Rot A. Ccr7 and its ligands: Balancing immunity and tolerance. *Nat Rev Immunol* (2008) 8(5):362–71. doi: 10.1038/nri2297

62. Bui TM, Wiesolek HL, Sumagin R. Icam-1: A master regulator of cellular responses in inflammation, injury resolution, and tumorigenesis. *J Leukoc Biol* (2020) 108(3):787–99. doi: 10.1002/jlb.2mr0220-549r

63. Domingueti CP, Dusse LM, Carvalho M, Gomes KB, Fernandes AP. Hypercoagulability and cardiovascular disease in diabetic nephropathy. *Clin Chim Acta* (2013) 415:279–85. doi: 10.1016/j.cca.2012.10.061

64. Reininger AJ. Function of Von willebrand factor in haemostasis and thrombosis. *Haemophilia* (2008) 14 Suppl 5:11–26. doi: 10.1111/j.1365-2516.2008.01848.x

65. Xu H, Jia J. Immune-related hub genes and the competitive endogenous rna network in alzheimer's disease. *J Alzheimers Dis* (2020) 77(3):1255–65. doi: 10.3233/jad-200081

66. Ljubicic S, Bezzi P, Brajkovic S, Nesca V, Guay C, Ohbayashi N, et al. The gtpase Rab37 participates in the control of insulin exocytosis. *PLoS One* (2013) 8 (6):e68255. doi: 10.1371/journal.pone.0068255

67. Wang Q, Li P, Wu W. A systematic analysis of immune genes and overall survival in cancer patients. *BMC Cancer* (2019) 19(1):1225. doi: 10.1186/s12885-019-6414-6

68. Lu J, Bi Y, Zhu Y, Huipeng S, Duan W, Zhou J. Cd3d, gzmk, and Klrb1 are potential markers for early diagnosis of rheumatoid arthritis, especially in anti-citrullinated protein antibody-negative patients. *Front Pharmacol* (2021) 12:726529. doi: 10.3389/fphar.2021.726529

69. Stentz FB, Kitabchi AE. Activated T lymphocytes in type 2 diabetes: Implications from in vitro studies. *Curr Drug Targets* (2003) 4(6):493–503. doi: 10.2174/1389450033490966

70. Iżykowska K, Rassek K, Żurawek M, Nowicka K, Paczkowska J, Ziółkowska-Suchanek I, et al. Hypomethylation of the promoter region drives ectopic expression of Tmem244 in sézary cells. *J Cell Mol Med* (2020) 24(18):10970–7. doi: 10.1111/jcmm.15729

71. Salmena L, Poliseno L, Tay Y, Kats L, Pandolfi PP. A cerna hypothesis: The Rosetta stone of a hidden rna language? *Cell* (2011) 146(3):353–8. doi: 10.1016/j.cell.2011.07.014

72. Zhao W, Meng X, Liang J. Analysis of circrna-mrna expression profiles and functional enrichment in diabetes mellitus based on high throughput sequencing. *Int Wound J* (2022) 19(5):1253–62. doi: 10.1111/iwj.13838

73. Zhang F, Zhang R, Zhang X, Wu Y, Li X, Zhang S, et al. Comprehensive analysis of circrna expression pattern and circrna-Mirna-Mrna network in the pathogenesis of atherosclerosis in rabbits. *Aging (Albany NY)* (2018) 10(9):2266–83. doi: 10.18632/aging.101541

74. Yu XH, Deng WY, Chen JJ, Xu XD, Liu XX, Chen L, et al. Lncrna Kcnq1ot1 promotes lipid accumulation and accelerates atherosclerosis *Via* functioning as a cerna through the mir-452-3p/Hdac3/Abca1 axis. *Cell Death Dis* (2020) 11 (12):1043. doi: 10.1038/s41419-020-03263-6

75. Zhang R, Ji Z, Yao Y, Zuo W, Yang M, Qu Y, et al. Identification of hub genes in unstable atherosclerotic plaque by conjoint analysis of bioinformatics. *Life Sci* (2020) 262:118517. doi: 10.1016/j.lfs.2020.118517

76. Massaro JD, Polli CD, Costa ESM, Alves CC, Passos GA, Sakamoto-Hojo ET, et al. Post-transcriptional markers associated with clinical complications in type 1 and type 2 diabetes mellitus. *Mol Cell Endocrinol* (2019) 490:1–14. doi: 10.1016/j.mce.2019.03.008

Advantages of publishing in Frontiers

OPEN ACCESS
Articles are free to read for greatest visibility and readership

FAST PUBLICATION
Around 90 days from submission to decision

HIGH QUALITY PEER-REVIEW
Rigorous, collaborative, and constructive peer-review

TRANSPARENT PEER-REVIEW
Editors and reviewers acknowledged by name on published articles

Frontiers
Avenue du Tribunal-Fédéral 34
1005 Lausanne | Switzerland

Visit us: www.frontiersin.org
Contact us: frontiersin.org/about/contact

REPRODUCIBILITY OF RESEARCH
Support open data and methods to enhance research reproducibility

DIGITAL PUBLISHING
Articles designed for optimal readership across devices

FOLLOW US
@frontiersin

IMPACT METRICS
Advanced article metrics track visibility across digital media

EXTENSIVE PROMOTION
Marketing and promotion of impactful research

LOOP RESEARCH NETWORK
Our network increases your article's readership